UNIVERSITY OF SOUTHAMPTON

FACULTY OF NATURAL AND ENVIRONMENTAL SCIENCE

School of Chemistry

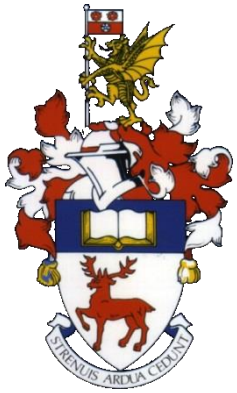

The Structural Analysis of Porphyrin Modified DNA and the Construction of a Molecular Wire

by

James William Wood

Thesis for the degree of Doctor of Philosophy

March 2015

UNIVERSITY OF SOUTHAMPTON

ABSTRACT

FACULTY OF NATURAL AND ENVIRONMENTAL SCIENCES

SCHOOL OF CHEMISTRY

Thesis for the degree of Doctor of Philosophy

THE STRUCTURAL ANALYSIS OF PORPHYRIN MODIFIED DNA AND THE CONSTRUCTION OF A MOLECULAR WIRE

James William Wood

During this work, porphyrins have been attached onto oligonucleotides using several different methods with the aim of creating an organic electronic wire. Due to their planar, aromatic nature, porphyrins can interact with each other and transfer electrons along a self-assembled chain.

Porphyrins, as a substance class have been studied extensively over the years due to their potential application in making optoelectronic devices. DNA, on the other hand has only recently been found to be an ideal supramolecular scaffold for the construction of functional molecules. Hence, combining the chemical properties of porphyrins and DNA opens the door to produce multiporphyrin arrays that have applications for example, in molecular electronic devices.

Two systems have been investigated. The first, named a Zipper array, relies on π-stacking of porphyrins which are held in close proximity by the DNA scaffold. The second is designed to covalently link porphyrins in a DNA directed reaction.

As well as producing a porphyrin wire, the effects of increasing modification on the circular dichroism signature and other spectroscopic techniques was investigated. This sought a greater understanding of the porphyrin-DNA structure and modified DNA in general. Circular dichroism spectroscopy was used to probe the effect porphyrin-modified nucleobases have on the DNA's helical structure, and how porphyrins in different numbers and positions interact with each other.

Contents

ABSTRACT i

Contents i

List of figures v

List of schemes xi

List of tables xiii

DECLARATION OF AUTHORSHIP xv

Acknowledgements xvii

Definitions and Abbreviations xix

1. Introduction 1

1.1 The Structure and Properties of Porphyrins 1
1.2 The Synthesis of Porphyrins 6
1.3 The Structure of 2'-Deoxyribonucleic Acid 12
1.4 The Synthesis of Oligonucleotides 17
1.5 Modification of oligonucleotides 23
1.6 DNA Nanotechnology and Supramolecular Structures 29

2. Aims 35

3. Self-Assembled Porphyrin Zipper Array 37

3.1 Introduction to the Porphyrin Zipper Array 37
3.2 Synthesis of Porphyrin Monomer with Flexible Amide Linker 40
3.3 Synthesis of Porphyrin Monomer with Rigid Acetylene Linker 44
3.4 The Synthesis of Six Porphyrin Oligonucleotides 47
3.5 Single Molecule Spectroscopy of Porphyrin-Modified DNA 54
3.6 Conclusions: Porphyrin Zipper Array 57

4. Click Chemistry for the Attachment of Porphyrins onto DNA 59

4.1 Introduction to the Copper Catalysed Azide-Alkyne Cycloaddition 59
4.2 Labelling Oligonucleotides with Porphyrins using the Baseclick Oligo-Click Kit 64
4.3 Introduction to Copper-Free Click Chemistry 73
4.4 Copper-Free Click Chemistry with Porphyrins 77
4.5 Conclusions: Copper Catalysed and Copper-Free Click Chemistry for the Production of Porphyrin-Modified DNA 82

5. Conjugated Porphyrin-DNA Wire 85

5.1 Introduction to the Conjugated Porphyrin System 85
5.2 Synthesis of the Di-Acetylene Porphyrin 90
5.3 Synthesis of Di-Acetylene Porphyrin Azide and Amine 96
5.4 Attachment of Di-Acetylene Porphyrin to 5'-Modified DNA 102
5.5 Construction of a Porphyrin Wire using a Tetraphenyl Porphyrin Analogue 111
5.6 DNA Directed Glaser-Hay Coupling to Form the Conjugated Porphyrin Wire 117
5.7 Conclusions: Conjugated Porphyrin-DNA Wire 122
6. Structural Analysis of Porphyrin-Modified DNA 125
6.1 Introduction to Circular Dichroism Spectroscopy 125
6.2 Synthesis of Porphyrin-Modified DNA for Circular Dichroism Spectroscopy 129
6.3 Circular Dichroism Spectra of Porphyrin-Modified DNA 134
6.4 Ultraviolet-Visible and Fluorescence Studies of Porphyrin-Modified DNA 154
6.5 Synthesis of Truncated Monomers for Further Structural Analysis ... 157
6.6 Circular Dichroism Spectra of Non-Porphyrin-Modified DNA 160
6.7 Melting Studies of Modified DNA 165
6.8 Conclusions: Structural Analysis of Porphyrin-Modified DNA 175
7. Concluding Remarks 177
8. General Experimental Methods 181
8.1 Suppliers 181
8.2 Column Chromatography and Thin Layer Chromatography 181
8.3 Nuclear Magnetic Resonance Spectroscopy 181
8.4 Mass Spectrometry 181
8.5 Ultraviolet-Visible Spectroscopy 182
8.5.1 UV-Vis Scans 182
8.5.2 UV Melting Experiments 182
8.6 Fluorescence Spectroscopy 182
8.6.1 Fluorescence Scans 182
8.6.2 Fluorescence Melting Experiments 183
8.7 Solid Phase Oligonucleotide Synthesis 183
8.8 Purification of Oligonucleotides by Fluorous Affinity 183
8.9 Purification of Oligonucleotides by Glen-Pak™ 184
8.10 High Performance Liquid Chromatography 185
8.11 Annealing DNA Duplexes 185
8.12 Porphyrin-DNA Coupling Reactions 185

8.12.1 Copper Catalysed Azide-Alkyne Cycloaddition with the Baseclick Oligo-Click Kit 185
8.12.2 Copper-Free Click Chemistry 186
8.12.3 Post Synthetic Labelling of Carboxy Modified DNA with Amino-Modified Porphyrin 187
8.13 DNA Templated Glaser-Hay Reactions 187
8.14 Gel Electrophoresis 188
8.15 Circular Dichroism Spectroscopy 191
9. Synthetic Procedures 193
9.1 Synthesis of 5-(*p*-methyl benzoate)-10, 15, 20-triphenyl porphyrin .. 193
9.2 Synthesis of 5-p-(benzoic acid)-10, 15, 20-triphenyl porphyrin 195
9.3 Synthesis of 5'-DMT-5-Iodo-deoxyuridine 197
9.4 Synthesis of 5'-DMT-5-propargylamine-deoxyuridine 199
9.5 Synthesis of 5'-DMT-5-propargyl-dU-10'', 15'', 20''-triphenyl-5''-(P-benzamide)- porphyrin 201
9.6 Synthesis of 5'-DMT-(5-propargyl-dU)-10'', 15'',20''-triphenyl-5''-(P-benzamide)-porphyrin-3' amidite 203
9.7 Synthesis of 4-(3-hydroxy-3-methylbut-1-ynyl)benzaldehyde 204
9.8 Synthesis of 5-P-(3-methyl-3-hydroxyl-1-butynl) phenyl – 10, 15, 20-triphenyl porphyrin 206
9.9 Synthesis of Zn(II)-5-P-(3-methyl-3-hydroxyl-1-butynyl)-10,15,20 triphenyl porphyrin 208
9.10 Synthesis of 5-P-ethynylphenyl-10, 15, 20-triphenyl porphyrin 210
9.11 Synthesis of 5'-DMT-(5''-P-ethynylphenyl)-10'', 15'', 20''-triphenyl-Zn (II)- porphyrin-dU 212
9.12 Synthesis of 5'-DMT-5-(5''-p-ethynylphenyl)-10'', 15'',20''-triphenyl-Zn(II)- porphyrin-dU-3' amidite 214
9.13 Synthesis of 1-amino-3-propylazide 216
9.14 Synthesis of dipyrromethane 217
9.15 Synthesis of 5-(p-methyl benzoate)-15-phenyl porphyrin 218
9.16 Synthesis of 5-(p-methyl benzoate)-15-phenyl, 10, 20-dibromo porphyrin 220
9.17 Synthesis of Zn(II)-5-(P-methylbenzoate)-15-phenyl-10,20 dibromo porphyrin 222
9.18 Synthesis of Zn(II)-5-(P-methylbenzoate)-15-phenyl-10,20 di-(trimethylsilyl) acetylene porphyrin 224
9.19 Synthesis of Zn(II)-5-(P-methylbenzoate)-15-phenyl-10,20 di-acetylene porphyrin 226
9.20 Synthesis of Zn(II)-5-(P-benzoic acid)-15-phenyl-10,20 di-acetylene porphyrin 228
9.21 Synthesis of 5-p-(benzoic acid NHS-ester)-10, 15, 20-triphenyl porphyrin 230

9.22 Synthesis of Zn (II)-5-(P-benzoic acid)-15-phenyl-10, 20-dibromo porphyrin 232
9.23 Synthesis of Zn (II)-5-(P-benzoic acid)-15-phenyl-10, 20-di-(trimethylsilyl) acetylene porphyrin 234
9.24 Synthesis of Zn (II)-5- *p*-(*N*-(3-azidopropyl) benzamide)-15-phenyl-10, 20-di-(trimethylsilyl) acetylene porphyrin 236
9.25 Synthesis of Zn (II)-5-p-(N-(3-Fmoc-aminopropyl)benzamide-15-phenyl-10, 20-di-(trimethylsilyl) acetylene porphyrin 238
9.26 Synthesis of Zn (II)-5-p-(3-aminopropyl)benzamide-15-phenyl-10, 20-di-(trimethylsilyl) acetylene porphyrin 240
9.27 Synthesis of 5-p-(N-(3-hydroxypropyl)benzamide)-10, 15, 20-triphenyl porphyrin 242
9.28 Synthesis of 5-*p*-(*N*-(3-Bromopropyl)benzamide)-10, 15, 20-triphenyl porphyrin 244
9.29 Synthesis of 5-*p*-(*N*-(3-azidopropyl)benzamide)-10, 15, 20-triphenyl porphyrin 246
9.30 Synthesis of 5-*p*-(*N*-(3-Fmoc-aminopropyl)benzamide)-10, 15, 20-triphenyl porphyrin 248
9.31 Synthesis of 5-p-(N-(3-aminopropyl)benzamide)-10, 15, 20-triphenyl porphyrin 250
9.32 Synthesis of 5-*p*-(*N*-(3-azidopropyl)benzamide)-10, 15, 20-triphenyl porphyrin 252
9.33 Synthesis of 5'-DMT-5-trimethylsilylacetylene-deoxyuridine 254
9.34 Synthesis of 5'-DMT-5-phenylacetylene-deoxyuridine 256
9.35 Synthesis of 5'-DMT-5-propargylbenzamide-dU 258
9.36 Synthesis of 5'-DMT-5-trimethylsilylacetylene-deoxyuridine -3' amidite 260
9.37 Synthesis of 5'-DMT-5-phenylacetylene-deoxyuridine-3' amidite ... 261
9.38 Synthesis of 5'-DMT-5-propargylbenzamide-deoxyuridine-3' amidite 262

Appendix 263

Bibliography 275

List of figures

Figure 1.1 The structures of free base tetraphenyl porphyrin, Haem B and c2. 1

Figure 1.2 UV-Vis spectra of Fb-TPP and Zn-TPP. 3

Figure 1.3 The dipoles present in a D_{2h} free base porphyrin and a D_{4h} zinc metalated porphyrin. 4

Figure 1.4 The molecular orbital's of free base and zinc porphyrin 4

Figure 1.5 The four bases of DNA and the Watson-Crick base pairs. 12

Figure 1.6 Example nucleoside 2'-deoxyadenosine and a tri-nucleotide. 13

Figure 1.7 Molecular models of the A, B and Z-DNA. 14

Figure 1.8 The *syn* and *anti* conformations of 2'deoxyadenosine. 15

Figure 1.9 The 2'-endo and 3'-endo conformations of the furanose ring 15

Figure 1.10 The major and minor grooves of a DNA helix 16

Figure 1.11 The structures of a universal linker and a linker pre-loaded with the 3'-end base. 17

Figure 1.12 The structures of the protected nucleosides. 22

Figure 1.13 The commercially available iodinated nucleosides 23

Figure 1.14 Examples of different ways to modify nucleobases.. 24

Figure 1.15 Examples of different ways to modify the furanose ring. 26

Figure 1.16 Examples of nucelotide replacements. 26

Figure 1.17 A simple molecular beacon designed using a hairpin loop. 29

Figure 1.18 Examples of DNA nanotechnology structures 31

Figure 1.19 Representation of the action of a DNA walker. 33

Figure 2.1 The two porphyrin-modified DNA systems. 35

Figure 3.1 Schematic of the porphyrin system produced by Drain. 38

Figure 3.2 The amide and acetylene linked porphyrin nucleosides. 39

Figure 3.3 The twelve porphyrin Zipper array spanning a lipid bilayer. 39

Figure 3.4 Three porphyrins obtained from the porphyrin synthesis. 41

Figure 3.5 Deprotonated porphyrin acid and protonated porphyrin..... 42

Figure 3.6 NMR spectrum of the porphyrin nucleoside 1' and 3' protons. 46

Figure 3.7 The full sequences of the porphyrin Zipper array. 47

Figure 3.8 Trityl yield obtained after each coupling of a oligonucleotide synthesis..... 50

Figure 3.9 HPLC chromatograms for the crude products obtained when synthesising ODNs 1 and 2. 51

Figure 3.10 Structure of the biotin modifier 54

Figure 3.11 Sequences of ODN's 3 – 8 55

Figure 4.1 The TBTA ligand and the water soluble THPTA ligand..... 62

Figure 4.2 The C8-Alkyne-dU modifier. 65

Figure 4.3 The porphyrin azides synthesised by Vasilis Nikolaou. 66

Figure 4.4 HPLC chromatograms for CuAAC single labelling reactions using the Baseclick Oligo-Click kit with ODN 9. 68

Figure 4.5 MALDI-ToF mass spectra for each of the products produced by the single labelling CuAAC reactions 70

Figure 4.6 HPLC chromatogram for CuAAC multiple labelling reaction using the Baseclick Oligo-Click kit and porphyrin J-TPP.. 71

Figure 4.7 Energy level diagrams for copper-free click chemistry 74

Figure 4.8 Sequence of ODN 11 77

Figure 4.9 HPLC chromatograms produced by the Cu-free click reaction between ODN 11 and the porphyrin azides 78

Figure 4.10 DBCO-dT and Cyclooctyne modified nucleoside 80

Figure 5.1 Schematic of the covalently linked porphyrin wire. 85

Figure 5.2 Oligo(phenylene ethylene) units and di-acetylene porphyrin strands with associated template DNA for Glaser-Hay coupling 86

Figure 5.3 Carboxy-modifier C10 and TPP amine. 102

Figure 5.4 HPLC chromatograms of a crude and pure Carboxy-TPP DNA. 103

Figure 5.5 HPLC chromatogram following the coupling of the di-acetylene porphyrin amine to carboxy-modified DNA. 105

Figure 5.6 Strained alkyne modifier for copper-free click chemistry 107

Figure 5.7 HPLC chromatogram following the coupling of the di-acetylene porphyrin azide to strained alkyne-modified DNA. 107

Figure 5.8 Schematics representing the TPP 1P, 2P, 3P and 4P systems. 111

Figure 5.9 Native page gel of 1P – 4P TPP systems 112

Figure 5.10 UV-Vis and fluorescence spectra of the 1 – 4P systems 114

Figure 5.11 Urea PAGE gel for the Glaser-Hay coupling using Gothelf's reaction conditions. 119

Figure 5.12 Urea PAGE gel for the DNA templated Glaser-Hay coupling reaction between two porphyrins in chlorinated solvent 120

Figure 6.1 Diagram showing the conversion of un-polarised light to circular polarised light. 125

Figure 6.2 An example CD spectra produced by unmodified B-DNA 127

Figure 6.3 The eight duplexes assembled containing 0 - 4 porphyrin modifications 129

Figure 6.4 The amide linked and acetylene linked porphyrin modifications included in the synthesised duplexes. 130

Figure 6.5 HPLC chromatograms of a Porph Amide 1P single strand produced after oligonucleotide synthesis and HPLC purification 131

Figure 6.6 UV-Vis spectra of the porphyrin region for the two peaks shown in the Porph Amide 1P pure chromatogram 132

Figure 6.7 Full CD spectra acquired for the duplexes containing the porphyrin amide modification. 135

Figure 6.8 Expanded DNA region of the porphyrin amide spectra. 136

Figure 6.9 Expanded porphyrin region of the porphyrin amide spectra. 137

Figure 6.10 Example molecular model and Newman projections of the porphyrin-modified DNA. 140

Figure 6.11 Full CD spectra acquired for the duplexes containing the porphyrin acetylene modification. 144

Figure 6.12 Expanded DNA region of the porphyrin acetylene spectra. 145

Figure 6.13 Expanded porphyrin region of the porphyrin acetylene spectra. 145

Figure 6.14 Full CD spectra acquired for the duplexes containing the tri acid porphyrin acetylene modification. 148

Figure 6.15 Full CD spectra acquired for the mixed porphyrin duplexes. 151

Figure 6.16 UV-Vis and fluorescence spectra of the Porph Amide and Porph Acet duplexes. 154

Figure 6.17 The three truncated modifications 157

Figure 6.18 CD spectra of the duplexes containing the acetylene modified T base. 160

Figure 6.19 CD spectra of the duplexes containing the phenyl acetylene modified T base. 161

Figure 6.20 CD spectra of the duplexes containing the Phenyl Amide modified T base. 162

Figure 6.21 The changes in the spectra of the 2X/Un duplex when building up from the unmodified duplex to the porphyrin modification. .. 164

Figure 6.22 Graphical representation showing the melting temperature of a DNA duplex 165

Figure 6.23 A typical DNA melting curve 167

Figure 6.24 Fluorescence melting curves for the Acet, Porph Acet and Porph Amide duplex sets 169

Figure 6.25 Melting curves for the Porph Amide duplexes. 172

List of schemes

Scheme 1.1 Early poprhyrin syntheses 7

Scheme 1.2 Mechanism for the formation of a tetrasubstituted porphyrin 8

Scheme 1.3 Oxidation mechanism to convert a porphyrinogen into a porphyrin using DDQ. 9

Scheme 1.4 Examples of dipyrromethanes and dipyrromethenes 10

Scheme 1.5 The synthesis of a diphenyl porphyrin from a dipyrromethane and formaldehyde. 11

Scheme 1.6 Detritylation step using 3 % TCA in DCM. 18

Scheme 1.7 Activation step to increase the reactivity of the incoming nucleotide 19

Scheme 1.8 Coupling step for the addition of the next monomer to the growing oligonucleotide chain. 19

Scheme 1.9 Capping step mechanism using acetic anhydride and 10 % methylimidazole. 20

Scheme 1.10 Oxidation of phosphorus (III) to phosphorus (V). 20

Scheme 1.11 Cleavage of an oligonucleotide from a DNA synthesis column. 21

Scheme 1.12 Mechanism of phosphate backbone deprotection. 22

Scheme 3.1 Full scheme for the formation of the amide linked porphrin nuclesoide. 40

Scheme 3.2 Full scheme for the formation of the acetylene linked porphrin nuclesoide 44

Scheme 4.1 General reaction scheme for the azide-alkyne cycloaddition with and without a Cu(I) catalyst. 60

Scheme 4.2 Full catalytic cycle of the copper catalysed azide-alkyne cycloaddtion (CuAAC) reaction. 61

Scheme 4.3 Production of zinc tetraphenyl porphyrin azide (J-TPP). 64

Scheme 4.4 Mechanism of copper free Click chemistry using a strained cyclooctyne. 73

Scheme 5.1 Examples of three different copper catalysed methods of forming 1, 3-diynes. 87

Scheme 5.2 Suggested mechanism of the Glaser-Hay coupling reaction. 88

Scheme 5.3 Full scheme for the formation of the di-acetylene porphrin NHS ester. 90

Scheme 5.4 Bromination and Zn metalation of the porphyrin. 92

Scheme 5.5 Sonogashira coupling of TMS acetylene to the poprhyrin meso positions. 93

Scheme 5.6 Conversion from TMS protected porphyrin ester to the deprotected porphyrin acid. 94

Scheme 5.7 Reaction scheme for the synthesis of TPP NHS ester. 95

Scheme 5.8 The second full scheme for the formation of the di-acetylene porphrin NHS ester. 96

Scheme 5.9 Formation of di-TMS acetylene azide and amine. 98

Scheme 5.10 Schematic showing three different routes attempted to produce a TPP azide. 99

Scheme 6.1 Synthetic routes to produce the acetylene, phenyl acetylene and phenyl amide monomers. 158

List of tables

Table 4.1 Calculated molecular masses and values obtained by MALDI-ToF mass spectrometry for the singly modified oligonucleotide reacted with each of the three porphyrins. 70

Table 4.2 Calculated molecular mass values, values obtained by MALDI-ToF mass spectrometry and yields for ODN 11 reacted with each of the three porphyrins by copper-free click chemistry. 79

Table 5.1 Strand name and sequence for TPP modified DNA produced by coupling TPP amine carboxy modified DNA. 103

Table 5.2 Amount of pure porphyrin-DNA isolated when coupling the TPP amine with carboxy-modified DNA. 104

Table 5.3 The amounts of purified di-acetylene-modified DNA obtained from one amide labelling. 106

Table 5.4 The amount of di-acetylene porphyrin-modified DNA isolated by the copper-free click chemistry method starting with 20 nmoles of DNA. 108

Table 5.5 Values for Soret peak widths using full width at half maximum. .. 115

Table 5.6 Values for the emission intensity for each of the samples with and without the addition of the template strands. 116

Table 5.7 The reaction conditions employed by Gothelf *et al*. to covalently link oligo(phenylene ethylene) units. 117

Table 6.1 Data compiled from the experimentally obtained CD spectra of the Porph Amide duplexes and the molecular modelling 142

Table 6.2 The angle between porphyrins in the Porph Acet duplex systems and the amplitude of the measured CD spectra in the porphyrin region 147

Table 6.3 Sequences of the oligonucleotides containing the tri acid porphyrin modification..... 149

Table 6.4 The mixed porphyrin duplexes..... 150

Table 6.5 The calculated molecular weights (MW) and the values measured by LC-MS for each oligonucleotide containing one of the three truncated modifications. 159

Table 6.6 Melting temperatures of duplexes containing acetylene, phenyl acetylene or phenyl amide modifications..... 168

Table 6.7 Melting temperatures of the Porph Amide and mixed Porph duplexes as measured by UV melting. 172

DECLARATION OF AUTHORSHIP

I, James William Wood

declare that the thesis entitled

The Structural Analysis of Porphyrin Modified DNA and the Construction of a Molecular Wire

and the work presented in the thesis are both my own, and have been generated by me as the result of my own original research. I confirm that:

- this work was done wholly or mainly while in candidature for a research degree at this University;
- where any part of this thesis has previously been submitted for a degree or any other qualification at this University or any other institution, this has been clearly stated;
- where I have consulted the published work of others, this is always clearly attributed;
- where I have quoted from the work of others, the source is always given. With the exception of such quotations, this thesis is entirely my own work;
- I have acknowledged all main sources of help;
- where the thesis is based on work done by myself jointly with others, I have made clear exactly what was done by others and what I have contributed myself;
- parts of this work have been published as: J. R. Burns *et. al*, *Angew. Chem.-Int. Edit.*, 2013, **52**, 12069-12072

Signed: ……

Date:……

Acknowledgements

Over the past four years I have received help and support from many individuals in a variety of roles. Whilst I cannot name everyone here, I am truly grateful to you all. There are however some who I must mention.

The first thank you has to go to Dr Eugen Stulz for enabling me to carry out this work and for the continued support and encouragement on the many occasions the chemistry did not go to plan.

I must also thank Dr Dorcas Brown and ATDBio for helping me with oligonucleotide synthesis and purification, as well as Dr Giuliano Siligardi and Dr Rohanah Hussain for their help with CD spectroscopy. The work of Vasilis Nikolaou to acquire the MALDI-ToF spectra is also greatly appreciated. Another big thank you to Dr Jim Tucker and James Carr-Smith of the University of Birmingham for their help in obtaining UV melting data.

To everyone I have worked alongside in lab 5003, thank you for your help, humour and your friendship. I would not have reached this point without you all keeping me sane. I would especially like to thank Dr Daniel Singleton for providing me with far more help than I had any right to expect.

For the much needed distractions and helpful suggestions I need to thank my friends. You guys really do make my life a lot more interesting.

Finally to my family, and most importantly of all, my parents, who have supported me in so many ways. Whilst I don't always show it, I really do appreciate everything you have done and continue to do for me. Thank you for always being there.

The last four years have been frustrating and at times infuriating, but the help and support from everyone has enabled me to complete this thesis. So for every contribution, in whatever way, thank you.

Definitions and Abbreviations

Å	angstrom
δ	chemical shift in ppm
Δ	heat
λ	wavelength
λ_{ex}	excitation wavelength
λ_{em}	emission wavelength
2PA	Two photon absorption
5-I-dU	5-iodo-2'-deoxyuridine
A	Adenine
AFM	Atomic force microscopy
BCN	Bicyclo[6.1.0]nonyne
C	Cytosine
CCMS	Convergence chromatography mass spectrometry
CEP-Cl	2-cyanoethyl *N*,*N*-diisopropylchlorophosphoramidite
CPG	Controlled pore glass
d	doublet
DBCO	Dibenzo-cyclooctyne
DBU	1,8-diazabicyclo[5.4.0]undec-7-ene
DCE	1, 2-dichloroethane
DCM	Dichloromethane
DDQ	2, 3-dichloro-5, 6-dicyano-*p*-benzoquinone
DIC	*N*, *N*'-diisopropylcarbodiimide
DIPEA	*N*, *N*-diisopropylethylamine
DMAP	4-dimethylaminopyridine
DME	Dimethoxyethane (ethylene glycol dimethyl ether)
DMF	Dimethylformamide
DMT	4, 4'- Dimethoxytrityl
DMT-Cl	4, 4'- Dimethoxytrityl chloride
DNA	2'-deoxyribonucleic acid
DPPA	Diphenyl phosphoryl azide
EA	Ethyl acetate
EDTA	Ethyldiaminetetraacetic acid
equiv.	equivalents
Fmoc	fluorenylmethyloxycarbonyl
FWHM	Full width at half maximum
G	Guanine
H_2O	Water
HATU	1-[Bis(dimethylamino)methylene]-1*H*-1,2,3-triazolo[4,5-*b*]pyridinium 3-oxid hexafluorophosphate
HCl	Hydrochloric acid
HFIP	Hexafluoroisopropyl
HOBt	Hydroxybenzotriazole
HOMO	Highest occupied molecular orbital
HPLC	High performance liquid chromatography
HPLC-MS	High performance liquid chromatography – mass spectrometry
Hz	Hertz
J	coupling constant
KOH	Potassium hydroxide

LNA	Locked nucleic acid
LUMO	Lowest unoccupied molecular orbital
m	multiplet
M	molar
MALDI MS	Matrix-assisted laser desoption/ionisation mass spectrometry
MeOH	Methanol
min	minutes
mmol	millimoles
N_2	Nitrogen
nm	nanometres
nmol	nanomoles
NBS	*N*-Bromosuccinimde
NEt_3	Triethylamine
ODN	oligonucleotide
Oligo	oligonucleotide
PAGE	Polyacrylamide gel electrophoresis
Pd-C	10 % palladium on carbon
$Pd_2(dba)_3$	Tris(dibenzylideneacetone)dipalladium (0)
$Pd(PPh_3)_4$	Tetrakis palladium triphenyl phosphine
Pet.	Petroleum ether 40 – 60 ˚C
PNA	Peptide nucleic acid
PPh_3	Triphenyl phosphine
PyBrop	Bromotripyrrolidinophosphonium hexafluorophosphate
Pyr	Pyridine
RP-LCMS	Reverse phase liquid chromatography mass spectrometry
RT	room temperature
s	singlet
T	Thymine
TBAF	Tetrabutylammonium fluoride
TBTA	Tris (benzyltriazolylmethyl)amine
TCA	Trichloroacetic acid
TEA	Triethylamine
TEAA	Triethylammonium acetate
TEA-HFIP	8.6 mM triethylamine / 100 mM hexafluoroisopropanol buffer
TFA	Trifluoroacetic acid
THF	Tetrahydrofuran
THPTA	Tris (3-hydroxypropyltriazolylmethyl)amine
TLC	Thin layer chromatography
T_m	Melting temperature
TMEDA	
Tosyl chloride	p-toluenesulfonyl chloride
TSU	*N*, *N*, *N*', *N*'-tetramethyl-*o*-(*N*-succinimidyl)uronium
TTP	5, 10, 15, 20-tetraphenyl porphyrin
UNA	Unlocked nucleic acid
UV-Vis	Ultra violet - visible

1. Introduction

1.1 The Structure and Properties of Porphyrins

Porphyrins are a group of heterocyclic macrocycles consisting of four pyrrole rings linked at the α-position by a methine bridge. Porphyrins are widely found in nature and play key roles in many biological functions. The porphyrins Haem B and Chlorophyll c2, highlighted in Figure 1.1, are vital for the existence of human and plant life respectively.[1, 2] The Haem porphyrin acts as the oxygen carrier in blood whereas the Chlorophyll porphyrins play an important role in converting sunlight to chemical energy in the process of photosynthesis.

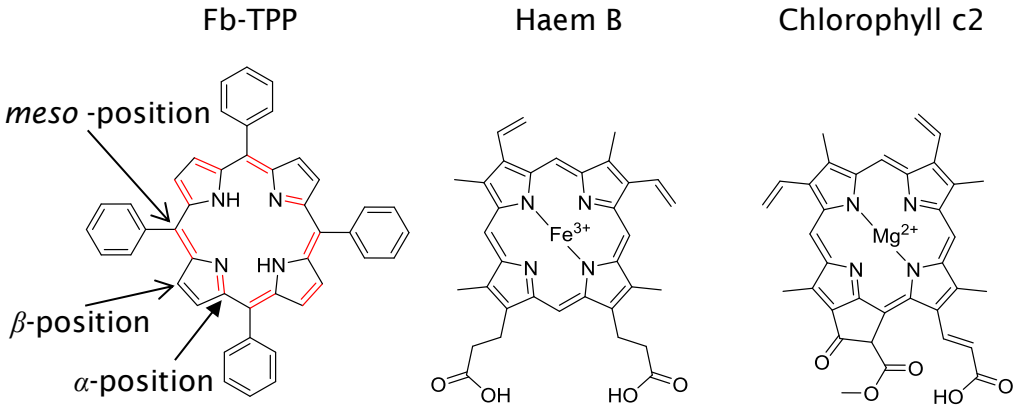

Figure 1.1 The structures of the free base porphyrin 5, 10, 15, 20-tetraphenyl porphyrin (Fb-TPP), the naturally occurring iron metalated Haem B found in oxyhaemoglobin, and magnesium metalated chlorophyll c2.

Porphyrins are aromatic compounds containing 18 π-electrons in conjugation around the planar macrocycle. The 18 π-electrons obey the Huckel 4 n + 2 rule for aromaticity and are highlighted in red in the first structure of Figure 1.1. This leaves two double bonds which are not contributing to the aromaticity of the structure. The large number of conjugated double bonds in the aromatic system results in a small energy gap between the highest occupied molecular orbital (HOMO) and the lowest unoccupied molecular

orbital (LUMO). This property gives porphyrins intense absorptions in the visible region resulting in brightly coloured compounds. These strong absorbance properties make the porphyrins strong light harvesting molecules as is shown by Chlorophyll and the process of photosynthesis.[3, 4] When Chlorophyll (and other porphyrins) absorbs energy from light, an electron is promoted to an excited state. This excited electron can then be transferred to another molecule starting a redox process between carbon dioxide and water. This transfer of an excited electron from a porphyrin forms the basis of this work.

The internal cavity of a porphyrin is approximately 4 Å across allowing a variety of transition metals to bind to the nitrogen atoms forming metalloporphyrins.[5, 6] Smaller metal ions such as Fe^{3+} and Mg^{2+} can fit within the cavity in a square planar geometry without distorting the porphyrin ring. The larger transition metals (e.g. Re^{+}, Hf^{4+}) however, are too big to fit inside this cavity.[7] In order to bind these ions, the planar porphyrin ring is distorted and the ion sits above the cavity.[8] Sandwich complexes of the largest ions between two porphyrins can also be formed.[9] A porphyrin without an associated metal is referred to as free base (Fb).

The electronics and optical properties of the porphyrin can be altered or tuned by changing the metal centre, oxidation state or the modifications around the macrocyclic ring.[10] Figure 1.2 shows the ultra violet-visible (UV-Vis) spectra of Fb-TPP (black) and zinc metalated TPP (Zn-TPP, red). Porphyrins have characteristic absorbances which can be shifted or changed depending on the metalation state and other properties of the molecule.[11]

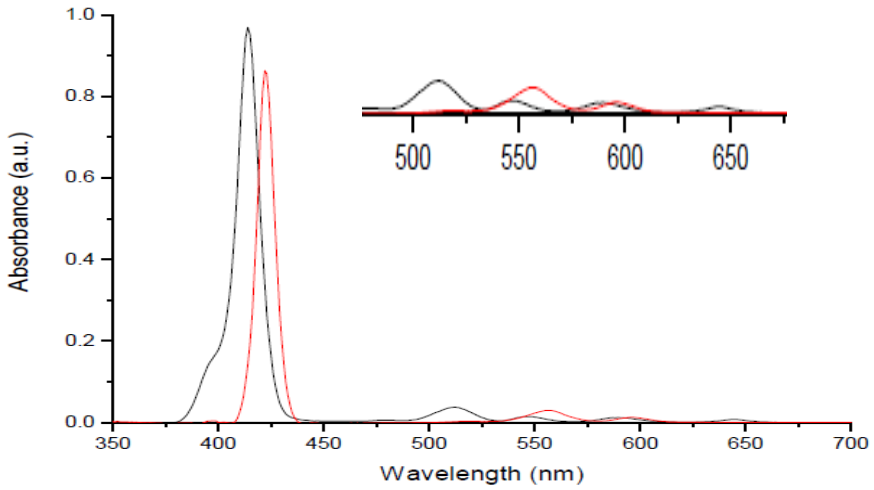

Figure 1.2 UV-Vis spectra of Fb-TPP (black) and Zn-TPP (red).

If the free base spectrum is considered first, five absorption bands can be seen in the visible region. The large peak at approximately 420 nm is called the Soret (or B) band and has a molar extinction coefficient of approximately 4.4 × 10^5 mol $^{-1}$ dm^3 cm^{-1} in tetraaryl porphyrins.[12] This absorption results from two quasidegenerate transitions with perpendicular polarisation.[13] These are referred to as B_x and B_y as shown in Figure 1.3. The peak is actually a superposition of two peaks which tend to appear at the same wavelength when measured in solution. For this reason the Soret band is commonly referred to as a single entity but the two peaks have been shown to separate when π-stacking is present in the sample.[14, 15]

A series of four smaller peaks appear between 500 and 700 nm and are referred to as the Q-bands. These have a molar extinction coefficient of approximately 1 × 10^4 mol^{-1} dm^3 cm^{-1}, and are responsible for the bright colours of the porphyrins.[16] Metalated porphyrins however, show fewer Q-bands as demonstrated by the two present in the spectra of Zn-TPP (red line). This reduction is due to the increase in symmetry from D_{2h} to D_{4h} as the metal ion replaces the two hydrogen atoms in the porphyrins cavity. In the free base porphyrin, two transition dipole moments (B_x and B_y) exist. The B_x transition dipole moment can be viewed along the N-H H-N axis and the B_y perpendicular to this. By inserting an ion into the cavity, the transition dipole moments become equivalent and the corresponding energy levels degenerate. This

causes the reduction in the number of Q-bands from four to two, and two Soret bands to just one.

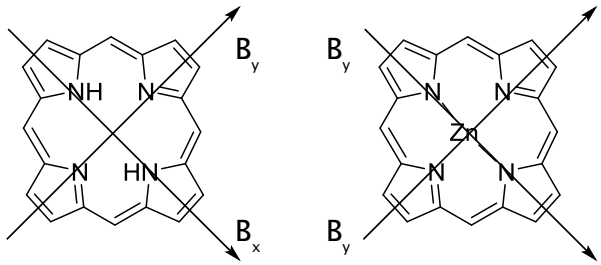

Figure 1.3 The transition dipole moments present in a D_{2h} free base porphyrin and a D_{4h} zinc metalated porphyrin.

This was explained further by the Gouterman four orbital model.[17-21] This states that the peaks in the absorbance spectra of a free base porphyrin are caused by the transitions between the two HOMOs, a_{1u} and a_{2u} (π), and the two LUMOs, $e_{g,x}$ and $e_{g,y}$ (π^*). Upon metalation and an increase in the symmetry, the e_g orbitals become degenerate resulting in fewer HOMO-LUMO transitions and as a result, fewer absorbance peaks. Molecular orbital diagrams for these transitions are shown in Figure 1.4. By changing the metal centre, the type, or position of substituents around the ring, the energies of these transitions can be altered causing a change to the porphyrins electronic characteristics.[11]

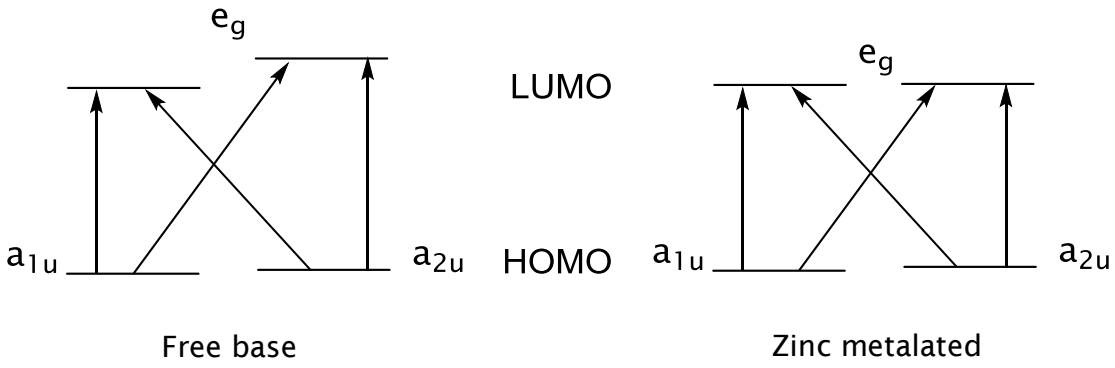

Figure 1.4 The molecular orbital's of a free base and zinc metalated porphyrin as described by the Gouterman four orbital model. Also shown are the HOMO-LUMO transitions responsible for the peaks in porphyrin absorbance spectra.

From the molecular orbital diagrams, transitions between all four orbitals are allowed as long as the polarisation is correct. The B and Q-bands arise from the interaction of two different single electron transitions, one constructive, the other destructive. The constructive interaction can be viewed as the sum of the transitions and the destructive as the difference. For a free base compound, transitions between the nearly degenerate HOMOs and non-degenerate LUMOs have different energies. Interactions between these transitions will therefore give both constructive and destructive interactions. For a metalated porphyrin with degenerate LUMOs, the transition energies become equal. As such the destructive interactions will cancel out (difference = 0). Fewer interactions lead to the reduction in the number of B and Q-bands seen in the UV-Visible spectra of metalated porphyrins.

1.2 The Synthesis of Porphyrins

The chemical synthesis of porphyrins has been widely studied since the first synthesis of Haem was reported by Fisher and Zeile in 1929.[22] Subsequently, improved methods were suggested by Rothemund in the 1930's[23, 24] and Adler and Longo in 1967.[25] These one pot syntheses focused on simple symmetric porphyrins, the simplest being porphin (Scheme 1.1). The synthesis of porphin has been reported by many groups using varying methods. Fischer published a synthesis using pyrrole-α-aldehyde in boiling formic acid (Scheme 1.1 a).[26] Shortly after, Rothemund used formaldehyde and pyrrole with the presence of a Lewis acid to achieve the same product (Scheme 1.1 b).[24] Rothemund also showed using a different aldehyde (for example benzaldehde) would produce a symmetric meso-substituted porphyrin such as the tetraphenyl porphyrin shown in Figure 1.1. Lindsey advanced the synthesis of porphyrins further using a mixture of different aldehydes to form unsymmetrically substituted porphyrins at the *meso*-positions (Scheme 1.1 c).[27, 28] These reactions produce a statistical mixture of porphyrin products based on the ratio of the combined aldehydes. The Stulz group has since developed a method for the synthesis of mono-functionalised tetraphenyl porphyrins. The details of this method are discussed in further detail in section 3.2.

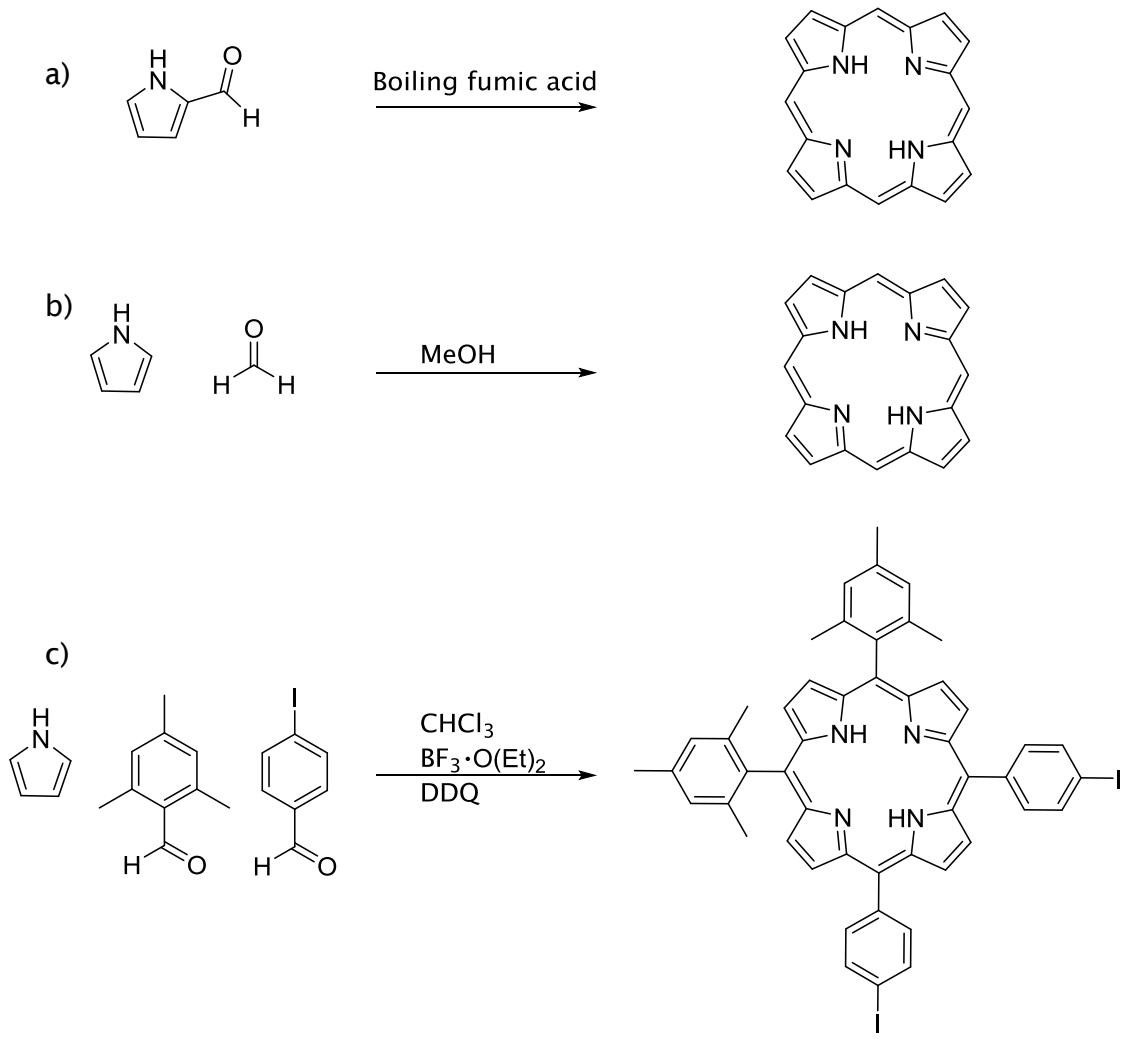

Scheme 1.1 a) Fischer's synthesis of the unsubstituted porphin from pyrrole-α-aldehyde.[22] b) Rothemond's synthesis of the unsubstituted porphin from formaldehyde and pyrrole.[24] c) Lindsey's synthesis of an unsymmetrically substituted porphyrin.[28]

As shown above, porphyrins can be easily synthesised with different modifications at the meso positions by using different aldehydes in the reaction. Modifications can also be made at the β-positions of the porphyrin. This has been achieved after the porphyrin has been formed, but it is generally easier to use modified pyrroles when forming the porphyrin. These different techniques allow a huge variety of modified porphyrins to be synthesised with differing characteristics for all kinds of uses (see section 1.6).

The mechanism for the formation of a simple tetrasubstituted porphyrin from pyrrole and an aldehyde is shown in Scheme 1.2. This mechanism requires the presence of a Lewis acid such as Boron trifluoride etherate and needs to be carried out in the dark due to the photosensitivity of porphyrins.

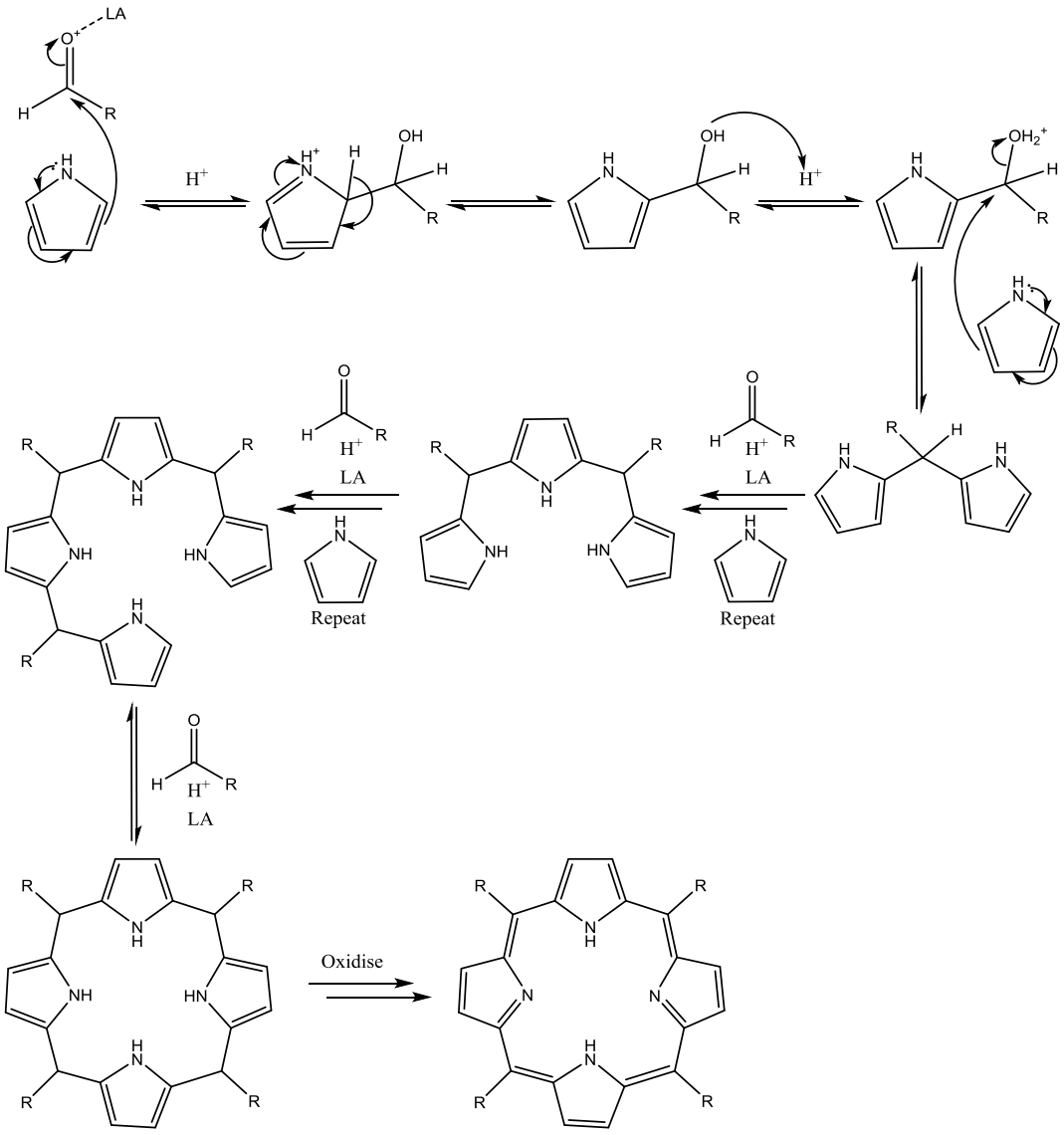

Scheme 1.2 The abbreviated mechanism for the formation of a tetrasubstituted porphyrin starting with pyrrole and an aldehyde. LA = Lewis acid.

Initially, four pyrroles are combined into a ring structure called a porphyrinogen. This structure can then be oxidised into the porphyrin using an oxidising agent such as 2, 3-dichloro-5, 6-dicyano-*p*-benzoquinone (DDQ) or 2, 3, 5, 6-tetrachlorobenzoquinone (Chloranil) as shown in Scheme 1.3. This method of chemical oxidation is preferred to the original technique of heating to reflux and using atmospheric oxygen to form the porphyrin.[25] These harsh conditions affect the range of functional groups available for porphyrins and hence the use of a benzoquinone has become commonplace.

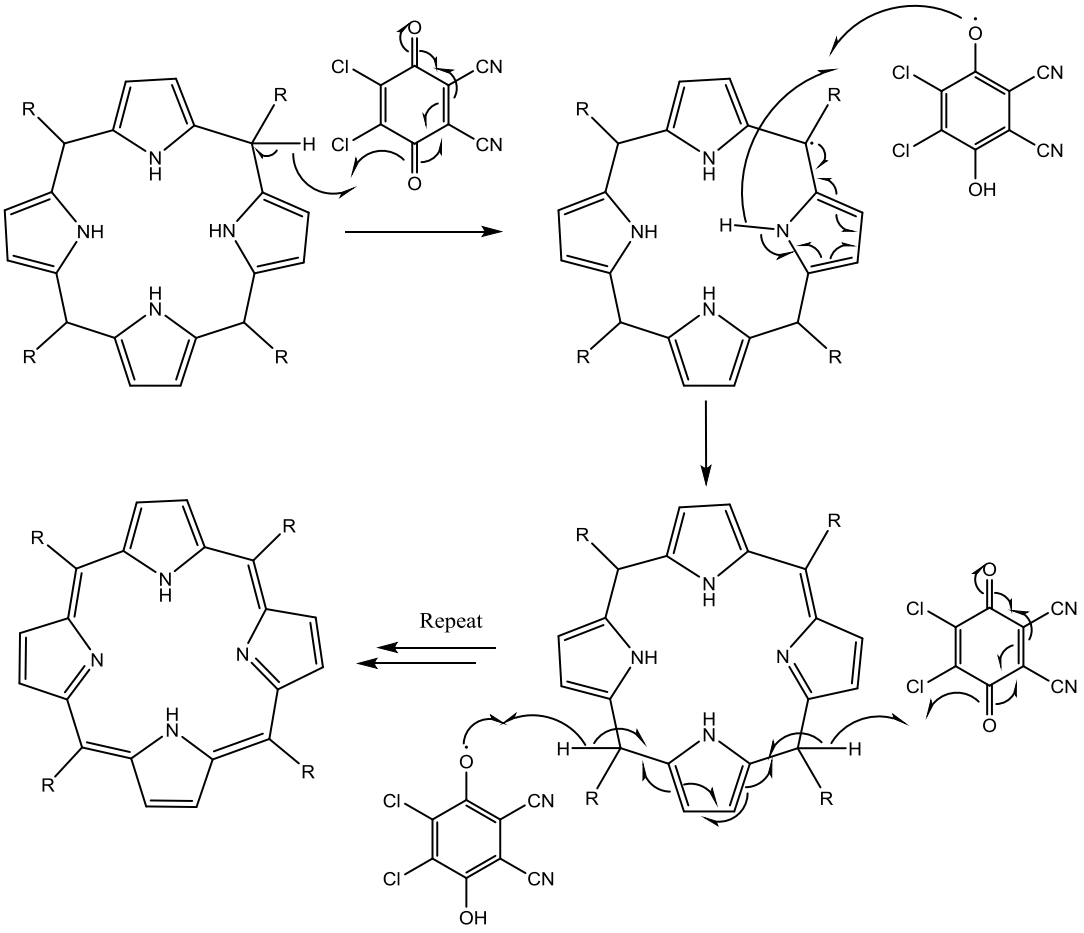

Scheme 1.3 Oxidation mechanism to convert a porphyrinogen into a porphyrin using the oxidising agent 2, 3-dichloro-5, 6-dicyano-*p*-benzoquinone (DDQ).

Pre-formed dipyrrolic intermediates can also be used in porphyrin synthesis. Dipyrromethene salts were used by Fischer *et al*. in the 1930's[29] and dipyrromethanes used by Lindsey in the 1990's.[30, 31] Pre-forming these units has the advantage of increased control over the β and meso substituents

allowing for higher substituted porphyrins to be produced with greater ease and in higher yields. The bridging (meso) carbon can be left free by using a 2-formylpyrrole as shown in Scheme 1.4 a, or specific substituents can be added with 2-unsubstituted pyrroles and the appropriate aldehyde (Scheme 1.4 b). This approach is used in section 5.2.

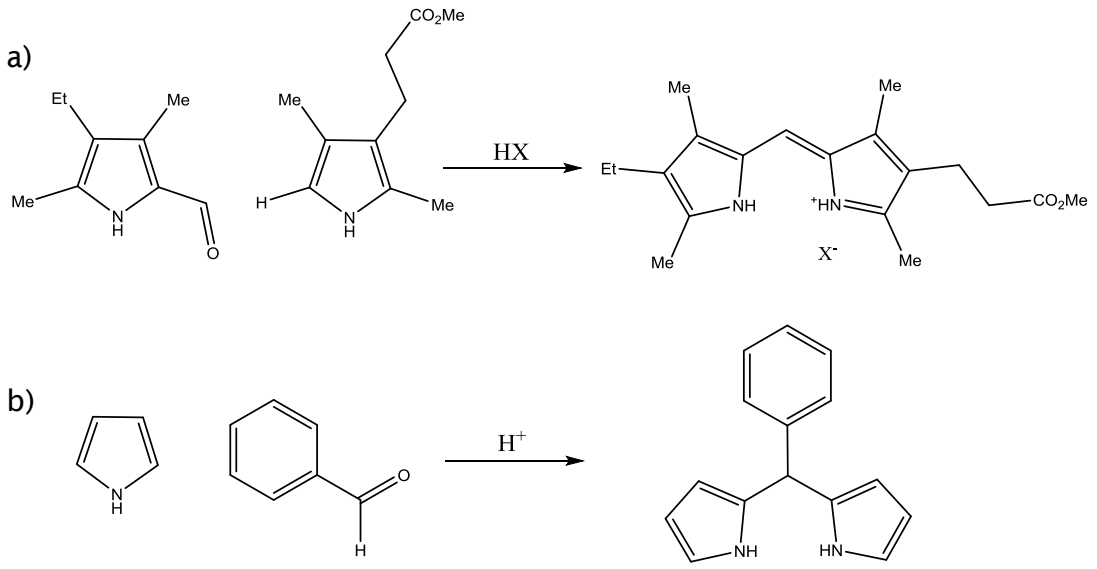

Scheme 1.4 a) Example of an unsymmetrically substituted dipyrromethene formed by the acid catalysed condensation of a 2-formylpyrrole with a 2-unsubstituted Pyrrole.[32] b) A meso-phenyl dipyrromethane formed by the acid catalysed condensation of Pyrrole and benzaldehyde.[31]

Once formed, the dipyrrolic intermediates can replace the pyrrole in the reaction to form the porphyrin. An example of this type of synthesis carried out by the Dolphin group is shown in Scheme 1.5.[33]

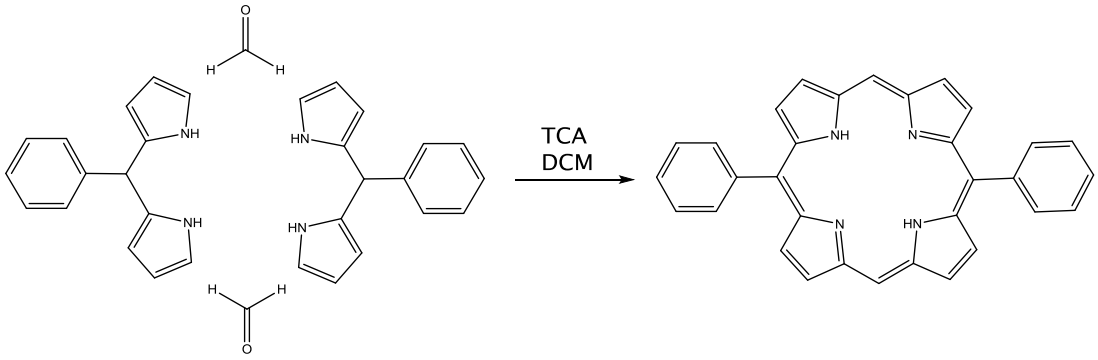

Scheme 1.5 The synthesis of a diphenyl porphyrin from a dipyrromethane and formaldehyde.

1.3 The Structure of 2'-Deoxyribonucleic Acid

2'-deoxyribonucleic acid (DNA) carries the genetic code that forms the basis of life. This code consists of the four bases, adenine (A), cytosine (C), guanine (G) and thymine (T) pictured in Figure 1.5.

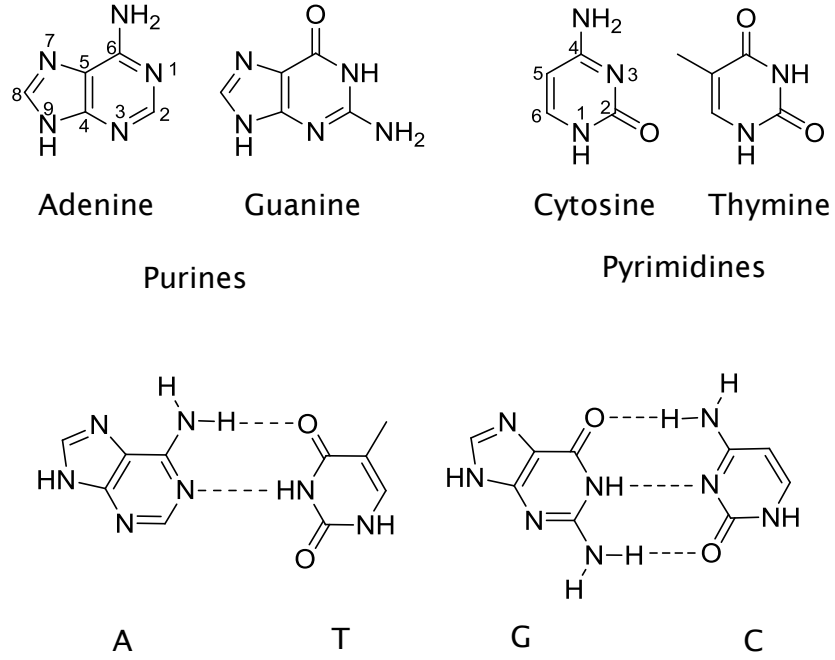

Figure 1.5 The four bases of DNA and the Watson-Crick base pairs.

These bases are attached to 2'-deoxyribose rings forming nucleosides (Figure 1.6). Nucleosides are coupled together via phosphodiester linkages between the 5'-hydroxyl of one unit and the 3'-hydroxyl of the next unit to form a biopolymer. This is referred to as single stranded DNA. A strand will have a free 5'-hydroxyl at one end and a free 3'-hydroxyl at the other. This gives the strand directionality and allows the sequence of a polynucleotide to be read in a specified direction. Figure 1.6 shows an example of a trimer with the sequence 5'-CGA-3'.

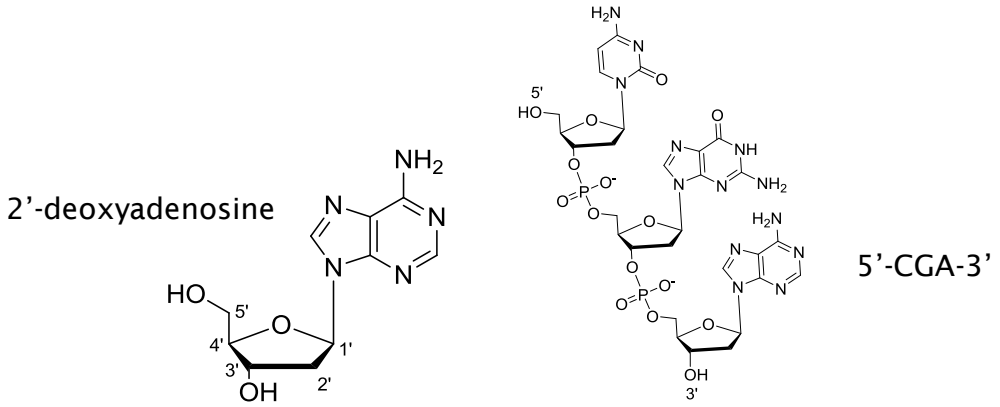

Figure 1.6 Example nucleoside 2'-deoxyadenosine and a tri-nucleotide.

The four bases can pair up, A with T and C with G, matching hydrogen-bond donors with hydrogen-bond acceptors. These are the Watson-Crick base pairs shown in Figure 1.5.[34] Two complementary (matching) single strands can bind through their Watson-Crick base pairs to form double stranded DNA. The structure of double stranded DNA was investigated for many years with several different models proposed before the actual structure was deciphered. In 1950, Chargaff discovered that double stranded DNA contained the same number of adenosines and thymidines.[35] The same is true for C and G. This led to the discovery of the base pairing and in 1953 Watson, Crick, Wilkins and Franklin reported the now famous double helix.[36-38] This structure consists of two antiparallel strands coiling around each other with the hydrophobic bases in the middle and the hydrophilic phosphate backbone on the outside. The term antiparallel denotes that if one strand is situated in the 5' to 3' direction, then it's complementary strand alligns 3' to 5'.

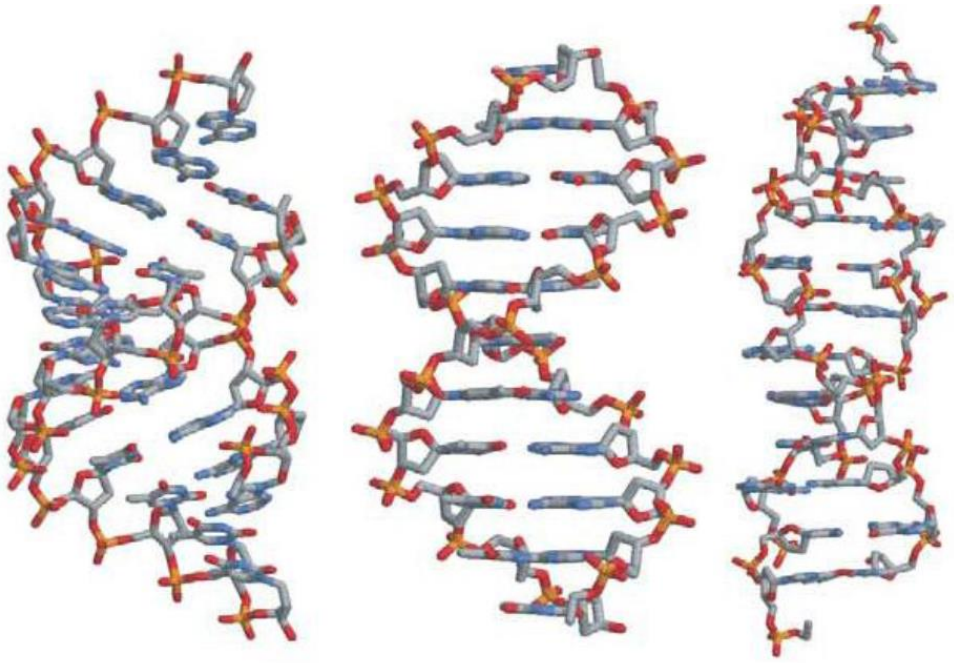

Figure 1.7 Molecular models of the A[39], B[40] and Z-DNA.[41] Picture re-produced with permission from Arnott.[42]

The DNA duplex can exist in more than one form dependent on the sequence and surroundings.[43] B-DNA is most commonly found in nature and is a right handed helix with approximately 10.5 base pairs per helical turn.[40] This single helical turn corresponds to approximately 36 Å in length. In this form, the base pairs sit directly over the helical axis and are almost perpendicular to it. B-DNA is favoured in low salt environments as there are fewer cations to balance out the negative charge on the phosphate backbone. This leads to the hydrophobic bases stacking on the inside of the duplex away from the hydrophilic surroundings.

A-DNA is a more squashed duplex, shorter and wider. The right handed helix has approximately 11 base pairs per helical turn covering a distance of 28 Å. The ribose rings are parallel to the helix axis displacing the bases from the axis by approximately 4.5 Å. This displacement gives in the duplex a hollow core 3 Å in diameter. A-DNA is favoured in high salt environments where the negatively charged phosphates are shielded by cations. This allows the bases to be more stable towards the edge of the duplex leaving the hollow core.

Z-DNA differs from A and B being a left handed helix. This type of helix is mainly seen with GC rich sequences and high salt concentrations. This helix is also longer and thinner than the B-DNA having 12 base pairs per helical turn spanning 44 Å.

The bases can arrange themselves into two conformations, *syn* and *anti* relative to the ribose ring (Figure 1.8). Normally the *anti* conformation would be the preferred due to the steric clash with the 5'-carbon. However, for an ideal left handed duplex, all the bases would be in the *syn* conformation. As this is not possible, Z-DNA adopts a *syn-anti* mixture with cytosine adopting the *syn* conformation and guanines the *anti*.[43]

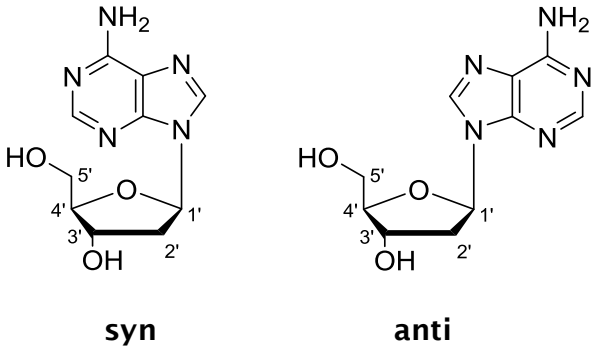

Figure 1.8 The *syn* and *anti* conformations of 2'deoxyadenosine.

The furanose ring of the nucleoside can also exist in one of two possible conformations (Figure 1.9). The 2'-endo conformation is mostly seen in DNA duplexes whereas the 3'-endo conformation is more associated with RNA duplexes.

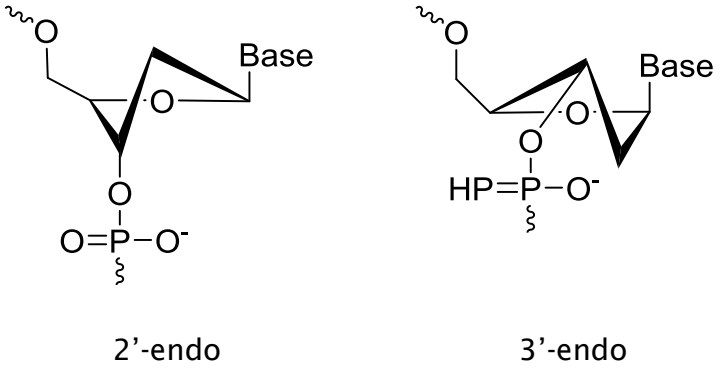

Figure 1.9 The 2'-endo and 3'-endo conformations of the furanose ring.

All duplexes have two grooves formed by the two strands twisting around each other (Figure 1.10). The backbones are closer to each other on one side than they are on the other leading to a major groove and a minor groove reflecting the relative sizes. The size of the grooves varies with the different forms of DNA, but for B-DNA the major groove is approximately 22 Å wide and the minor groove 12 Å.[40]

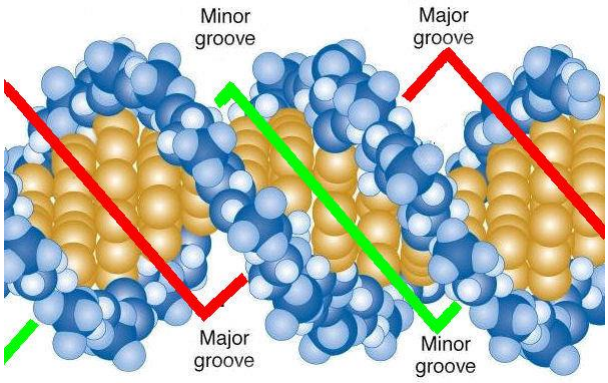

Figure 1.10 Representation of a DNA double helix with the locations of the major and minor grooves highlighted by the red and green lines respectively.[44] The Phosphate backbone is shown in blue with the nucleobases in gold.

As mentioned above, hydrogen bonding between the bases of complementary strands allows a duplex to form. The stability of this duplex is however affected by several other interactions. π-stacking of the heterocyclic bases, the hydrophobic effect within the duplex, dipole-dipole interactions and the negatively charged backbone of the DNA all contribute to the duplex's binding strength.[45] The presence of water molecules which can form hydrogen-bonds and other weak interactions with the DNA bases and phosphate backbone are also very important in stabilising the DNA structure.[46] The first single crystal structure of B-DNA is known as the Dickerson-Drew dodecamer[40] and showed a spine of hydration in the minor groove.[47, 48] Later work by Egli *et al.*[49] showed the number of water molecules present to be much higher than originally reported. The level of hydration not only stabilises the double helical structure, but can even cause transformations between the different duplex forms.

1.4 The Synthesis of Oligonucleotides

Oligonucleotides (oligos) are short single stranded DNA molecules which are widely synthesised in the laboratory using automated solid phase oligonucleotide synthesis.[50] This technique uses controlled pore glass (CPG) beads as the solid support. Oligonucleotides are synthesised inside the cavities of these porous glass beads growing from linkers attached to the surface. For small oligos (< 30 bases), a typical pore diameter is 500 Å. Pore diameters of 1000 Å and 3000 Å are also available for the synthesis of longer oligos. These beads can be purchased pre-packed into columns to place directly onto a DNA synthesiser and are available as universal supports or pre-loaded with one of the four bases (Figure 1.11).

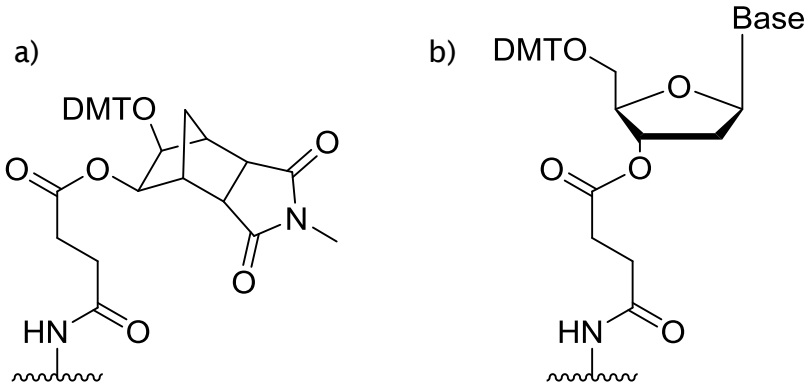

Figure 1.11 a) The structures of a universal linker. B) A linker pre-loaded with the 3'-end base.

The universal columns can be used to synthesise any sequence containing only a linker attached to the glass bead. More commonly, columns are manufactured with the first nucleotide of the sequence already attached to the column. As solid phase oligonucleotide synthesis occurs in the 3' – 5' direction this will be the 3'-end base. This nucleobase is attached to the resin via a base labile linker which allows the oligonucleotide to be cleaved from the column once the full sequence has been synthesised. The universal support has the advantage of only needing one type of column for any synthesis. The first coupling can be any of the natural bases or a modified base allowing the synthesis of 3'-modified oligonucleotides.

A nucleotide pre-attached to the column has the 5'-OH position protected by a 4, 4'-dimethoxytrityl (DMT) group. The first stage of solid phase oligonucleotide synthesis is detritylation, the removal of the DMT protecting group (Scheme 1.6). This is achieved by passing 3 % trichloroacetic acid (TCA) in DCM through the column releasing the bright orange DMT cation. The synthesiser can measure the trityl yield with an in-built absorption spectrophotometer to give a real time measurement of the amount of DNA present and the coupling efficiency of each cycle.

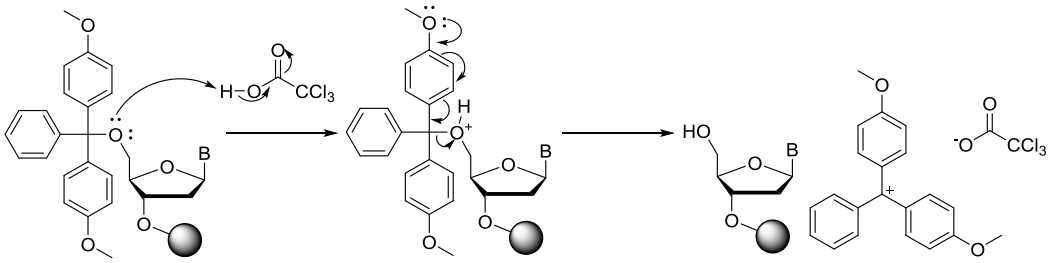

Scheme 1.6 Detritylation step using 3 % TCA in DCM.

Each new nucleotide to be added to the growing DNA chain has this 5'-position protected. This is required for two reasons. Firstly, in order to create the correct structure the 3'-OH must be converted to a highly reactive phosphoramidite (Scheme 1.7). The 5'-OH however is less sterically hindered and therefore more reactive. Without this protecting group, the 5'-phosphoramidite would be formed leading to an incorrect backbone.

The second reason for 5'-DMT protection is to prevent a polymer of the same nucleobase forming. As is shown in the coupling step (Scheme 1.8), a new nucleotide is added to the growing DNA chain by the reaction between the 5'-OH of the DNA strand and the incoming 3'-phosphoramidite. If this incoming nucleotide was also 5'-deprotected the molecules would be able to react with each other forming, for example, the sequence AAAAAAAAA. Protecting this 5'-position of the incoming nucleotide ensures the oligo only grows by one base per cycle.

After detritylation, the incoming 5'-DMT-protected-3'-phosphoramidite is activated by replacing the di-*iso*-propylamino group with tetrazole to create a better leaving group (Scheme 1.7). The free 5'-OH on the growing oligo can

displace this leaving group in the coupling step increasing the oligonucleotide chain by one nucleotide (Scheme 1.8).

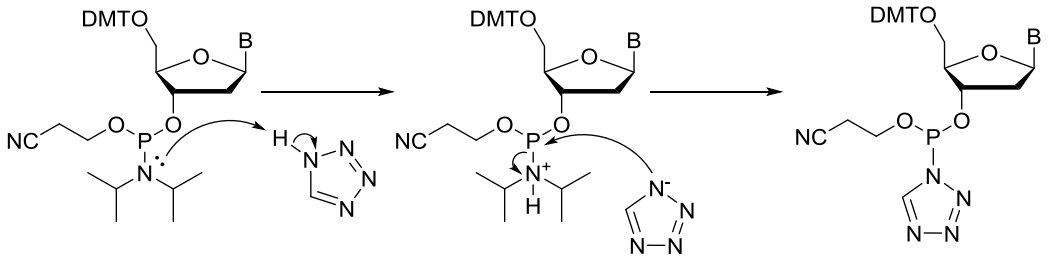

Scheme 1.7 Activation step to increase the reactivity of the incoming nucleotide.

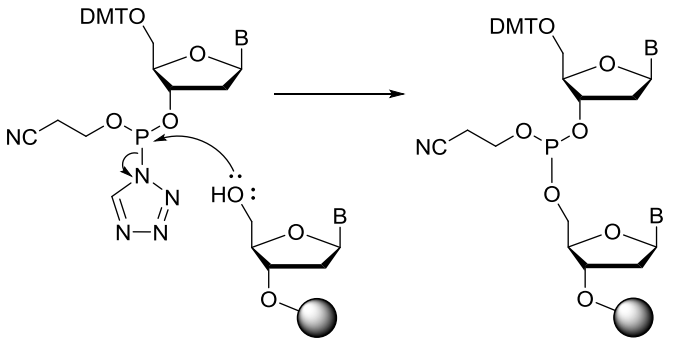

Scheme 1.8 Coupling step for the addition of the next monomer to the growing oligonucleotide chain.

Coupling in solid phase DNA synthesis is 99 % efficient, however after coupling, any un-reacted 5'-hydroxyls need to be capped to prevent undesired strands from being synthesised (Scheme 1.9). If trying to synthesise the strand ACGT (to a column preloaded with A), the first coupling required is the addition of C. If a small number of A nucleobases are left un-reacted, then come the addition of the next nucleotide G, the sequence AG will be formed as well as the desired ACG. This problem would surface in every cycle leading to a whole range of undesired truncated sequences. By adding acetic anhydride and N-methyl imidazole to cap the unreacted 5'-hydroxyls before the addition of the next nucleotide, all failure sequences should be blocked and unable to continue with the synthesis.

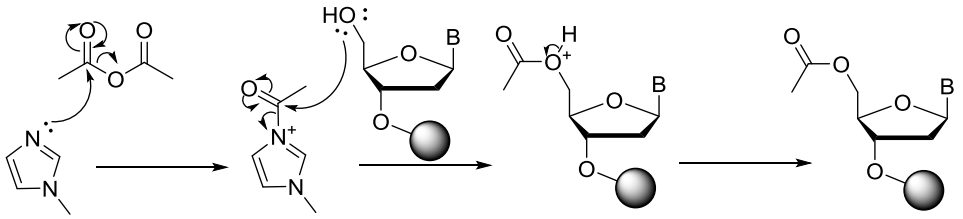

Scheme 1.9 Capping step mechanism using acetic anhydride and 10 % methylimidazole.

The phosphite triester, P(III), formed in the coupling step (Scheme 1.8) is unstable under acidic conditions (such as the detritylation step conditions) so must be oxidised to the stable P(V) species prior to the next step. Oxidation is carried out using a mixture of iodine, water and pyridine (scheme 1.10).

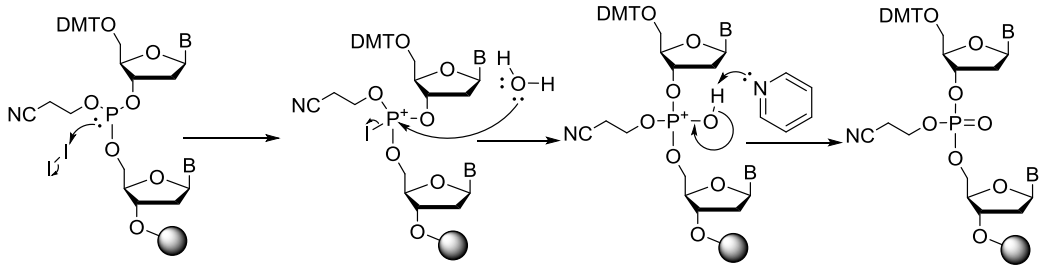

Scheme 1.10 Oxidation of phosphorus (III) to phosphorus (V).

With the growing chain stabilised, the cycle can start again by deprotecting the 5'-hydroxyl and coupling the next nucleotide in the sequence. By repeating this cycle the full oligonucleotide can be synthesised on the solid support. At this point the oligo needs to be cleaved from the beads and collected. As acid is a key part of the synthetic cycle (detritylation step), the linker holding the oligo to the bead (Figure 1.11) needs to be stable towards acidic conditions. As a result, the linker is designed to be base labile. The fully synthesised oligo is detached from the bead by passing ammonium hydroxide through the CPG column. A simple ester hydrolysis will cleave the oligo from the non-universal solid support. A slightly more complicated mechanism of an ester hydrolysis

followed by an intramolecular dephosphorylation is required to cleave from a universal support. These mechanisms are shown in Scheme 1.11.

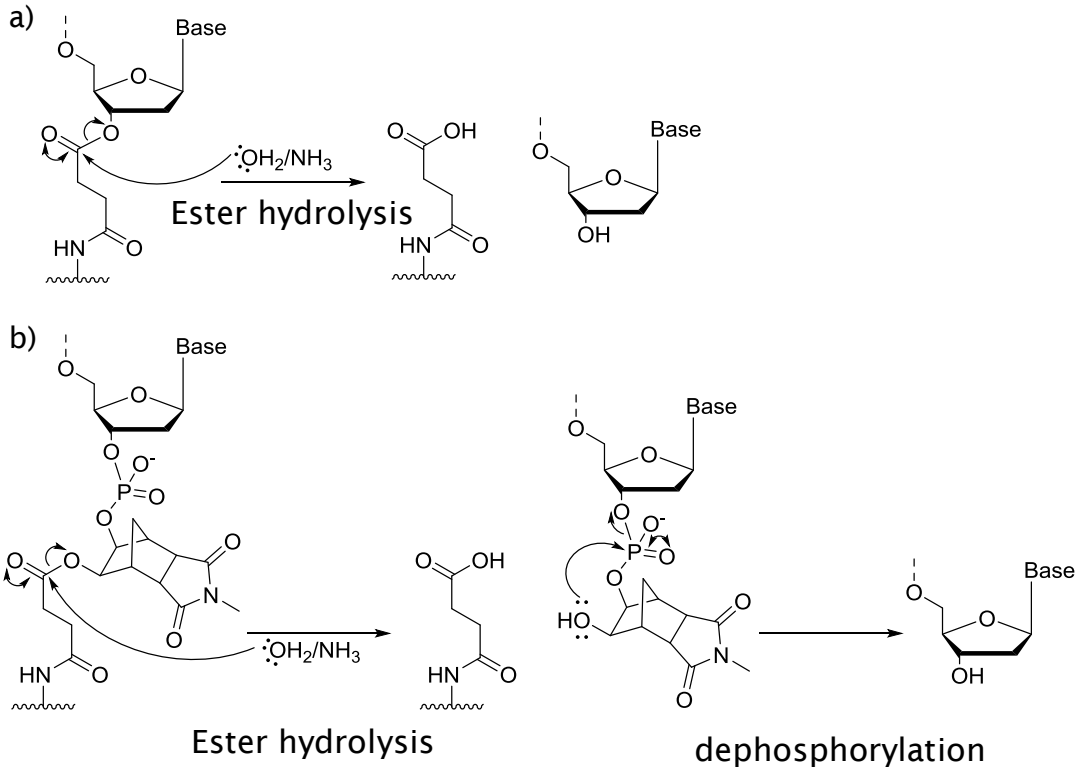

Scheme 1.11 Cleavage of an oligonucleotide from a) a column loaded with the first base. b) a universal column.

The final step of the synthesis before purification is carried out is to deprotect the bases and the backbone. The coupling reaction is a nucleophilic substitution with the 5'-OH as the nucleophile. However, the A, G and C bases all contain amine groups capable of acting as nucleophiles. If these amine groups are not blocked, competing reactions can occur and the wrong molecule formed. The protected bases are shown in Figure 1.12. Concentrated ammonium hydroxide is used to deprotect the bases with full deprotection possible in 4 hours by raising the temperature to 55 °C.

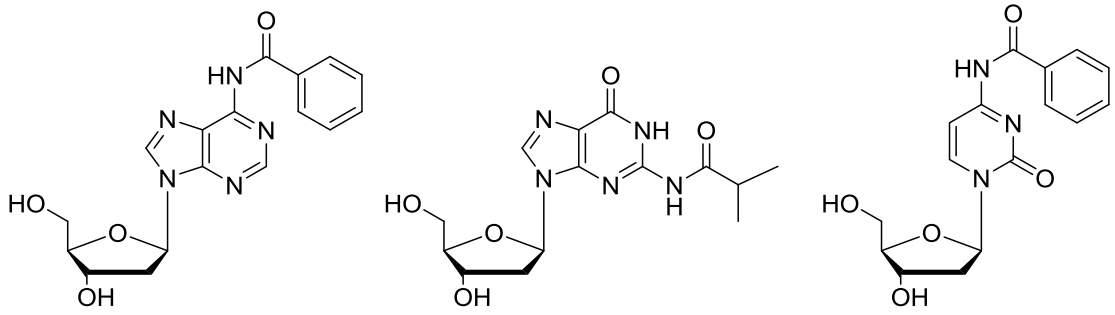

Figure 1.12 The protected nucleosides N(6)-benzoyl dA, N(2)-isobutyryl dG and N(4)-benzoyl dC.

The phosphate backbone of the oligonucleotide is also protected during the synthesis as 2-cyanoethyl phosphotriesters. This deprotection occurs at the same time as the base deprotection using concentrated ammonium hydroxide to release acrylonitrile. The mechanism of this cleavage is shown in Scheme 1.12.

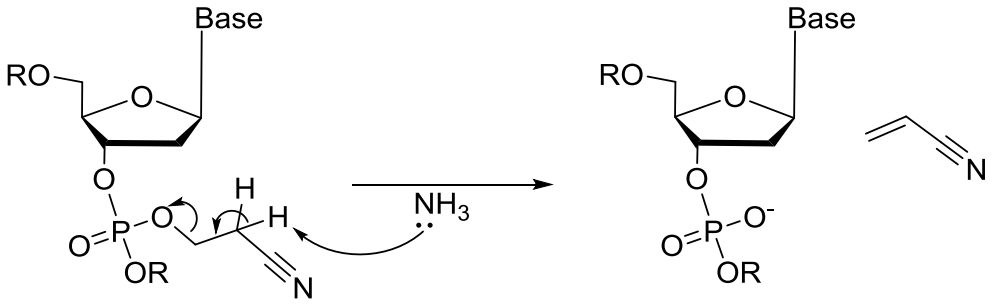

Scheme 1.12 Mechanism of phosphate backbone deprotection.

With the full sequence synthesised, cleaved form the solid support and the bases and backbone deprotected, the crude oligonucleotide is ready to be purified. This purification is usually carried out by high performance liquid chromatography (HPLC). HPLC is an automated technique which is used to separate compounds of different polarities as they are passed through a column. The polarity of the solvent mixture can be increased at a pre-determined rate to elute the higher polarity compounds. For oligonucleotides, hydrophobic C18 columns are commonly employed. Examples of obtained HPLC chromatograms are presented in later sections.

1.5 Modification of oligonucleotides

Whilst naturally occurring DNA is a very important molecule, the ability to include different modifications into a sequence opens up a huge variety of potential uses in areas such as diagnostics, therapeutics and electronics.[51-53] DNA sequences can be adapted at various locations with subtle changes, or large additions to the structure.[54] Combining these modifications with the self-assembling properties of a DNA duplex allows researchers great control over systems on the nanometre scale.

Unnatural phosphoramidites can be included in solid phase synthesis to create modified oligonucleotides. This can be achieved in many different ways. The four natural nucleosides are all commercially available with an iodo-modification as is shown in Figure 1.13. Organic molecules containing a terminal alkyne can be substituted for the iodine atom on the nucleobase using palladium catalysed Sonogashira cross coupling.[55-58] Standard phosphoramidite chemistry and solid phase synthesis (as described above) can then be used to make a modified nucleotide which can be incorporated into an oligonucleotide at any position. This method provides a route to a huge array of modified bases with control over the modifications position in a sequence.

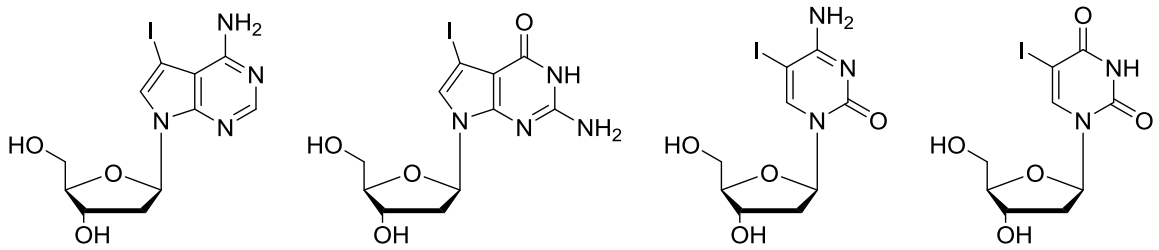

7-deaza-7-iodo-dA 7-deaza-7-iodo-dG 5-iodo-dC 5-iodo-dU

Figure 1.13 The commercially available iodinated nucleosides.

Modification of DNA is not limited to additions to the nucleobases. The base can be re-designed, replaced entirely, or changes can be made to the ribose ring at the 2', 3' and 5'-positions. Figure 1.14 shows examples of different

ways to modify the nucleobases. These modifications need to be carefully designed as removing or disrupting a hydrogen bonded base pair can drastically reduce the stability of the duplex.[59]

First is an example of a modified base formed using Sonogashira coupling to attach an alkyne containing molecule to the iodo-modified thymine nucleobase as described above. This type of modification may not have much effect on the duplex stability as all hydrogen bonding sites are left unhindered. However, the presence of a large modification sticking out from the backbone may cause disruption in other ways (see Chapter 6).

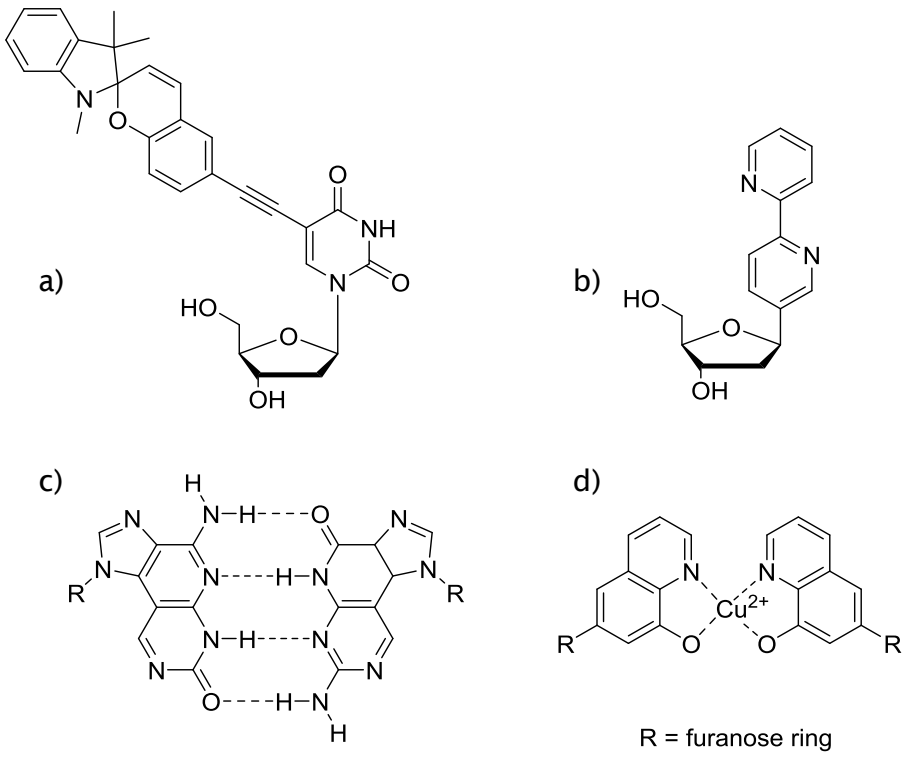

Figure 1.14 Examples of different ways to modify nucleobases. a) Attachment of a molecule via Sonogashira coupling to iodo-modified nucleobase.[60] b) Artificial nucleobase with no Watson-Crick base pairing but π-stacking interactions for added stability.[61] c) Artificial nucleobase with more hydrogen bond pairs.[62] d) Artificial nucleobase using metal chelation instead of hydrogen bonding.[63]

The second example is a base replacement.[64, 65] Modifications like the example shown, do not add any stabilisation to the DNA duplex through hydrogen

bonding as the Watson-Crick base pairing has been removed. However, they are usually planar aromatic molecules (like the natural bases) which allows stabilisation of the duplex through π-stacking with neighbouring base pairs. Leumann and co-workers have shown by using biphenyl base replacements, the π-stacking can even increase the stability of the DNA duplex compared to the natural sequence.[61]

The third example shows a base pair where both bases have been adapted to include more hydrogen bond donor/acceptor sites.[62, 66] Swapping an A-T base pair for the pair shown above doubles the number of hydrogen bonds and as such will have a stabilising effect on the duplex.

The final example shown in Figure 1.14 again involves the replacement of the nucleobases and hydrogen bonding. In these types of modification, metal chelating groups are included in place of the bases.[67, 68] Each pair of modified bases then binds to an ion which sits inside the DNA helix. This metal ion binding can be much stronger than the natural base pairing. Including a metal ion chelating pair in the middle of a 15mer duplex was reported to increase the melting temperature of the natural duplex from 41.3 °C with an A-T pair, or 44.6 °C with a G-C pair, to 65 °C.[63]

Modification is not limited to the nucleobases. There are also several ways to modify the deoxyribose ring with examples shown in Figure 1.15. Example b is modified at the 2'-position. These compounds can be made by modifying the 2'-OH of ribonucleic acid (RNA, Figure 1.15 a). Example b shows a terminal amine included which can be used for further modification via an amide coupling post oligonucleotide synthesis.[69] Other small modifiers such as thiols and azides can be included into oligonucleotides in this way opening up a variety of possible reactions.[70, 71] These molecules can all be converted to nucleotides using the standard phosphoramidite chemistry and then included in the solid phase olionucleotide synthesis. This allows the facile inclusion of a single, or multiple modifications into a designed sequence.

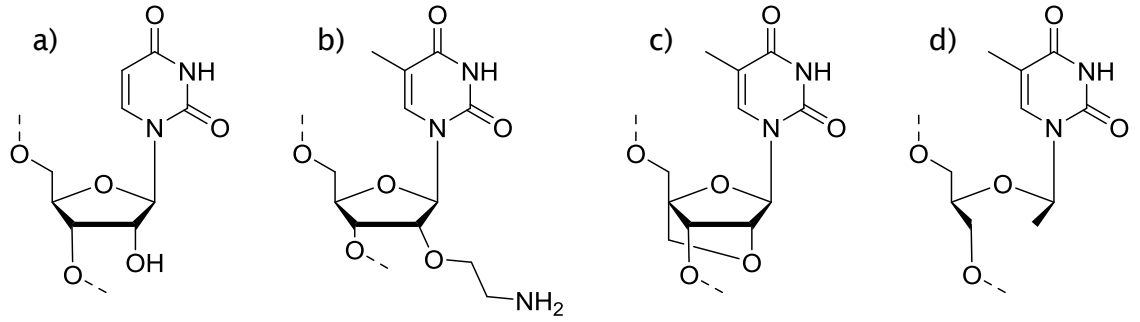

Figure 1.15 a) Unmodified RNA with a uracil nucleobase. b) 2'-modification[69]. c) LNA. d) UNA.

Modification to the ribose ring is not limited to the inclusion of reactive groups. Locked nucleic acid (LNA, Figure 1.15 c) can be formed by modifying RNA nucleotides.[72-74] A link is made between the 2'-O and the 4'-carbon of the ribose ring via a methylene bridge. This bridge locks the ribose in the 3'-endo conformation associated with A-form duplexes. This enhances the base stacking and backbone pre-organisation increasing the stability of the duplex. Unlocked nucleic acid (UNA, Figure 1.15 d) is the opposite, reducing the base stacking and pre-organisation by removing the bond between the 2' and 3'-carbons making the structure a lot more flexible.[75]

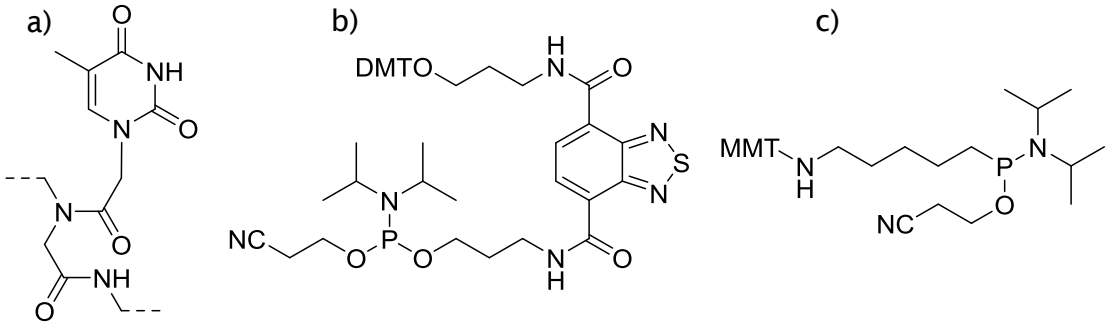

Figure 1.16 a) PNA. b) Internal nucleotide replacement.[76] c) MMT protected 5'-end amino modifier.

As well modifying the ribose ring, this along with the phosphate backbone can be replaced entirely. Peptide nucleic acid (PNA, Figure 1.16 a) is a polymer synthesised from a series of monomers linked by amide couplings.[77] The

monomers contain a nucleobase so duplexes can be formed between two PNA strands, or chimera DNA/PNA or RNA/PNA duplexes can be synthesised.[78] The advantage of the peptide backbone is its neutral charge. The PNA strands have no repulsive interactions between them, unlike the negatively charged phosphate backbones of DNA and RNA. This makes duplexes containing a PNA strand more stable.

The DNA backbone can be modified with the inclusion of a synthetic compound in place of a nucleotide.[79] The example in Figure 1.16 b was synthesised by Haner *et al*. and shows what is required from these modifying units.[76] A hydroxyl is located at each end of the molecule, one to be converted to a phosphoramidite and the other to be protected with a DMT group. This then resembles the 3' and 5'-ends of a natural nucleotide and as such can be included at any position in solid phase oligonucleotide synthesis.

Functional groups can be included into oligos with non-nucleotide phosphoramidites. The commercially available amino-modified phosphoramidite (Figure 1.16 c) contains no nucleobase and no 5'-OH.[80] This modifier therefore, cannot continue the growing chain so is designed to be incorporated at the 5'-terminus of the oligonucleotide. The amine is free to react allowing a huge range of compounds to be attached onto oligonucleotides post synthesis.[81] Other functional groups, such as thiols, are also popular and can be added in the same way.[82]

As shown, modifications can easily be included into oligonucleotides internally or at the 5'-terminus via modified phosphoramidites. Modification at the 3'-terminus however, is a trickier proposition. This is due to the nature of solid phase oligonucleotide synthesis which proceeds in the 3' to 5' direction. Reverse DNA synthesis, i.e. in the 5' to 3' direction, can be achieved but is more difficult.[83, 84] This is due to the relative reactivity's of the primary 5'-OH and the secondary 3'-OH when acting as nucleophiles in the normal and reverse phase DNA synthesis respectively (see Scheme 1.8). Owing to the greater difficulty and the associated cost with this method, it is not a widely used technique. More commonly, modified solid supports are designed with the desired 3'-modification pre-loaded onto the CPG beads. The oligonucleotide synthesis can then proceed as normal with the cleaved strand

containing the required modification at the 3'-terminus. With end-modified oligonucleotides easily producible with the modification included at the 5'-terminus it may appear that there is little point going through the extra effort to modify the 3'-end. However, 3'-modified oligonucleotides act as polymerase chain reaction (PCR) blockers as this requires a 3-OH. They have also been shown to resist digestion by 3'-exonucleases.[85] These qualities are important when designing diagnostic probes and antisense oligonucleotides.

1.6 DNA Nanotechnology and Supramolecular Structures

Supramolecular chemistry looks beyond the molecule at large chemical systems made up of a discrete number of assembled molecular subunits.[86] The forces involved in holding these molecular units together are usually the weaker non-covalent interactions such as hydrogen bonding or π-π interactions. An important concept in supramolecular chemistry is molecular self-assembly where molecules can arrange themselves into larger systems to form a functioning device.

Duplex DNA can be regarded rather like a stick with its rigid double helix. The potential of DNA however is far greater. Our understanding of DNA structure and sequence specific binding makes it a very attractive building block from which to create supramolecular structures. Advances in oligonucleotide synthesis have allowed researchers to design and synthesise any sequence they wish.[50] Owing to the Watson-Crick base pairing, the self-assembly of DNA structures becomes very predictable and controllable. These principles can be put to use in very simple systems such as the molecular beacon shown in Figure 1.17.[87]

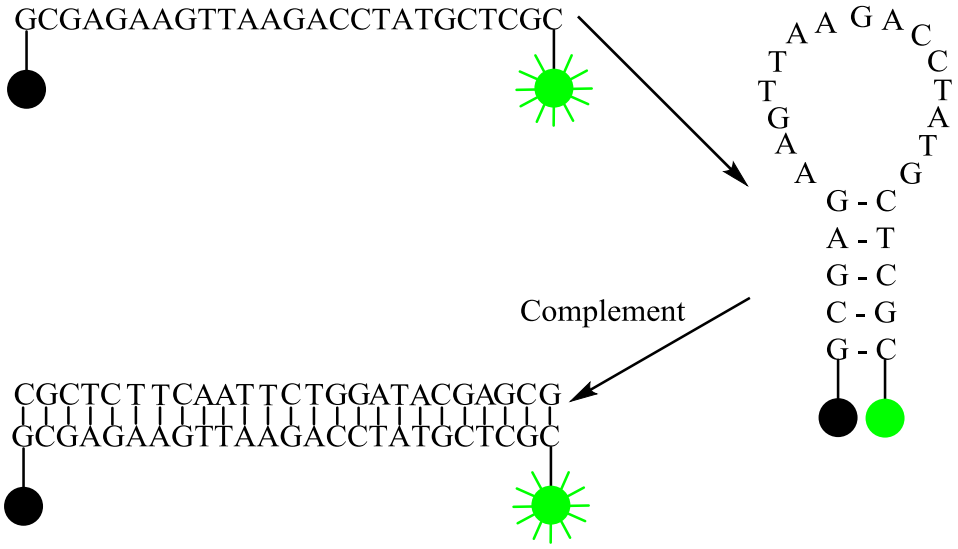

Figure 1.17 A simple molecular beacon designed using a hairpin loop.

The molecular beacon is based on a hairpin loop. This is a single stranded oligonucleotide with the two ends designed to be complementary. This results in the DNA folding and annealing to itself forming a loop. By attaching a fluorophore at one end of the strand, and a quencher at the other, a simple signalling device is created. The single strand folding into a loop brings the fluorophore into close proximity with the quencher. This stops the emission from the fluorophore and no signal can be detected. By adding the complementary strand, the loop is opened up and the quencher moved away from the fluorophore allowing an emission to be measured.

This design, and other simple systems based on fluorescently labelled DNA, have been widely used to detect PCR products, check sequences and detect mismatches (single nucleotide polymorphisms).[88-91] DNA structures are not limited to these small probes however. Using the recognition and self-assembly properties of DNA, much larger two and three dimensional structures can spontaneously form given the right sequences and conditions.

The use of DNA to form these large structures in this way has been termed DNA nanotechnology and was pioneered by Ned Seeman in the 1980s.[92-94] The aim of DNA nanotechnology, according to Seeman, is the construction of specific geometrical and topological targets from DNA.[95] Forming these structures can require many carefully designed sequences of DNA with each one partially complementary to more than one other strand. This allows many duplexes to be linked together enabling the DNA to become less of a helical stick, and more of an intelligent glue.[96] A few of the vast array of structures produced are presented in Figure 1.18.

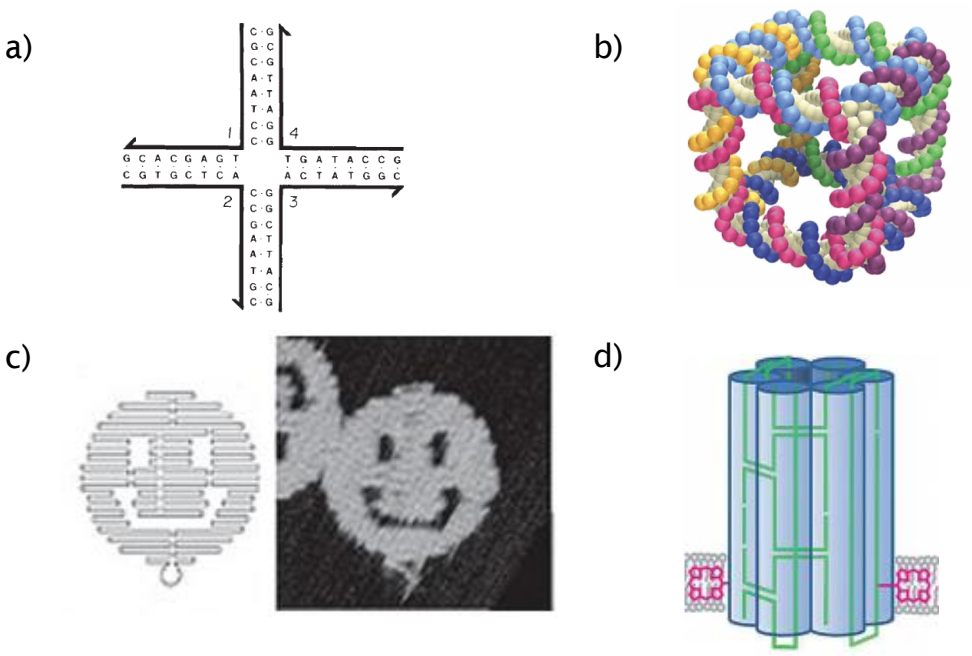

Figure 1.18 a) A four branch Holliday junction.[97] b) Representation of a three dimensional DNA cube constructed by Seeman *et al*.[98] c) DNA origami face produced by Rothemund (schematic on the left, AFM image on the right).[99] d) A DNA-Nanopore with attached porphyrins to anchor into a lipid membrane.[100]

The first wave of structures produced using the concepts of DNA nanotechnology were all very simple 2 dimensional shapes based around hairpin loops and branched junctions (Figure 1.18 a). Branches consisting of three, four, five and more arms have all been reported.[101] By designing overhangs (sticky ends) into the sequences, many more strands could be attached to form a variety of shapes.

The use of DNA in this way is not limited to two dimensions. The famous cube (Figure 1.18 b) produced by Seeman was created from six interconnecting strands.[98] This structure advanced the field of DNA nanotechnology inspiring further research into the area resulting in the creation of many more polyhedra. These three dimensional cages are now being investigated for potential real world uses such as drug delivery capsules.[102, 103]

With time, and the assistance of more advanced computer programs, more complicated structures could be produced. Rothemund has constructed a series of two dimensional shapes like the face presented in Figure 1.18 c.[99] This was achieved using a single very long strand of viral DNA and over two hundred shorter "staple strands" to fold the DNA and hold the scaffold together. Rothemund named this approach DNA origami. Whilst these structures have no practical application of their own, they show the level of control and range scientists now have in this field. This technique has since been adopted in the construction of three dimensional shapes.[104, 105]

In recent years, DNA nanotechnology has advanced further in the pursuit of functional molecular devices. The name DNA architectonics has been acquired by the field reflecting the use of DNA as the building blocks of much greater systems.[96] Modifications can be included into these DNA structures to incorporate the desired properties needed for a certain use. In a collaboration led by Stefan Howorka, the principles of DNA nanotechnology were used to interconnect six duplexes (represented by the blue cylinders, Figure 1.18 d) from several intertwined single strands (green lines). This produced a nanopore which has been placed in a lipid bilayer using the Stulz group's porphyrin modifications as a hydrophobic anchor to keep the DNA within the hydrophobic bilayer.[100]

Supramolecular porphyrin arrays have been widely studied due to the interest in their electronic properties. Chains of covalently linked porphyrins have been tested for their electrical conduction[106] and as optoelectrical switches.[107] Light harvesting devices[108-110] have also been constructed from this type of multi-porphyrin array and look to mimic photosynthetic systems.[111] Porphyrins are also being used as molecular electronic components for a variety of functional devices.[112]

With its reliable recognition and well defined structure, DNA is an obvious candidate to aid the construction of these types of systems. Porphyrin-DNA conjugates have been employed by many groups looking to exploit the porphyrins characteristics with the added stability of a DNA support.[113-117]

All the examples presented in Figure 1.18 can be described as static systems. Due to the transient nature of the hydrogen bonding between base pairs, competing binding sites can be included in a design. This creates a dynamic system as strands switch between binding sites. By taking advantage of these binding properties, the groups of Seeman[118] and others[119, 120] have created DNA walkers capable of travelling along a designed DNA track with the assistance of a number of "fuel" strands. These consist of a set strand to bind the walker to the track at a certain point. An unset strand can then bind this set strand releasing the walker's foot. The addition of a second set strand will then attach the walker to the track at a different position and hence the molecule is walking. This movement is represented by the cartoon in Figure 1.19. Dynamic systems such as these walkers have been dubbed molecular machines.

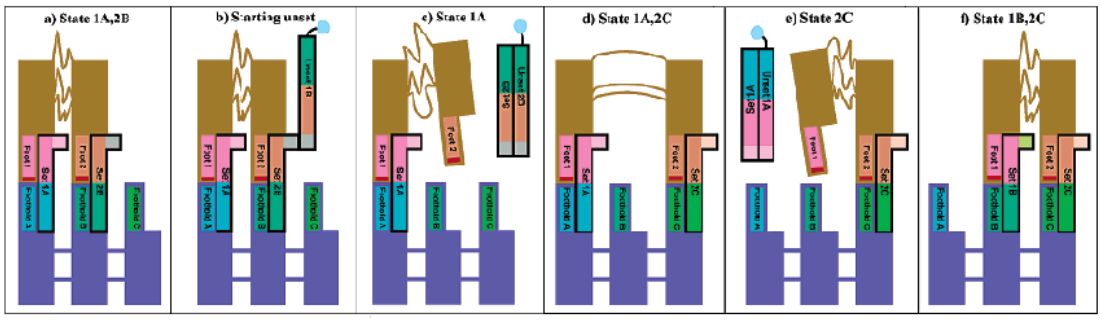

Figure 1.19 A cartoon reproduced with permission from Seeman *et al.* to represent the action of his DNA walker.[118]

DNA has also been investigated as a potential for a molecular wire. Barton and others have shown a DNA duplex itself can act as a charge carrier, but reports on the level of conductivity vary.[121-124] This charge transfer occurs through the π-stacking of the base pairs. Mismatches in the duplex backbone, or a structural distortion (e.g. by binding to a protein) impairs the DNA's conductivity. Achieving charge transfer over long distances (> 40 nm) in this manner is therefore a concern[125] which led Porath *et al.* to create a molecular wire from G-quadruplex DNA.[126] The larger structure provides a stiffer wire with additional charge transfer pathways within the molecule. This allows a current to be passed over a much greater distance (> 100 nm) than with a duplex.

As well as transferring charge themselves, DNA nanostructures have found uses as support structures for electronic devices. By attaching nanoparticles or chromophores to a DNA backbone, plasmonic[127] and light harvesting[128] devices have been constructed. Pike *et al.* used DNA as a template to grow a polymer nanowire with the monomer units attached to the scaffold using click chemistry.[129] DNA is also being used as a template for more conventional metal wires. Braun *et al*. used the negatively charged backbone to chemically deposit silver ions onto a DNA duplex to form a 12 μm long, 100 nm wide conductive silver wire. Control experiments showed the current was being carried solely by the silver.[130, 131]

The aim of DNA nanotechnology is to provide controllable assembly on the nanoscale to produce static structures, dynamic machines and therapeutic techniques.[132] The early work in the field was very much proof of concept and discovering how to increase the complexity of these systems whilst retaining the control. Over thirty years after the concept of DNA nanotechnology was introduced, the research is starting to produce systems with real world applications. DNA origami cages are already being used to investigate new therapeutic techniques such as drug delivery systems. Molecular wires and other electronic devices are of great interest. Many groups are using the recognition capabilities of DNA to template the construction of these wires using a wide variety of conductive materials. DNA nanotechnology is also reaching much further into biological systems. The potential to study and even control enzymatic reactions using DNA's recognition capabilities could be of huge significance in increasing our understanding of these systems. This will hopefully lead to innovative medicinal treatments.[133, 134]

DNA nanotechnology is an exciting field with a wide scope for creating functional biological devices. The control over DNA binding, stemming from the Watson-Crick base pairing, and the growing numbers of potential uses is leading many researchers to use nucleic acids as the building blocks towards novel functional structures.

2. Aims

This project focused on two main aims. Firstly, to synthesise the components required to form two self-assembled porphyrin arrays based on a DNA templating approach. The connectivity of the two porphyrin systems differs, but they are both designed to function as an electronic wire. Whilst one will yield a π-stacked porphyrin array with the porphyrins positioned in the major groove of the DNA helix, the other is aimed at connecting the porphyrins covalently at the end of a DNA template (Figure 2.1). Different strategies of attaching porphyrins to the DNA backbone (during and post oligonucleotide synthesis) were to be investigated during the project.

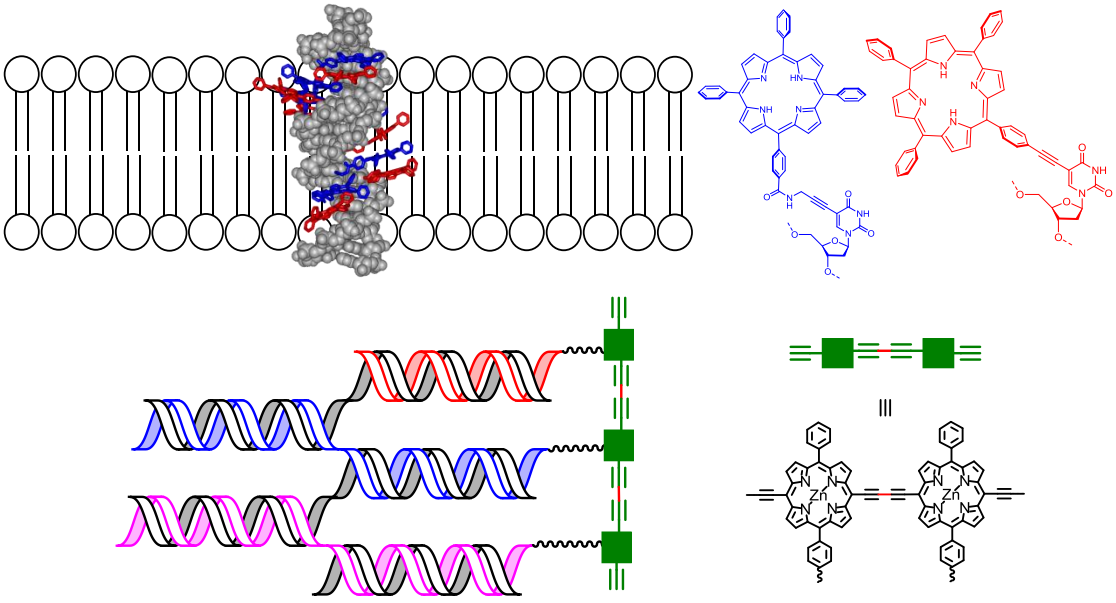

Figure 2.1 Top) Schematic representation of a porphyrin Zipper array embedded within a lipid bilayer. The two porphyrin-modified nucleobases are also shown. Bottom) Schematic representation of an acetylene-linked porphyrin wire templated by DNA duplex formation.

Both wires use porphyrin chains to transfer electrons, and DNA as a molecular scaffold to direct the self-assembly of the system and hold the porphyrins in the desired position. A self-assembled porphyrin chain has previously facilitated electron transfer across a lipid bilayer, but the system based on

hydrogen bonding was not very stable (see section 3.1). Through the use of a DNA scaffold a more durable molecular wire was targeted.

In parallel, circular dichroism spectroscopy was to be used for structural analysis of modified DNA. Through this work we aimed to investigate the effects of increasing modification on the CD signature of a DNA duplex and obtain a better understanding of general aspects of DNA modification. Small and large (porphyrin) modifications were to be included in short oligonucleotides, and studied in conjunction with molecular modelling. By obtaining this data we hoped to gain a greater understanding of how porphyrin modifications alter the structure of the DNA backbone, and interact with each other.

3. Self-Assembled Porphyrin Zipper Array

3.1 Introduction to the Porphyrin Zipper Array

The aim of this project was to create a molecular scale electronic wire using porphyrin-modified DNA. A DNA duplex was designed to act as a scaffold to hold a series of porphyrins in the correct positions. Once aligned, electron transfer along the porphyrin chain should result in a measurable current.

This project was inspired by previous work presented by Charles Michael Drain in 2002.[135] Drain reported the transfer of energy across a lipid bilayer by inserting porphyrins into the membrane and taking advantage of their electronic characteristics. Drain synthesised his porphyrins to contain either hydrogen bond donor/acceptor groups or metal ion coordination sites. When inserted into the membrane, these porphyrins could self-assemble into a linear porphyrin array spanning the bilayer. The length of the assembly was influenced by the properties of the bilayer and so could self-adjust to the thickness of the membrane. An aqueous soluble electron donor was placed on one side of the membrane, and an electron acceptor on the other. Illuminating with white light excites the system, and a current was measured across the membrane. The photocurrent was only observed with the fully assembled structure showing the system acts as a molecular wire. A schematic representing Drain's system is shown in Figure 3.1.

Porphyrin Zipper Array

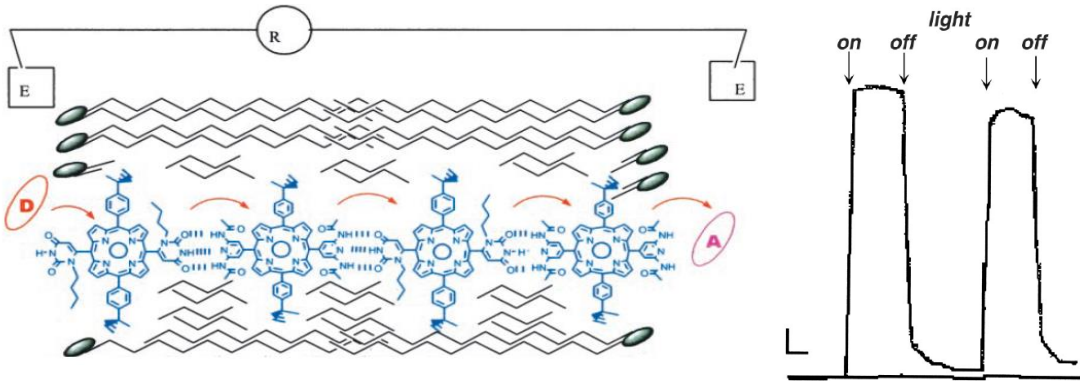

Figure 3.1 Left) Schematic of the porphyrin system produced by Drain.[135] The porphyrins are inserted into the lipid membrane and self-assemble using hydrogen bonding. D = electron donor. A = electron acceptor. The arrows show movement of electrons along the porphyrin chain. Right) The photocurrent measured by Drain showing the drop in measured current over time. Vertical scale bar = 6.9 nA, horizontal scale bar = 1 minute.

This system, whilst able to transfer the energy across the membrane, was not very stable being "limited to a few hours, at most a day". This stemmed from the fact the porphyrins were not joined by strong covalent bonds. The system breaking down resulted in a drop in the measured energy transfer with repeated cycles. This drop off in signal was demonstrated by Drain and is shown here in Figure 3.1.

With the stability of this design in mind, a new system was planned around a DNA duplex. This duplex was intended to act as a scaffold to hold the porphyrins in close proximity to each other, whilst adding the increased stability of covalent bonding. This system has been named a "Zipper array" and consists of two complementary oligonuceotides each containing six porphyrin modifications. The porphyrins are included in the oligonucleotide by producing porphyrin-modified nucleosides. Phosphoramidite chemistry can then be used and the modified nucleotides included in solid phase oligonucleotide synthesis. Two different porphyrin monomers were produced and included in the design of the Zipper array. These are pictured in Figure 3.2.

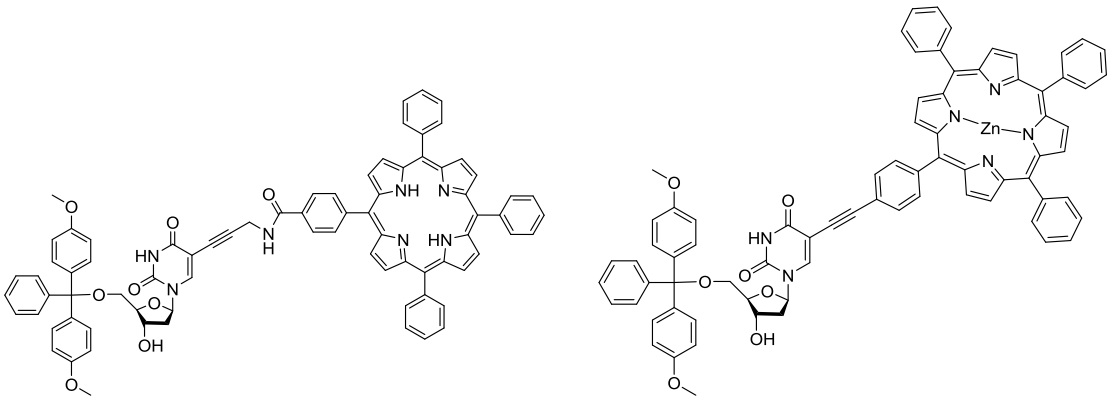

Figure 3.2 The structure of the amide and acetylene linked porphyrin nucleosides.

The two porphyrin-modified nucleosides produced each contain a thymine base modified at the 5-position. The porphyrins are attached to the nucleobase via a linker. This linker is the difference between the two compounds. The first is connected by an amide linker and the second by an acetylene linker. The synthesis of the two porphyrin-modified nucleosides is described in sections 3.2 and 3.3 respectively where the reasons for having the two different linkers will also be explained.

Using the porphyrin-modified nucleosides, the two complementary porphyrin containing strands could be synthesised and annealed to form the Zipper duplex. Like Drain's system, the Zipper array can be inserted into a lipid bilayer. By placing an electron donor on one side of the membrane, and an electron acceptor at the other, an electron transfer through the bilayer will hopefully be measured.

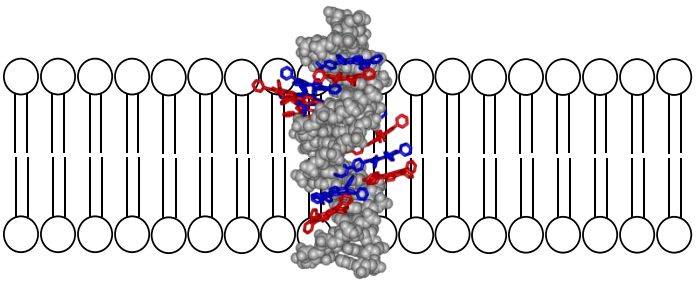

Figure 3.3 Representation of the twelve porphyrin Zipper array spanning a lipid bilayer.

3.2 Synthesis of Porphyrin Monomer with Flexible Amide Linker

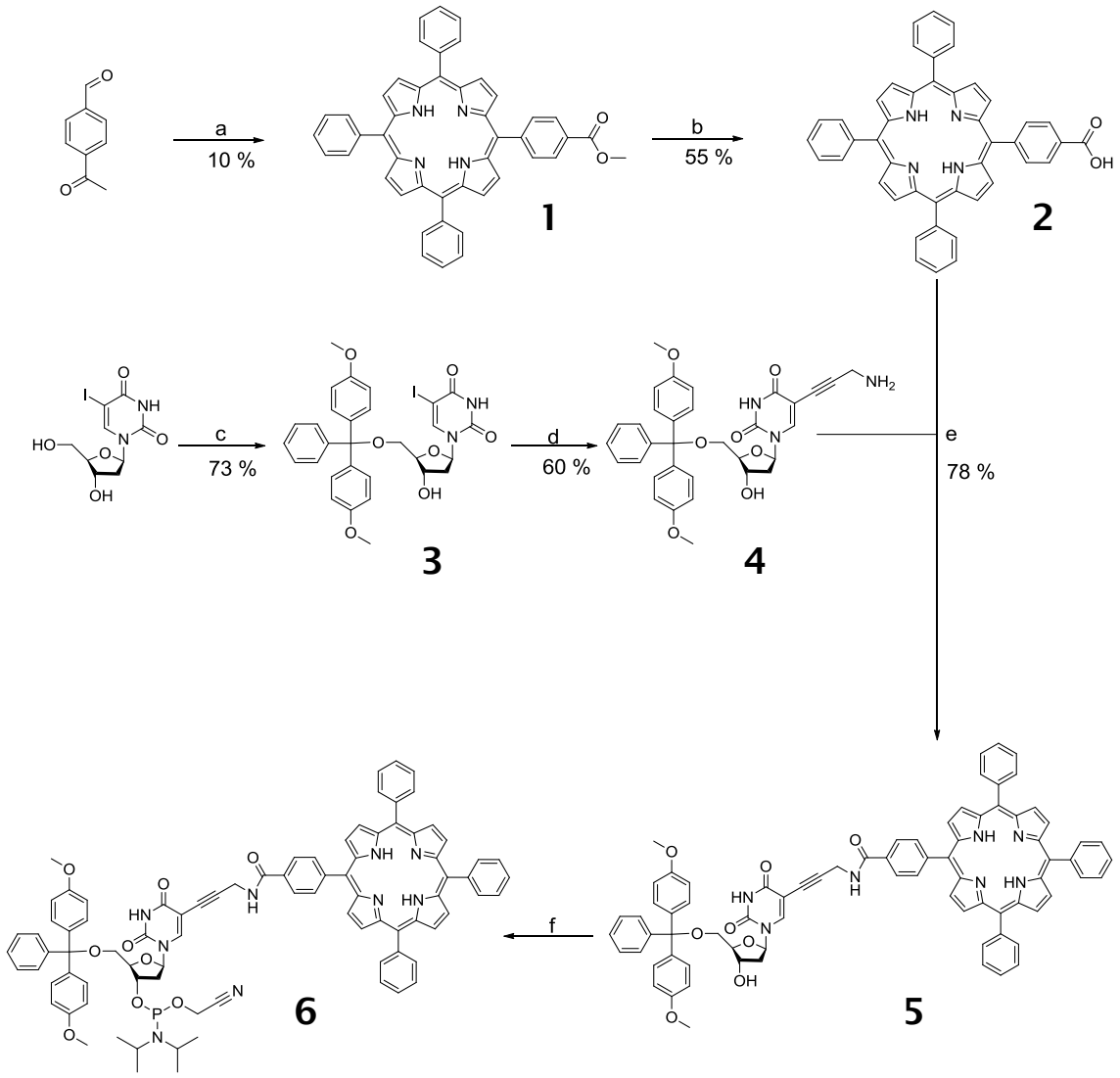

Scheme 3.1 a) i) Pyrrole, Benzaldehyde, Boron trifluoride etherate, $CHCl_3$ ii) DDQ. b) Pyridine, KOH, H_2O, Δ. c) DMT-Cl, Pyridine. d) Propargylamine, CuI, $Pd(PPh_3)_4$, DMF, NEt_3. e) DMAP, HOBt, DIC, DCM. f) CEP-Cl, DIPEA, DCM, N_2.

The synthesis of a porphyrin nucleotide with an amide linker was carried out following a procedure established previously by members of the Stulz group.[115] This amide linker was designed to add a degree of flexibility to the system and allow multiple porphyrins to stack. The synthetic route is outlined in Scheme 3.1.

5-(*p*-methyl benzoate)-10, 15, 20-triphenyl porphyrin (**1**) was first synthesised achieving a yield of 10 %. A yield this low is normally unacceptable in organic synthesis, however it is common place in porphyrin syntheses.[27] These reactions are low yielding due to multiple porphyrin products (Figure 3.4) being formed as well as polypyrrole side products. In this synthesis the tetraphenyl porphyrin (TPP) and bis-substituted porphyrins are made along with the desired mono-substituted porphyrin. Adjusting the ratio of pyrrole and the aldehydes can change the statistical balance of the reaction making the desired porphyrin more likely to form and increasing the yield from the reaction. A 1:6:6 ratio of methyl-4-formylbenzoate, benzaldehyde and pyrrole was used to synthesise this porphyrin as test reactions have shown this ratio to produce the highest proportion of the methyl ester compared to the tetraphenyl porphyrin and higher substituted porphyrins.

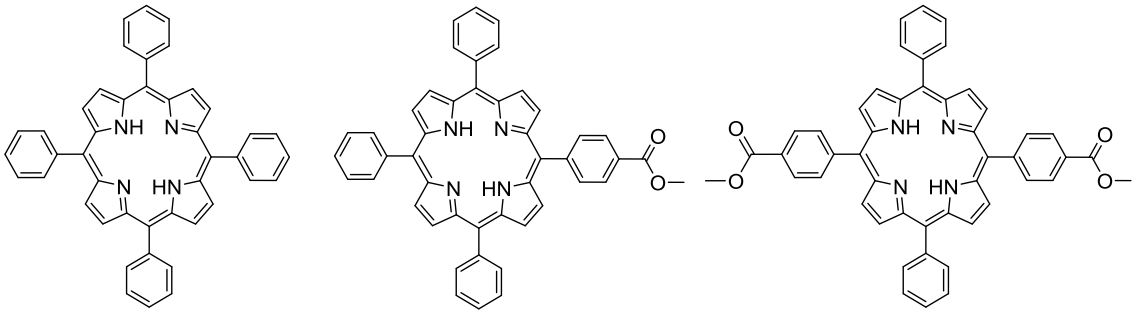

TPP Mono-substituted porphyrin Bis-substituted porphyrin

Figure 3.4 Three different porphyrins obtained from the porphyrin synthesis step a. Left) tetraphenyl porphyrin. Middle) mono ester product. Right) A bis-substituted porphyrin.

The methyl ester porphyrin was converted to the carboxylic acid (**2**) by base catalysed hydrolysis. A huge excess (50 equivalents) of the potassium hydroxide was used to push the reaction forward, whilst the reaction time was shortened by heating to 40 ˚C. The addition of a small amount of acid was required during the aqueous extraction to neutralise the solution. Without this neutralisation both the deprotonated porphyrin acid, and the protonated porphyrin are slightly water soluble meaning no separation is achieved during the extraction (see Figure 3.5). With the solution neutralised all the porphyrin becomes soluble in the organic phase greatly aiding the separation. An

undesired consequence of adding too much acid was a change in colour from a red/purple to bright green as the two previously un-protonated nitrogens at the centre of the porphyrin ring are protonated. Van der Waals repulsion of these inner hydrogens causes the pyrroles to tilt from the mean plane of the nitrogens, moving the phenyl groups at the meso positions into the same plane as the porphyrin ring. This increases the molecule's conjugation resulting in a change in the energy and wavelength of absorbance causing the change in the compounds colour.[136] A yield of 55 % was achieved for this step.

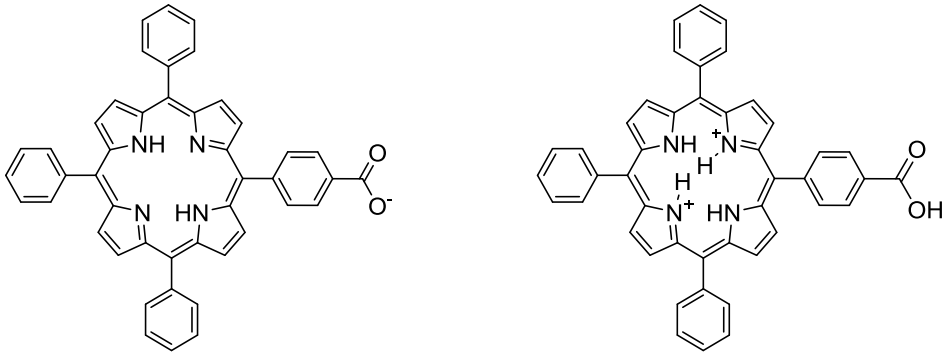

Figure 3.5 Left) Deprotonated porphyrin acid. Right) Protonated porphyrin.

The porphyrin carboxylic acid (**2**) was attached to an amino-modified uridine monomer (**4**) by the formation of an amide bond. The modified uridine base 5-iodo-2'-deoxyuridine (5-I-dU), was first protected at the 5' position with 4, 4'-dimethoxytrityl (DMT), the standard 5'-protecting group used in solid phase DNA synthesis. DMT chloride was added portion wise over 5 hours to the 5-I-dU. This slow addition was used to stop double addition of the DMT protecting group to the 3'-OH as well as the 5'-OH of the ribose ring. The least hindered 5'-OH is favoured for nucleophilic reaction, but the 3' position will react with DMT-Cl if a large excess of the protecting group is present.

With the 5'-OH protected, the nucleoside was modified at the 5-position of the pyrimidine ring. A palladium catalysed Sonogashira coupling was used to substitute the iodine for propargylamine to produce 5'-DMT-5-propargylamine-dU (**4**). The use of oven dried glassware and the addition of 3 Å molecular sieves was found to be very important when improving the yield of this reaction. The reaction has since been repeated successfully several times with a yield of 60 % being achieved.

With the porphyrin carboxylic acid (**2**) and the amine nucleoside (**4**) both synthesised, an amide coupling was carried out producing the porphyrin nucleoside (**5**) with a yield of 78 %. This reaction progressed with no problems, however, monitoring the progress did present an issue. Separating the carboxylic acid starting material and the amide product by TLC analysis proved tricky. The TLC plate needed to be run twice to increase the separation. This produced clearer results showing the formation of the amide product.

The porphyrin phosporamidite (**6**) was synthesised to complete the synthesis of the porphyrin-DNA monomer with the flexible amide linker. Phosphoramidites are used in solid phase DNA synthesis due to their highly reactive nature towards nucleophiles. They are however also highly reactive to oxygen and are readily oxidised from the phosphorus (III) species to the phosphorus (V) under atmospheric conditions. For this reason all phosphoramidite chemistry is carried out under inert atmosphere for the entirety. As the porphyrin-modified phosphoramidite has previously shown itself to be unstable resulting in a short lifetime, it was immediately coupled to the oligonucleotide. Column chromatography can be carried out under inert atmosphere but again due to the stability of the phosphoramidite, recrystallisation (DCM / hexane) was the only purification technique used before DNA synthesis. It is vital that the reaction goes to completion using this method otherwise the chlorophosphitylating reagent can couple to the oligo instead.

3.3 Synthesis of Porphyrin Monomer with Rigid Acetylene Linker

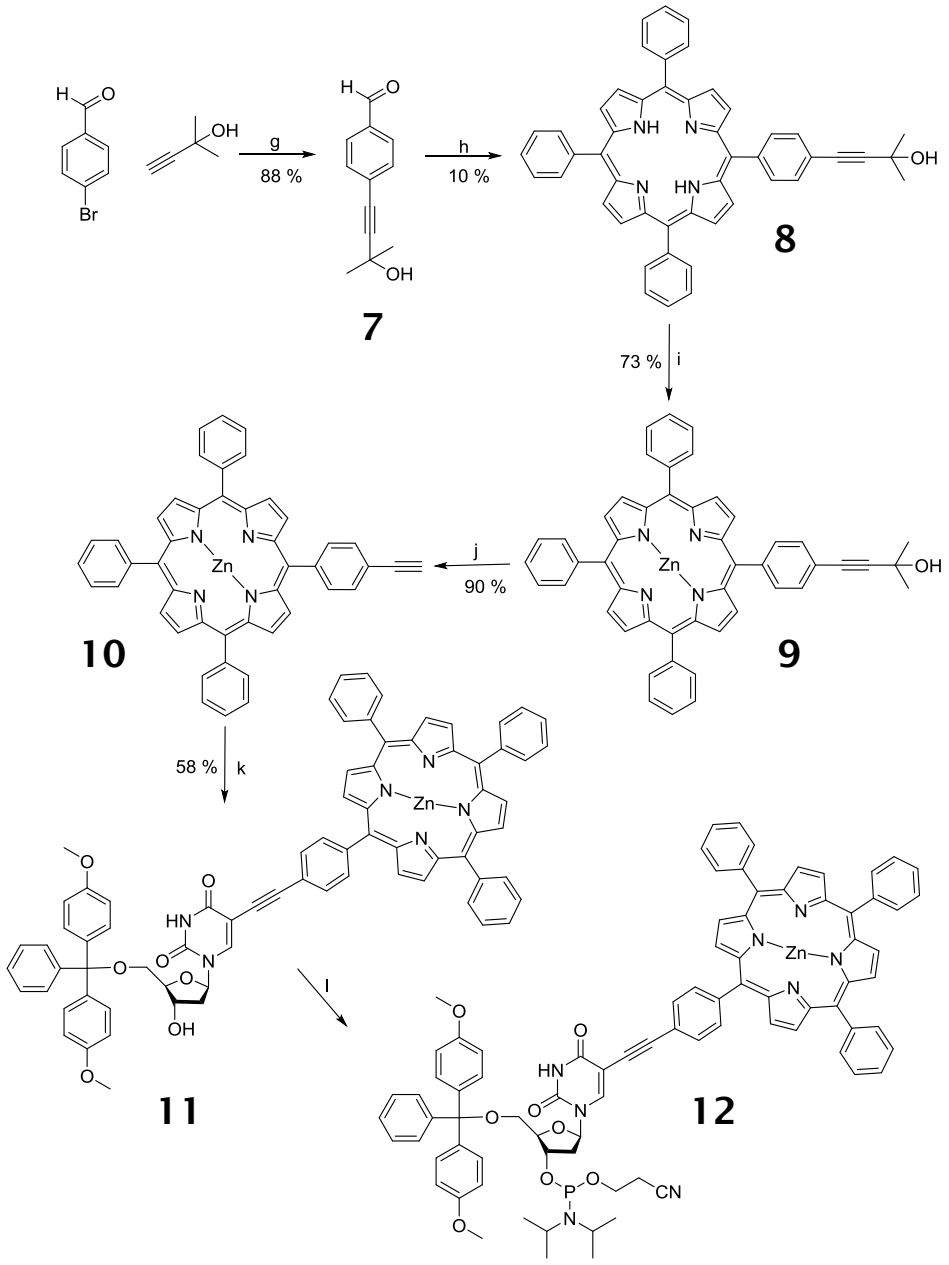

Scheme 3.2 g) Pd-C, PPh_3, CuI, K_2CO_3, DME/H_2O, N_2, Δ. h) i) Pyrrole, Boron trifluoride etherate, $CHCl_3$. ii) DDQ. i) $Zn(OAc)_2$, DCM/MeOH, Δ. j) Toluene, NaOMe, Δ. k) 5-I-dU, $Pd(PPh_3)_4$, CuI, NEt_3, DMF, N_2. l) CEP-Cl, DIPEA, DCM, N_2.

The second porphyrin nucleotide to be synthesised contained a more rigid acetylene linker. Where the more flexible amide linker was designed to give a small amount of flexibility in multiporphyrin systems, the acetylene linker

added rigidity and a bit more control. The synthesis was carried out following the synthetic route outlined in Scheme 3.2.

The protected acetylene (2-methyl-3-butyn-2-ol) was attached to 4-bromobenzaldehyde by Sonogashira coupling using palladium on carbon as the catalyst. This reaction produced the product in good yield (88 %). The mono-substituted porphyrin (**8**) was then synthesised using the same 1:6:6 ratio with pyrrole and benzaldehyde as applied in the synthesis of the amide porphyrin. As before, a yield of 10 % was achieved with large amounts of TPP and bis-substituted porphyrins being formed. The mono-substituted porphyrin (**8**) was then metalated with zinc. This metalation is required as the Sonogashira coupling of the porphyrin to the modified nucleobase (step k, Scheme 3.2) will not work with the free base porphyrin. This is because copper can itself metalate the porphyrin and therefore becomes unavailable to act as the catalyst in the reaction. A decent yield of 73 % was achieved for the zinc metalation, but this was not as high as hoped. By heating with a large excess of zinc acetate (40 equivalents), there should be no reason why all the porphyrin cannot be metalated. It is believed that the uncollected product was lost during the purification as the compound seemed to stick to filters and silica gel and could not be removed very easily. This led to changes for subsequent attempts. It was decided to remove the excess zinc acetate by phase separating between ethyl acetate and water and avoiding drying with Na_2SO_4 which would also capture the product. This step was dropped from many subsequent reactions, instead removing any residual water in the crude product *in vacuo*. Column chromatography after the zinc metalation reaction was also dropped. This could be left out entirely as in theory, all the porphyrin should be zinc metalated and so unable to bind the catalytic copper. Re-crystallisation was investigated as a purification method, but as filtering was required could again prove tricky to get a perfect yield.

Before the coupling of porphyrin to the iodo-modified nucleoside (**3**) could be carried out, the acetylene on porphyrin **9** needed to be deprotected. By heating under reflux with a large excess of sodium methoxide, a good 90 % yield was achieved. Once deprotected, the acetylene (**10**) was available for Sonogashira coupling to the nucleoside to produce compound **11**. This reaction proceeded without incident but the purification proved tricky. Difficulties were brought about by the fact that the product and the DMT

protected 5-I-dU starting material appear at almost identical R_f values on a TLC plate. This made analysis of the progression of the reaction difficult, but more importantly complicated the purification by column chromatography. Purification of the product was achieved by column chromatography using silica with 10 % silica H. Silica H is a finer powder which aids the separation. This was still not easy however with two, sometimes three, rounds of chromatography being required to collect all of the product free from starting material. It is critical to remove all the starting nucleoside at this point otherwise two nucleotides could be formed in the phosphitylation step leading to competition to couple to the oligonucleotide.

A change in analysis was also used as it was not clear on a TLC plate if the starting nucleoside was present or not. To check, different fractions were collected and analysed by NMR spectroscopy. The presence of the starting material could be established by the emergence of a set of peaks corresponding to the 1' – 5' protons of the deoxyribose ring. These peaks are slightly displaced from those produced by the porphyrin monomer deoxyribose ring so two nucleosides could be detected.

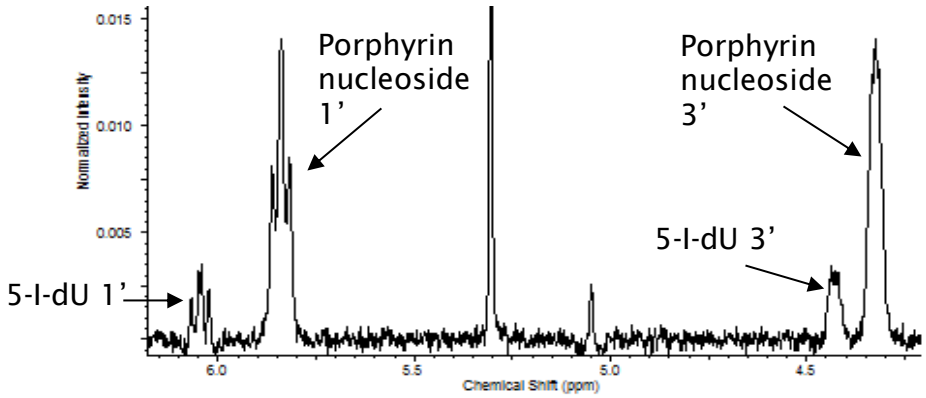

Figure 3.6 NMR spectrum showing the porphyrin nucleoside 1' and 3' proton peaks as well as the corresponding peaks for the starting 5'-DMT-5-I-dU.

The synthesis of the porphyrin nucleotide with rigid acetylene linker was completed by forming the phosphoramidite (**12**). As previously mentioned these compounds are not air stable so as with the amide monomer, this phosphoramidite was used straight away for solid phase DNA synthesis.

3.4 The Synthesis of Six Porphyrin Oligonucleotides

The porphyrin Zipper array consists of two oligonucleotides, the first containing six porphyrins attached via the amide linker (ODN 1), the second contains six porphyrins attached by the acetylene linker (ODN 2). The two oligos are partially complementary and contain an overhang at each end. These sticky ends are intended as binding sites for the electron donor and acceptor. The sequences are designed with an adenine base alternating with a porphyrin modified base to give a PAPAPA sequence in the porphyrin region. The complementary strand is designed to line up so that each porphyrin modified T base can form a base pair with an opposite A base. By doing this, no hydrogen bonds are lost compared to the unmodified duplex as the porphyrin does not obstruct these sites. The Zipper array is named as such due to the alternating porphyrins interlocking like the teeth of a zip. This can be seen in the full sequence of the Zipper duplex shown in Figure 3.7.

5' – GGC CAT CGT CGC **P**A**P** A**P**A **P**A**P** A**P**A TTA T ODN 1

3' – A GCG A**P**A **P**A**P** A**P**A **P**A**P** AAT ACC GTA TGG ODN 2

Figure 3.7 The full sequences of the porphyrin Zipper array. ODN 1 contains six amide linked porphyrin modifications represented by **P**. ODN 2 contains six acetylene linked porphyrin modifications represented by **P**. An overhang was designed into each side of the duplex in order to attach an electron donor and electron acceptor.

As mentioned previously, the amide linker was included to add flexibility to the system whilst the rigid acetylene was designed to hold the porphyrins in the correct positions. This combination was used to maximise π-stacking of the porphyrins aiding the electron transfer capacity and the stability of the system. The Stulz group has shown in the past that arranging porphyrin units in this

alternating Zipper style stabilises the duplex by approximately 0.3 °C per porphyrin modification.[115]

Dependent on their properties and substituents, porphyrins are able to stack in several ways. Face-to-face H-aggregates[137] and edge-to-edge J-aggregates[138] can be achieved. Sanders however, reports the optimum geometry consists of a pyrrole from one porphyrin sitting over the central cavity of another porphyrin ring. Previous modelling work within the Stulz group (Macro-Model, AMBER) suggested the porphyrins in this zipper system aggregate into a slipped stack geometry with the porphyrins parallel, but slightly displaced.[115]

Once synthesised, the porphyrin-modified nucleotides were included in solid phase oligonucleotide synthesis to make the two Zipper strands. The oligonucleotide synthesis was carried out as per an unmodified sequence (section 8.7) with the porphyrin-modified phosphormidite placed on the synthesiser as would be done with any phosphoramidite. The only difference was the solvent used on the DNA synthesiser. The synthesiser is designed for phosphoramidites dissolved in acetonitrile. However, the porphyrin phosphoramidite is not readily soluble in pure acetonitrile. For this reason a 50:50 mixture of acetonitrile and DCM was used. The drawback with this solvent is the vapour pressure of the DCM being much higher than the acetonitrile. This results in the synthesiser taking up more monomer than it would do using pure acetonitrile, meaning more porphyrin-modified monomer is required than normal. Whilst wasteful, this is a necessary price to pay in order to solubilise the monomer.

The phosphorus (III) species in all phosphoramidites is unstable and is prone to oxidation to the more stable phosphorus (V) species. The porphyrin phosphoramidites appeared even more unstable than the natural bases oxidising rapidly when exposed to oxygen. For this reason the phosphoramidites are not stored and no time was wasted after the phosphitylation. Even when putting the monomer onto the DNA synthesiser immediately, achieving good coupling efficiencies can prove tricky. To try and improve on this, an extended six minute coupling time is used when coupling the porphyrin monomer. A slight improvement can be seen with this method but it is not substantial. This is by no means a limited occurrence with Glen Research and Link Technologies (commercial suppliers of phosphoramidites)

recommending extended coupling times as well as extra de-blocking and capping steps for many of their commercially available modifiers. Once a porphyrin modifier had been coupled to the growing oligonucleotide and the oxidation step carried out, the porphyrin unit appeared stable.

Including a single porphyrin modification into an oligonucleotide in this way is easily achievable. The coupling of the porphyrin monomer may be a little lower than a natural base reducing the overall yield, but working on a 1 μmol scale should provide ample modified DNA for what is required. Six porphyrin modifications however can be a bigger problem.

Standard couplings on a solid phase DNA synthesiser are 99 % efficient as a minimum. This is needed because synthesising oligos can require 20, 30 or 100 couplings. If a monomer only couples with 75 % efficiency then you instantly lose a quarter of the product. Two couplings with this monomer would then give a 56 % overall yield. It then becomes easy to see how a bad monomer can swiftly result in a tiny yield. This was the problem experienced trying to form the six porphyrin strands during this project. The graph below (Figure 3.8) shows the trityl yield (total absorption of the released DMT cation) from a synthesis of one of these multiply modified oligonucleotides. Porphyrin monomers are represented by the 5's. From this graph, a dramatic drop in the yield after each porphyrin has been added can be clearly seen resulting in a tiny trityl yield compared to where it was at the start of the synthesis.

Porphyrin Zipper Array

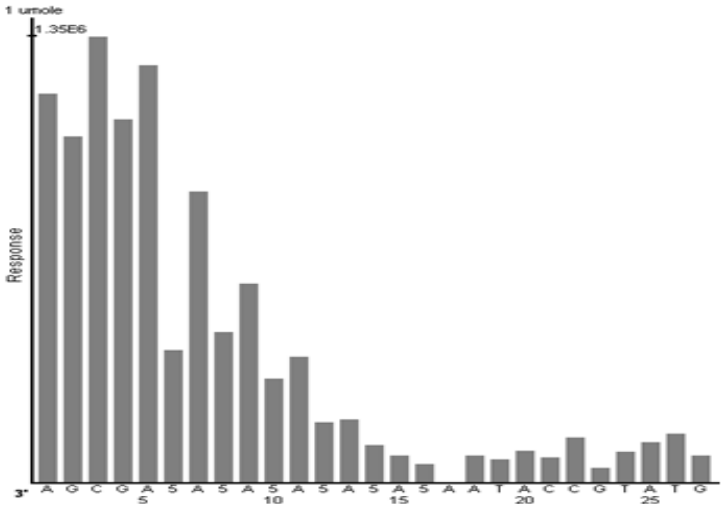

Figure 3.8 Trityl yield obtained after each coupling of a oligonucleotide synthesis. The modified porphyrin monomer is added from the 5 position of the synthesiser.

As well as low yields, the poor coupling makes the purification much trickier. An unmodified oligo synthesised with all 99 % plus couplings should produce a single product peak by HPLC. Any incomplete sequences that have been capped will result in side product peaks. Glen-Pak cartridges were used during this project as a purification method pre-HPLC. These consist of a hydrophobic resin designed to capture any oligo containing a dimethoxy trityl (DMT) group. Therefore, if the oligo is synthesised without removing the final DMT, all complete strands will be held on the resin and all truncated strands will pass straight through. Treating the column with acid then cleaves the DMT group releasing the product strand from the column. Unfortunately, due to the hydrophobic nature of porphyrins, any strand containing a porphyrin modification is retained on the Glen-Pak column. Due to this the six porphyrin strands were directly purified by HPLC.

As expected, the less than ideal coupling efficiencies resulted in lots of truncated strands, much of which contained 1 – 5 porphyrins. All these extra strands made the separation of the peaks by HPLC challenging. To try and create as much separation as possible a long, slow gradient was used, and to a degree was successful. Distinct, sharp peaks were achieved making it possible to isolate single peaks. Two HPLC chromatograms are shown in Figure 3.9.

The first shows the crude product from the synthesis of ODN 1 containing six amide liked porphyrin modifications. Below is a trace of ODN 2 containing six acetylene linked modifications.

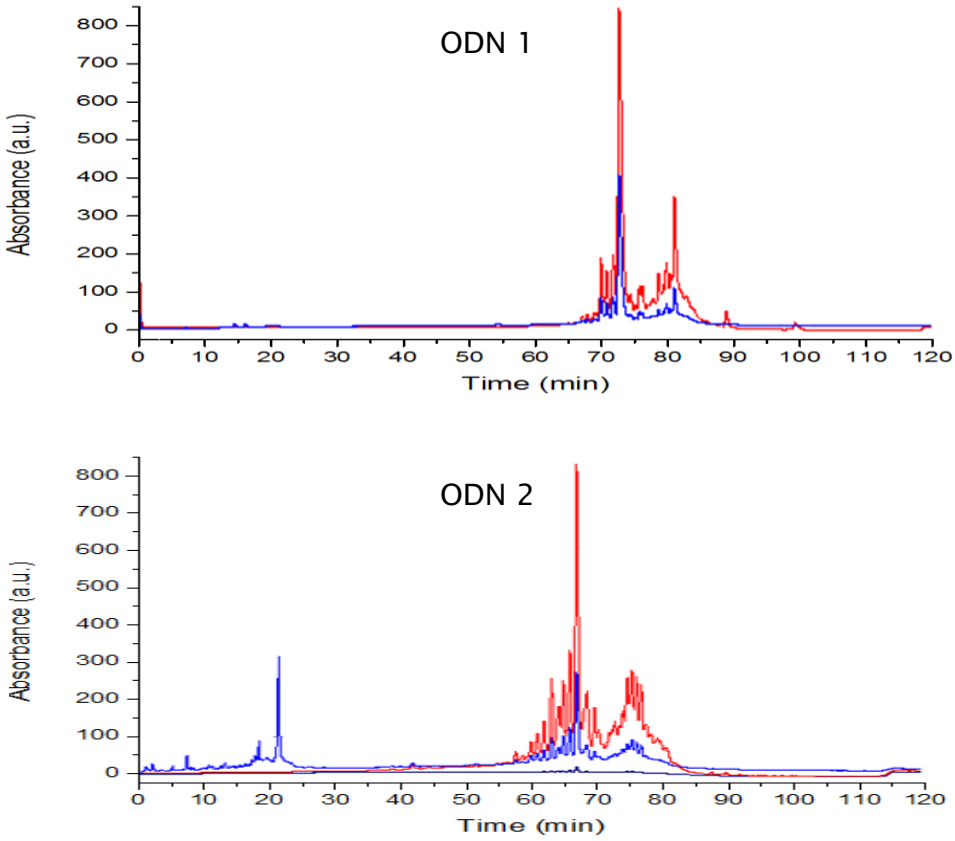

Figure 3.9 HPLC chromatograms for the crude products obtained when synthesising ODNs 1 and 2. Blue lines show absorbance monitored at 260 nm, red lines show absorbance monitored at 420 nm. A Waters XBridge OST C18 2.5 µm column (10 X 50 mm) column was used at 50 °C with buffer A – 8.6 mM TEA/100 mM HFIP and buffer B - methanol. Gradient used [time (mins) (% buffer B)]; 0 (0 %), 90 (100 %), 110 (100 %). Flow rate = 1 mL min^{-1}.

The chromatograms show two traces representing the absorbance of DNA at 260 nm (blue line) and the porphyrin absorbance at 420 nm (red lines). The absorbance was monitored by a UV-Vis spectrometer built into the HPLC system. As can be seen from the chromatograms, there are lots of peaks showing both DNA absorbance (blue) and porphyrin absorbance (red) between 60 and 80 minutes. This would suggest these peaks all represent porphyrin-modified DNA. The retention time of these compounds is also a positive sign.

Porphyrin Zipper Array

Porphyrins are highly hydrophobic and as such will have a strong affinity for the hydrophobic C18 column. When considering this with the percentage of methanol needed in the solvent mixture before these compounds come off the column, it suggests that these are all oligonucleotides containing porphyrin modifications.

With so many porphyrin-DNA peaks, it is hard to determine which peak corresponds to the full oligos. Based on the fact that there can be no more than six porphyrins on any strand, it was assumed that the desired product would show the highest absorbance at 420 nm. As more porphyrins are added, the hydrophobic nature of the oligo will increase resulting in longer retention times for the compounds containing the most poprhyrins. By this logic, the desired peak should be the largest in terms of DNA absorbance, have the largest ratio of porphyrin to DNA absorbance and have a higher retention time than the truncated strands. This gives one peak substantially larger than the rest in each chromatogram which was collected as the product.

Having said the desired oligo should be the last compound to come off the column, a few small peaks do appear at higher retention time. As even the coupling of the unmodified bases was not perfect, these peaks have been assigned as strands containing all six porphyrins, but not all of the unmodified bases after. As such, there would be the same number of porphyrins on a shorter strand, making the overall compound more hydrophobic than the desired oligo.

By carrying out the porphyrin-modified oligonucleotide syntheses and purifications as described, 108 nmol of ODN 1and 42 nmoles of ODN 2 were collected. These values were calculated by measuring the absorbance of a sample in water at 260 nm and using the Beer-Lambert law (Equation 1).

$$A = \varepsilon cl$$

Equation 1 The Beer-Lambert law. A = Absorbance. ε = molar extinction coefficient (M^{-1} cm^{-1}). c = Concentration (M). l = Pathlength (cm). The molar extinction coefficient was calculated using the ATDBio Oligo calculator[139] replacing the value of a T base (7830 M^{-1} cm^{-1}) with 13460 M^{-1} cm^{-1} for every porphyrin modification as determined by Fendt *et al.*[14]

The only way to confirm that the correct products have been collected is to acquire mass spectrometry data. However, due to the number of porphyrins on the oligo, this has yet to be achieved by any mass spectroscopy method.

With the Zipper strands synthesised and purified the electron transfer experiments can be carried out. However, these experiments were not attempted during the course of this work as the necessary equipment and expertise were not available to us. For this reason, the other parts of this work were prioritised. A plan is now in place however to continue this work in collaboration with Professor Jerzy Radecki (Olsztyn, Poland). Previous work with Prof. Radecki has provided excellent experience in the electrochemical analysis of porphyrin-modified DNA.[140] With this experience it is hoped that the desired electron transfer along the porphyrin Zipper array can be measured to complete this project.

3.5 Single Molecule Spectroscopy of Porphyrin-Modified DNA

A second goal of this project was to try and establish whether this Zipper array forms an extended π-system over the whole molecule, or if the porphyrins behave as individual electronic units. The plan was to investigate this using single molecule spectroscopy in collaboration with Dr Andrew Hudson, University of Leicester. For this, the ODNs containing six porphyrin modifications needed to be re-made.

The single molecule spectroscopy requires the oligos to be attached to a surface. This led to a further modification of one of the sequences attaching a 5'-biotin modification (Figure 3.10). Biotin is a naturally occurring molecule which can be bound by the avidin and streptavidin proteins.[141, 142] This binding produces the highest binding constant found in nature. Using a surface bound streptavidin and a biotin labelled duplex, a single duplex can be captured and held on the surface.

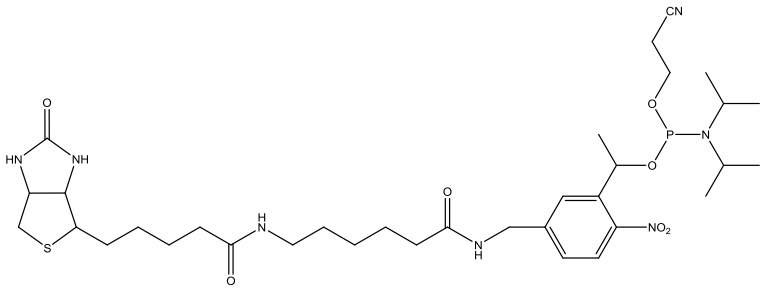

Figure 3.10 Structure of the biotin modifier commercially available from Link Technologies.

As well as the Zipper strands, the unmodified strands and strands with a single porphyrin modification were designed as controls. The sequences of ODNs 3 – 8 are shown in Figure 3.11.

5’ – GGC CAT CGT CGC **PAP** A**P**A **PAP** A**P**A TTA T – 3’	ODN 3
5’ – GGC CAT CGT CGC TAT ATA **P**AT ATA TTA T – 3’	ODN 4
5’ – GGC CAT CGT CGC TAT ATA TAT ATA TTA T – 3’	ODN 5
3’ – A GCG A**P**A **PAP** A**P**A **PAP** AAT ACC GTA TGG – Biotin - 5’	ODN 6
3’ – A GCG ATA TA**P** ATA TAT AAT ACC GTA TGG – Biotin - 5’	ODN 7
3’ – A GCG ATA TAT ATA TAT AAT ACC GTA TGG – Biotin - 5’	ODN 8

Figure 3.11 Sequences of ODN’s 3 – 8 designed for single molecule spectroscopy. The amide linked porphyrin modifications are represented by **P**. The acetylene linked porphyrin modifications are represented by **P.**

With differing combinations of these oligos, single molecule spectroscopy was to be used to analyse the unmodified duplex, two porphyrin system, six porphyrin strand with its unmodified complement and all the way up to the full Zipper array.

The initial synthesis attempted to make ODNs 3 and 4, the six acetylene linked porphyrin oligo and its one porphyrin analogue. This work was carried out alongside Dr Iwona Mames of the Stulz group. The coupling of the porphyrin monomer, whilst not brilliant, was enough to produce both the six porphyrin strand and the one porphyrin strand. Dr Mames purified the crude products by HPLC collecting 5.0 nmoles of the purified ODN 3 and 28.5 nmoles of ODN 4. Subsequently, Dr Mames has synthesised ODNs 6 and 7 collecting 4.7 nmoles and 33.6 nmoles respectively.

Dr Hudson requested a 1 mL sample of a 50 nM solution to carry out single molecule spectroscopy. This corresponds to 50 pmoles of DNA in the sample. This shows to obtain the measurements that are wanted, the porphyrin oligonucleotide synthesis does not need to be that high yielding. However, a better synthesis with more product is easier to handle and much easier to purify.

Porphyrin Zipper Array

Time restrictions prevented any further work on this system being carried out as part of this project. The work has since been carried on by Dr Mames who has been working to prepare the samples ready to be tested by single molecule spectroscopy.

3.6 Conclusions: Porphyrin Zipper Array

The porphyrin Zipper array proved to be a challenging part of the project. The syntheses of the two porphyrin-modified nucleotides threw up several difficulties but these were all overcome and both nucleotides were successfully synthesised.

Numerous attempts have been made to synthesise the six porphyrin oligonucleotides using automated solid phase DNA synthesis. However, none of these attempts have produced the required strand in a good yield. There are many potential reasons why this synthesis has not been very successfully, and a combination of reasons is likely the cause. The quality of the phosphoramidite plays a major role in oligonucleotide synthesis. This nucleotide could be degrading or oxidising at any point in the phosphitylation reaction, or when on the synthesiser. The phosphitylating reagent may itself not be of the highest quality resulting in poor couplings. An argon atmosphere was employed during the phosphitylation as a better alternative to nitrogen, and fresh phosphitylating reagent purchased at regular points during the project. These steps should minimise the chances of obtaining a bad porphyrin nucleotide. There were also no errors observed in technique whilst carrying out the phoshitylation so hopefully this is not the source of the problem.

There is further room for error on the synthesiser. Lots of solvents and reagents are used during oligonucleotide synthesis which all need to be oxygen and water free. Using fresh reagents did improve couplings a little, but not remarkably. The Stulz group has previously reported the synthesis of oligonucleotides with six or more porphyrin modifications showing it to be possible.[115] Getting this synthesis working with higher coupling efficiency is the key to taking this project forward.

Although the oligonucletide syntheses were low yielding, some six porphyrin strands were successfully synthesised. HPLC purification of the crude product was the next step and brought its own challenges. A lot of time was spent optimising a protocol for this purification and has been fairly successful. Lots of porphyrin containing products were seen on the chromatograms, but the

optimised gradient separated these into clear sharp peaks which could be isolated.

After this point, this system took a back seat as other areas of the project were prioritised, and little further progress was made. Another member of the Stulz group will now take this system forwards. To do this she must first synthesise the oligos with acceptable yields. Once a pure six porphyrin strand has been isolated, attempts need to be made to characterise and confirm this product. All attempts at this so far have proven unsuccessful.

The next step would be to test the system for its electron transfer properties and stability in a lipid bilayer. The electron donor, $K_4Fe(CN)_6$, and electron acceptor, anthraquinonesulfate, used by Drain will be utilized with the Zipper system.

The other measurements required are for the single molecule spectroscopy. With the six porphyrin strands containing a biotin modification now synthesised these measurements should be obtained fairly rapidly.

Porphyrins connected by hydrogen bonding and metal ion coordination have been shown to transfer electrons across a lipid bilayer when using white light as an excitation source. The Zipper system was designed to mimic this electron transfer but in a more stable system. The aim of this part of the project was to test this electron transfer of the full Zipper array in a lipid membrane. These measurements could not be obtained but good strides have been made and the work will be continued following a clear path.

4. Click Chemistry for the Attachment of Porphyrins onto DNA

4.1 Introduction to the Copper Catalysed Azide-Alkyne Cycloaddition

The copper catalysed azide-alkyne cycloaddition (CuAAC) is one of a group of reactions described by the term click chemistry, a phrase coined by K Barry Sharpless. Click chemistry is designed with nature's preferred methods in mind, combing small molecules in quick, easy and reliable reactions.[143] Developed from the Huisgen 1, 3-dipolar cycloaddition,[144, 145] the CuAAC reaction, as the name suggests, reacts an azide with an alkyne to form a stable triazole. To Sharpless, cycloaddition reactions involving heteroatoms represent the ideals of click chemistry. The hetero-Diels-Alder[146, 147] reaction has been widely employed by chemists, but it is the Huisgen 1, 3-dipolar cycloaddition of azides and alkynes which Sharpless regards as "the cream of the crop", owing to its high dependability and specificity.[143, 148]

Azides are reactive towards alkynes without the presence of a catalyst, but this requires elevated temperatures and long reaction times. This results in a mixture of the 1, 4 and 1, 5 products (Scheme 4.1) from the concerted cycloaddition reaction. Despite their reactivity towards each other, azides and alkynes are amongst the least reactive functional groups in organic chemistry. This lack of interaction with solvents and other molecules makes the azide-alkyne cyclooaddition a valuable tool for biological systems. The general reaction scheme is shown in Scheme 4.1.

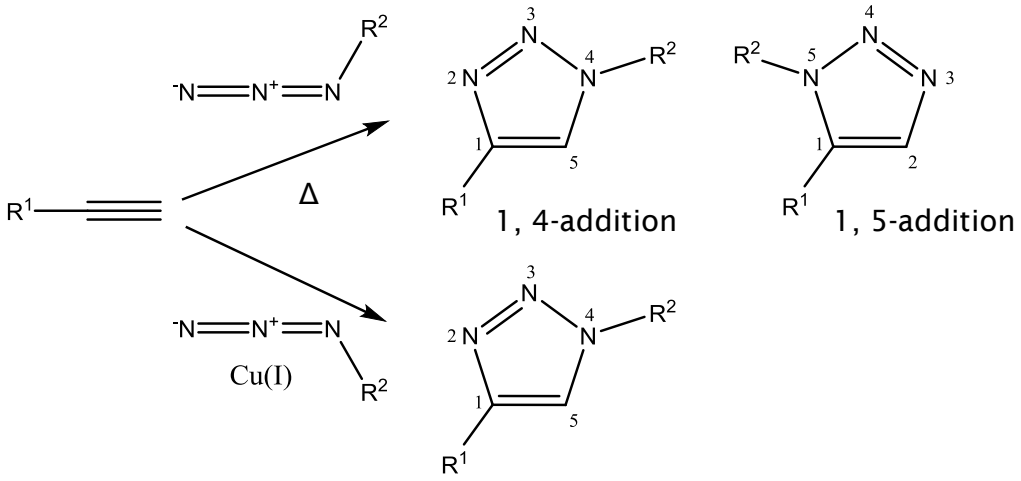

Scheme 4.1 General reaction scheme for the azide-alkyne cycloaddition with and without a Cu(I) catalyst. The copper (I) source is usually in the form of a copper (I) halide.

Whilst a mixture of products is seen from the reaction without copper, the 1, 4-addition is favoured over the 1, 5-addition. This arrangement places the majority of the two molecules (the R groups) at opposite ends of the system reducing the steric clash and resulting in a lower energy system.

The addition of a copper (I) catalyst leads to complete conversion to the 1, 4 product. This is formed via a six-membered ring intermediate as is demonstrated in the full catalytic cycle (Scheme 4.2) suggested by Sharpless and Fokin.[149] The activation energy to form this ring system has been calculated at 14.9 kcal mol^{-1}.[150] This is considerably lower than the barrier of 25.7 kcal mol^{-1} for the uncatalysed reaction and results in a 10^6-fold increase in the rate of reaction whilst allowing it to be carried out at ambient temperature.

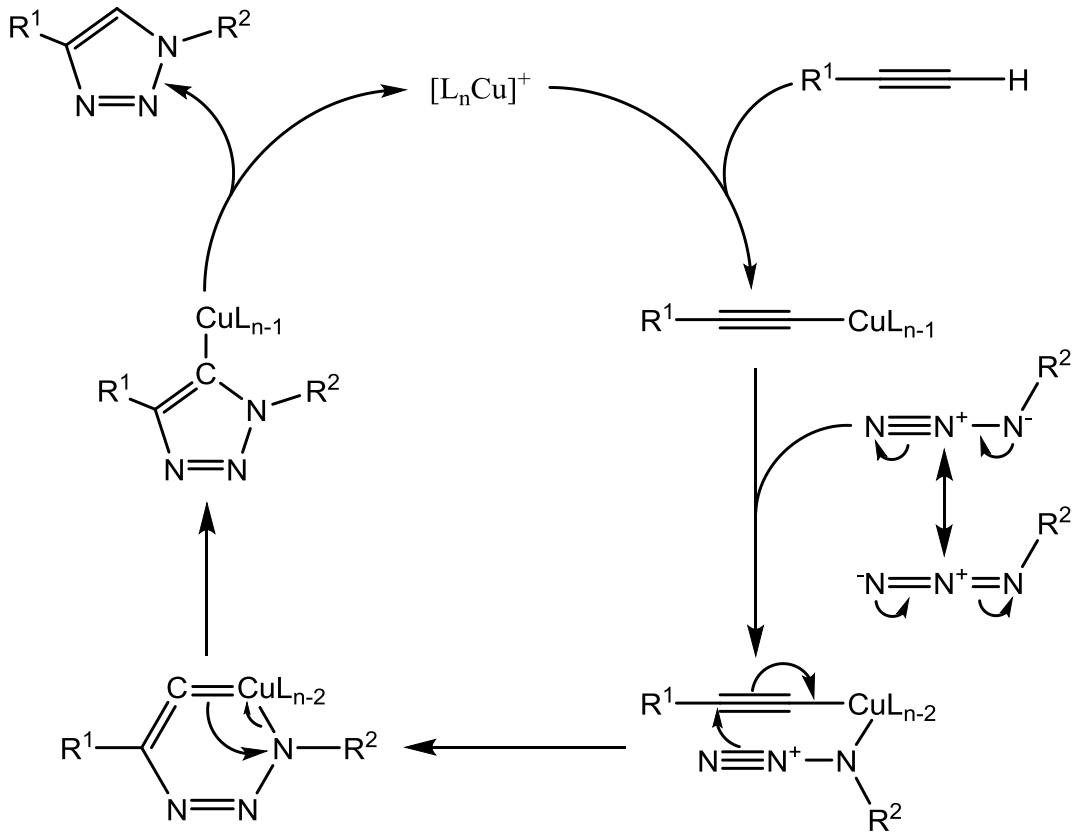

Scheme 4.2 Full catalytic cycle of the copper catalysed azide-alkyne cycloaddtion (CuAAC) reaction.[150]

Copper (I) as a catalyst drastically increases the rate of reaction but is not without its problems. The thermodynamic instability of Cu (I) quickly results in oxidation to Cu (II) and/or disproportionation to Cu (0) and Cu (II).[151-153] For this reason, reactions involving a copper (I) catalyst (such as Sonogashira coupling) require carefully controlled conditions free of oxygen. Historically, soft ligands such as nitriles and guanidines have been used to stabilise the copper.[152] However, these ligands either bound the copper too loosely to stop the degradation, or too tightly suppressing the catalytic activity. This led to a series of copper (I) stabilising ligands, the most common of these being tris (benzyltriazolylmethyl)amine (TBTA).[152] The structure of this ligand is shown in Figure 4.1 along with its water soluble version tris (3-hydroxypropyltriazolylmethyl)amine (THPTA).[154] As these compounds contain three triazole groups, they are themselves formed using click chemistry. These ligands are able to bind the copper preventing oxidation, whilst retaining the catalytic activity.

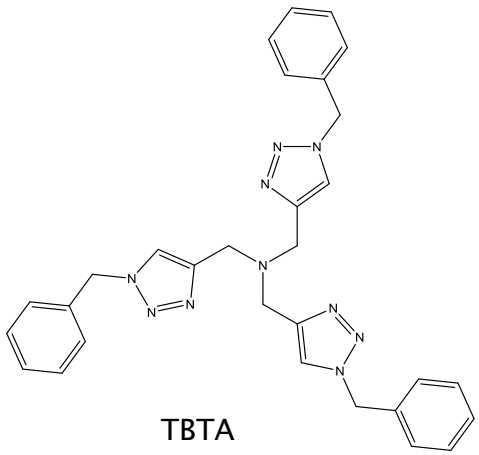

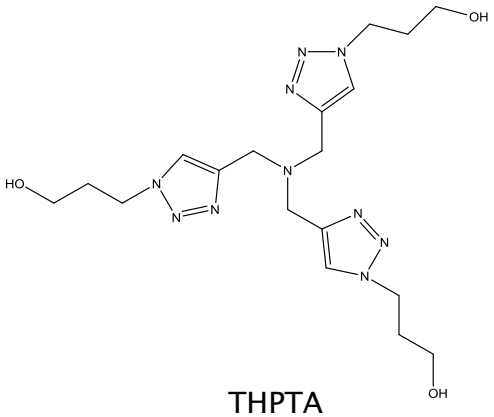

Figure 4.1 The structure of the TBTA ligand and the water soluble THPTA ligand.

The water soluble THTPA ligand is of great use for biological conjugations which take place in completely aqueous environments. Labelling of cells, proteins and DNA are all of great interest and the THPTA ligand allows biocompatibility for the click reaction whilst removing concerns of denaturing secondary structures.[155]

In biological systems, the copper oxidation process causes much bigger problems than just the loss of catalytic activity. Copper is cytotoxic and can generate reactive species such as superoxide radicals, hydroxyl radicals and hydrogen peroxide which can damage biomolecules and disturb the metabolic balance of the target system.[156-158] Proteins can be irreversibly oxidised and lose their biological functionality, whereas the structure of the DNA double helix can be altered or broken by a number of mechanisms.[153, 159] Carell and others have reported a range of adducts corresponding to strand breaks when attempting copper catalysed click reactions using DNA without the presence of a stabilising ligand.[160-162] This potential damage makes the presence of the stabilising ligand of even greater importance when carrying out click chemistry on biological systems.

Since the early 2000s, click chemistry and the copper catalysed Huisgen reaction, have found a wide variety of uses ranging from combinatorial chemistry to the labelling of different biomolecules. Sharpless *et* al. produced large chemical libraries using solution phase synthesis,[148] whereas polymer

bound azides have been employed by the group of Yli-Kauhaluoma.[163] Proteins and enzymes have also been the subject for click reactions with Sharpless and Finn employing click chemistry *in situ* with the enzyme acetylcholinesterase to synthesise its own inhibitor.[164]

Fluorescence labelling of biomolecules has been the focus of many groups. Finn *et al*.[165] were able to use the copper catalysed azide-alkyne cycloaddition to attach a fluorescein dye molecule to a virus, whilst Ju *et al.* fluorescently tagged oligonucleotides for the purpose of DNA sequencing.[166] The attachment of dye molecules is not the only use found for the click reaction with DNA.[167] Immobilisation, ligation and cross-linking of oligonucleotides have all been reported.[168-170]

The copper catalysed azide-alkyne cycloaddition has proved to be one of the most popular click reactions and with good reason. The lack of reactivity of the components, except towards each other, makes the reaction highly selective and reliable. Combined with its aqueous compatibility, the cycloaddition becomes an extremely useful bioorthogonal reaction with a wide variety of uses.

4.2 Labelling Oligonucleotides with Porphyrins using the Baseclick Oligo-Click Kit

An oligonucleotide labelling kit was provided by Dr Antonio Manetto of Baseclick, Tutzing, Germany.[171] This kit was designed for the labelling of oligonucleotides with fluorescent dyes using the copper catalysed azide-alkyne cycloaddition. The reagents were supplied, and included an azide modified fluorescein dye molecule.

However, this project was not designed for the attachment of a fluorescein modification. Instead, a porphyrin azide molecule was to be the modifier. This was produced by first converting 3-bromoproylamine hydrobromide into 1-amino-3-propyl azide (**13**) following the procedure of Nolte *et al.*[172] An amide coupling reaction was then carried out with zinc metalated TPP acid to produce the porphyrin azide. This is summarised in Scheme 4.3. Further details can be found in section 5.3.

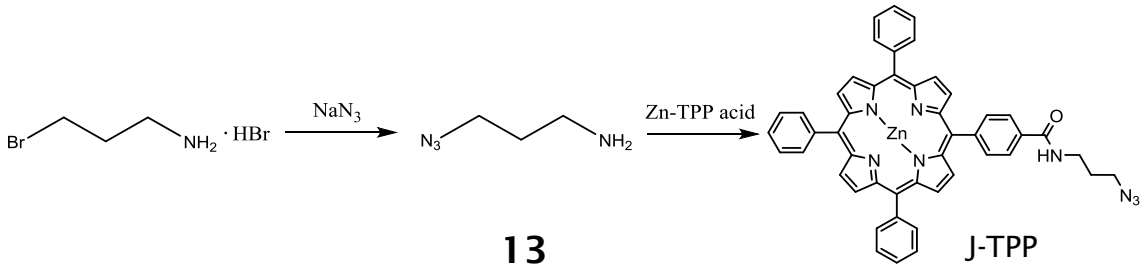

13 J-TPP

Scheme 4.3 Production of zinc tetraphenyl porphyrin azide (J-TPP).

Using copper catalysed azide-alkyne cycloaddition to modify oligonucleotides with porphyrins provides an alternative to the porphyrin nucleosides synthesised in Chapter 3. This post synthetic labelling would allow the porphyrin to be attached to the pre-synthesised oligo and could prove to be a better method for synthesising porphyrin-modified DNA. As has been shown in this work (section 3.4), achieving high level coupling with this kind of modified phosphoramidite can prove tricky. Having a highly efficient post synthetic labelling alternative would be highly valuable.

As the porphyrin was modified with an azide functional group, the DNA needed to be modified with an alkyne. This alkyne-modified DNA was again provided by Baseclick and used a C8-alkyne modified thymine base (Figure 4.2) first employed by Thomas Carell.[160] This nucleoside contains an eight carbon chain with a terminal alkyne from the thymine 5-position. The long linker is incorporated to reduce steric restrictions when attaching multiple molecules onto a single oligonucleotide.

Two oligonucleotides were provided, the first (ODN 9) containing a single alkyne modification at the 5'-terminus, the second (ODN 10) with five internal modified bases. The different oligos allowed both single and multi-labelling click reactions to be tested.

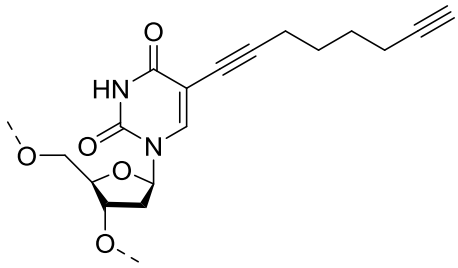

5' – **X**TG GTA TCG CTA TCG CTA TGG C – 3' ODN 9

5' – CA**X** TGA **X**GG CGG CC**X** TCG TA**X** GGA AAA **X**A – 3' ODN 10

Figure 4.2 Alkyne modified monomer (C8-Alkyne-dU) used for the porphyrin-DNA CuAAC reactions. Also shown are the sequences of the singly and multiply modified oligonucleotides provided by Baseclick. **X** = C8-Alkyne modification.

As well as the DNA, the copper (I) source was provided by Baseclick in the form of copper metal. This solid, heterogeneous catalyst is air stable and remains insoluble in both aqueous and organic solvents. This was used in place of the more common CuBr or CuI catalysts to ease handling. An activator solution was also included in the Oligo-Click kit. This solution contains the copper binding ligand and is to be added to the catalyst before the addition of the other reagents. The recommended solvent for the reactions was a 3:1 mixture of DMSO and t-BuOH, but for this project a DMF/water mixture was used

instead. An aqueous/organic extraction was to be used to work-up the reaction instead of the suggested ethanol precipitation in order to remove the excess porphyrin. It was feared the DMSO could be difficult to remove by this method and so was best avoided.

The Zn metalated tetraphenyl porphyrin azide J-TPP (shown in Scheme 4.3) was used to test the click reaction along with two similar porphyrin azides (Figure 4.3). These two compounds were synthesised by Vasilis Nikolaou working under the supervision of Prof Athanassios Coutsolelos at the University of Crete, Greece. The three porphyrin compounds will be referred to as J-TPP, V-TPP and V-DMP as labelled in the figures.

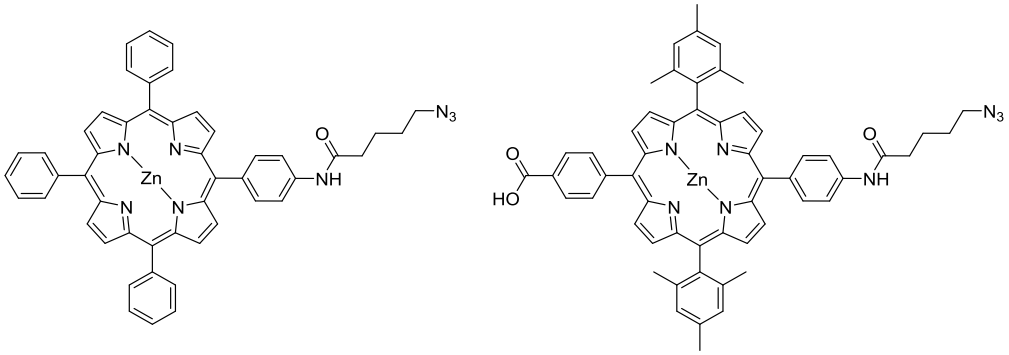

V-TPP V-DMP

Figure 4.3 The porphyrin azides synthesised by Vasilis Nikolaou. These are a tetraphenyl porphyrin (V-TPP) and a 5-(4-carboxyphenyl)-15-[4-(5-azidopentanamidophenyl)]-10, 20-bis(2, 4, 6-trimethylphenyl)porphyrin (V-DMP).

The full synthetic procedure for these CuAAC reactions is outlined in section 8.12.1, and is briefly described here.

The activator (ligand) solution was first added to the copper catalyst in a reactor vial thoroughly flushed with argon. To this was added the alkyne-modified oligonucleotide in water (5 nmoles in 5 µL), and the porphyrin azide in DMF (50 µL). A large excess of DMF was used compared to the water due to the insolubility of all three porphyrins in aqueous solvent. A sample with more water than DMF (2:1) was tested but the porphyrins precipitated out of solution and no reaction took place. Once all reagents were added, the reactor vial was

sealed under argon. The reaction mixture was maintained at 25 °C with shaking. Varying time scales over the range of a few hours to five days were tested with 24 – 48 hours found to produce the best results. After this time no progression in the reaction could be detected by HPLC.

When the reactions were deemed to be complete, a mini extraction with water and ethyl acetate was carried out to remove the large excess of porphyrin (50 equiv. to the DNA) used in each reaction. The aqueous layer was sequentially washed with aliquots of ethyl acetate until the dark red/purple colour of the first wash was replaced by a colourless organic layer. This lack of colour suggested the majority of the free porphyrin had been removed from the vial.

During this process any DNA, porphyrin modified or unreacted, remained in the aqueous layer. A slight red colour to this aqueous layer (when the organic was colourless) was an early indication that the reaction had been successful to at least some degree. The progress of the reaction was quantified and the porphyrin-modified DNA isolated using HPLC. Chromatograms of single labelling reactions with ODN 9 and each of the three porphyrins are shown in Figure 4.4.

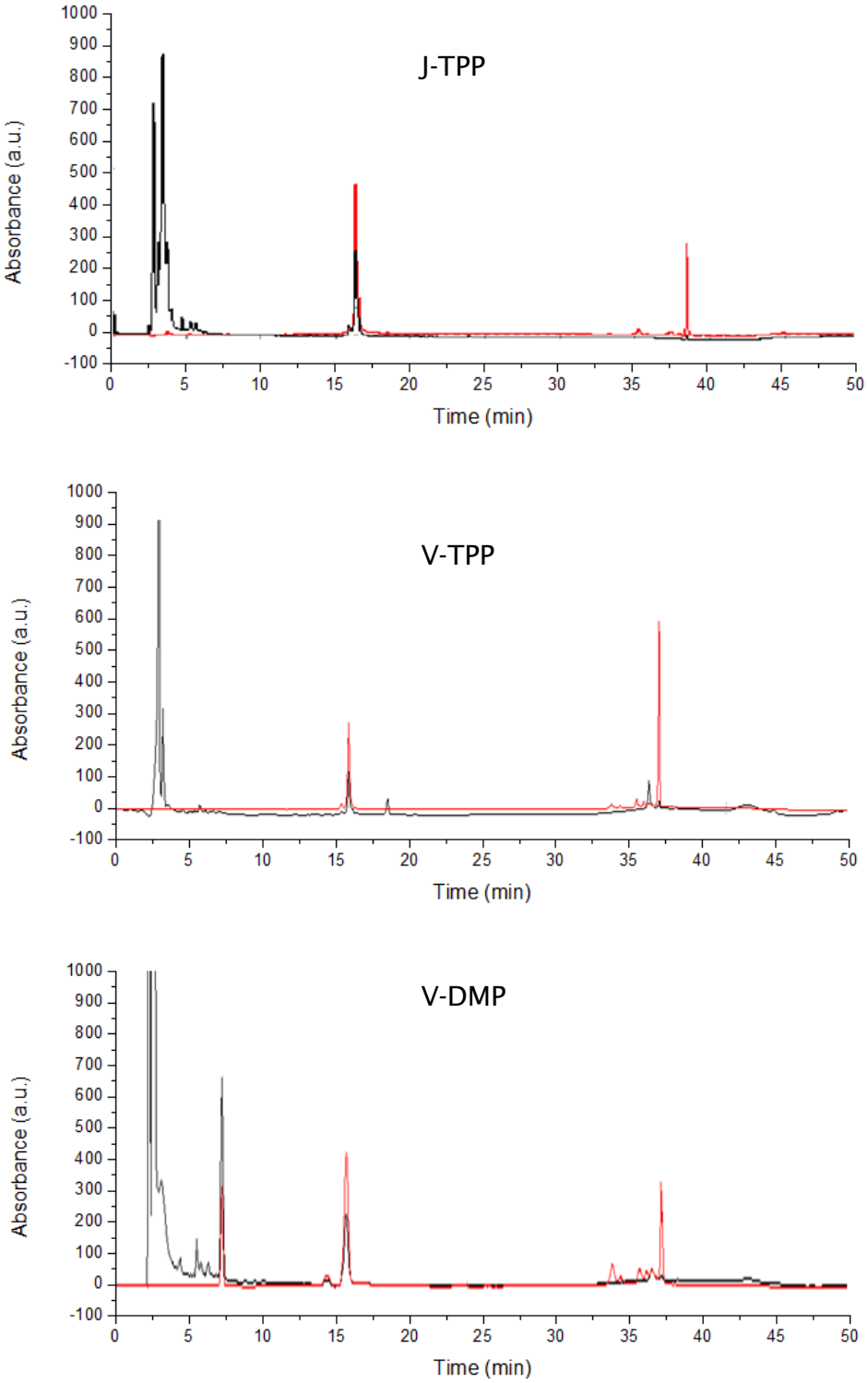

Figure 4.4 HPLC chromatograms for CuAAC single labelling reactions using the Baseclick Oligo-Click kit with ODN 9 and each of the three porphyrins. Chromatograms taken at reaction time 48 hours. A Polaris 3 C18-A 150 × 4.6 mm column was used at 60 ˚C with buffer A – 8.6 mM TEA/100 mM HFIP with 0.5 mM EDTA and buffer B - methanol. Gradient used [time (mins) (% buffer B)]; 0 (0 %), 15 (60 %), 30 (70 %), 35 (100 %). Flow rate = 1 mL min^{-1}.

Two traces are displayed on the chromatograms, the absorbance measured at 260 nm to monitor for the presence of DNA (black lines) and 420 nm for porphyrin absorption (red lines). There are three clear areas of interest in the chromatograms. A single peak at approximate retention time of 38 minutes shows absorbance at 420 nm but not at 260 nm. This suggests there is a small amount of free porphyrin remaining in the aqueous layer after the work-up. Below five minutes is a group of peaks showing absorbance at 260 nm but not 420 nm, suggesting this is all unreacted DNA. Assuming the oligo provided by Baseclick had been purified, a single peak would be expected. Multiple peaks suggest multiple strands, and could therefore suggest some degradation products are present despite the inclusion of the stabilising ligand.

The most important peaks appear at approximately 17 minutes in each of the chromatograms. As shown by both red and black traces, these compounds are absorbing at both 260 nm and 420 nm, suggesting the presence of porphyrin-modified DNA. This is supported by the UV-Vis spectrometer built into the HPLC which shows characteristic porphyrin-DNA spectra (peaks = 260 nm – DNA, 420 nm – Soret band, 500 – 700 nm 2 Q-bands). The shifted retention time is also a strong indicator of a successful reaction. The large hydrophobic porphyrin modification would be expected to slow the porphyrin-modified DNA's progression through the column, retaining it for longer. Taking all this into account strongly suggests each of the three porphyrins have been attached to ODN 9 using the CuAAC reaction. From the relative intensities of the peaks however, it does appear there is far more unreacted DNA remaining than there is porphyrin-modified DNA produced.

One more peak of interest can be seen in the V-DMP chromatogram. A peak appearing to be porphyrin-DNA is seen at approximately 7 minutes. This was also seen in the chromatograms produced by the other two porphyrins when the reactions were left for five days. This suggests this peak could be a degradation product which has formed in the V-DMP much earlier than the other reactions. The reason for this however is unknown.

Confirmation of the singly modified products was given using MALDI-ToF mass spectrometry carried out by Vasilis Nikolaou at the University of Crete, Greece. The acquired spectra are shown in Figure 4.5, with the calculated masses of

the unmodified and porphyrin-modified oligo's, and the experimentally obtained peak maxima combined in Table 4.1.

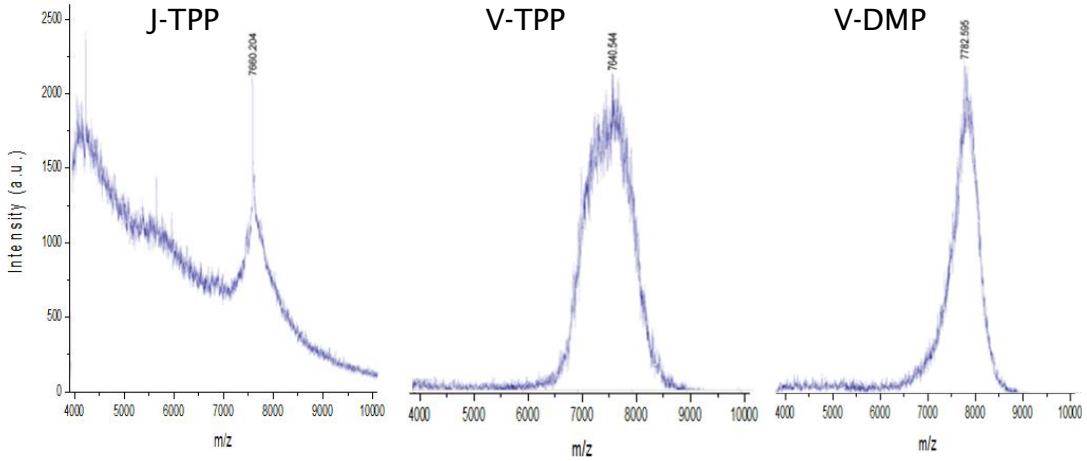

Figure 4.5 MALDI-ToF mass spectra for each of the products produced by the single labelling CuAAC reactions using each of the three different porphyrins. Data acquired on a Bruker UltrafleXtreme MALDI-ToF spectrometer.

ODN	Calculated Molecular Mass	Peak maximum by MALDI
ODN 9 (unmod)	6822	-
ODN 9 + J-TPP	7626	7660
ODN 9 + V-TPP	7638	7640
ODN 9 + V-DMP	7768	7782

Table 4.1 Calculated molecular masses and values obtained by MALDI-ToF mass spectrometry for the singly modified oligonucleotide reacted with each of the three porphyrins.

None of the values obtained from the MALDI-ToF mass spectrometer are perfect, but they are all in the correct region and significantly higher than the 6822 expected if only unmodified ODN 9 remained in the reaction mixture. Further to this, in all the acquired spectra only a single peak is seen. This however, is a very broad peak but does cover the calculated mass.

This work has shown the CuAAC reaction can be used to attach porphyrins onto alkyne-modified DNA. However, in its current form the reaction appears

low yielding. This reaction was attempted numerous times with varied reaction times, temperatures and reactant ratios but no improvement could be found. Higher yielding conditions may yet be found given more time and further work on this project.

With the single labelling reaction complete the multiple labelling was attempted using ODN 10 (Figure 4.2) and each of the three porphyrins.

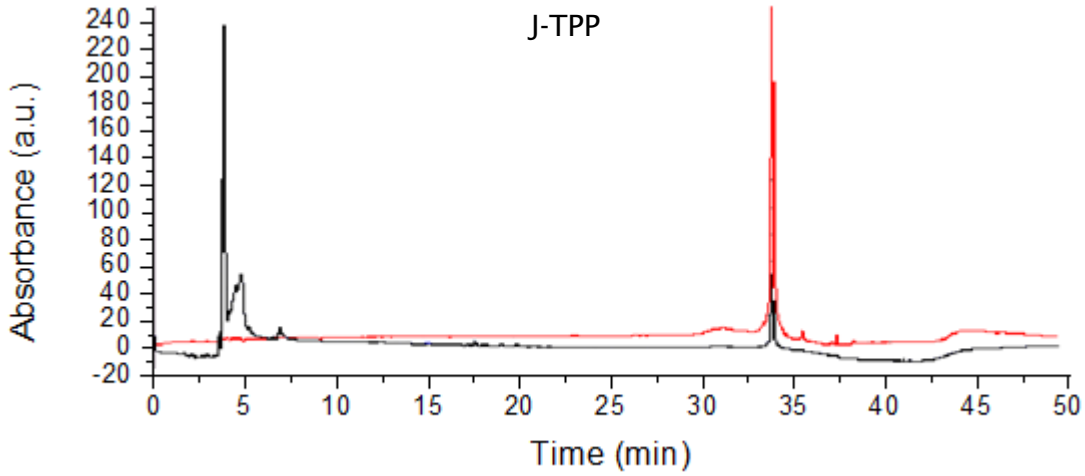

Figure 4.6 HPLC chromatogram for CuAAC multiple labelling reaction using the Baseclick Oligo-Click kit and porphyrin J-TPP. A Polaris 3 C18-A 150 × 4.6 mm column was used at 60 °C with buffer A – 8.6 mM TEA/100 mM HFIP with 0.5 mM EDTA and buffer B - methanol. Gradient used [time (mins) (% buffer B)]; 0 (0 %), 15 (60 %), 30 (70 %), 35 (100 %). Flow rate = 1 mL min^{-1}.

The chromatogram presented in Figure 4.6 is that produced by the multi-labelling reaction between ODN 10 and the porphyrin J-TPP. Only two peaks are present, unreacted DNA below 5 minutes, and unreacted porphyrin around 35 minutes. A small 260 nm component (black trace) is present in the peak at 35 minutes. When considering the aim to attach five porphyrins onto a single oligonucleotide, the 420 nm (red) absorbance would be expected to be much greater than the black. This initially led to the belief the reaction had been successful. However, smaller peaks corresponding to 1, 2, 3 and 4 attached porphyrins were expected, and is indeed what was observed by Carell and his

team during their attempts at labelling oligos with different azide compounds.[160] These are not present in the produced chromatogram suggesting no porphyrins had been attached at all. Further proof of this was provided by the UV-Vis spectra of the peak at 35 minutes. Absorptions for the porphyrin B and Q bands were clearly visible, but no clear DNA absorbance could be seen. The small absorbance at 260 nm on the HPLC chromatogram has been attributed to the porphyrin and the attached phenyl groups. No labelling was observed when using one of the other two porphyrin azides either.

It is strange that absolutely no labelling has been observed with ODN 10 given that the single labelling reaction did produce some porphyrin-modified DNA. ODN 9 contains only one alkyne modification and this is located on the terminal nucleobase. All five modifications in ODN 10 are internally situated. It is therefore possible that modifying a terminal nucleobase with the porphyrins is possible, but internal modification is not. This is perhaps due to increased sterics at the internal modification sites compared to at the end of the DNA strand. To check whether this is the case an oligo with a single internal modification would need to be acquired and tested under the same reaction conditions.

From the experiments carried out and the results presented in this section, it is clear that the Baseclick Oligo-Click kit can be used to attach a porphyrin azide onto alkyne-modified DNA using the copper catalysed azide-alkyne cycloaddition reaction. However, using the current method, only terminal modification can be achieved and then only in low yields. There is also evidence suggesting the unmodified oligonucleotide is being degraded during the course of the reaction. In order to produce porphyrin-modified DNA in any substantial quantity requires further tuning of the method and reactants. Furthermore, attempts at labelling five positions on a single oligonucleotide in a one pot reaction have produced no positive results. This lack of reactivity may be a result of the internal modifications but further investigations are required to determine the full potential of the multiple coupling reaction.

4.3 Introduction to Copper-Free Click Chemistry

The copper mediated damage of biomolecules and the inclusion of a copper stabilising ligand in the CuAAC reaction were discussed in section 4.1. Another way to avoid this damage to cells and biomolecules is to remove the copper from the system entirely. Copper-free click chemistry has been pioneered by Carolyn Bertozzi and was designed to proceed rapidly and selectively *in vivo* without perturbing native biochemical functionality.[173, 174] In order for the reaction to occur without the copper catalyst, the activation energy needs to be lowered in a different way. This is done using a strained alkyne and is demonstrated by the energy level diagrams produced by Bertozzi *et al.* shown in Figure 4.7.[175]

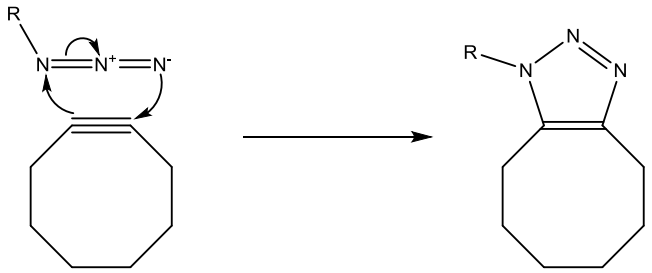

Scheme 4.4 Mechanism of copper free Click chemistry using a strained cyclooctyne.

The energy level diagrams below show the differing energy pathways for click reactions involving a normal, linear alkyne and a strained cyclooctyne. The values for these energy diagrams were calculated using a density functional theory based transition state model following on from the work of Houk and co-workers.[21, 176, 177]

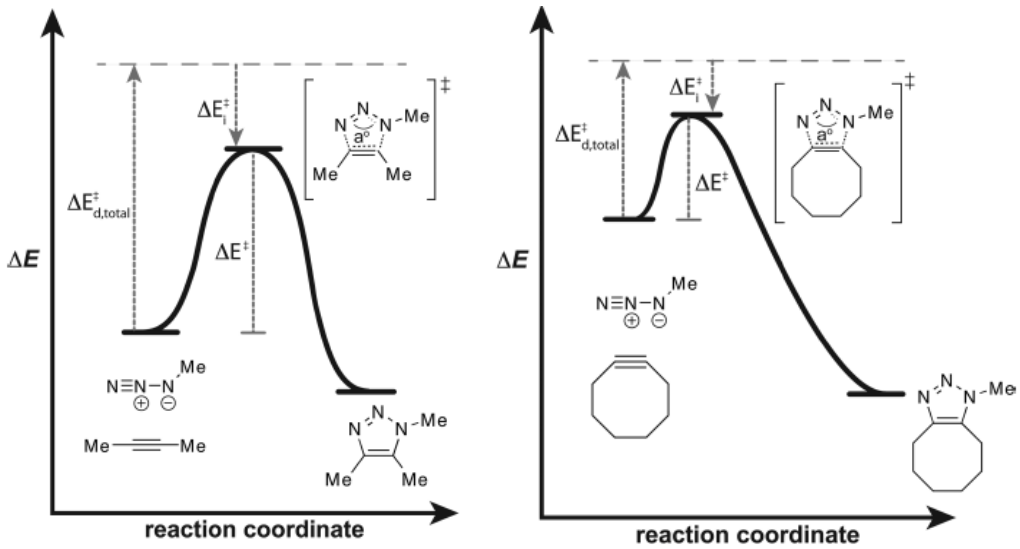

$\Delta E^{\ddagger}_{d,butyne} = 10.1\ kcalmol^{-1}$
$\Delta E^{\ddagger}_{d,azide} = 19.8\ kcalmol^{-1}$
$\Delta E^{\ddagger}_{d,total} = 29.9\ kcalmol^{-1}$
$\Delta E^{\ddagger}_{i} = -9.0\ kcalmol^{-1}$
$\Delta E^{\ddagger} = 20.9\ kcalmol^{-1}$
$a° = 137°$

$\Delta E^{\ddagger}_{d,cyclooctyne} = 2.1\ kcalmol^{-1}$
$\Delta E^{\ddagger}_{d,azide} = 15.2\ kcalmol^{-1}$
$\Delta E^{\ddagger}_{d,total} = 17.3\ kcalmol^{-1}$
$\Delta E^{\ddagger}_{i} = -6.9\ kcalmol^{-1}$
$\Delta E^{\ddagger} = 10.4\ kcalmol^{-1}$
$a° = 141°$

Figure 4.7 Energy level diagrams reproduced from Bertozzi *et al.*[175] showing the difference between a normal, unstrained alkyne (left) as is used in the CuAAC reaction, and the strained cyclooctyne used in copper-free click chemistry. $\Delta E^{\ddagger}$ = activation energy. $\Delta E^{\ddagger}_{d}$ = distortion energy. $\Delta E^{\ddagger}_{i}$ = interaction energy.

The activation energy is broken up into two parts, distortion ($\Delta E^{\ddagger}_{d}$) and interaction ($\Delta E^{\ddagger}_{i}$). The interaction energy is the reduction in energy caused by a favourable orbital overlap as the azide and alkyne react. The reaction with the linear but-2-yne actually has a greater decrease in energy upon interacting, favouring this reaction over the copper-free click reaction.

The distortion energy represents the energy that is required to distort both the azide and the alkyne into their desired transition state conformations. The cyclic nature of the cyclooctyne forces the triple bond into an unnatural (non-linear) bond geometry. The inherent strain destabilises the cyclooctyne increasing its energy compared to the but-2-yne and making it more reactive. The cyclooctyne also has the added advantage of being a lot more product-like

in its appearance, therefore, it requires a lot less energy to distort into the required transition state geometry.

The amount of distortion in the azide also varies between the two reactions. The distortion angle of the azide (a˚, Figure 4.7) was calculated by Bertozzi to be 137˚ when reacting with the but-2-yne and 141˚ for the cyclooctyne. This has been attributed to the destabilisation of the cyclooctyne causing a transition state earlier in the reaction coordinate for the copper-free reaction. This reduces the distortion needed for the azide to reach its transition state geometry. The change in position of the transition state also fits with the Hammond postulate, a method used to predict reaction coordinates.[178] This states that the transition state of a reaction resembles either the products or the reactants, to whichever it is closer in energy. The small but significant decrease in the distortion of the azide, along with the strain of the cyclooctyne, results in a smaller distortion energy for the copper-free click reaction.

The overall activation energy is calculated by the sum of the distortion and interaction energies ($\Delta E^{\ddagger} = \Delta E_{d}^{\ddagger} + \Delta E_{i}^{\ddagger}$). As can be seen from the energy diagrams, the distortion has a much greater effect, significantly reducing the activation energy required for the copper-free click reaction. Therefore, the strained bond angle of this cyclooctyne is enough to allow the azide-alkyne cycloaddition to occur in the absence of the catalytic copper.

This technique has proved highly efficient with Cu-free reactions having been carried out in many biological systems.[179] As with the copper catalysed reaction, attaching fluorescent labels to biomolecules is a major use of copper-free click chemistry. Bertozzi *et al*. led the way selectively labelling cells which had azidosugars attached to their surfaces.[180] Neef and Schultz then reversed this, including a cyclooctyne in the cell membrane and labelling with a fluorescent azide.[181] Yin took this further labelling bacteriophage without damaging the host cell.[182] Tom Brown *et al.* are at the forefront of oligonucleotide research and have adopted copper-free click as a method to attach fluorescent dyes onto oligonucleotides for the purposes signalling devices such as HyBeacons.[183]

Proteins have also been probed using the copper-free reaction. The Burkart group crosslinked domains in order to study protein-protein interactions in non-ribosomal peptide biosynthesis.[184] A cyclooctyne immobilised on a solid

phase has also been synthesised and used for the capture of azido-peptides from a complex mixture.[185]

One potential problem with the copper-free method is the lack of regioselectivity caused by the symmetrical cyclooctyne. This results in a regioisomeric mixture of triazole products. If regioselectivity is of high importance for a certain reaction, the CuAAC reaction would be better suited. However, the majority of biocompatible work revolves around labelling the biomolecules with molecules such as fluorescent dyes. In this case the regioselectivity is not important as long as the target has been tagged.

Like its copper catalysed predecessor, copper-free click chemistry has proven to be a reliable reaction in many different situations. The real draw of this method, its fast reaction rates in the absence of copper and elevated temperatures, makes it that much more compatible with biological systems and as such, a highly attractive tool in biochemistry.

4.4 Copper-Free Click Chemistry with Porphyrins

As an alternative to the copper catalysed click reaction using the Baseclick Oligo-Click kit, copper-free click chemistry was attempted using the same three porphyrins, J-TPP, V-TPP and V-DMP pictured in Scheme 4.3 and Figure 4.3. The sequence used for these experiments was different to those used with the Oligo-Click kit and contained a strained alkyne modification at the 5'-terminus of the strand. This oligo was supplied by ATDBio. The sequence and structure of the strained alkyne modification are shown in Figure 4.8.

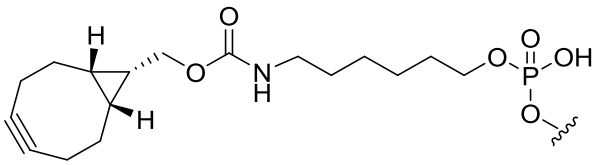

5'- **X** ATG CTA AAG GTT CGA TCG ACT GTA CGG T – 3' ODN 11

Figure 4.8 Sequence of ODN 11, the strand containing the pictured bicyclo[6.1.0]nonyne (BCN) strained alkyne modification at position **X**. ODN 11 was provided by ATDBio.

The conditions used were similar to the CuAAC reactions with the obvious exception of the copper. DNA (10 nmoles) and porphyrin azide (100 nmoles, 10 equivalents) were dissolved in water (10 µL) and DMF (40 µL) and maintained at 25 °C for 24 hours. As with the CuAAC tests, a range of times and temperatures were previously tested with little reaction progress witnessed after 24 hours. A work-up between water and ethyl acetate was carried out to remove the unreacted porphyrin and the reaction progress checked by HPLC. The chromatograms for the copper-free click reactions with each of the three porphyrins are presented in Figure 4.9 along with their associated MALDI-ToF mass spectra. Using these conditions, 2.1 nmoles, 6.2 nmoles and 4.8 nmoles of porphyrin-modified DNA were collected for the reactions with J-TPP, V-TPP and V-DMP respectively.

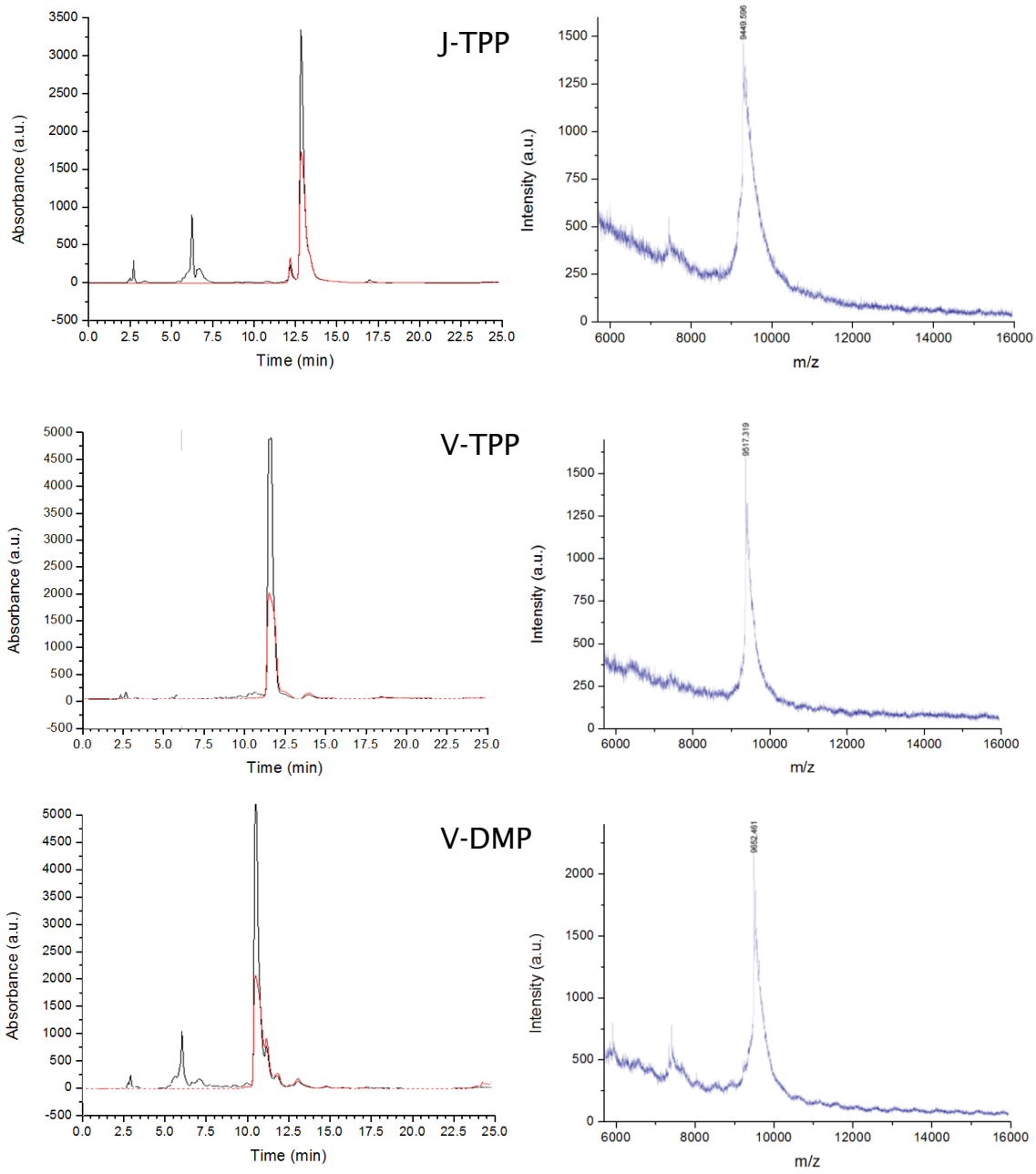

Figure 4.9 Left) HPLC chromatograms produced by the Cu-free click reaction between cyclooctyne containing ODN 11 and the porphyrin azides J-TPP, V-TPP and V-DMP. Absorbance monitored at 260 nm (black lines) and 420 nm (red lines). A Polaris 3 C18-A 150 × 4.6 mm column was used at 60 ˚C with buffer A – 8.6 mM TEA/100 mM HFIP with 0.5 mM EDTA and buffer B - methanol. Gradient used [time (mins) (% buffer B)]; 0 (0 %), 10 (50 %), 20 (60 %), 25 (100 %). Flow rate = 1 mL min^{-1}. Right) MALDI-ToF mass spectrometry data from the product peaks.

The presence of a peak showing DNA (260 nm, black line) and porphyrin (420 nm, red line) absorbance in each chromatogram immediately suggests the reactions have progressed. The earlier peaks (approx. 6 mins) show absorbance at 260 nm but not 420 nm, indicating some unreacted DNA does still remain.

As expected, and as was seen in the CuAAC reactions, the porphyrin-modified DNA is the peaks at higher retention time. These show absorbance at 260 and 420 nm with the corresponding UV-Vis spectra showing all the expected absorptions for DNA, Soret band and Q-bands.

In contrast to the CuAAC HPLC chromatograms, once the reactions had been tuned, the peaks produced by the porphyrin-modified DNA are a lot bigger than for the unreacted DNA peaks. This suggests that the coupling efficiency of the copper-free click method is much better than for the copper catalysed alternative. With no copper in this reaction to damage the DNA and no evidence the cyclooctyne modifier, porphyrin azide or porphyrin-modified DNA are unstable, the reaction should reach completion given sufficient time.

The oligos labelled with each of the three porphyrins were sent to Crete for confirmation by MALDI-ToF mass spectrometry and the results summarised in Table 4.2.

ODN	Calculated Molecular Mass	Peak maximum by MALDI	Reaction yield
ODN 11 (unmod)	8685	-	-
ODN 11 + J-TPP	9489	9449	21 %
ODN 11 + V-TPP	9503	9517	62 %
ODN 11 + V-DMP	9631	9652	48 %

Table 4.2 Calculated molecular mass values, values obtained by MALDI-ToF mass spectrometry and yields for ODN 11 reacted with each of the three porphyrins by copper-free click chemistry.

The mass spectrometry results show the same as for the previous samples. The measured values are in the vicinity of the calculated masses without being perfect.

From the HPLC, UV-Vis and mass spectra, it has been clearly shown that copper-free click chemistry is a viable reaction for attaching an azide-modified porphyrin onto an oligonucleotide containing a 5'-cyclooctyne modification. Greater coupling efficiencies have been achieved using this method as opposed to the CuAAC reaction. The reactions are easy to set up and the porphyrin-modified DNA product has been shown to be easily isolated by HPLC purification.

One test that has not been carried out is a multi-labelling reaction using internal modifications as was done with the CuAAC. This was not attempted because at the time of the work no internal cyclooctyne modifier was commercially available. One has since become accessible from Glen Research,[186] whilst Wagenknecht *et al.* have also recently published a cyclooctyne-modified nucleoside.[187] It would be very interesting to see if coupling can be achieved with copper-free click chemistry where the copper catalysed version failed using one of these internal modifiers.

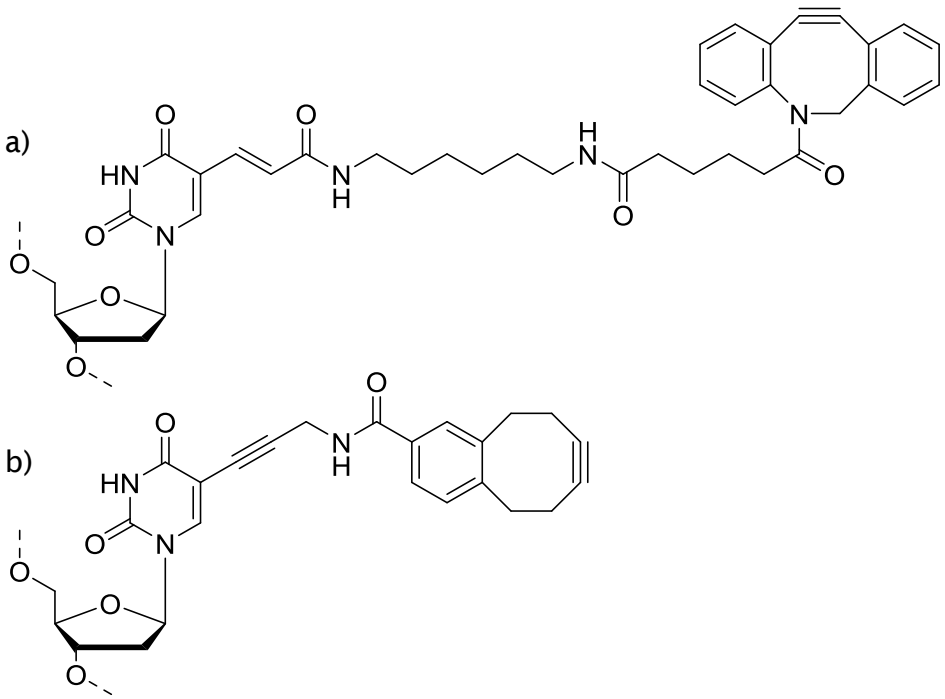

Figure 4.10 a) DBCO-dT available from Glen Research. b) Cyclooctyne modified nucleoside presented by Wagenknecht *et al.*[175, 187]

This internal modifier available from Glen Reseach is slightly different to the BCN 5'-modifier used previously. Firstly, instead of BCN, a dibenzo-cyclooctyne (DBCO) unit is employed as the cyclooctyne. This unit has been shown to be more reactive than the single cyclooctyne ring. Secondly, the linker length is much longer in this modifier than for the C8-Alkyne-dU. This increased distance from the backbone will make the alkyne less sterically hindered and therefore more available to react. As the linker length and the cyclooctyne unit will be changed as well as removing the copper from the reaction, a direct comparison between the different reactions will not be possible. Wagenknechts cyclooctyne bears a closer resemblance to the BCN unit and is a similar length to the C8-Alkyne-dU. This nucleoside would therefore be better for direct comparisons, but would need to be synthesised in the lab first.

4.5 Conclusions: Copper Catalysed and Copper-Free Click Chemistry for the Production of Porphyrin-Modified DNA

This chapter has shown an alternate way of including porphyrins into oligonucleotides to that presented in Chapter 3. Post synthetic attachment of the porphyrins to oligos was attempted using both the copper catalysed azide-alkyne cycloaddition and copper-free click chemistry. Not having to produce the porphyrin-modified phosphoramidite removes the problem of low coupling efficiencies during DNA synthesis.

It has been shown that porphyrins can be attached to oligonucleotides using either the copper catalysed or copper-free methods when the alkyne modifier is at the terminus of the single strand. HPLC, UV-Vis spectroscopy and MALDI-ToF mass spectrometry have all been used to confirm the porphyrin-DNA product for both reactions. The results presented here favour the copper-free reaction, which consistently produced higher coupling efficiencies than the copper catalysed alternative.

As a modified nucleobase, the C8-Alkyne-dU used for copper catalysed click chemistry with the Baseclick Oligo-Click kit, can be incorporated at any position in a DNA sequence. However, absolutely no coupling has been observed when trying to attach any of the porphyrin azides to a strand containing multiple internal modifications. Until very recently, no strained alkyne internal modifier existed. As such, porphyrins have, so far, only been tested for coupling at the 5'-terminus of an oligonucleotide using this technique. As copper-free click chemistry has produced the better results thus far, it is hoped the newly available internal modifier will provide good coupling to multiple modified sites in a single oligonucleotide. This would allow the construction of multi-porphyrin systems like the Zipper array discussed in Chapter 3.

One potential way of improving the coupling with these strained alkyne units is to further modify the alkyne containing ring. The click reaction involves the highest occupied molecular orbital (HOMO) of the azide and the lowest unoccupied molecular orbital (LUMO) of the alkyne. If an electron withdrawing group can be added to the cyclooctyne, the LUMO will be lowered and the

alkyne will become more reactive. Using this theory, the Bertozzi group added different electron withdrawing groups to their cycloocytnes. The addition of a single fluorine to the ring system increased the reaction rate constant 3-fold.[157, 180] Two fluorine atoms on the same carbon made the reaction 60 times faster than their starting molecule.[188] Another possibility is to use the more reactive DBCO modification as has been done with the internal DBCO-dT.

A good start has been made to this project with proof of concept work showing porphyrins can be attached to oligonucleotides post synthetically using both copper catalysed and strained promoted click chemistry. Further work is now required to tune the reaction conditions and hopefully increase yields. The multiple labelling CuAAC reaction is of concern as at least some coupling was expected but so far has not been observed. No definitive explanation has been found for why this is the case. More work is required on this system to see if coupling can be encouraged with different conditions or the addition of the complementary strand. The newly available internal strained alkyne modifier also needs to be tested and can hopefully lead to a multi-porphyrin system.

5. Conjugated Porphyrin-DNA Wire

5.1 Introduction to the Conjugated Porphyrin System

A second DNA templated system was devised to differ from the Zipper array described in Chapter 3. The Zipper system was designed to self-assemble by taking advantage of the π-stacking and strong electronic interactions between porphyrins in close proximity. The second system is designed to form a conjugated chain of covalently linked porphyrins. This system expands on the work of Gothelf and co-workers who reported the construction of conjugated molecular wires from oligo(phenylene ethylene) building blocks.[189] A schematic of the porphyrin conjugated wire is shown in Figure 5.1 along with the sequences of the designed oligos.

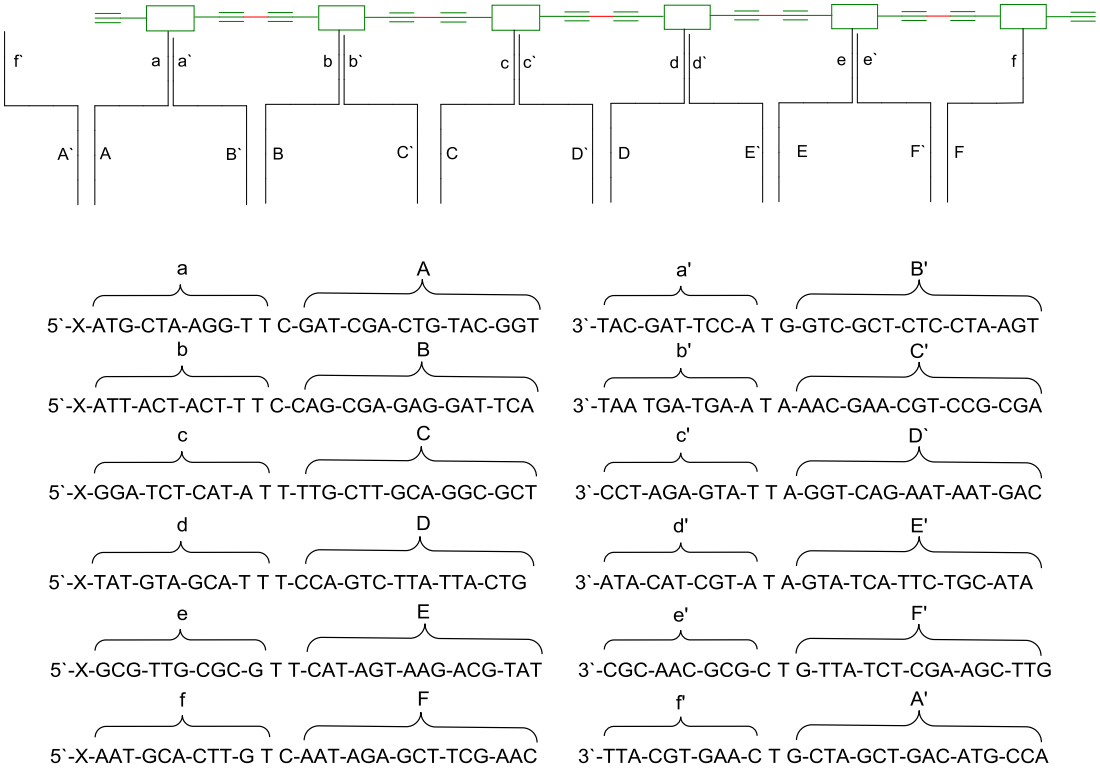

Figure 5.1 Top) Schematic of the covalently linked porphyrin wire. Black lines represent DNA and green boxes are porphyrins. The red lines show the bond formed by a DNA templated Glaser-Hay coupling as used by Gothelf with his oligo(phenylene ethylene units. Bottom) Sequences of the porphyrin modified strands (e.g. aA) and unmodified template strands (e.g. a'B').

Conjugated Porphyrin-DNA Wire

The conjugated porphyrin system, as shown in Figure 5.1, consists of a set of oligonucleotides modified with a porphyrin at the 5'-terminus and a corresponding set of unmodified template strands. One template strand (e.g. ODN a'B') has half its sequence that is complementary to one porphyrin containing strand, and the other half complementary to a second porphyrin containing strand (ODNs aA and bB for this example, see Figure 5.2 b). Upon annealing, the two porphyrins are brought into close proximity and are free to react with each other.

The desired reaction is widely referred to as a Glaser-Hay coupling.[190] This is a copper catalysed, oxidative coupling used to form a carbon-carbon bond between two terminal acetylenes, in this case attached to the meso position of the porphyrins. This reaction was used by Gothelf *et. al* to covalently bond their oligo(phenylene ethylene) units using this DNA templating method (Figure 5.2 b). Once the porphyrins are covalently bound, a conjugated π-system is formed through all the connected porphyrins. The butadiyne linkage between porphyrins is ideal as it provides an unusually high excitonic and electronic coupling between porphyrin centres, whilst being sterically unhindered and rotationally flexible.[191, 192]

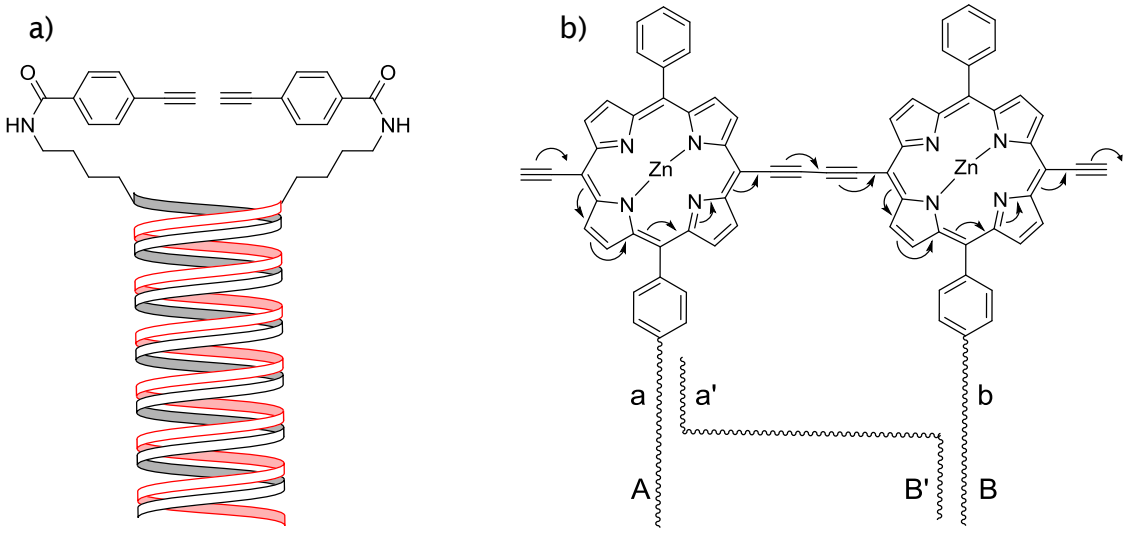

Figure 5.2 a) Two oligo(phenylene ethylene) units used by Gothelf *et al.* with associated template DNA prior to Glaser-Hay coupling.[189] b) Two di-acetylene porphyrin strands (aA and bB) with associated template DNA (a'B') after Glaser-Hay coupling forming the acetylene-acetylene bond. Also shown is the conjugation throughout this system.

This way of covalently linking molecules was originally introduced by Carl Glaser in 1869[193, 194] and improved by Allan Hay in the 1960's with the inclusion of the copper stabilising ligand tetramethylethylenediamine (TMEDA) to prevent oxidation of the copper.[195, 196] Hay's work also showed how this method could be used for the synthesis of polymers. Various other groups have adapted this reaction over the years with the aim of improving yields or varying reaction conditions.[197-202] One such variation was reported by Eglinton and Galbraith who showed that copper (II) acetate can be used in place of a copper (I) source given the right conditions.[203, 204] This method could also be carried out under high dilution conditions giving access to macrocyclic systems. Examples of some of the different conditions used for forming 1, 3-diynes are shown in Scheme 5.1 with the mechanism for the Glaser-Hay coupling in Scheme 5.2.

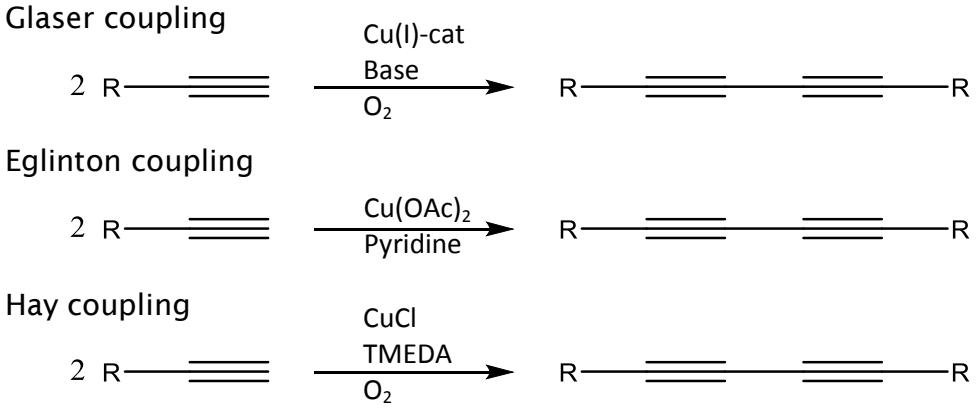

Scheme 5.1 Examples of three different copper catalysed methods of forming 1, 3-diynes. Top) The original Glaser coupling using a copper (I) source with a base. Middle) Eglinton coupling using copper (II) acetate. Bottom) Hay coupling using CuCl with TMEDA as a copper binding ligand.

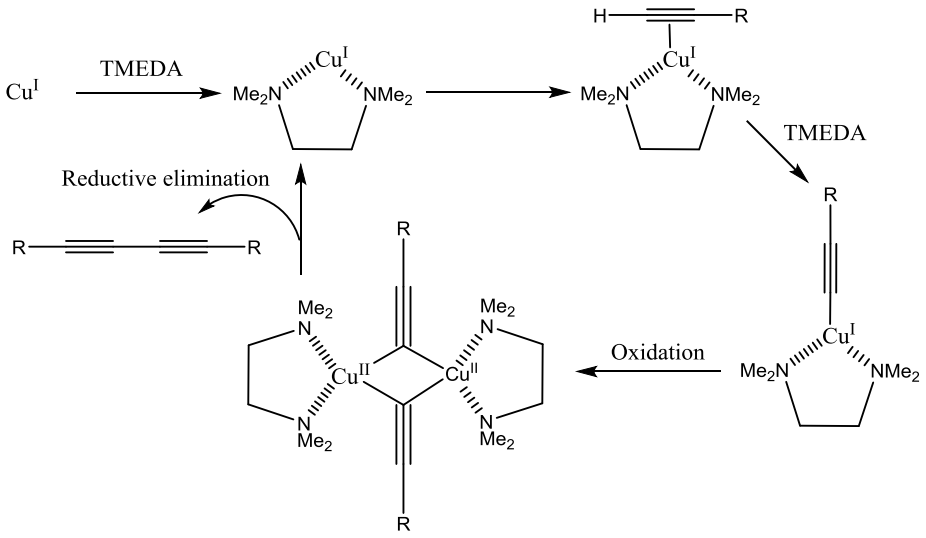

Scheme 5.2 Proposed mechanism of the Glaser-Hay coupling reaction.[190]

Other reactions, such as Sonogashira coupling,[55] can be used to form carbon-carbon bonds from terminal acetylenes but require expensive palladium catalysts. The comparatively cheap and freely available Cu (I) and (II) salts make Glaser-Hay type couplings an attractive option for the homocoupling of acetylenic compounds.[200]

Since the first synthesis of a butadiyne linked porphyrin dimer by Arnold *et al.* in 1978,[205] several groups have used Glaser-Hay couplings on porphyrins to form larger order systems.[192, 206-209] These large porphyrin structures are of great interest for their electrical, redox, and light harvesting properties as well as for their potential use in functional devices. Ethyne and butadiyne linked porphyrin dimers, trimers and oligomers have been investigated for their spectroscopic and electrochemical characteristics in organic solvent.[192, 210] These studies will provide a basis for the porphyrin wire attached to the DNA scaffold.

The construction of this conjugated porphyrin wire starts with the synthesis of the di-acetylene porphyrin.[211, 212] Once this is made, an oligonucleotide is synthesised with a reactive 5'-end modification. This reactive site is then to be coupled with the porphyrin post DNA synthesis. This method of including porphyrins into an oligo differs from the phosphoramidites used to make the Zipper system in Chapter 3. Once the porphyrin oligonucleotides have been

synthesised, the template strands can be added to bring the porphyrin strands into close proximity to enable the Glaser-Hay couplings to take place. By adding more porphyrin strands and template strands into the system, molecular wires containing 3, 4, 5 porphyrins can be constructed and tested for their electron transfer properties.

5.2 Synthesis of the Di-Acetylene Porphyrin

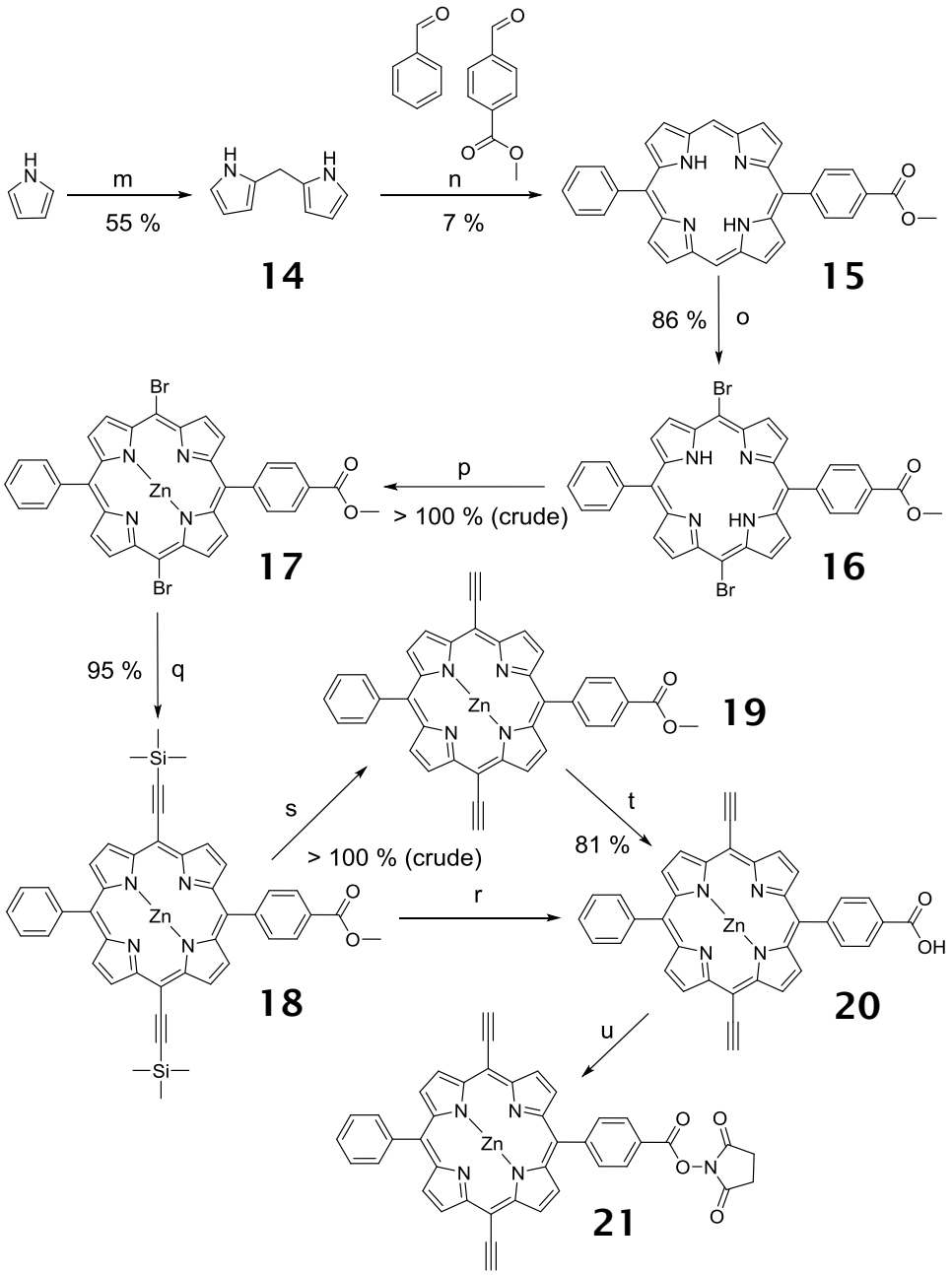

Scheme 5.3 m) i) Paraformaldehyde, TFA, DCM, N_2, Δ. ii) NaOH. n) i) Benzaldehyde, methyl-4-formylbenzoate, Boron trifluoride etherate, DCM, N_2. ii) DDQ. o) NBS, pyridine, $CHCl_3$, 0 ˚C. p) $Zn(OAc)_2$, DCM/MeOH, Δ. q) $Pd_2(dba)_3$, CuI, PPh_3, pyridine, NEt_3, trimethylsilylacetylene, N_2, Δ. r) KOH, pyridine, H_2O, Δ. s) TBAF, DCM. t) NaOH, pyridine, H_2O. u) TSU, DIPEA, DMF, N_2.

The synthesis of a di-acetylene, mono-NHS ester porphyrin (**21**) was designed with the synthetic route outlined in Scheme 5.3. This porphyrin differs from the previous two in a couple of ways which affect the synthesis. Firstly, it is not a mono-substituted tetraphenyl porphyrin so cannot be made using pyrrole and two benzaldehydes in a 6:6:1 ratio, as was done in both the previous cases. Secondly, the porphyrin was designed to be attached to a DNA strand via an amide bond from 5'-amino-modified DNA in a post synthetic labelling reaction. This approach means the porphyrin does not need to be made into a phosphoramidite for solid phase oligonucleotide synthesis.

Instead of carrying out the porphyrin synthesis from pyrrole as per the previous syntheses, dipyrromethane (**14**) was first synthesised and this reacted with a mixture of aldehydes. This reaction forms a porphyrin (**15**) with two free meso positions allowing a way to directly modify the porphyrin ring. The dipyrromethane was synthesised following the procedure laid out by Lindsey and produced a pure white product in a 55 % yield.[31] The dipyrromethane then replaced pyrrole in the porphyrin formation step and was reacted with benzaldehyde and methyl-4-formylbenzoate in a 1:1:1 ratio. The rest of the porphyrin synthesis was carried out following the same protocol as the previous porphyrins using boron trifluoride etherate (0.9 equiv.) as the Lewis acid catalyst. However, several attempts at this reaction produced no porphyrin. After consulting the work of Gorbunova, the amount of boron trifluoride etherate used was decreased to 0.1 equivalents.[213] Keeping with Gorbunova's work, the amount of DDQ used to oxidise the porphyrinogen to the porphyrin was also reduced from 6 equivalents to just 1.5 equivalents. This combination solved the problem and the porphyrin was collected with a yield of 7 %. No explanation has been found to why the higher concentration of the acid prevented the formation of the porphyrinogen.

Bromination at the two free meso positions was achieved using N-bromosuccinimide to form porphyrin **16** (step o). This reaction worked well (86 %) and produced a purple solid as with all previous porphyrins. However, unlike all previous porphyrins synthesised, the bromine attachments caused the porphyrin to lose its fluorescence. This phenomenon is called the heavy atom effect.[214-217] The loss in fluorescence is caused by the non-radiative transition of the excited electron from the singlet state to the triplet state. The presence of a heavy atom, such as a bromine or iodine, in the vicinity of the

excited electron makes this singlet to triplet transition more probable by strengthening spin-orbit coupling. This causes a shift in energy levels allowing an easier transition from the excited singlet state to the triplet state.

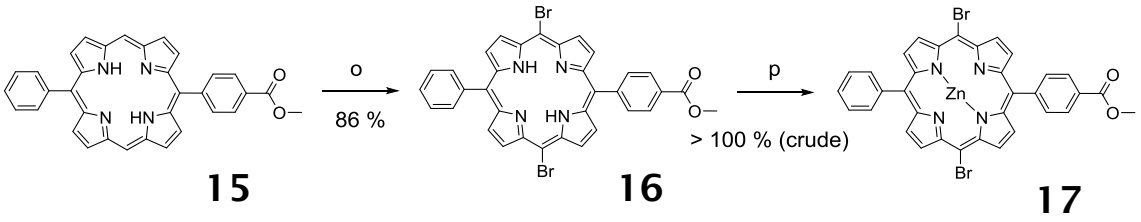

15 **16** **17**

Scheme 5.4 Step o) Bromination at the free meso positions. Step p) Zn metalation of the porphyrin.

Upon metalation with zinc, further differences were noticed from that of previous porphyrins. Whilst porphyrin **17** still dried to a purple solid product, in solution it appeared to have a slight blue/green tinge to the colour. This colour change became further apparent with the substitution of the bromines for trimethylsilane protected acetylene (TMS acetylene) (**18**, step q). Removal of the bromines returned the fluorescence of the porphyrin and resulted in a permanent change in colour to blue/green for both the dry solid and the compound in solution.

As discussed in section 3.3, a large excess of $Zn(OAc)_2$ is used in the metalation step so that in theory 100 % of the porphyrin is metalated quickly. At the completion of the reaction the excess zinc acetate is removed by filtration. As with the acetylene linked porphyrin, the product was retained in the filter. A similar problem was found with an attempt at purification by column chromatography. The same approach was adopted as before, removing the excess zinc with an aqueous work-up and carrying the product through to the next step without further purification. The collected crude yield was measured as > 100 %, so there must therefore be some zinc remaining, but this did not harm the next step.

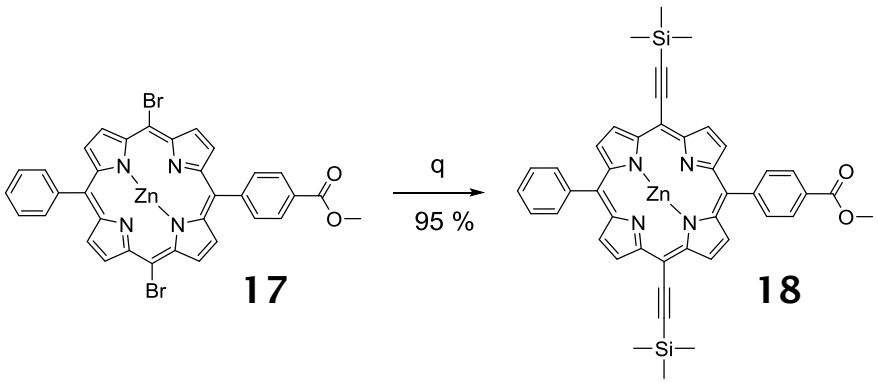

Scheme 5.5 Step q) Sonogashira coupling of TMS acetylene to the poprhyrin meso positions.

Substituting the bromines for the TMS acetylene (step q) worked a lot better than the previous step producing the purified product (**18**) in 95 % yield. The same could not be said for step **r**. This was to be the simultaneous removal of the TMS groups from the two acetylenes, and the hydrolysis of the methyl ester to the carboxylic acid (**20**) using KOH in pyridine and water. Several attempts at this were made without success. These conditions also appeared to degrade the porphyrin as no evidence of the characteristic green colour or the fluorescence could be detected. It was therefore decided to split this into two steps, deprotecting the acetylenes before hydrolysing.

The removal of the TMS groups producing porphyrin **19** (step **s**) was carried out using tetrabutyl ammonium fluoride (TBAF) and consistently produced crude yields of greater than 100 %.[212] The crude product was carried forward to the next reaction as the crude as a substantial amount of product was again lost during attempts at purification. Using the crude product did not seem to affect the hydrolysis (step **t**) and the carboxylic acid product (**20**) was collected in its crude form.

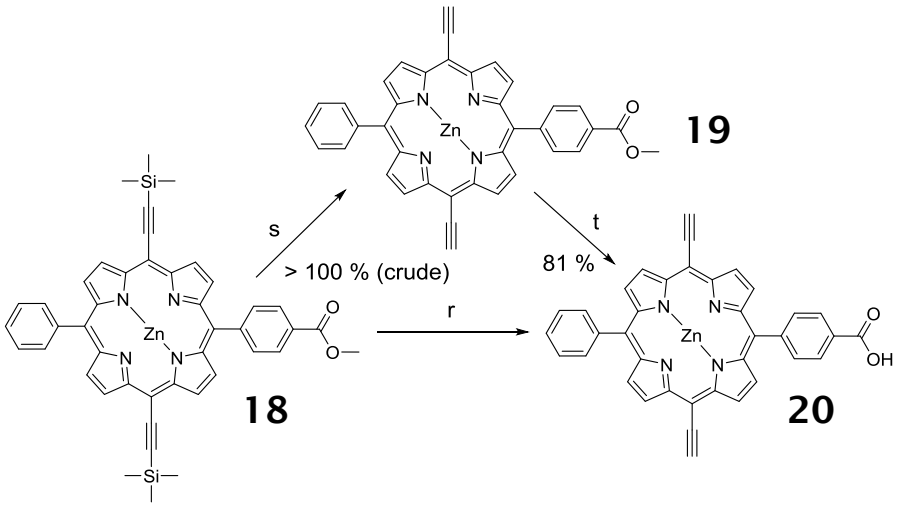

Scheme 5.6 Step r) Attempted conversion from TMS protected porphyrin ester **18** to the deprotected porphyrin acid **20** in a single step. Step s) Removal of TMS groups. Step t) Hydrolysis of ester.

Fears over column chromatography remained so an attempt at purification by re-crystallisation (hot toluene and cold hexane) was made for step **t**. A green/blue solid did crash out of solution, but when analysed by NMR showed the sample to be much less clean than the crude product. TLC analysis of this product showed the appearance of an orange/red spot slightly above that of the green product spot clearly showing the change.

Finally an attempt at column chromatography was made but without success. As with the previous attempts, multiple fractions of different colours were collected with no sign of any being pure product. This all suggests that the compound was not stable and was degrading.

With these two attempts at purifying the porphyrin product **20** failing, it was decided to carry on with the final step using an un-purified sample. Although not purified, a small amount (50 mg) of crude porphyrin **20** had produced an NMR spectrum which was much cleaner than the others and looked acceptable to carry forward. The acid (**20**) was to be converted to the more reactive NHS ester to produce final porphyrin product (**21**, Scheme 5.3).

Due to the difficulties in procuring a small amount of compound **20**, a TPP analogue of the NHS ester product (**22**) was synthesised and used to test the

coupling reaction between an NHS ester porphyrin and 5'-amino-modified DNA. Despite several attempts employing different reaction conditions, these tests proved unsuccessful. Different solvents (DMF/water, DMF/aqueous buffer, pure DMF) with the addition of the base DIPEA were all tested with varying reaction times and temperatures. These reactions were monitored by HPLC but at no point showed any evidence porphyrin-modified DNA had been produced.

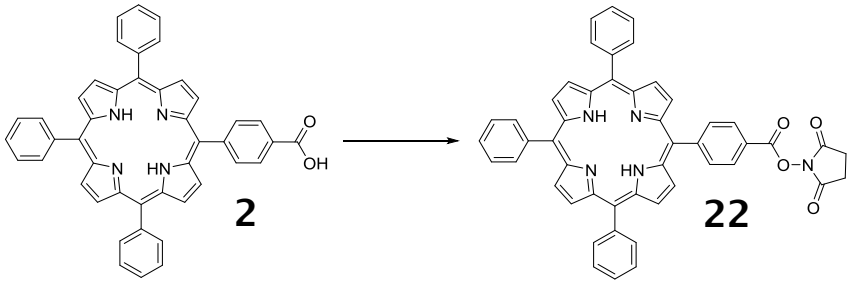

Scheme 5.7 Reaction scheme for the synthesis of TPP NHS ester.

With the synthesis of the di-acetylene NHS ester (**21,** Scheme 5.3**)** proving difficult, and attempts at coupling a porphyrin NHS ester to amino-modified DNA failing, the decision was taken to abandon this route and rethink the synthesis and method of attachment to the oligonucleotide.

5.3 Synthesis of Di-Acetylene Porphyrin Azide and Amine

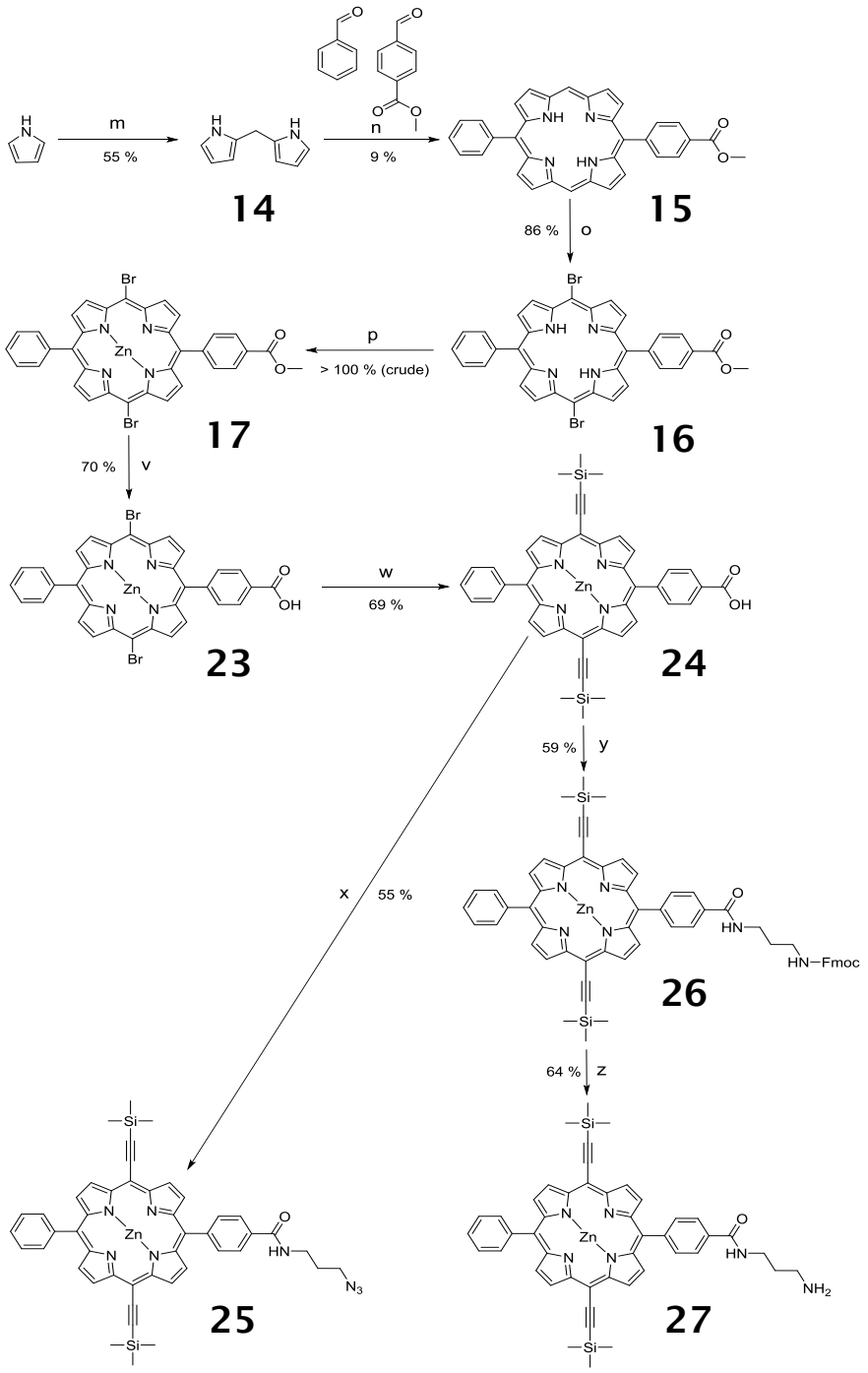

Scheme 5.8 m) i) Paraformaldehyde, TFA, DCM, N_2, Δ. ii) NaOH. n) i) Benzaldehyde, methyl-4-formylbenzoate, Boron trifluoride etherate, DCM, N_2. ii) DDQ. o) NBS, pyridine, $CHCl_3$, 0 ˚C. p) $Zn(OAc)_2$, DCM/MeOH, Δ. v) KOH, pyridine, H_2O, Δ. w) $Pd_2(dba)_3$, CuI, PPh_3, pyridine, NEt_3, trimethylsilylacetylene, N_2, Δ. x) 1-amino-3-propylazide, HATU, DIPEA, DMF, N_2. y) Fmoc-diaminopropane.HCl, HATU, DIPEA, DMF, N_2. z) 20 % piperidine in DMF.

Two alternatives to the di-acetylene porphyrin were designed and successfully synthesised. The first is an amine designed for amide coupling to carboxy-modified DNA in the reverse to the original design (amino DNA and carboxy porphyrin). The second is an azide porphyrin designed for attachment to DNA via copper-free click chemistry (see Chapter 4).

The first four steps of this new synthetic route (steps **m** – **p**) are the same as those in the original synthesis (section 5.2) to make compound **17**. At this point the syntheses diverge. In the original design, TMS protected acetylene is attached to the free meso positions, deprotected and finally the methyl ester hydrolysed. The major problems in the original route began when the TMS groups were removed. It was therefore decided that the TMS groups could be left on during the synthesis, and removed with ammonia after coupling the porphyrin to the DNA.[218] As the basic conditions for hydrolysing the ester would also remove the TMS groups (as was attempted in step **r**), this hydrolysis needed to be performed before attachment of the TMS acetylene groups.

This plan was not without its problems. The carboxylic acid porphyrins **23** and **24** being polar stuck to a silica column resulting in low yields. Re-crystallisation of compound **23** was more successful giving a 70 % yield. The TMS acetylenes were then attached using Sonogashira coupling as before. The reaction proceeded without trouble producing compound **24** in a much quicker, easier way than was used to make compound **20**.

At this point, two different amide couplings were used to make the compounds **25** and **27**. These differing routes are outlined in Scheme 5.9.

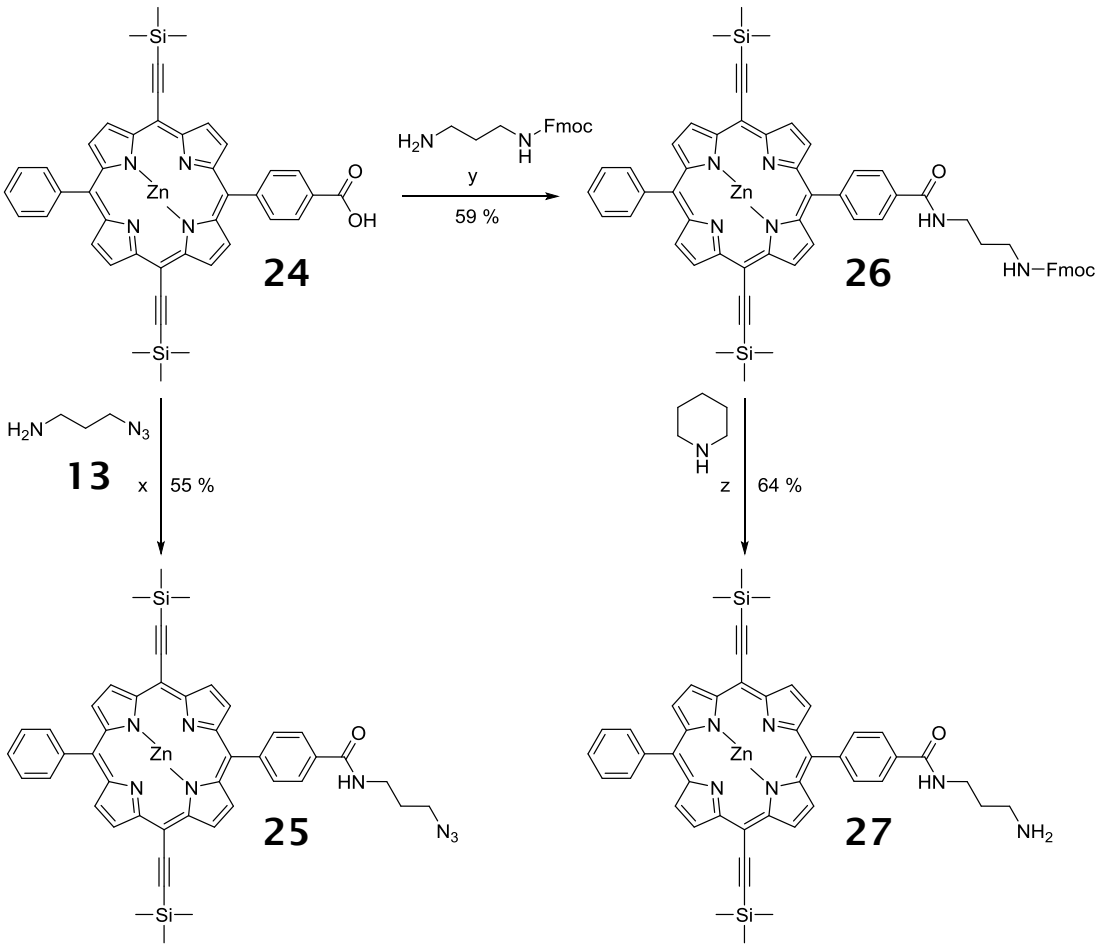

Scheme 5.9 Step x) Formation of di-TMS acetylene azide. Steps y and z) Formation of di-TMS acetylene amine.

As was shown in Scheme 4.3 (section 4.2), 1-amino-3-propyl azide (**13**) can be coupled with a carboxylic acid porphyrin to produce the porphyrin azide **25**. This however was not the first attempt at making a porphyrin azide. Several other routes had been tested previously before deciding to use this method. The attempted pathways for converting The TPP acid **2** into the azide are outlined in Scheme 5.10.

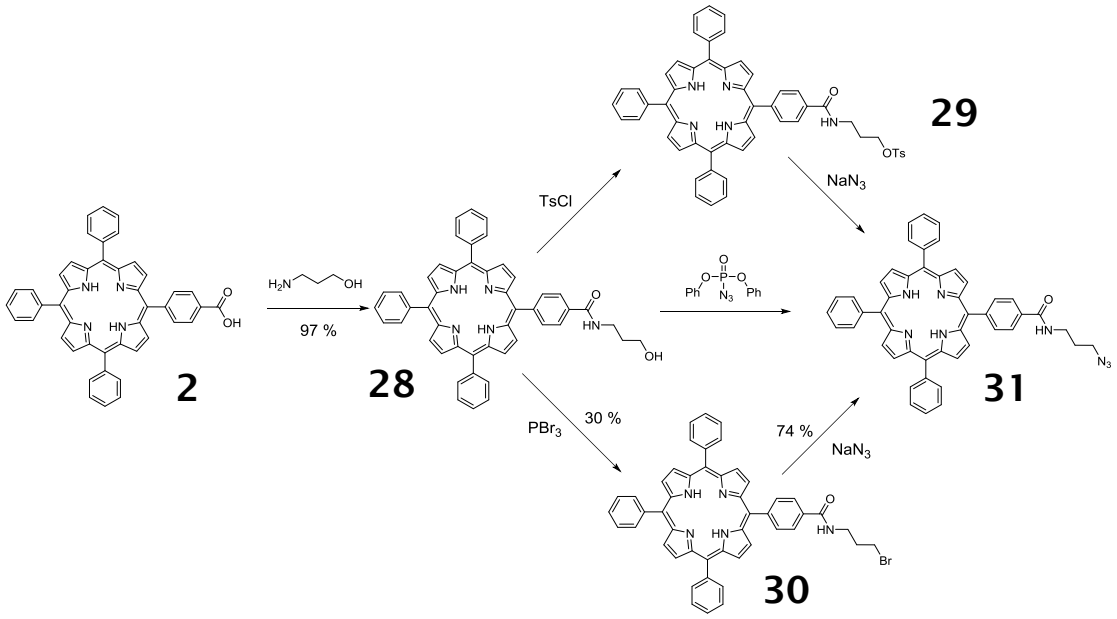

Scheme 5.10 Schematic showing three different routes attempted to produce a TPP azide. Top) TsCl, NaN_3. Middle) DPPA. Bottom) PBr_3, NaN_3.

The first step got off to a good start with the amide coupling to an amino alcohol producing compound **28** with a 97 % yield. This alcohol was then to be activated with *p*-toluenesulfonyl chloride (tosyl chloride) before conversion to the azide using sodium azide (Scheme 5.10, top). Despite the well documented reaction between primary alcohols and tosyl chloride,[219] no product could be isolated from this reaction. Qi *et al*. have reported that benzyl alcohols with electron withdrawing substituents can give the corresponding chloride rather than the tosylate.[220] Due to the large aromatic porphyrin ring it is possible that the chloride has been formed in this instance.

The next route attempted was to first convert the porphyrin alcohol to the bromide using phosphorus tribromide before converting to the azide with NaN_3 (Scheme 5.10, bottom).[221] This route was successful and the TPP azide **31** was isolated meaning this route was viable for the diacetylene porphyrin. However, a yield of only 30 % was consistently achieved for the bromination. This was again surprising considering the yields of similar reactions reported in the literature and is not really high enough to make this route feasible.[222]

Due to this low yield a third route was attempted (Scheme 5.10, middle). This aimed to convert the alcohol directly to the azide using diphenyl phosphoryl

azide (DPPA).[223] This though was once again unsuccessful and the azide porphyrin **31** was not isolated.

It was at this point that the focus was switched to synthesising 1-amino-3-propyl azide (**13**, Scheme 4.3).[172] The three routes described in Scheme 5.10 all involved the attachment of an amino propyl alcohol to the porphyrin. This alcohol was then to be converted to the azide. This approach however, involved at least two further reactions on porphyrin compounds after the porphyrin acid had been made. By producing the 1-amino-3-propyl azide before coupling to the porphyrin, only one further reaction was required on a porphyrin compound. Due to the stability issues highlighted earlier, the fewer the number of steps after attaching the TMS acetylene groups (step **w**) the better.

Coupling 1-amino-3-propyl azide to the TPP acid gave a 95 % yield so was considered the best method and was used to produce the di-acetylene porphyrin azide **25**.

The production of the porphyrin amine **27** (Scheme 5.9) also suffered a false start. TPP acid **2** was first reacted with 1, 3-diaminopropane. The formation of some diporphyrin compound from both ends of the diamine reacting was expected so a large excess (4 equivalents) of the diamine was used. This produced a single new porphyrin spot on a TLC plate and a clean NMR. However, the correct product mass could not be found by mass spectrometry. The reason for this became apparent when attempting to couple the compound to carboxy-modified DNA. No amide coupling occurred suggesting no amine was present. As the integration of the peaks in the NMR suggested a 1:1 ratio of porphyrin to C3 linker it appears the isolated compound is not the diporphyrin compound. The mass spectra could not confirm any compound and shed any light on the issue. For this reason it is not known what had been formed.

A mono Fmoc-protected 1, 3-diaminopropane hydrochloride salt was then found to be commercially available. This was coupled to the TPP acid producing an Fmoc-protected amine (**32**, see section 9.30) as confirmed by NMR and mass spectrometry. Upon deprotection with piperidine, a different

single compound to that obtained when using the diamine was isolated. This compound however, did provide the correct product mass by mass spectrometry and proved to be the TPP amine compound **33** (Figure 5.3). Using this route the di-acetylene porphyrin amine **27** was also produced in 64 % yield.

The di-TMS acetylene porphyrin has been made with two different functionalities. These compounds were now ready to be taken forward and attached to oligonucleotides. Having the two different porphyrins allowed two different coupling methods to be tested so the most suitable technique could be used in future. Once a protocol for post synthetically modifying oligonucleotides with porphyrins was established, the porphyrin-modified DNA could be used to investigate the DNA directed Glaser-Hay coupling.

5.4 Attachment of Di-Acetylene Porphyrin to 5'-Modified DNA

The di-acetylene porphyrin amine **27** was designed for attachment to oligonucleotides using amide coupling. This required the oligos to be modified with an activated ester modifier. A 5'-carboxy-modifier C10 phosphoramidite was purchased from Glen Research and was included in solid phase oligonucleotide synthesis.[224]

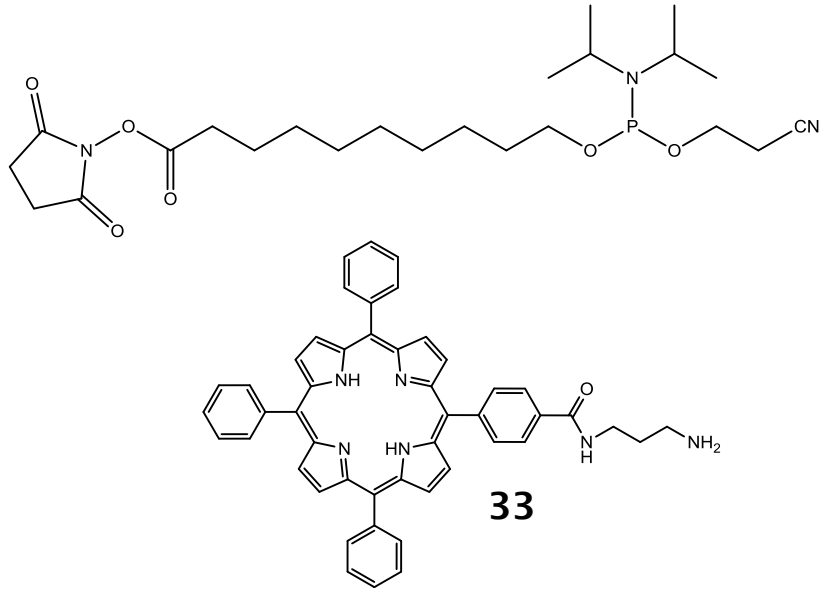

33

Figure 5.3 10-Carboxy-decyl-(2-cyanoethyl)-(N,N-diisopropyl)-phosphoramidite N-hydroxysuccinimide ester purchased form Glen Research and TPP amine.

Initially four of the designed oligos (Table 5.1) were synthesised by solid phase oligonucleotide synthesis and the carboxy modifier included at the 5'-end of the strands. These were used to test the coupling to the TPP amine porphyrin **33**. This coupling was carried out using 5 equivalents of porphyrin (compared to the 1 μmol DNA synthesis) with DIPEA in 1 mL of DMF. The reaction was designed as an on-bead labelling and was achieved by passing the porphyrin solution back and forth through the DNA synthesis column for 2 hours. The excess porphyrin was washed from the column with several aliquots of DMF. Once the solvent being passed through the column remained colourless, and the CPG beads remained a red porphyrin colour, it was clear this coupling had been successful. Cleavage and deprotection of the oligonucleotide was carried

out with ammonium hydroxide using the standard method discussed in section 1.4.

HPLC purification was required as unreacted carboxy-DNA was visible by analytical HPLC showing the coupling had not been 100 % efficient (Figure 5.4). None the less, a significant amount of porphyrin modified DNA was isolated. The peak showing the largest DNA and porphyrin absorbance (approx. 16 mins) was isolated due to this ratio of porphyrin to DNA and due to the UV-Vis spectra produced by the peak. Samples were sent to the group of Athanassios Coutsolelos at the University of Crete to confirm by MALDI-ToF mass spectrometry. This information is summarised in Table 5.2.

Strand name	Sequence
Carboxy-TPP aA	5' - X ATG CTA AGG TTC GAT CGA CTG TAC GGT
Carboxy-TPP bB	5' - X ATT ACT ACT TTC CAG CGA GAG GAT TCA
Carboxy-TPP cC	5' - X GGA TCT CAT ATT TTG CTT GCA GGC GCT
Carboxy-TPP dD	5' - X TAT GTA GCA TTT CCA GTC TTA TTA CTG

Table 5.1 Strand name and sequence for TPP modified DNA produced by coupling TPP amine **33** with carboy modified DNA. X = TPP modification.

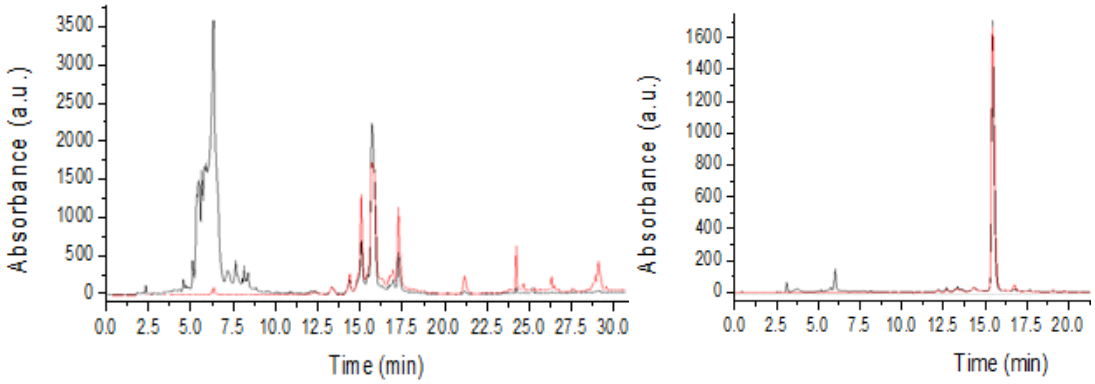

Figure 5.4 Left) Crude HPLC chromatogram of a Carboxy-TPP sample showing absorbance at 260 nm in black and absorbance at 420 nm in red. Right) Purified sample. A Polaris 3 C18-A 150 × 4.6 mm column was used at 60 °C with buffer A – 8.6 mM TEA/100 mM HFIP with 0.5 mM EDTA and buffer B - methanol. Gradient used [time (mins) (% buffer B)]; 0 (0 %), 15 (60 %), 20 (63 %), 25 (100 %). Flow rate = 1 mL min^{-1}.

Strand name	Pure DNA isolated (nmoles)	Molecular mass	Mass by MALDI
Carboxy-TPP aA	14.3	9275	9343
Carboxy-TPP bB	7.8	9203	9266
Carboxy-TPP cC	11.0	9217	9263
Carboxy-TPP dD	7.1	9175	9253

Table 5.2 Amount of pure porphyrin-DNA isolated when coupling the TPP amine **33** with carboxy-modified DNA. Also shown are the calculated molecular masses and the values obtained experimentally by MALDI-ToF mass spectrometry.

Once the carboxy-TPP strands had been made the same coupling was attempted using the di-acetylene porphyrin amine **27**. This however, did not appear to couple as well. A very small amount of porphyrin-modified DNA could be identified by HPLC showing signs the reaction can work, but it was mostly unreacted carboxy-DNA which remained. As this method did not provide the desired coupling efficiency an alternative was attempted.

The carboxy-modified oligo was synthesised via solid phase synthesis as before, but this time the CPG beads were removed from the column and placed in an eppendorf tube. The porphyrin reaction solution (porphyrin, 3 equivs. DIPEA, 6 equivs. DMF, 500 μL) was added to this tube and left for 18 hours at 25 °C in a thermomixer to agitate. As can be seen from the chromatogram (Figure 5.5), this new method was a lot more effective producing substantially more porphyrin-modified DNA. The porphyrin absorbance was monitored at 430 nm instead of the 420 nm used for the tetraphenyl porphyrins. This was only done as the absorbance maximum of the di-acetylene porphyrins is higher than that of the others.

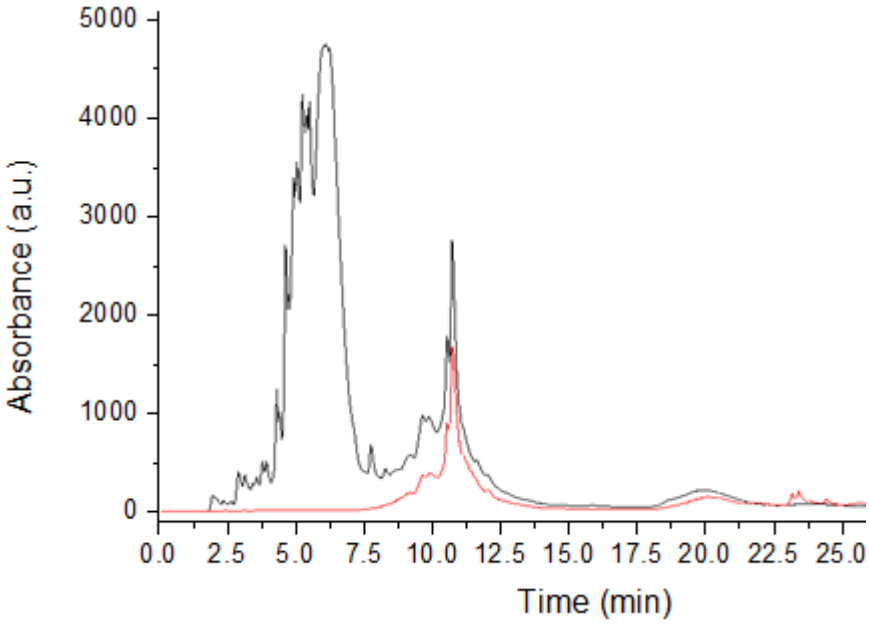

Figure 5.5 HPLC chromatogram following the coupling of the di-acetylene porphyrin amine **27** to carboxy-modified DNA. The CPG class beads were removed from the DNA synthesiser column after oligo synthesis and submerged in porphyrin/base solution overnight with shaking. A Polaris 3 C18-A 150 × 4.6 mm column was used at 60 ˚C with buffer A – 8.6 mM TEA/100 mM HFIP with 0.5 mM EDTA and buffer B - methanol. Gradient used [time (mins) (% buffer B)]; 0 (0 %), 10 (46 %), 16 (52 %), 25 (100 %). Flow rate = 1 mL min^{-1}.

As with standard solid phase oligonucleotide synthesis the DNA needed to be cleaved from the CPG beads and the bases deprotected. Following the standard procedure, ammonia was added to the beads which were later separated from the DNA in solution. It was hoped the addition of ammonium hydroxide would play one other role. Carell *et al.* have previously shown that when treating a resin bound oligonucleotide containing a TMS protected C8-Alkyne-dU (see Figure 4.2) with concentrated aqueous ammonia to cleave and deprotect, the TMS group is also removed.[218] The TMS groups on the porphyrin need to be removed to allow a Glaser-Hay coupling to proceed. It was therefore hoped that the groups protecting the porphyrin meso acetylenes would also be removed under these conditions. To check, the samples were sent for MALDI-ToF mass spectrometry. As with previous MALDI spectra, all measured values are higher than those calculated (Table 5.3). These values are

at the tips of very broad peaks however. Due to these broad peaks, it is impossible to confirm whether the TMS groups have been cleaved or not without better quality mass spectrometry data. The spectra can be viewed in the appendix.

Once the DNA was cleaved from the CPG resin and the bases and phosphates deprotected, the porphyrin-modified oligonucelotides were purified by HPLC and the amount of pure DNA collected was quantified by UV-Vis spectroscopy using the Beer-Lambert law.

Strand name	Pure DNA isolated (nmoles)	Molecular mass	Mass by MALDI
Carboxy di-acetylene aA	2.9	9235	9328
Carboxy di-acetylene bB	5.9	9163	9402
Carboxy di-acetylene cC	5.0	9177	9344
Carboxy di-acetylene dD	6.9	9135	9319

Table 5.3 The amounts of purified di-acetylene-modified DNA obtained from one amide labelling. Also shown are the calculated molecular masses of the oligonucleotides and the values obtained experimentally by MALDI-ToF mass spectrometry.

Only a small amount of pure porphyrin-modified DNA was isolated for each strand, but this was enough to carry out preliminary Glaser-Hay coupling tests.

As shown earlier, a second variant of the di-acetylene porphyrin was synthesised with an azide functionality. The di-acetylene and TPP azide porphyrins (**25** and **31**) were designed for attachment to DNA using copper-free click chemistry (see sections 4.3 and 4.4). As previously described, this coupling required oligonucleotides modified with a 5'-strained alkyne (Figure 5.6). These strands were provided by ATDBio having been cleaved from the solid support. The method for the copper-free click reactions would

therefore need to differ slightly from that used for the on-bead amide coupling above.

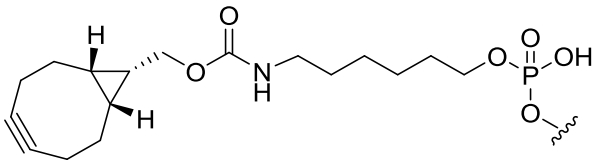

Figure 5.6 Strained alkyne modifier for copper-free click chemistry. Formed from a coupling reaction between amino C6 oligonucleotide and BCN NHS ester. Provided by ATDBio.

As with the carboxy modifier, a test reaction was carried out using the TPP azide **31**. The experimental conditions and results of copper-free click chemistry between a TPP azide and strained alkyne modified DNA have already been discussed in section 4.4. This showed a successful coupling and the production of TPP-modified DNA.

Having shown that copper-free click chemistry can work with a porphyrin azide, the reaction was attempted using the di-acetylene porphyrin azide **25** to make the sequences aA and bB as shown in Table 5.1. The reactions were carried out on 20 nmoles of DNA with 200 nmoles of porphyrin in DMF and heated to 35 ˚C for 36 hours. Reaction progress was monitored by HPLC.

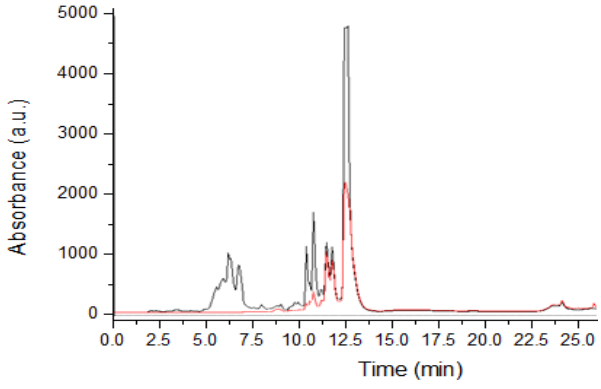

Figure 5.7 HPLC chromatogram following the coupling of the di-acetylene porphyrin azide **25** to strained alkyne-modified DNA. A Polaris 3 C18-A 150 × 4.6 mm column was used at 60 ˚C with buffer A – 8.6 mM TEA/100 mM HFIP with 0.5 mM EDTA and buffer B - methanol. Gradient used [time (mins) (% buffer B)]; 0 (0 %), 10 (50 %), 20 (60 %), 25 (100 %). Flow rate = 1 mL min^{-1}.

Conjugated Porphyrin-DNA Wire

As before, the di-acetylene porphyrin-modified DNA was purified by HPLC and quantified by UV-Vis spectroscopy. Unlike the carboxy-linked porphyrin DNA, these samples had not been treated with ammonia and so the acetylenes would still be TMS protected (see structures in Scheme 5.9). These groups needed to be removed before the Glaser-Hay coupling reaction. As it had not been conclusively proven that the ammonia does remove the TMS group from the porphyrin, the samples in water (400 µL) were treated with TBAF (1 M in THF, 50 µL, 25 °C, 30 mins). TBAF has been shown to remove the TMS groups from the meso acetylenes both in this work (section 5.2) and by others.[212] After treating the DNA with TBAF, the excess was removed using a size exclusion NAP column. Samples of the DNA, with and without treatment with TBAF, were sent to the Coutsolelos group to confirm the TMS groups had indeed been removed. The measured values are displayed in Table 5.4 whilst the spectra can be seen in the appendix.

Strand name	Pure DNA isolated (nmoles)	Molecular mass	Mass by MALDI
Cu-free di-acetylene aA TMS ON	5.2	9529	9605
Cu-free di-acetylene aA TMS OFF	-	9385	9564
Cu-free di-acetylene bB TMS ON	5.6	9457	9468
Cu-free di-acetylene bB TMS OFF	-	9313	9373

Table 5.4 The amount of di-acetylene porphyrin-modified DNA isolated by the copper-free click chemistry method starting with 20 nmoles of DNA. Also shown are the molecular masses measured by MALDI-ToF mass spectrometry before and after treatment with TBAF to remove the TMS groups.

As can be seen from the measured molecular masses of the corresponding TMS ON and TMS OFF samples, there is a drop in mass after treatment with TBAF. This is a strong indication that the TMS groups have indeed been removed. Removal of both TMS groups from a porphyrin reduces the molecular mass by 144.4 g mol^{-1}. The measured decrease after TBAF for strand aA = 41.5 and for strand bB = 94.7. These values are a lot lower than

expected so could signal that most molecules in the samples have only one or neither of the TMS groups removed. However, as shown previously, the peaks produced on the MALDI spectra are far from sharp and cover mass ranges in the region of hundreds. The measured values therefore cannot be taken as exact. As NMR spectra of the porphyrins has previously shown both TMS groups have been removed, and as a large excess of TBAF was added to the samples, it was deemed highly likely that both TMS groups have been removed leaving the acetylenes free to react in the Glaser-Hay coupling reactions.

This work has shown that it is possible to attach porphyrin compounds onto oligonucleotides modified at the 5'-position. This has been achieved using two different reactions, an amide coupling with a porphyrin amine and by copper-free click chemistry with a porphyrin azide. The coupling methods appeared to work equally well. The preferred method will come down to several factors and depend on what is to be done next.

From a financial point of view the BCN chemistry to form the strained alkyne modification is a lot more expensive than the carboxy-modifier (on top of the rest of the synthesiser reagents). However, by purchasing the strained alkyne DNA from ATDBio, the purified samples were available quicker than could be achieved in the Stulz lab.

In terms of yields, when using the copper-free method with the di-acetylene porphyrin, 20 nmoles of DNA were used in the reaction producing 5-6 nmoles of porphyrin DNA. Around 100 nmoles of strained acetylene DNA per strand was provided by ATDBio meaning these reactions could be carried out several times or on a larger scale. This is a lot higher yield than the 3-7 nmoles of porphyrin-modified DNA produced from a 1 µmol oligonucleotide synthesis for the carboxy method. So although the Cu-free method is potentially more expensive, it does appear more productive.

For the moment, both routes have provided plenty of sample with the different attachments offering further options. The triazole produced by copper-free click chemistry is more stable than the amide linkages. The ability to cleave the porphyrins from the amide linked DNA using harsh hydrolysing conditions however, could be a big advantage for many applications. Having formed the

conjugated porphyrin wire by DNA directed Glaser-Hay coupling, the covalently bound porphyrins may be detached from the DNA scaffold if this is no longer required for a particular use.

5.5 Construction of a Porphyrin Wire using a Tetraphenyl Porphyrin Analogue

Four porphyrin modified oligonucleotides were made by coupling the TPP amine **33** to carboxy-modified DNA (see Table 5.1, section 5.4). These strands were used to make control systems for the di-acetylene porphyrin wire. Systems containing 1 porphyrin (1P), 2 porphyrins (2P), 3 porphyrins (3P) and 4 porphyrins (4P) with the appropriate template strands were made up and annealed. The same systems were also set up but without the template strands. This was done to monitor any interactions between porphyrins without the template strands bringing them into close proximity. Representations of these systems are shown in the schematics in Figure 5.8.

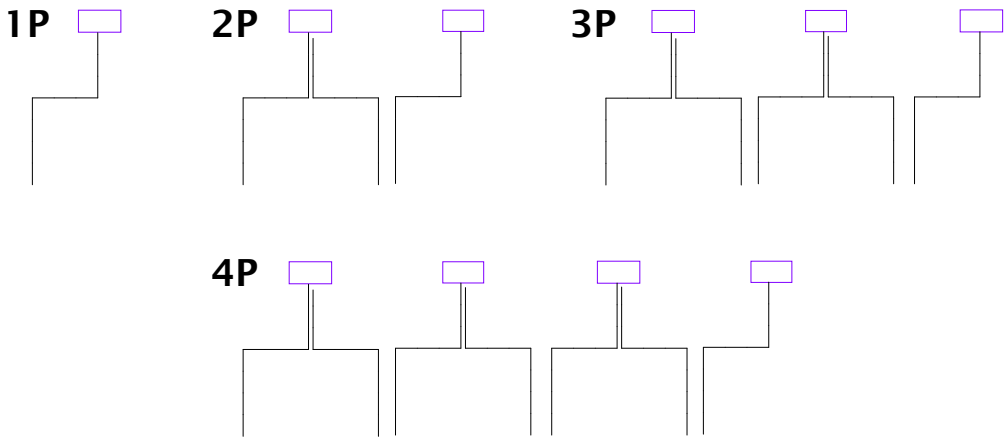

Figure 5.8 Schematics representing the 1P, 2P, 3P and 4P systems with associated template strands included. The same systems were also produced without the inclusion of the template strands. Black lines represent DNA and purple boxes are porphyrins.

Analysis was carried out by UV-Vis spectroscopy, fluorescence spectroscopy and native polyacrylamide gel electrophoresis (native PAGE). These techniques were used to first show whether the template strands were annealing to the porphyrin strands, and then to see if there was any interaction between porphyrins.

Gel electrophoresis of nucleic acids is commonly done using agarose gels or polyacrylamide (PAGE) gels. Both techniques separate oligonucleotides by size, shorter strands moving further through the gel matrix as they face less residence from the medium. This movement is caused by placing a potential across the gel. Due to the negatively charged phosphate backbone of DNA, the molecules are pulled towards the anode at the far end of the gel from where the samples were loaded. Agarose gels are generally used for relatively large DNA molecules and polyacrylamide for greater separation of shorter DNA. Polyacrylamide gels can also be native or denaturing. The addition of a denaturing agent, such as urea, to a gel disrupts the secondary structure of a DNA duplex resulting in only single stranded DNA. For this TPP system, a native gel was required. This does not break up the secondary structure of the molecules so a fully annealed 4 porphyrin system (4P) should be retained more on the gel than the 1P sample due to its greater size. This technique was therefore used to check that the systems were being fully formed upon annealing and the resulting gel shown in Figure 5.9. The systems were set up with 2.5 nmoles of each strand in a sample (a 1:1:1 ratio of aA : template : bB etc.).

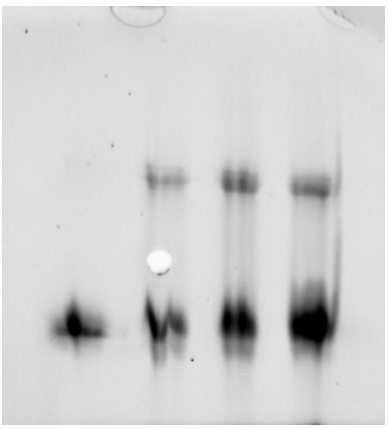

Figure 5.9 Native PAGE gel (20 % acrylamide, 37.5 : 1 crosslinking) of systems 1P – 4P with associated template strands. Visualised under UV light (no stain). Direction of travel from top to bottom.

From the gel in Figure 5.9, two sets of bands can be seen clearly. The lower bands align with the single porphyrin 1P strand. This suggests that there is a large proportion of the DNA remaining in the single stranded form in all samples and therefore the annealing process was not very successful. The 4P band appears brighter than the rest. This is to be expected as there was more porphyrin containing strands in this sample than the rest. The second set of bands did not move as far through the gel and there is no 1P band associated with this set. This all suggests that some annealing has taken place and multi-porphyrin systems have been formed. The presence of a band in the 2P lane for this set suggests that this set of bands corresponds to two porphyrins connected by the one template strand (2P). Potentially, a very faint band could be seen higher up the gel in the 3P and 4P lanes, but was by no means conclusive. With more sample, or a slower annealing method, these bands may have become clearer but this was not tested. It is also possible that the 3P and 4P systems have been formed to some extent but the sample was too bulky to enter the gel.

This gel has shown that porphyrin DNA strands can be brought together by template strands, but adding more porphyrins into the system makes this much lower yielding.

Further investigation into these systems was carried out using UV-Vis and fluorescence spectroscopies (Figure 5.10). As well as the fully annealed systems, a second set of samples was made up without the inclusion of the template strands. Porphyrins in close proximity interact with each other by π-stacking. By comparing the full systems and systems without the template strands to bring the porphyrins into close proximity, the spectroscopic methods could probe these interactions.

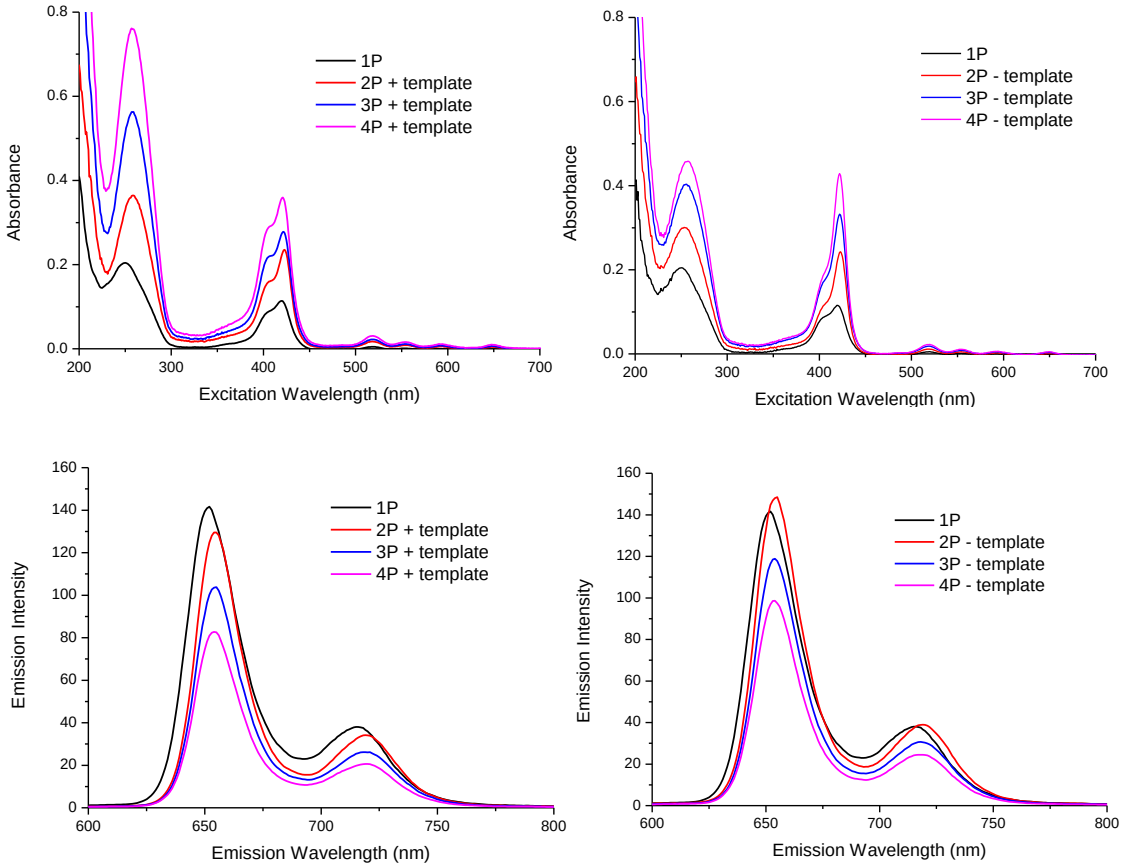

Figure 5.10 Top) UV-Vis spectra of the 1 – 4P systems. Bottom) Fluorescence spectra of the 1 – 4P systems, λ_{ex} = 420 nm. In both cases; left) Fully annealed systems. Right) Systems minus the template strands.

If the UV-Vis data is considered first, the peaks at 260 nm, as expected, show a stronger absorbance when more DNA is present. The intensity of the porphyrin Soret band also increases with the inclusion of more porphyrins into the system, again, as would be expected. The Soret peaks produced by the systems with the template strands (left) show broader peaks compared to the samples without the templating (right) caused by a more pronounced shoulder at the lower wavelength side of the main peak. This broadening of the peak shows the porphyrins are interacting with each other.[212] Values for this broadening in the form of full width at half maximum (FWHM) are given in Table 5.5.

Sample	Full Width at Half Maximum (nm)	
	With template strands	Without template strands
1P	35	35
2P	35	25
3P	37	28
4P	37	21

Table 5.5 Values for Soret peak widths using full width at half maximum.

Without the template strands (right), a bit of broadening is seen as the porphyrins can still interact in solution, but the peaks are clearly a lot sharper. This suggests that the templating of the porphyrin strands is having an effect by bringing the porphyrins closer together to allow an interaction. What is interesting is these peaks become sharper the more porphyrin strands there are in solution. The 1P sample which contains only 2.5 nmoles of the single porphyrin strand is a lot broader than the 4P sample without template strands.

Fluorescence spectroscopy can also monitor the interactions between porphyrins. The samples used were the same as above, therefore, 1P contains 2.5 nmoles of porphyrin DNA, whereas 2P contains 2 × 2.5 nmoles of porphyrin DNA plus the 2.5 nmoles of template strand. It might be expected that more porphyrins in the system would lead to a higher fluorescence due to the increased number of fluorophores. This however, is not the case. Poprhyrins in close proximity fluorescently quench leading to lower emission intensity with more fluorophores present.[225-228] This trend is shown in both sets of fluorescence spectra where the emission intensity decreases as more porphyrins are introduced to the system (1P → 4P). Values for the emission maxima at approximate wavelengths 653 nm and 718 nm (peak maxima) for each of the samples are displayed in Table 5.6. The decreasing emission intensity for the samples without the template strands shows that the porphyrins can interact in solution without this templating. The one outlier in this data is the 2P without template sample which shows higher fluorescence than the single porphyrin strand. This is most likely due to the concentration of the sample.

Sample	Emission Intensity at the stated wavelength			
	With template strands		Without template strands	
	653 nm	**718 nm**	**653 nm**	**718 nm**
1P	141.6	38.0	141.6	38.0
2P	129.5	34.2	148.5	38.9
3P	103.8	26.2	118.8	30.7
4P	82.7	20.6	98.6	24.5

Table 5.6 Values for the emission intensity at the maximum of both peaks for each of the samples with and without the addition of the template strands.

Differing emission intensity of samples with and without the addition of the template strands can also be observed. The emission maxima for corresponding samples (2P + template and 2P – template etc.) all show lower fluorescence in the samples containing the template strand(s). The fluorescence quenching demonstrated by this data provides further evidence that the template strands are having the desired effect and bringing the porphyrin units into close proximity where there is a stronger interaction.

The spectroscopic data along with the acquired native PAGE gel all suggests that, to at least some extent, the template strands are having the desired effect and upon annealing bring the porphyrins into closer proximity. This is a key result in showing the DNA can provide a template for the porphyrin Glaser-Hay reactions.

5.6 DNA Directed Glaser-Hay Coupling to Form the Conjugated Porphyrin Wire

With evidence collected to show the two porphyrin-DNA strands can be linked by a template strand, the DNA directed Glaser-Hay coupling could be attempted. Highlighted previously was the work of Gothelf who carried out Glaser-Hay coupling to link oligo(phenylene ethylene) units in aqueous solvent.[189] Anderson and Bradley have used Glaser-Hay coupling on di-acetylene porphyrins to form a conjugated porphyrin polymer in organic solvent.[210]

Both the reactions mentioned here have aspects in common with the DNA directed Glaser-Hay coupling but use very different solvent systems. The best conditions needed to be carefully considered. Due to the insolubility of DNA (porphyrin-modified or otherwise) in dichloromethane, as used by Anderson in his porphyrin reactions, the conditions laid out by Gothelf were the starting point. These are displayed in Table 5.7.

Component	Concentration
DNA	30 pmoles per strand (1 μM)
CAPS buffer	10 mM
$NaCl_{aq}$	100 mM
THPTA ligand	6.9 mM
CuOAc	0.1 mM
$CuSO_4$	1 mM

Table 5.7 The reaction conditions employed by Gothelf *et al*. to covalently link oligo(phenylene ethylene) units. These conditions were followed to attempt the DNA directed Glaser-Hay coupling of the di-acetylene porphyrin-modified DNA with the inclusion of the template strand.

30 pmoles of each DNA strand was initially annealed in CAPS buffer and $NaCl_{aq}$. A catalytic mixture of THPTA ligand (see Figure 4.1), CuOAc and $CuSO_4$ was then added and the samples shaken at 25 °C overnight.

Conjugated Porphyrin-DNA Wire

Gothelf's system has two oligos modified with the phenylene ethylene unit which are fully complementary to each other and hence there was no need for a template strand (Figure 5.2). This lead to a slight change in the conditions used with the porphyrin-DNA to take this required template strand into account. Equal amounts of the three strands were combined increasing the overall concentration of DNA in the reaction mixture. As the number of reacting acetylenes remained the same however, the concentrations of all other reagents were left unchanged.

The TMS groups blocking the terminal alkynes had previously been removed using either ammonia or TBAF depending on the linker (amine or azide) connecting porphyrin to DNA. This enabled the porphyrin-modified DNA produced by both methods to be tested in a Glaser-Hay coupling. The reactions were set up using the conditions discussed above with more detail provided in section 8.13. Whilst the reactive part of the molecule, the acetylene groups, were the same for each DNA strand, the linkers may have some effect on the reactivity so both sets of porphyrin DNA needed to be tested. If the Glaser-Hay coupling works in both cases, this would act as proof that both the ammonia and the TBAF methods can be used to deprotect the TMS acetylenes.

The reactions were followed by gel electrophoresis as was done for the TPP test system in section 5.5. However, this time denaturing PAGE was used to determine if the porphyrins had been covalently linked. Whereas native PAGE gels leave the secondary structure of DNA intact, denaturing PAGE gels break up any formed duplexes. As a result, the template strand will be removed from this system. This will leave either a lot of porphyrin-DNA single strands indicating the reaction has not occurred, or a band will be seen on the gel which has not moved as far as the single porphyrin-DNA strands. This will indicate the reaction has been successful as the covalently linked strands will be twice as long and contain one more porphyrin than the single strands making it a lot bigger and slowing the progress through the gel.

The denaturing PAGE gel for the Glaser-Hay coupling using Gothelf's reaction conditions as stated above is shown in Figure 5.11.

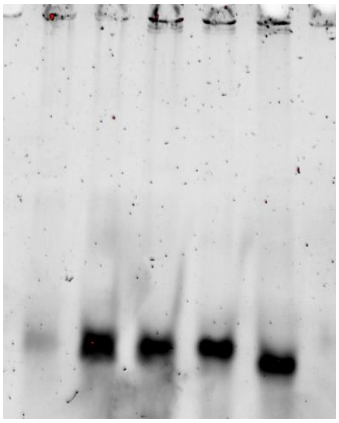

Lane 1 2 3 4 5

Figure 5.11 Urea PAGE gel for the Glaser-Hay coupling using Gothelf's reaction conditions. 15 % acrylamide, 200 volts, 2 hours, stained with Sybr gold. Lane 1 = Single stranded template strand. 2 = Single stranded porphyrin DNA. 3 = negative control. 4 = Reaction with amide linker. 5 = Reaction with click chemistry triazole linker. The negative sample was fully annealed but no copper was added. Gel run from top to bottom.

As can be seen from the gel, there appears to be a lot of single stranded DNA present in all lanes and no evidence that the DNA directed Glaser-Hay coupling has been successful.

Given this result, a series of other conditions were tested to attempt to achieve a positive outcome. Different copper (I) and (II) catalysts were tested with varying concentrations (up to 10 × more copper). Samples were left for longer (up to 72 hours) and heated to 35 °C as well as cooled to 4 °C. Different bases (NEt_3, Pyr, TMEDA) were added to try and aid the reaction.

No matter the combination of conditions, no evidence was found to suggest any Glaser-Hay coupling had taken place between porphyrins in any of the tested samples.

As the reactions had been unsuccessful in aqueous solvent, a new approach was attempted. In all the previous work attempting Glaser-Hay couplings on porphyrins by the likes of Anderson *et al*. highlighted above, more traditional

Hay type conditions were used (see Scheme 5.1). These reactions were all carried out in chlorinated solvents. As previously mentioned, DNA is insoluble in these types of solvents. To solubilise the Poprhyrin-DNA, half an equivalent to the number of phosphate groups of tetrabutylammonium hexafluorophosphate (TBA PF_6) was added to the DNA in water. This means 13 equivalents of TBA PF_6 was added to the 27-mer DNA (one less phosphate than bases). The mixture was gently heated until all the TBA PF_6 was dissolved then the solvent was removed *in vacuo*. Addition of 1, 2-dichloroethane (DCE) re-dissolved the DNA proving this experiment a success. DCM was trialled initially but the solvent all evaporated overnight despite a sealed reaction vessel.

With the annealed two porphyrin system now soluble in a chlorinated solvent, the coupling could be attempted using CuCl (1 mM) and TMEDA (7 mM) to catalyse. The reaction was allowed to proceed in a similar fashion to the previous tests, 25 ˚C with shaking. Once again denaturing PAGE was used to check for any signs of product and is shown in Figure 5.12. The first sample was taken after 3 hours and the second after 24 hours. A much larger gel was used to make sure that any product was being separated from the single stranded DNA.

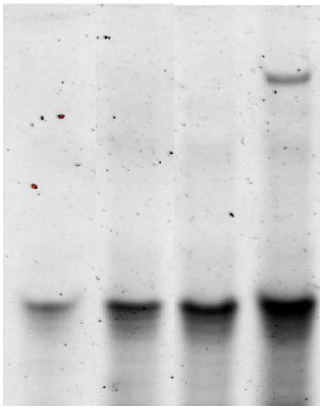

Lane 1 2 3 4

Figure 5.12 Urea PAGE gel for the DNA templated Glaser-Hay coupling reaction between two porphyrins in chlorinated solvent. 20 % acrylamide, 200 volts, 4 hours, stained with Sybr gold. Lane 1 = Single stranded porphyrin DNA. 2 = negative control. 3 = Reaction after 3 hours. 4 = Reaction after 24 hours. Gel run from top to bottom.

As can be seen from the gel, there are bands in each lane corresponding to single stranded DNA as was observed in all previous attempts. However, in lane 4 (reaction time 24 hours) there appears to be a second band visible towards the top of the gel. This could be product. The gel is denaturing so this band cannot be due to any duplex DNA and no long single stranded DNA was added to the sample. The higher band has moved less than half the distance through the gel compared to the lower band which would be expected for a product twice the size and containing an extra porphyrin.

Due to the reactions scale, all of the reaction mixture was used on the gel. For this reason no further analytical data could be obtained to confirm whether the DNA directed Glaser-Hay coupling has formed some covalently linked porphyrin-DNA.

This is an excellent result given the lack of positives from all previous experiments. Unfortunately, time restraints on the project meant no further results could be obtained, though a clear plan remains for progressing. Firstly, repeats of the reaction in chlorinated solvent must be carried out in order to confirm the results presented here. The conditions need to be optimised due to the large volume of unreacted porphyrin strands remaining in the sample even after 24 hours. With a fully optimised protocol, a larger amount of the product can be isolated either through PAGE or by HPLC. A mass spectrum and other spectroscopic data can then be obtained to prove the carbon-carbon bond has been formed and the two porphyrin-modified strands have indeed been linked in the DNA templated reaction.

5.7 Conclusions: Conjugated Porphyrin-DNA Wire

The aim of this part of the project was to produce a porphyrin wire with some differing characteristics to the Zipper array. A porphyrin with an acetylene group on two opposing meso positions was to be used to construct a covalently linked, conjugated system.

Many difficulties were encountered working on this system but huge advancements have been made. The porphyrin was originally designed to contain a carboxylic acid functional group in order to be coupled to amino-modified DNA. With this approach proving unsuccessful, a redesign of the synthetic route led to two new alternatives, a porphyrin amine and azide. The synthetic procedures to produce these two compounds are now fully established allowing the syntheses to be completed relatively quickly and efficiently. Through the use of different chemistries, both forms of the di-acetylene porphyrin have been attached to the 5'-terminus of oligonucleotides.

Extensive preliminary tests of the DNA directed Glaser-Hay coupling have been carried out trialling many different conditions. Initially the reactions were attempted using aqueous solvents but no evidence of a reaction could be seen by gel electrophoresis. No definitive explanation for the lack of reactivity has been found but it is potentially a result of the hydrophobic porphyrins not mixing well with the aqueous solvent. Porphyrins form π-stacks, and this characteristic is further promoted by the hydrophobic effect.[229] If the porphyrins are stacking face-to-face, this could explain why the acetylene groups are not aligning and able to react.[230]

There are many examples of Glaser-Hay type reactions being carried out on porphyrins, all of which proceed in chlorinated solvents. Using TBA PF_6 to make the DNA soluble in 1, 2-dichloroethane enabled the DNA directed Glaser-Hay coupling to be tested under these conditions. This appears to have been a lot more successful than previous tests with the emergence of a new band on the gel in a position consistent with that of a larger oligo. Only a single reaction has been carried out however, so more testing is required before the product can be confirmed.

Although a fully functioning multi-porphyrin wire could not be assembled and tested, great strides have been made towards this goal. The initial test of the DNA directed Glaser-Hay coupling has shown promising signs and a clear plan of action exists should this project be continued in the future.

6. Structural Analysis of Porphyrin-Modified DNA

6.1 Introduction to Circular Dichroism Spectroscopy

Circular dichroism (CD) spectroscopy is a technique which can be used to determine the secondary structure of macromolecules such as proteins and DNA.[231, 232] This is achieved using circularly polarised light from the UV-Visible region of the electromagnetic spectrum. Circularly polarised light originates from unpolarised light. This is how light is emitted from all natural and artificial sources. For unpolarised light the electric field vector oscillates in every possible direction. During this project, CD data were acquired at the Diamond Light Source, Didcot, Oxfordshire. Here a synchrotron creates the unpolarised light using an electron beam.[233] The resulting light is first polarised into plane polarised light using a polarising filter. This gives a wave with the electric field vector oscillating in a single plane. This can be illistrated as a single sine wave. Then using a birefringent crystal or a quarter-wave plate at 45˚ to the polarisation axis, the wave is rotated into a spiral thus creating circularly polarised light. In this waveform the electric field stays at the same strength but is continually changing direction, tracing out a helix as the wave moves forwards resulting in the helical wave. The steps in producing circularly polarised light are demonstrated in the diagram in Figure 6.1.

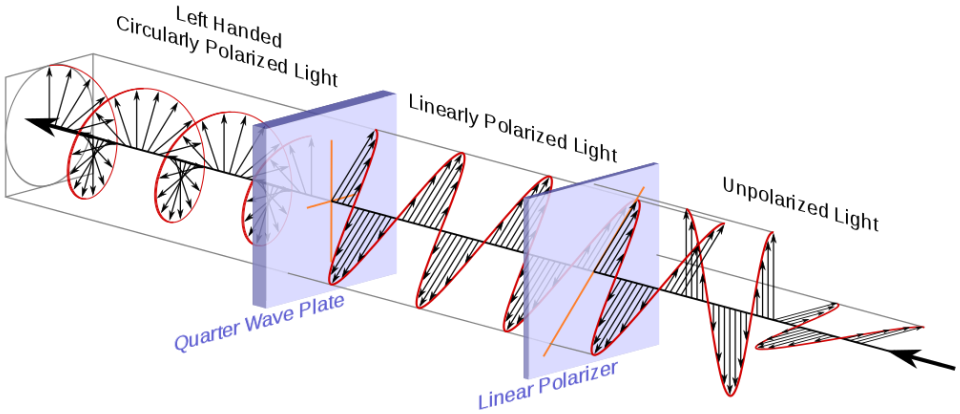

Figure 6.1 Diagram showing the conversion of un-polarised light to circularly polarised light.[234]

The light can be made to spiral in one of two opposite directions. These are termed left circularly polarised (LCP) and right circularly polarised (RCP) light. For LCP light, the direction of the electric field vector (black arrows, Figure 6.1) rotates anti-clockwise as the wave moves away from the source. RCP light has a clockwise rotation as observed from the source. Chiral molecules, such as proteins and DNA, absorb left and right circularly polarised light to different degrees. By measuring the molecule's absorbance of both forms of light (at the same wavelength) the difference can be found using Equation 2.

$$\Delta A = A_L - A_R$$

Equation 2 The difference in left and right circularly polarised light.

The absorbance can be measured over a range of wavelengths and the difference at each point plotted on a graph. An example of a spectrum produced by CD spectroscopy is shown in Figure 6.2. This is a spectrum of natural B-DNA. As can be seen, a bisignate curve is produced with the trace crossing zero at the absorption maximum (260 nm). This effect is termed the Cotton effect, named for Aimé Cotton the first person to observe this phenomenon in 1895.[231] B-DNA is an example of a positive Cotton effect followed by a negative Cotton effect as the spectrum first increases as the wavelength shortens. Different conformations of DNA and proteins have characteristic spectra which allows CD spectroscopy to be used for structural analysis. The amplitude of the CD signal is defined as, $\Delta\varepsilon_1 - \Delta\varepsilon_2$ where $\Delta\varepsilon_1$ and $\Delta\varepsilon_2$ are the intensities of the peak and trough respectively.

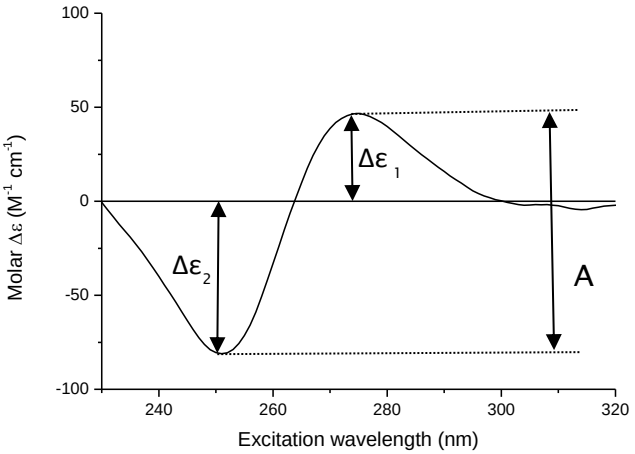

Figure 6.2 An example CD spectra produced by unmodified B-DNA showing a positive Cotton effect followed by a negative Cotton effect. A = amplitude. Δε = intensity of peak.

The CD spectrometer measures the difference in absorbance of left and right circularly polarised light in terms of ellipticity (millidegrees) using a sample of known concentration and a fixed path length. This is then converted into the concentration independent units of Molar Δε using Equation 3.

$$Molar\ \Delta\varepsilon = \frac{mdeg}{32980\ cL}$$

Equation 3 Formula for the conversion of millidegrees into the concentration independent units of Molar Δε. mdeg = measured difference in absorbance. c = concentration (mol dm^{-3}). L = pathlength (cm).

CD spectroscopy can also be used to probe the effect of chromophores attached to DNA.[235] Achiral molecules which would be optically inactive by CD spectroscopy can produce a CD signal if they are held in a chiral environment. Chirality is then induced into the molecule through the environment. Both the interactions between chromophores, and the structural changes these molecules cause to the DNA backbone can be studied using CD spectroscopy. Previous work in the Stulz group has used CD spectroscopy to look at porphyrin-DNA systems like the Zipper array described in Chapter 3.[14, 114, 115] Other groups, notably those led by Berova, Balaz and Purrello, have also

studied the relationship between porphyrin modifications and changes in the CD spectra in order to decipher the changes being caused to the DNA structure.[16, 231, 236-242] The appearance of the induced CD signal in the porphyrin region is affected by the nature of the porphyrin linker to the DNA and the conformation of the underlying DNA scaffold. These characteristic signals make porphyrins excellent chiroptical probes.[243]

6.2 Synthesis of Porphyrin-Modified DNA for Circular Dichroism Spectroscopy

The aim of this part of the project was to study the changes that occur in the CD spectra as more and more porphyrin modifications are added into the system. A set of DNA duplexes were designed which are adapted from the self-complementary Dickerson-Drew dodecamer.[40] Two complementary strands were designed (rather than one self-complementary strand) and are shown in Figure 6.3. Site **X** can be either a natural thymine base, or one of the porphyrin modified T bases (**P**) for which the synthesis is described in Chapter 3. This allows duplexes with 0, 1, 2, 3 and 4 modifications in all the different combinations to be made.

5' – CGC A**X**T ATA **X**GC
3' – GCG **X**AA TA**X** ACG

Duplex	Duplex name (Mods on strand A / Mods on strand B)
5' – CGC ATT ATA TGC 3' – GCG TAA TAT ACG	Un/Un
5' – CGC ATT ATA TGC 3' – GCG TAA TA**P** ACG	Un/1P
5' – CGC A**P**T ATA TGC 3' – GCG TAA TA**P** ACG	1P/1P (far)
5' – CGC ATT ATA **P**GC 3' – GCG TAA TA**P** ACG	1P/1P (near)
5' – CGC ATT ATA TGC 3' – GCG **P**AA TA**P** ACG	Un/2P
5' – CGC A**P**T ATA **P**GC 3' – GCG TAA TAT ACG	2P/Un
5' – CGC A**P**T ATA **P**GC 3' – GCG TAA TA**P** ACG	2P/1P
5' – CGC A**P**T ATA **P**GC 3' – GCG **P**AA TA**P** ACG	2P/2P

Figure 6.3 The eight duplexes assembled containing 0, 1, 2, 3 or 4 porphyrin modifications (**P**) in different positions.

As is shown in Figure 6.3, each duplex is named to describe the number of modifications on each strand. For example, the duplex 2P/1P has 2 porphyrin modifications in the A strand (top strand as shown in Figure 6.3), and 1 porphyrin modification in the B strand. There are two 1P/1P samples which have been distinguished with "near" and "far". This refers to the number of base pairs between the porphyrin modifications. For 1P/1P (near) the porphyrins are on adjacent base pairs. For 1P/1P (far) there are 3 unmodified base pairs between the porphyrins. The strands for these duplexes were synthesised twice. One set containing the amide linked porphyrin as the modification (see section 3.2), and the other containing the acetylene linked porphyrin (see section 3.3). From here on, to distinguish which modification is used, the duplexes will be referred to with the prefix's Porph Amide and Porph Acet, for example, Porph Amide Un/1P.

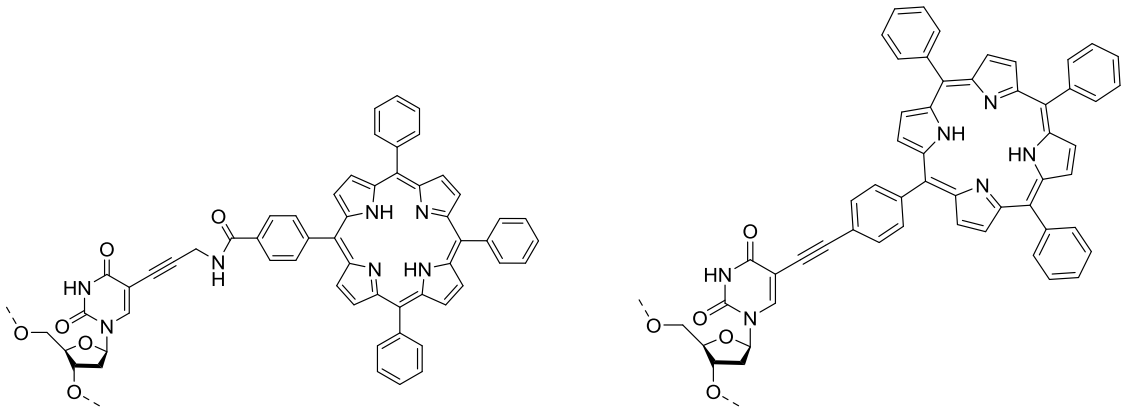

Figure 6.4 The amide linked (left) and acetylene linked (right) porphyrin modifications included in the synthesised duplexes.

Five single strands modified with one or two porphyrin units were required to make up each set of duplexes along with the two unmodified strands. These were all synthesised using solid phase oligonucleotide synthesis as described in section 3.4. The porphyrin monomers were converted into phosphoramidites using a chlorophosphitylating reagent and incorporated into DNA on the automated synthesiser with an extended six minute coupling time. The crude strands were then purified by HPLC. Example chromatograms are shown in Figure 6.5 of a single strand with 1 amide linked porphyrin modification before and after purification.

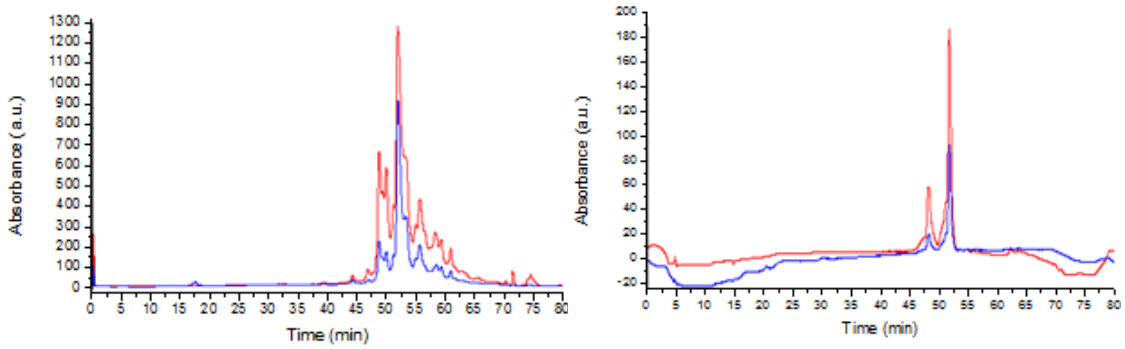

Figure 6.5 HPLC chromatograms of a Porph Amide 1P single strand produced after oligonucleotide synthesis (left) and after HPLC purification (right). Blue lines show absorbance monitored at 260 nm, red lines show absorbance monitored at 420 nm. A Polaris 3 C18-A 150 × 4.6 mm column was used at 60 ˚C with buffer A – 8.6 mM TEA/100 mM HFIP with 0.5 mM EDTA and buffer B - methanol. Gradient used [time (mins) (% buffer B)]; 0 (0 %), 20 (40 %), 60 (85 %), 65 (100 %).

As can be seen from the crude chromatogram there is one clear peak which shows the largest DNA absorption (in blue) and also a large porphyrin absorption (red). As the DNA synthesis only included one porphyrin nucleotide, the overall trityl yield measured on the synthesiser was fairly high meaning this largest peak should be the product. To try and confirm this theory the synthesis had been carried out with the last DMT group still attached. As this is a large hydrophobic group it should slow the desired products progression through the column resulting in a longer retention time. By taking a sample and adding a small amount of 2 % TFA the DMT group was cleaved. The sample was then neutralised with ammonium hydroxide. When injecting this sample onto the HPLC using the same method, the only peak that should come at a different retention time is the product strand which no longer contains the DMT group. This confirmed the large peak just after 50 minutes in Figure 6.5, was the desired product as this was the peak that was eluted from the column a little earlier following the removal of the DMT group.

With the desired product confirmed this peak was isolated. A sample of this collected pure product was then re-injected to check the purity. As can be seen from the chromatogram in Figure 6.5 (right), a large peak is seen just

after 50 minutes as expected, but a smaller peak is also present just before 50 minutes. A peak is seen at this time in the crude chromatogram but should not be contaminating the product as the collection of the desired peak did not begin until after the previous peak had finished eluting. It was initially hypothesised that this minor peak was the result of the porphyrin-DNA degrading. The absorption spectra of the two peaks were then consulted (Figure 6.6).

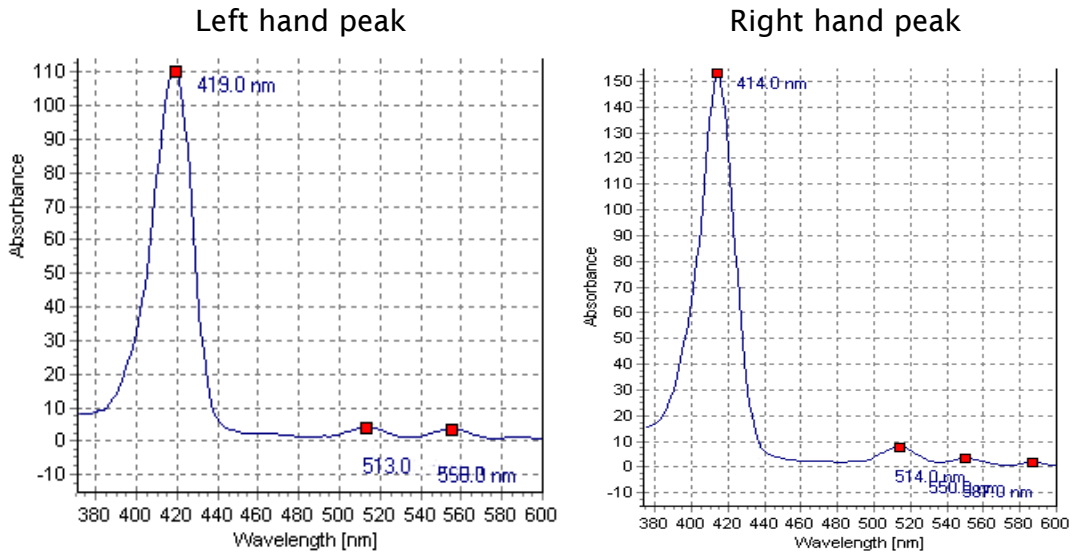

Figure 6.6 UV-Vis spectra of the porphyrin region for the two peaks shown in the Porph Amide 1P pure chromatogram (Figure 6.5, right). The left hand peak shows only two Q-bands suggesting metalation.

Analysing the peaks with the HPLC's in built UV-Vis spectrometer showed some differences. The clearest difference is the two peaks showing different wavelengths for the Soret band maxima. There is also a suggestion that there are two Q-bands present in the left hand peak and at least three in the right hand peak, though it is possible that additional Q-bands may exist at longer wavelength. Berova *et al.* have previously reported metalation of porphyrins during HPLC and suggested that there are metal ions in the buffers which are being complexed by the porphyrins.[240] To counter this, all following HPLC purifications of porphyrin-modified DNA were carried out with 0.5 mM EDTA added to the HFIP/TEA aqueous buffer. This addition of the metal ion

chelating ligand appeared to help the situation as the amount of metalation observed was reduced to leave a single product.

The acetylene linked porphyrin was zinc metalated during its synthesis, but the zinc is removed by the acid during the detritylation step on the DNA synthesiser. This is clearly visible by the colour change from purple to green as acid is flushed through the column. For this reason, these purifications also required the presence of the EDTA in the solvent.

Once all the single stranded DNA had been purified, the two sets of porphyrin-modified duplexes (Figure 6.3) were formed by annealing an A single strand with the appropriate B strand (2.5 nmoles each) in 500 μL of a 100 mM NaCl, 50 mM phosphate buffer, pH = 7. This gave samples with a 5 μM duplex concentration. The annealing process is described in section 8.11. Once annealed, the samples were taken to the B23 beamline at Diamond Light Source to be analysed by CD spectroscopy.

6.3 Circular Dichroism Spectra of Porphyrin-Modified DNA

The CD spectra of the porphyrin-modified duplexes (Figure 6.3) were acquired with two distinct regions of interest in mind. The first, 195 – 350 nm, is the DNA region of the spectra. Here changes to the secondary structure of the DNA can be monitored with increasing modification. The second region, 350 – 550 nm, is the porphyrin Soret band region. Here interactions between the porphyrins could be investigated, and it was hoped that important information about positioning and stacking could be obtained. The Q-band band region (500 – 750 nm) could also be observed, but due to the relative absorption intensities of these peaks compared to the Soret band, the CD spectra of this region is not very intense. It was therefore decided to only monitor the Soret region.

Due to the quality of the data obtained from the beamline in the different regions, two different systems were used to measure the CD spectra and the results combined. The B23 beamline provided the data for the DNA region of the spectra (195 – 350 nm). An Applied Photophysics Chirascan CD spectrometer was used for the porphyrin region (350 -550 nm) since the sensitivity of the beamline detector is rather low in the visible range. The full spectrum of the 5 μM porphyrin amide duplexes are shown in Figure 6.7 and the individual regions highlighted in Figure 6.8 and 6.9. All eight duplexes are plotted on the same graph so comparisons can be made and changes to the spectra followed as each modification is added. As highlighted in section 6.1, the CD spectrometers measure the difference in absorbance in units of millidegrees. All the following data are presented with these readings converted to the concentration independent units of molar $\Delta\varepsilon$ using Equation 3.

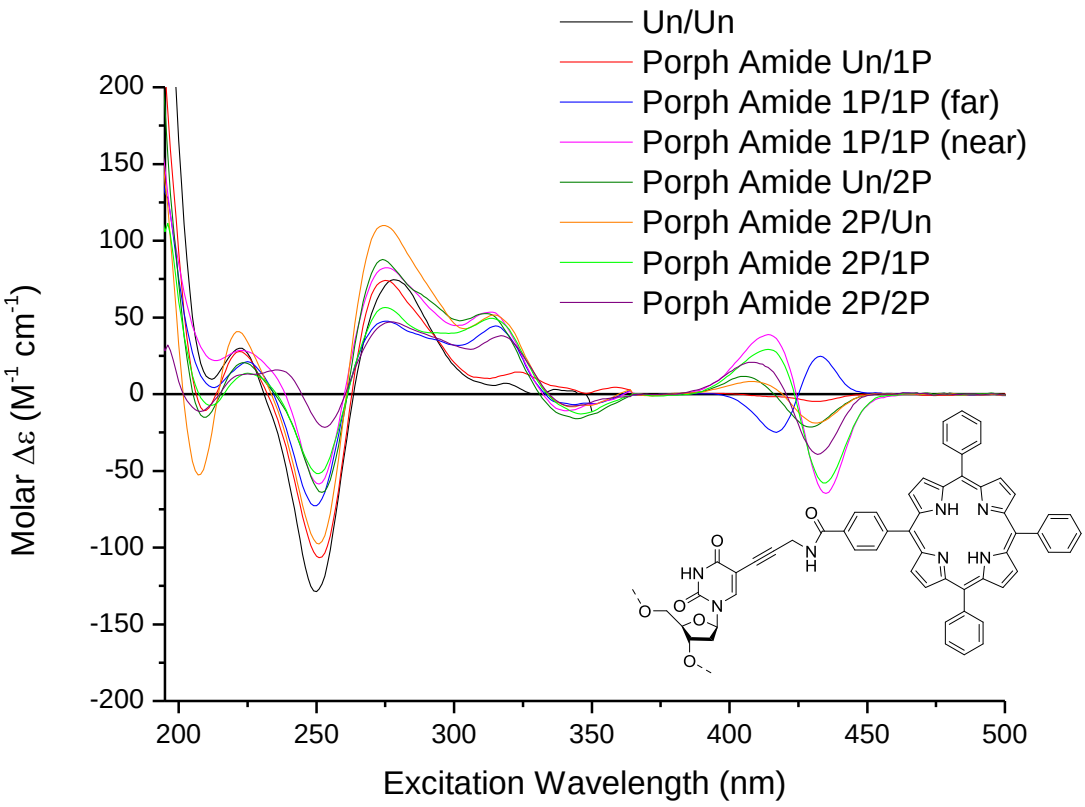

Figure 6.7 Full CD spectra acquired for the duplexes containing the porphyrin amide modification.

As can be seen, there are clear changes in both regions of the spectra as more porphyrin modifications are added into the system. Starting with the DNA region (195 – 350 nm, Figure 6.8) there appears to be changes in signal intensity at all maxima and minima. The clearest sign of this is the minimum at approximately 250 nm. This large trough for the unmodified duplex (black line) becomes much smaller by the time four porphyrins are included but a trough is still clearly visible. Another area of interest occurs between 225 and 250 nm. As the minima at 250 nm rise, the maxima at 225 nm appear to drop and a new peak begins to appear at approximately 230 nm as a shoulder. This is most clearly seen in the 2P/2P spectra (purple line) where this peak is actually larger than the original peak. The other effect caused by this new peak is a slight bathochromic shift in the trough at 250 nm, which increases by 3 nm for the 2P/2P sample.

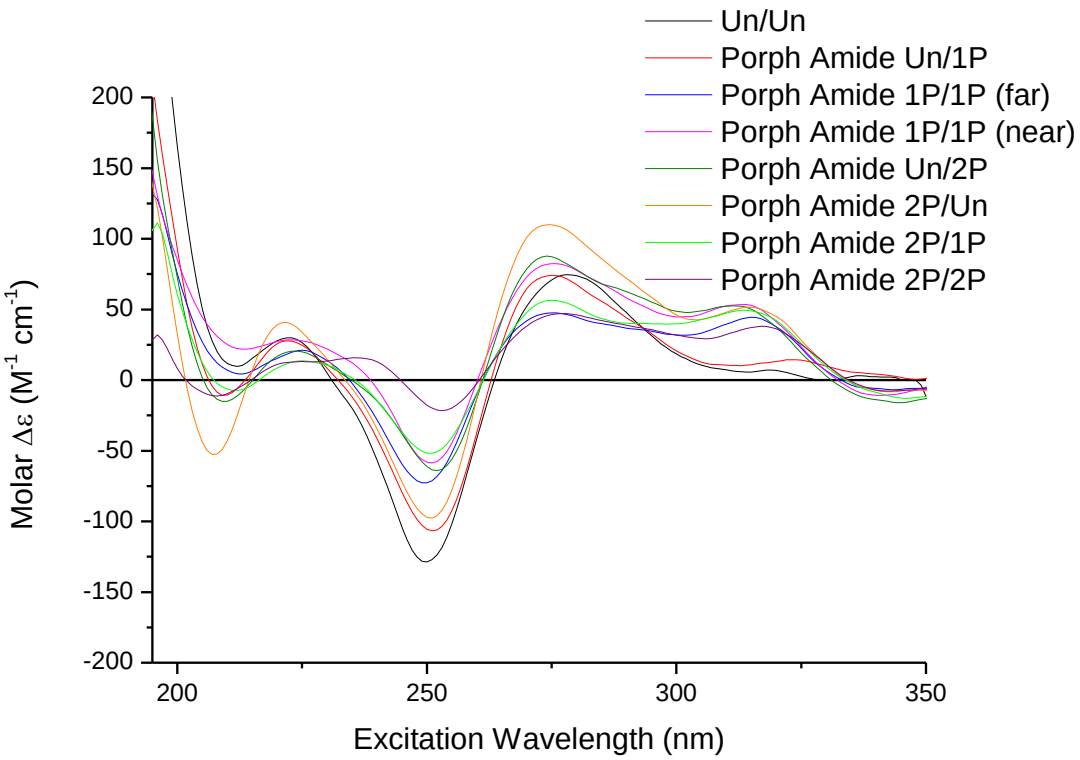

Figure 6.8 Expanded DNA region of the porphyrin amide spectra.

The other major areas in the region are at approximate wavelengths 280 nm and 320 nm. These positive peaks show significant differences, however, any patterns are not so obvious. There is no clear increase/decrease of the peak height as more modifications are added. There does however appear to be two different groups at 280 nm. The samples Un/Un (black), Un/1P (red), 1P/1P near (pink), Un/2P (dark green) and 2P/Un (orange) appear in a group with a slight gap to the other three spectra below. This observation is highlighted when comparing to the porphyrin acetylene spectra further below.

The final peak in the DNA region is seen at approximately 320 nm. Once again there is no obvious pattern other than the peak only occurring when there is more than one porphyrin present in the system. This suggests this is a direct result of the porphyrin amide modification.

Comparing the two samples 2P/Un and Un/2P shows an interesting difference. The 2P/Un sample (orange line) shows significantly stronger signals than the reverse Un/2P sample (dark green line). This could be due to an error in the

sample, for example, a higher concentration or excess of one single strand. However, when looking at the porphyrin region (Figure 6.9), the spectra are of almost identical intensity suggesting the samples are fine. This suggests these observed differences in the DNA region are sequence induced. The A and B strands are different and so the porphyrin modifications will be surrounded by different bases in each sample. This may be causing the porphyrins to be interacting differently in the two samples. This theory is backed up by the porphyrin region spectra where although the two spectra are of similar intensity, they are shifted slightly relative to each other suggesting the porphyrins are interacting with each other in a slightly different way.

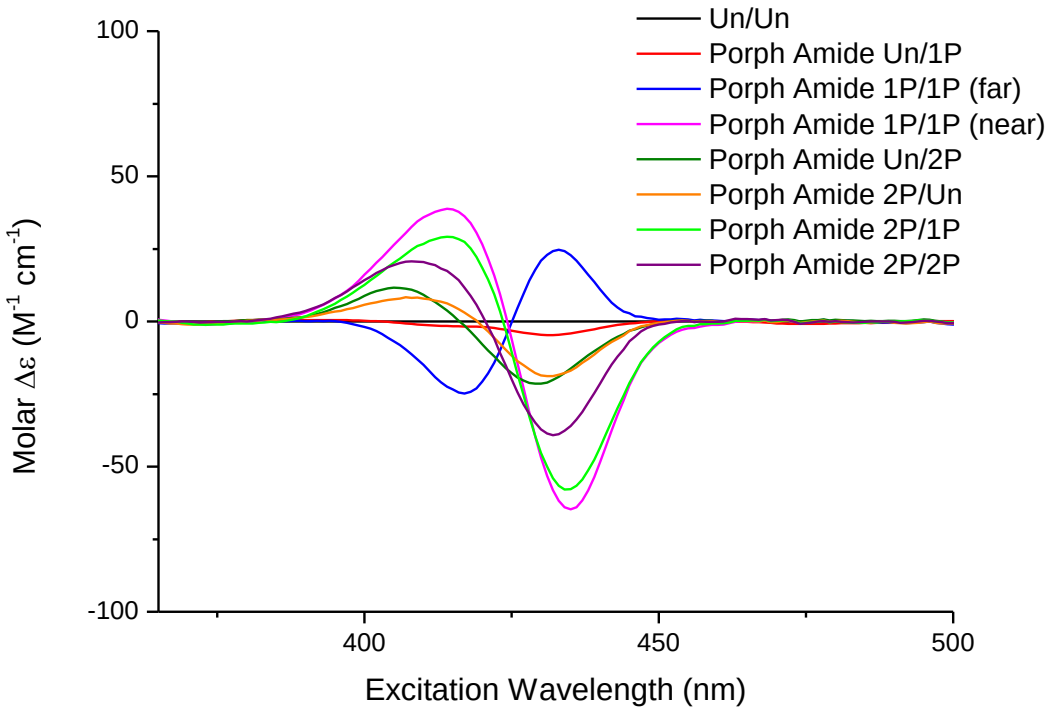

Figure 6.9 Expanded porphyrin region of the porphyrin amide spectra.

Looking at the porphyrin Soret band region of the spectra three features are immediately noticeable. Firstly, as expected, the unmodified DNA does not produce any signal in this region. Secondly, the spectra of all samples containing more than one porphyrin produce nice bisignate signals crossing the line Y = 0 at approximately 420 nm. This point corresponds to the λ_{max} of the Soret band. Finally, and most strikingly, six of the seven spectra show -/+ bisignate spectra (from longer wavelength), whereas one (1P/1P far, blue)

shows a +/- signal. The signals in this region are produced by exciton coupling interactions between two or more porphyrins.[237, 244] This is shown by the Un/1P spectra (red) only producing a tiny signal.

Upon excitation, chromophores undergo intense π – π* transitions. When a molecule contains two identical chromophores held in chiral positions, these electronically allowed transitions interact with each other resulting in the observed bisignate peak.[243] This pattern has been reported before in systems containing the flexible amide linker.[115] A bisignate spectrum is characteristic of linear oscillators. In this flexible system, the B_x and B_y transition dipoles of the porphyrins (see Figure 1.3) cannot be distinguished. This allows the porphyrin chromophores to be considered as simple point dipoles.[13] The direction of the bisignate peak is determined by the absolute sense of twist defined by the two dipoles (see below).[13, 237, 245] The porphyrins in the 1P/1P (far) duplex must be interacting with each other in a way that is opposite to the other systems.

Excitonic coupling between chromophores (porphyrins) is inversely proportional to the square of the interchromophore distance[246] and proportional to square of the extinction coefficients.[247] The amplitudes, and therefore the strength of the coupling, appear in a general order that would be expected when just considering distances between porphyrins. The 2P/Un and Un/2P samples (dark green and orange) have four base pairs between the two porphyrin containing pairs. These produce lower amplitude signals than the 1P/1P samples (blue and pink) which have the porphyrins closer together with none and three base pairs between porphyrins respectively. The 1P/1P (near) sample shows a greater coupling than the 1P/1P (far) as would be expected by this logic. Interestingly, the 2P/1P and 2P/2P samples (light green and purple) show weaker couplings than the 1P/1P (near). This could be due to the porphyrins being positioned in an orientation that either leads to weaker coupling or partial cancellation of the signal intensity. The measured values for the amplitudes of these samples are presented in Table 6.1 below.

Porphyrins have been shown to exhibit exciton coupling to at least a distance of 50 Å, well beyond the scale of these samples.[237] The distance between porphyrins in terms of base pairs, cannot be the sole factor affecting the amplitude of the signals. Porphyrins pointing into space on opposite sides of a duplex are less likely to couple effectively due not only to the distance, but

also due to the angle in respect to each other.[237] The angle between the porphyrins and location in space must also be considered when analysing coupling efficiency.

In order to gain a better understanding of the structure of the porphyrin-modified DNA and to link this in with the acquired CD data, molecular modelling was attempted using Schrodinger Maestro modelling software.[248] Due to the complexity of the systems and the different inter- and intra-molecular interactions between porphyrins, the produced models are limited and idealised. The amide linker is also somewhat flexible by design allowing the porphyrin to move around in space. The models only provide a snapshot of one position the porphyrins can be in and as such do not show the whole picture. Structural energy minimisation could not be carried out on these models as each time the two DNA strands were pulled completely apart. Whilst there may be some truth to the destabilising of the duplex, the extent to which the duplex was deformed looked too great and the model no longer resembled double stranded DNA. For this reason the models were left with the DNA backbone in its ideal configuration.

These models however, do provide a rough direction in which the porphyrins stick out from the DNA backbone. The angle between the porphyrins can be used to predict the direction of the bisignate signal in the porphyrin region of the spectra. An example of a produced molecular model is shown in Figure 6.10 with the models for the rest of the systems provided in the Appendix.

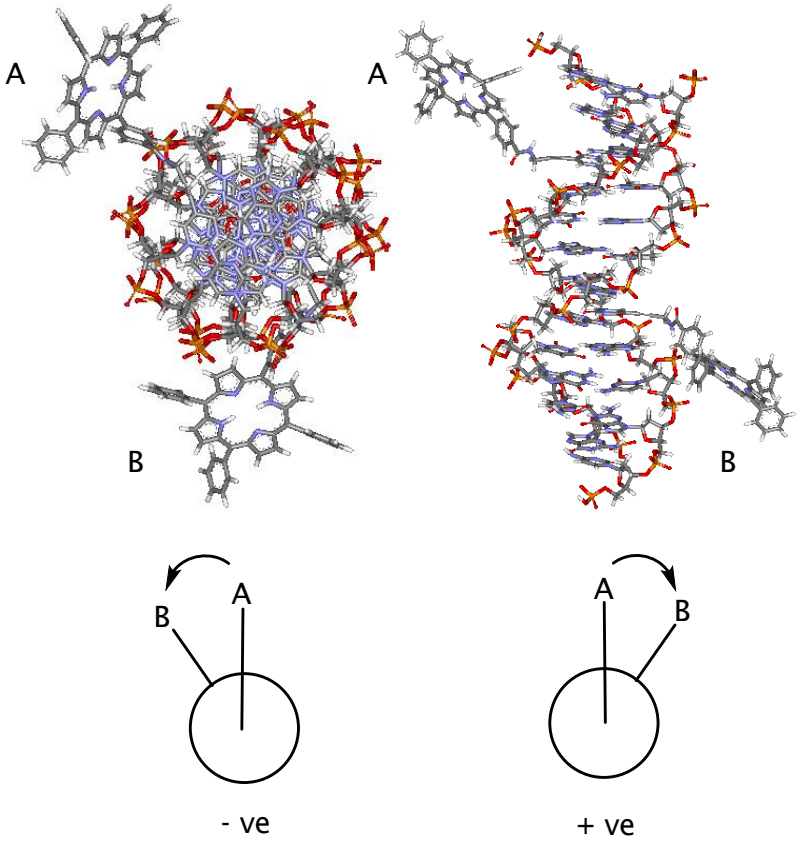

Figure 6.10 Top) Example molecular model showing the Porph Amide 2P/Un sample with the porphyrins labelled A and B to designate the same porphyrin. Bottom) Newman projections representing a negative, and a positive exciton chirality between the porphyrin chromophores. Porphyrin A is closest to the viewer.

The presented model is that of the Porph Amide 2P/Un system shown in two orientations. The two porphyrins have been labelled A and B with porphyrin A being at the top of the duplex (closest to the viewer looking down).

The Cotton effects seen in the porphyrin region can be predicted using the exciton chirality method.[231, 246, 249-251] This technique was pioneered by Harada and Nakanishi in the late 1960's and 70's and was used to establish the absolute configuration of a chiral compound without any reference (a non-empirical method). The original work established the chirality between benzoate groups and so was termed the "dibenzoate chirality rule". Since then, the exciton chirality method has expanded to encompass other chromophores, including porphyrins.[16] The bisignate signal reflects the "exciton chirality", the

helical sense between two electric transition dipole moments involved in the excitation.[243]

Looking down the axis of the chromophores, the offset of the two porphyrins is either described as “positive” or “negative” dependent on whether there is a clockwise screw (positive) or anticlockwise screw (negative) up to 180˚. For the porphyrin-DNA, looking down the helical backbone and starting with the upper porphyrin A, moving anti-clockwise to reach the lower porphyrin B gives a negative angle. Moving clockwise from A to B gives a positive angle. A Newman representation of this is shown below the models in Figure 6.10. As can be seen from the top down view of the modelled duplex, the lower porphyrin (B) is anti-clockwise from the upper porphyrin (A) and hence this is negative arrangement. A negative interaction corresponds to a negative exciton chirality which in turn should produce a bisignate signal with a negative Cotton effect followed by a positive Cotton effect in the porphyrin region. From the orange trace representing the Porph Amide 2P/Un sample in figure 6.9, this negative then positive Cotton effect can be seen clearly showing an agreement between the model and the collected spectroscopic data.

The predicted exciton chirality and the experimentally obtained Cotton effects for the set of Porph Amide duplexes has been combined in Table 6.1. Also included is a rough angle estimation between the porphyrins and the amplitude of the bisignate signals in the porphyrin region.

Porph Amide Duplex	Exciton Chirality	CD Cotton Effect	Angle Between Porphyrins	Amplitude of Bisignate Curve
Un/1P	N/A	N/A	N/A	5
1P/1P (far)	+ ve	+ ve	90˚	50
1P/1P (near)	+ ve	- ve	165˚	103
Un/2P	- ve	- ve	165˚	33
2P/Un	- ve	- ve	135˚	26
2P/1P	1 - 2) + ve 2 – 3) + ve 1 – 3) - ve	- ve	165˚ 90˚ 135˚	87
2P/2P	1 – 2) + ve 2 – 3) + ve 3 – 4) + ve 1 – 3) - ve 1 – 4) - ve 2 – 4) - ve	- ve	165˚ 90˚ 90˚ 135˚ 90˚ 165˚	60

Table 6.1 Data compiled from the experimentally obtained CD spectra of the Porph Amide duplexes and the molecular modelling. The porphyrins have been labelled 1 – 4 from the porphyrin at the top of the duplex down to the bottom. These assignments can be seen in the images in the appendix. 1 – 2) shows the interaction between porphyrins 1 and 2.

When considering the above data it is important to remember the flexible linker allows a degree of movement for the porphyrins. The direction that the porphyrin faces is also subject to how the model was connected about the nitrogen of the amide bond where two options were possible. The less hindered of these two options was chosen for presentation. Due to this flexibility, the stated values for angle between porphyrins must be considered as very rough and potentially not in the lowest energy state.

By comparing the exciton chirality with the observed Cotton effects it becomes clear that the +/- signal (opposite to the rest) displayed by Porph Amide 1P/1P (far) actually fits with the model. It is the Porph Amide 1P/1P (near) data which does not match. As the spectroscopic data does not lie, it suggests that the model of this structure is not quite correct, or there are more complicated

interactions that have not been considered. The models of the other two duplexes containing two porphyrins each match with the experimental data.

The systems containing more than two porphyrins get much more complicated due to the number of interactions possible. It is however interesting to note that the exciton chirality of the porphyrin pairs closest to each other (in terms of base pairs) all show positive interactions, and the longer range chiralities are negative. However, both spectra show -/+ signals. There is also nothing obvious in the angles to explain this observation. From this data it is far from easy, if not impossible, to explain the shape of these spectra in the porphyrin region by simple means.

A different method which could be useful for the analysis of these systems is the X-ray Bijvoet method.[252] In 1951 Bijvoet and co-workers were the first to experimentally determine the absolute configuration of a molecule. Later Harada conclusively proved that the X-ray Bijvoet and the exciton chirality methods result in the same assignment of a molecule's absolute configuration.[253] Obtaining the X-ray data could be useful in understanding the CD data and the structure of the porphyrin DNA. However, this is a crystallography technique and despite many efforts, to date, porphyrin-modified DNA has yet to be crystallised.

The second set of duplexes, containing the porphyrin acetylene linker, were then analysed by CD spectroscopy. As can be seen from the spectra in Figure 6.11, 6.12 and 6.13, the spectra are much more complicated, especially in the porphyrin region.

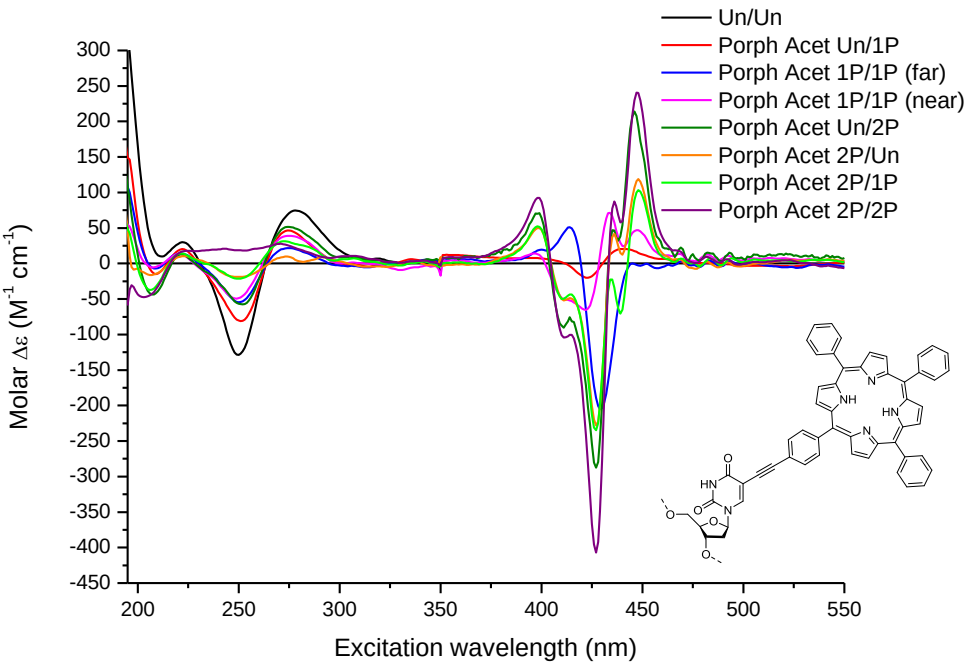

Figure 6.11 Full CD spectra acquired for the duplexes containing the porphyrin acetylene modification.

The changes in the DNA region are similar to those observed in the porphyrin amide spectra. The large trough at 250 nm decreases in size as more porphyrins are added into the system, but the small peak at 225 nm stays about the same size throughout. The most notable spectrum in this region is for the 2P/2P sample, which does not show characteristics resembling B-DNA but rather a broad signal across the wavelength scale.

The area at higher wavelength of the spectra is also slightly different from those that were produced by the porphyrin amide duplexes. There are no peaks at 320 nm, as are seen in the porphyrin amide spectra, suggesting these peaks (seen in Figure 6.8) are a result of the amide linker rather than the porphyrins. The peaks at approximately 275 nm however are similar to those produced by the amide linker. No obvious trend emerges as more modifications are introduced, but as mentioned above, the same samples (Un/Un, Un/1P, 1P/1P near and Un/2P) appear to show the stronger signals in this area. The glaring exception to this is the spectra for the 2P/Un sample in orange. In the previous samples it was noted that this sample showed a

stronger signal than it's opposite. This time round however, this sample shows a much weaker signal than the Un/2P sample.

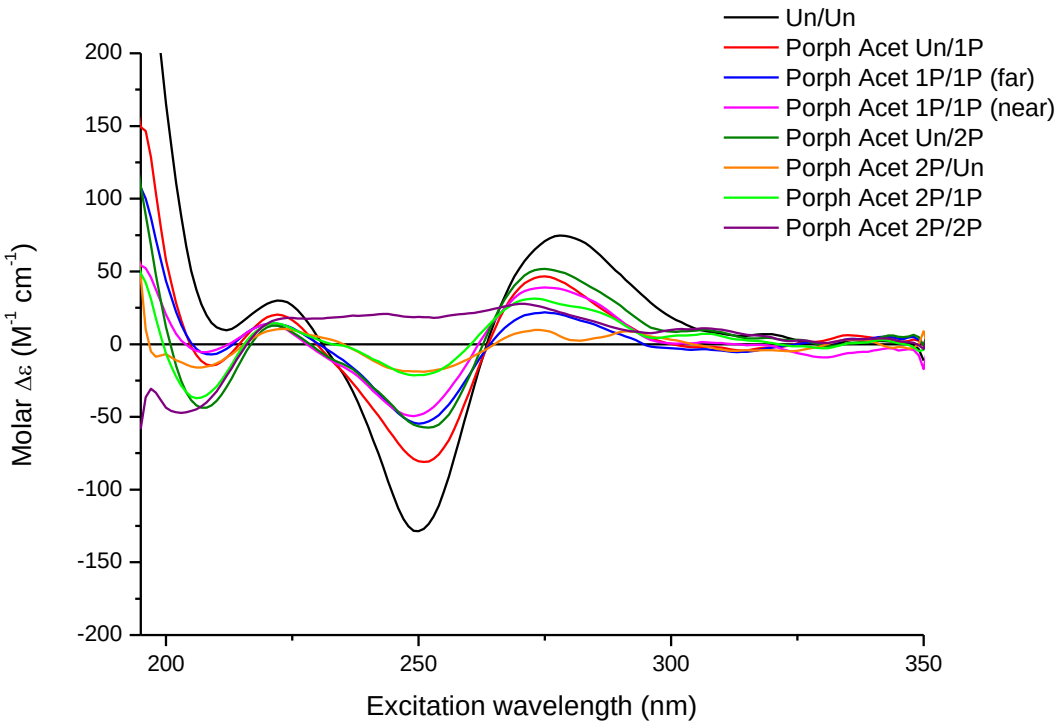

Figure 6.12 Expanded DNA region of the porphyrin acetylene spectra.

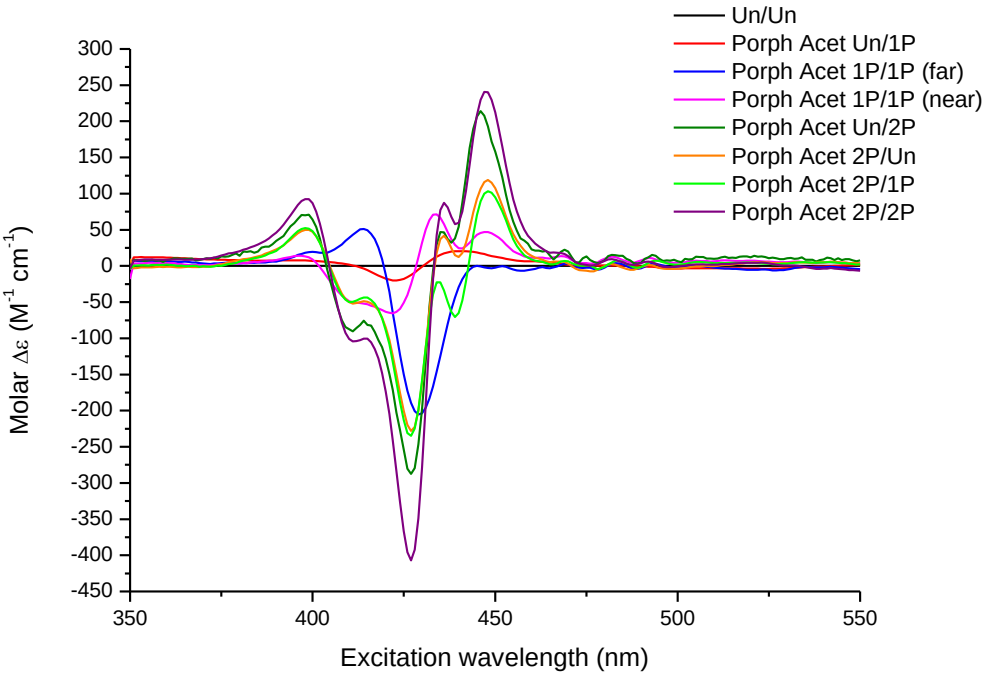

Figure 6.13 Expanded porphyrin region of the porphyrin acetylene spectra.

Structural Analysis

As mentioned previously, the porphyrin region of the spectra is a lot more complicated than those spectra produced by the duplexes containing the amide linked porphyrin. Whilst it can be said that there is a general +/-/+ trisignate trend, they are certainly not smooth curves. A +/-/+ signal is characteristic of a circular oscillator where the B_x abd B_y transitions both contribute to the excitonic coupling of the porphyrins.[13] As with the data of the amide series, this type of signal has previously been seen in other systems containing only the rigid acetylene linker.[115]

Once again the exception to this trend is the 1P/1P (far) duplex (shown in blue) which seems to lack the positive peak at 450 nm shown by the others. Instead it appears to show a comparatively smooth bisignate curve with a negative Cotton effect first. It is also interesting to note that this spectrum is the only one showing a negative Cotton effect in this series, whereas the corresponding amide linked duplex was the only one to show a positive Cotton effect followed by the negative. From the produced molecular model of this duplex, a positive exciton chirality would be expected suggesting there is more complexity to this interaction.

This increase in signal compared to the Porph Amide systems, both in terms of the amplitude and complexity, may not be that surprising when considering the structure of the modifications. The different linkers not only provide flexibility or rigidity, they also provide a different link from porphyrin to DNA. The amide linker consists of several single bonds, whereas the acetylene linker is directly attached to the nucleobase. This shorter linker allows much more information to be transferred between the porphyrin and the DNA backbone allowing for a stronger induced signal.

As with the previous set of data the values for the angle between porphyrins and the amplitude of the signal in the porphyrin region are shown in Table 6.2.

Porph Acet Duplex	Angle Between Porphyrins	Amplitude of signal
Un/1P	N/A	41
1P/1P (far)	90˚	257
1P/1P (near)	90˚	137
Un/2P	180˚	498
2P/Un	180˚	345
2P/1P	1 - 2) 90˚ 2 – 3) 90˚ 1 – 3) 180˚	337
2P/2P	1 – 2) 90˚ 2 – 3) 90˚ 3 – 4) 90˚ 1 – 3) 180˚ 1 – 4) 90˚ 2 – 4) 180˚	649

Table 6.2 The angle between porphyrins in the Porph Acet duplex systems and the amplitude of the measured CD spectra in the porphyrin region. The porphyrins have been labelled 1 to 4 from the porphyrin at the top of the duplex down to the bottom. These assignments can be seen in the images in the appendix. 1 – 2) shows the interaction between porphyrins 1 and 2.

The signals in the porphyrin region cannot solely be assigned to interactions between the porphyrins attached to the same duplex. Intermolecular interactions between porphyrin duplexes must also be playing a part and contributing to the spectra. Perhaps the most compelling evidence for this is shown by the Un/2P and 2P/Un samples. The models for these systems (see appendix) show the two porphyrins are pointing into space completely away from each other on opposite sides of the DNA backbone. With the short, rigid linker these porphyrins cannot bend around the duplex and π-stack. However, large signals are shown in the CD spectra. If the models are correct, then these large signals must be caused by different interactions, either through the linkage to the DNA backbone, or by exciton coupling to porphyrins on adjacent duplexes through space.

In an expansion of this project, Dr Mames of the Stulz group synthesised an analogue of the acetylene linked porphyrin monomer. This was still based on a

tetraphenyl porphyrin but contained a carboxylic acid group on each of the three meso phenyl rings. This extra functionalisation aimed to disrupt any intermolecular interactions allowing a simplified spectrum to be observed.

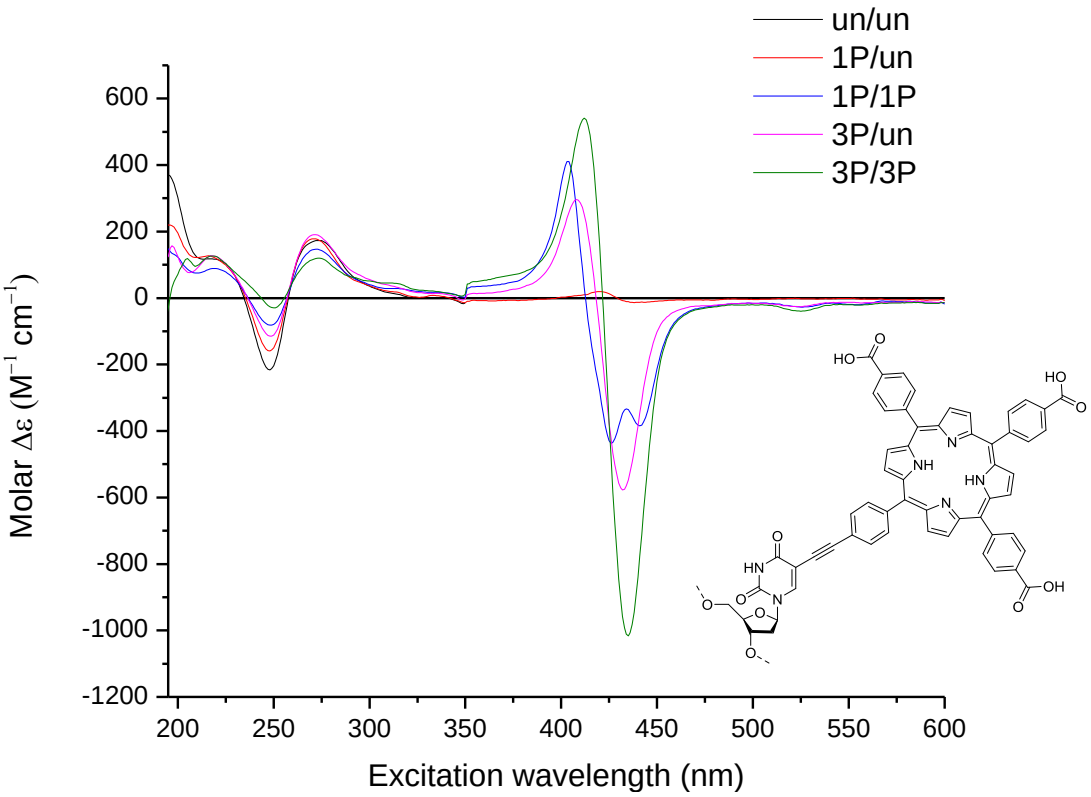

Figure 6.14 Full CD spectra acquired for the duplexes containing the tri acid porphyrin acetylene modification synthesised by Dr Iwona Mames. Also shown is the structure of this modification.

The oligos that contain this tri acid porphyrin are different to those used for the rest of this work as they were not designed solely for this project. These duplexes were again designed to include either a porphyrin modification or a natural T base at specific sites. The sequences can be seen in Table 6.3 with the modification sites represented by **P**. In a further difference from the Porph Amide and Porph Acet sequences, this duplex could incorporate up to three porphyrins per strand rather than the two of the previous.

Duplex	Duplex name (Mods on strand A / Mods on strand B)
5' – TCG CTA TAT ATA TAT ATT AT 3' – AGC GAT ATA TAT ATA TAA TA	Un/Un
5' – TCG CTA TAT A**P**A TAT ATT AT 3' – AGC GAT ATA TAT ATA TAA TA	1P/Un
5' – TCG CTA TAT A**P**A TAT ATT AT 3' – AGC GAT ATA **P**AT ATA TAA TA	1P/1P
5' – TCG CTA TA**P** A**P**A **P**AT ATT AT 3' – AGC GAT ATA TAT ATA TAA TA	3P/Un
5' – TCG CTA TA**P** A**P**A **P**AT ATT AT 3' – AGC GAT A**P**A **P**A**P** ATA TAA TA	3P/3P

Table 6.3 Sequences of the oligonucleotides containing the tri acid porphyrin modification represented by **P**.

From the spectra (Figure 6.14) several features are clear. The most important aspect of the spectra to note is the simplicity of the porphyrin region compared to the Porph Acet data (Figure 6.13) signalling a success with the design of disrupting intermolecular porphyrin interactions. Instead of the complex porphyrin region the spectra bears a much closer resemblance to the spectra of the Porph Amide duplexes (Figure 6.9) returning to a smooth -/+ bisignate signal. This could suggest a change in behaviour from the circular oscillator with the standard acetylene linker, to a linear oscillator by simply adding the acid groups. Once again a 1P/1P sample with porphyrin modifications on adjacent duplexes provides a bit of complication showing a double peak instead of the large negative signal the rest show around 430 nm.

The amplitude of the peaks in the porphyrin region has continued to increase as more porphyrins were added into the system. This is hardly surprising as six porphyrins in a duplex would be expected to have more of an interaction than if only two were present. The signal in the DNA region is also larger for these spectra. This though can be attributed to the longer sequences rather than any effect caused by the number or type of porphyrin. Unfortunately a sample has yet to be synthesised with two porphyrins 180° apart (like the Porph Acet Un/2P from above) so a comparison of the amplitudes cannot be made between these systems with and without the disrupting functionality.

Structural Analysis

The DNA region shows the same overall trend as that produced by the previous samples. The negative trough at 250 nm and the positive peak at 270 nm become less pronounced as more porphyrins are introduced. Interestingly, three tri acid porphyrins on each strand of the duplex (3P/3P) do not appear to have had such a big effect on the DNA structure as the Porph Acet 2P/2P system. Whilst having the smallest amplitude in this region, the shape of the signal is still clearly visible as opposed to the flat, broad signal produced by the Porph Acet 2P/2P sample. This is likely to be due to the longer duplex. As more Watson-Crick base pairs are formed, the more stable the duplex becomes and as such less easy to distort. Proportionally a third of the base pairs in the previous 2P/2P systems contained a porphyrin modification (4 out of 12). Here there is slightly less than a third with only 6 modified base pairs out of 20. There are also larger flanking regions of unmodified sequence either side of the porphyrins which would retain the B-DNA character.

A final set of three porphyrin-modified duplexes were created using the original 12-mers. These were a mixed system containing the Porph Acet modification on the A strand, and the Porph Amide modification in its complement. The three duplexes made were 1P/1P (near), 1P/1P (far) and 2P/2P as shown in Table 6.4.

Duplex	Duplex name (Mods on strand A / Mods on strand B)
5' – CGC A**P**T ATA TGC 3' – GCG TAA TA**P** ACG	Mix 1P/1P (far)
5' – CGC ATT ATA **P**GC 3' – GCG TAA TA**P** ACG	Mix 1P/1P (near)
5' – CGC A**P**T ATA **P**GC 3' – GCG **P**AA TA**P** ACG	Mix 2P/2P

Table 6.4 The mixed porphyrin duplexes. The amide linked porphyrin modifications are represented by **P**. The acetylene linked porphyrin modifications are represented by **P.**

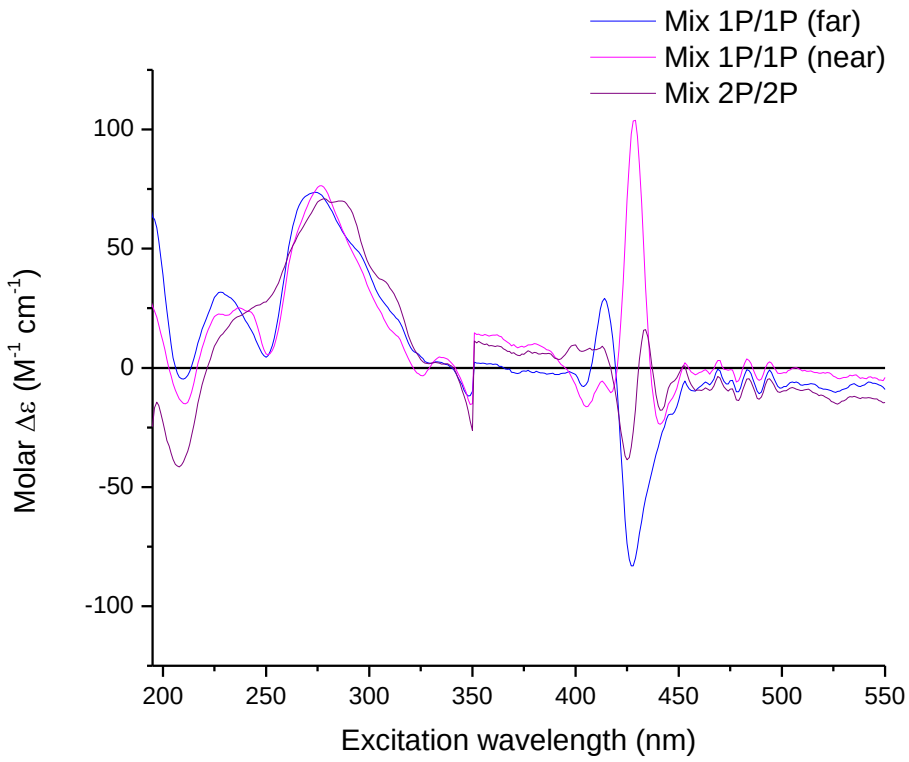

Figure 6.15 Full CD spectra acquired for the mixed porphyrin duplexes.

The mixed systems have clearly produced some quite different spectra to the ones containing only the one type of porphyrin. This is quite surprising as the previous work showed a mixed Zipper system to have a similar CD spectrum to the all amide zipper.[115] In the DNA region, all previous spectra have shown a major negative signal at 250 nm. The two 1P/1P samples (blue and pink) have a trough at 250 nm but it is substantially smaller than any of the previous. The 2P/2P sample (purple) does not show a peak here at all. Instead it flattens out in this region much like the Porph Acet 2P/2P system did (see Figure 6.12). The major peak in the DNA region is the positive peak around 275 nm in each of the spectra. These look like large peaks due to the scale of the graph, but they are in fact no bigger than any other sample which all have a corresponding signal with intensities in the region of 50 – 100 M^{-1} cm^{-1}. The DNA region of these spectra does not bare that much resemblance to unmodified B-DNA. This suggests the structure of the backbone is possibly being distorted more with the mixed porphyrins. This could be as a result of the combination between rigid and flexible. The amide linker allows the porphyrins to move around more to interact with each other. The rigid linker

doesn't allow movement so may well be holding the porphyrins in place. The mixed system may be more distorted as the limited flexibility is not enough to achieve a good interaction. As a result the DNA scaffold has to be distorted to accommodate this.

The porphyrin region also shows substantial differences, both between the mixed systems, and in comparison to the single porphyrin type samples. Out of the three, the 1P/1P (far) sample (blue) probably looks the most like the previous showing a smooth bisignate signal with a negative Cotton effect before a positive effect. In this way it looks a lot more similar to the Porph Acet system than the positive Cotton effect produced by the Porph Amide data. However, a positive exciton chirality is predicted based on molecular modelling, and therefore, a positive Cotton effect followed by a negative effect is expected.

The mixed 1P/1P (near) system (pink) however, looks nothing like either spectrum with the single type of porphyrin. The only major signal in the porphyrin region of this spectrum is a large positive peak. This different type of signal must mean the porphyrins are interacting with each other in a different way caused by the mixed flexibility and/or linkage.

The amplitudes of the signals in the porphyrin region are also worth noting. The 1P/1P samples amplitudes appear between those of the previous data (far = 112, near = 128). The 2P/2P sample shows an amplitude of 55. This signal is less intense than the two 1P/1P samples, showing the same trend as the Porph Amide data. Conversely, the Porph Acet 2P/2P produced a much more intense signal. This could be suggesting that the presence of the Porph Amide modification is having a greater effect on the signal.

By including multiple porphyrins into a short duplex, changes to the porphyrin structure were expected. The planar, aromatic and hydrophobic nature of the porphyrins gives a tendency for them to π-stack. It was therefore believed that the DNA backbone could be distorted by the porphyrins trying to reach each other. The short, rigid acetylene linker should make it harder for the porphyrins to move in order to interact with each other. If they are too far away, the porphyrins will either not be able to interact, or will have to

significantly alter the DNA structure in order to achieve this π-stacking. The amide linker on the other hand, being longer and more flexible, was thought to make achieving these porphyrin interactions easier. From the acquired spectra though a similar pattern is seen between the two linker systems and the number of porphyrins seems to have the bigger effect. Four porphyrins (two on each strand) in the 12-mer duplex seems to completely distort the DNA structure.

Surprisingly perhaps, the mixed system which was designed to be the best of both worlds in terms of rigidity and flexibility, shows the largest deviation from the unmodified B-DNA duplex.

In order to fully appreciate how the porphyrins are changing the DNA structure and interacting with each other, better quality molecular modelling needs to be carried out by someone with experience in this area. This modelling is currently in progress in collaboration with Dr Syma Khalid, University of Southampton.

6.4 Ultraviolet-Visible and Fluorescence Studies of Porphyrin-Modified DNA

Further spectroscopic data was acquired for the porphyrin modified duplexes in the form of UV-Vis and fluorescence spectroscopy. These spectra are presented in Figure 6.16.

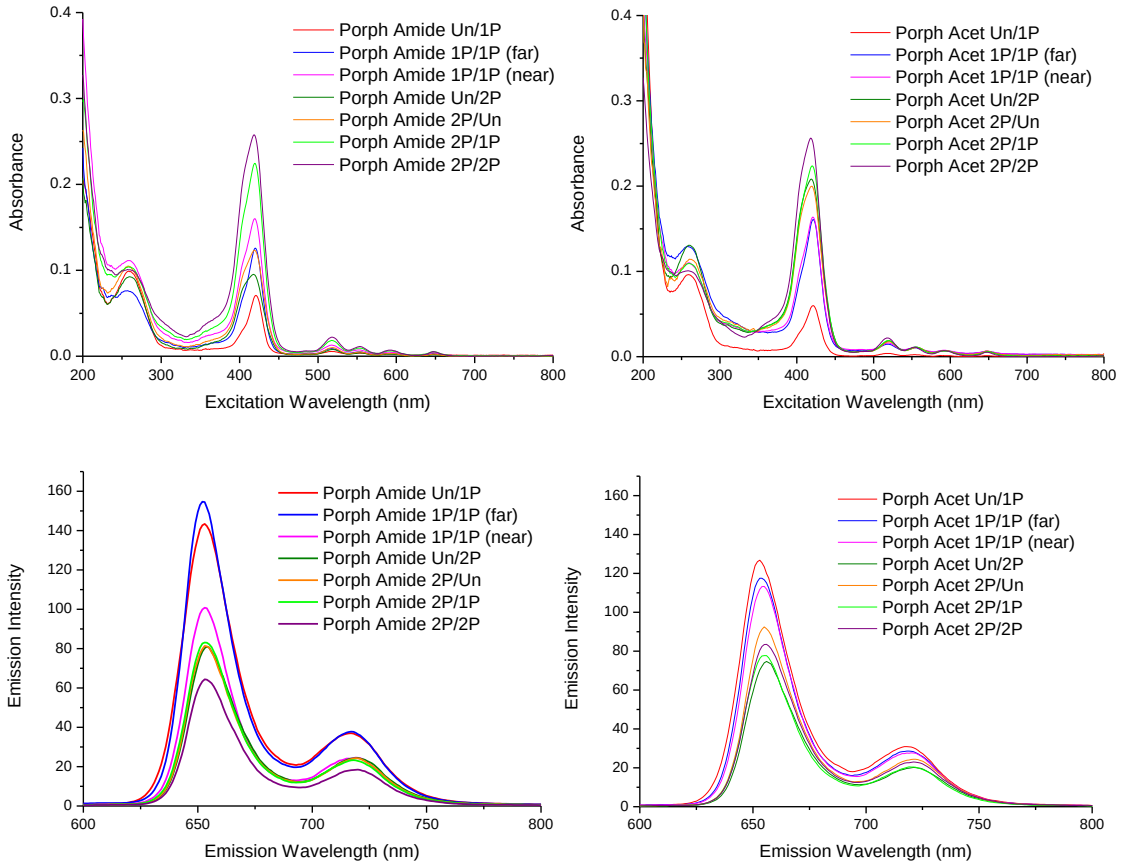

Figure 6.16 Top) UV-Vis spectra of the Porph Amide (left) and Porph Acet (right) duplexes obtained with a 1 mm pathlength cell. Bottom) Fluorescence spectra of the Porph Amide (left) and Porph Acet (right) duplexes obtained with a 1 cm pathlength cell. Samples concentration = 5 μM in 100 mM NaCl, 50 mM phosphate, pH = 7 buffer.

The fluorescence data were acquired with a fluorescence cell with a 1 cm pathlength. This is however a different cell to the one used for the above UV-Vis spectra. These were obtained with a 1 mm pathlength cell as the

absorbance readings were above 1.5 a.u. when using the 1 cm cell. Above this point the data becomes less accurate as the readings will stop following the Beer-Lambert law and become non-linear. The UV-Vis spectra acquired using the 1 cm pathlength fluorescence cell can be seen in the appendix.

Both sets of UV-Vis spectra show the same trends and are what would be expected. The absorptions at 260 nm, caused by DNA absorbance, all show a value consistent with the 5 μM duplex samples (within experimental error). The porphyrin absorbances (Soret band at approx. 420 nm and Q-bands) show increasing absorbance with increasing number of porphyrins as would be expected. It may be expected that if the duplex containing one porphyrin has absorbance of X, then duplexes containing two porphyrins would have absorbance of 2X. This is roughly the case in both sets of spectra, however, hypochromicity would be expected if the porphyrins are stacking due to the increased interactions.

The value of λ_{max} for the Soret band shows slight deviations between samples showing consistency with the crossing point of the porphyrin amide CD spectra (Figure 6.9). These values do not exactly match up, but the same samples show slightly higher or lower λ_{max} values in both spectra.

The two sets of fluorescent data again show comparable trends. As mentioned in section 5.5, poprhyrins in close proximity fluorescently quench leading to lower emission with more porphyrins present. This trend is shown in both the presented sets of fluorescence spectra.

The clear exception is the sample Porph amide 1P/1P (far) (blue, left) which shows the greatest emission of the set. The corresponding UV absorbance at 260 nm for this sample is lower than the rest suggesting it is slightly less concentrated. A lower concentration would mean less porphyrins in proximity to quench, and as such would give a higher emission. The Porph Amide 1P/1P (near) (pink) shows the highest absorbance at 260 nm. This sample may be slightly too high a concentration with the 1P/1P (far) slightly too low. Adjusting these concentrations would have the effect of bringing the emission of the two samples more into line with each other and what would be expected.

Emission values which are slightly too high or low can be seen in other spectra, but nothing that is beyond the realms of experimental or concentration error.

6.5 Synthesis of Truncated Monomers for Further Structural Analysis

Section 6.2 describes the production of two sets of porphyrin modified duplexes, one containing the amide linked porphyrin monomer and the other the acetylene linked monomer. These samples were studied for structural analysis using circular dichroism spectroscopy. UV-visible and fluorescence spectroscopy were also carried out all aimed at following the changes to the DNA structure as more and more porphyrin modifications were introduced into the system. The next part of the project looked to expand on this work.

The porphyrin modification is a large unit and can be attached with two different linkers. As can be seen in section 6.2, this can produce some really complicated spectra which are extremely difficult, if not impossible, to completely decipher without more data and crystal structures or high quality molecular models available. For this reason three truncated monomers were designed to systematically build up to the full porphyrin modification a bit at a time. The structures of these three monomers are shown in Figure 6.17.

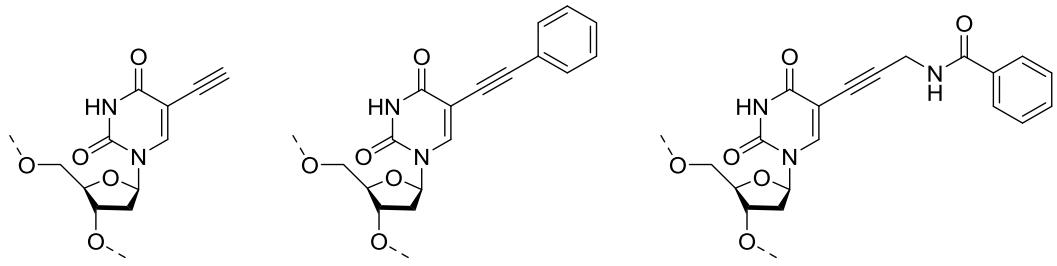

Figure 6.17 The three truncated modifications. Left) The acetylene modification (Acet). Middle) The phenyl acetylene modification (Phenyl Acet). Right) The phenyl amide modification (Phenyl Amide).

The first two monomers shown in Figure 6.17 are truncated versions of the acetylene linked porphyrin monomer. These have been named the acetylene modification (labelled Acet) and the phenyl acetylene modification (Phenyl Acet). These were designed to build up from the unmodified thymine base by

first adding an acetylene at the 5-position, then a phenyl ring is added on before the full porphyrin monomer is made.

The third truncated monomer shown is the phenyl amide monomer. This is designed as the linker of the amide linked porphyrin monomer with the porphyrin removed. A fourth monomer was originally designed with a propargylamine modification at the 5-position, leaving a primary amine. However, it was thought that protonation of this free amine could occur, and the resulting charged species may create artefacts and further complications in the spectra. For this reason it was decided not to make this fourth monomer.

Outlined below are the synthetic routes used to synthesise the three truncated monomers.

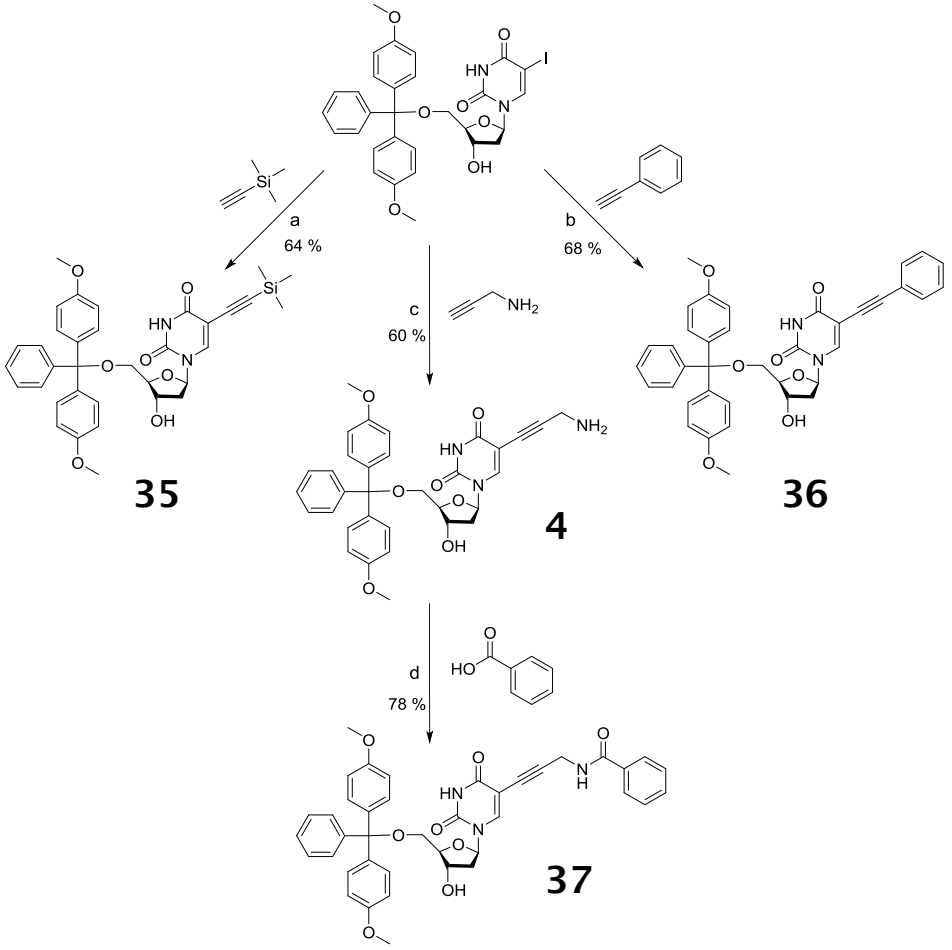

Scheme 6.1 Synthetic routes to produce the acetylene, phenyl acetylene and phenyl amide monomers. a) $Pd_2(PPh_3)_4$, CuI, NEt_3, DMF, trimethylsilylacetylene. b) $Pd_2(PPh_3)_4$, CuI, NEt_3, DMF, phenylacetylene. c) $Pd_2(PPh_3)_4$, CuI, NEt_3, DMF, propargylamine. d) Benzoic acid, HATU, DIPEA, DMF.

From Scheme 6.1 it can be seen that the truncated monomers have been made in a similar way to that used to make the porphyrin monomers in Figure 3.2. The same propargylamine monomer (**4**) that was used to make the amide linked porphyrin monomer was reacted with benzoic acid giving a yield of 78 %. The acetylene and phenyl acetylene monomers were made directly from the 5-iodo modified uridine via Sonogashira couplings to TMS acetylene and phenyl acetylene respectively. These monomers were all converted to phosphoramidites and included in solid phase oligonucleotide synthesis using an extended six minute coupling time as with the porphyrin monomers. The protecting TMS group was removed by ammonium hydroxide in the base de-protection step post oligonucletide synthesis. The five modified oligos needed to form all duplexes were then purified by HPLC and confirmed using LC-MS.

	Acet		**Phenyl Acet**		**Phenyl Amide**	
Sequence	MW	Measured	MW	Measured	MW	Measured
CGC A**X**T ATA TGC	3630.4	3629.6	3706.5	3705.6	3763.2	3762.3
CGC ATT ATA **X**GC	3630.4	3629.6	3706.5	3705.6	3763.2	3762.3
CGC A**X**T ATA **X**GC	3679.4	3678.6	3755.5	3754.6	3906.2	3905.3
GCA **X**AT AAT GCG	3640.4	3639.6	3792.6	3791.6	3813.2	3812.3
GCA **X**AT AA**X** GCG	3689.4	3688.6	3841.6	3840.6	3955.2	3954.3

Table 6.5 The calculated molecular weights (MW) and the values measured by LC-MS for each oligonucleotide containing one of the three truncated modifications.

6.6 Circular Dichroism Spectra of Non-Porphyrin-Modified DNA

The first of the truncated modification sets tested by CD spectroscopy was the acetylene modification, referred to as Acet. This is the smallest of the modifications and as such bears the closest resemblance to the natural DNA duplex.

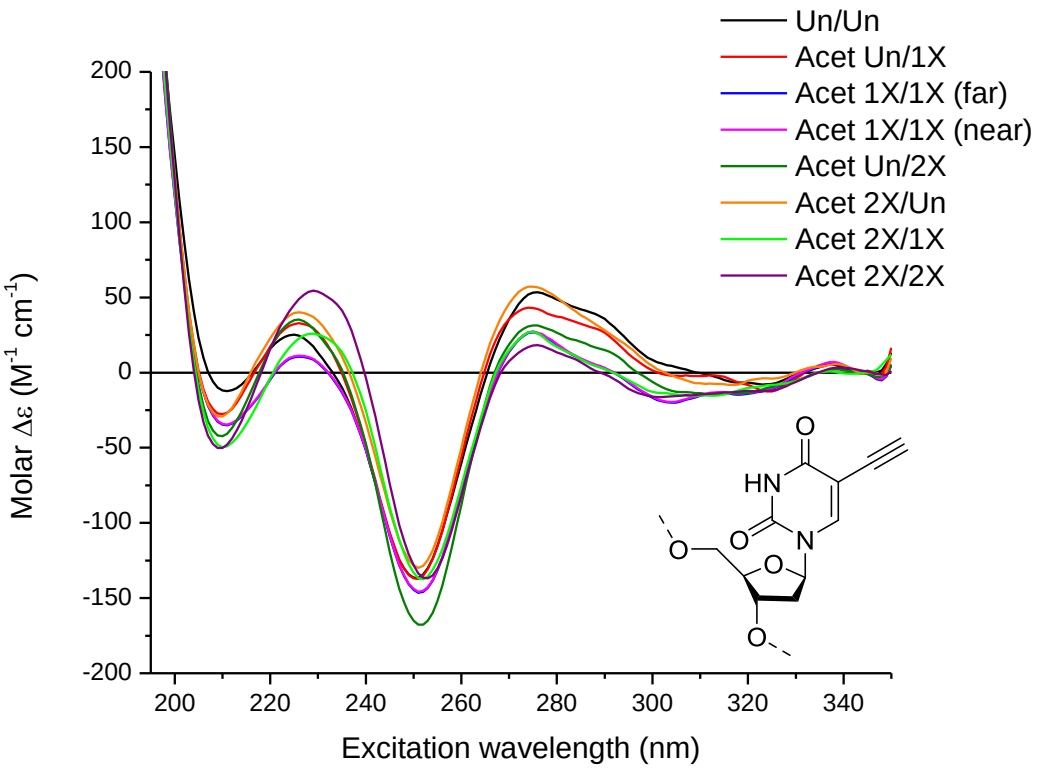

Figure 6.18 CD spectra of the duplexes containing the acetylene modified T base.

This close resemblance is also seen in the CD spectra where all traces are very similar to each other and to that of the unmodified duplex. The most notable change in the porphyrin spectra was the negative signal at 250 nm becoming a lot less negative, even flattening out in the case of the porphyrin acetylene modification. This trend is not seen at all with the acetylene modification with all spectra showing close to the same intensity. Slight variations are seen in the other two areas of interest (230 and 270 nm) but without further data it is

not possible to conclude whether this is a slight effect caused by the modification, or just natural variation when acquiring the data.

Building towards the acetylene linked porphyrin modification; the next set of samples tested contained the phenyl acetylene linker, referred to as Phenyl Acet.

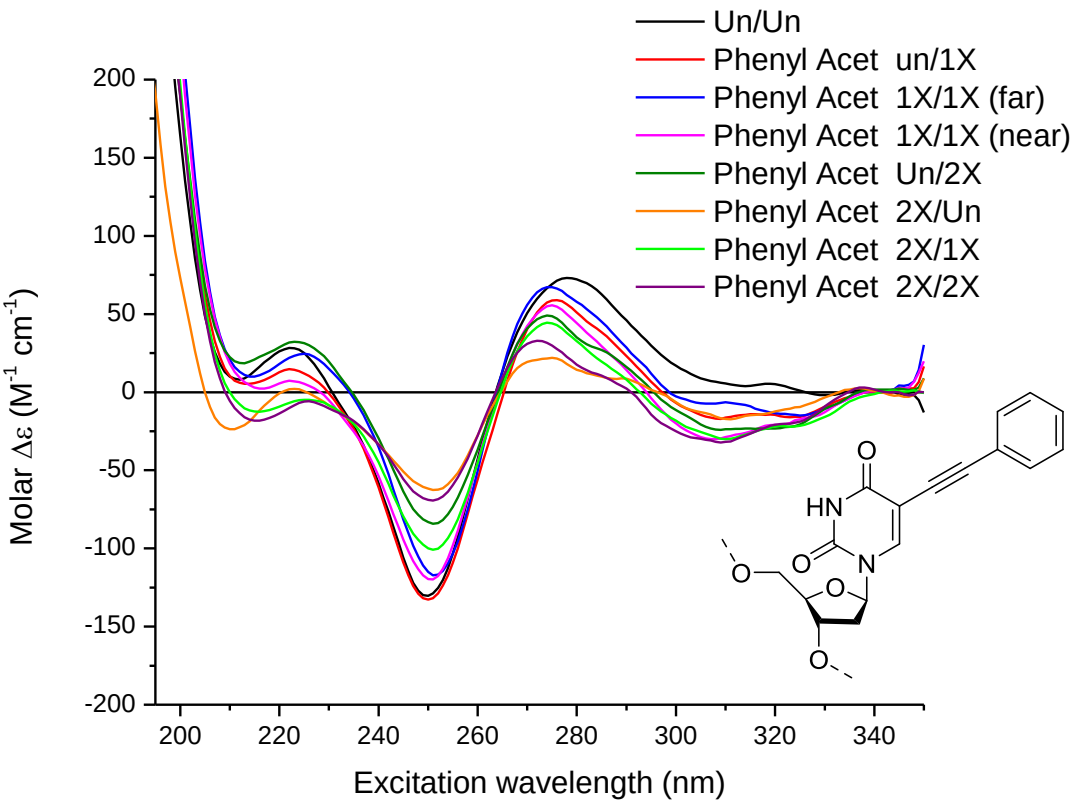

Figure 6.19 CD spectra of the duplexes containing the phenyl acetylene modified T base.

Adding this phenyl ring into the system clearly has a big effect as this dataset shows a lot more variation than the acetylene modification. The familiar reduction in the signal is seen in the peaks at 250 nm as well as 270 nm. This shows that the phenyl ring in the porphyrin modifications has an effect on the structure of the DNA. This should not be surprising considering the phenyl ring is a planar, aromatic molecule capable of π-stacking just like the porphyrins. Being smaller though the phenyl ring would be expected to have

less of an impact than the porphyrin and that is what is shown by the spectra. The traces clearly change as more modifications are added into the system but do not go as far as is seen with the porphyrin acetylene modified data in Figure 6.12.

The final set of duplexes tested by CD spectroscopy contained the phenyl amide modification as a building block to the amide linked porphyrin.

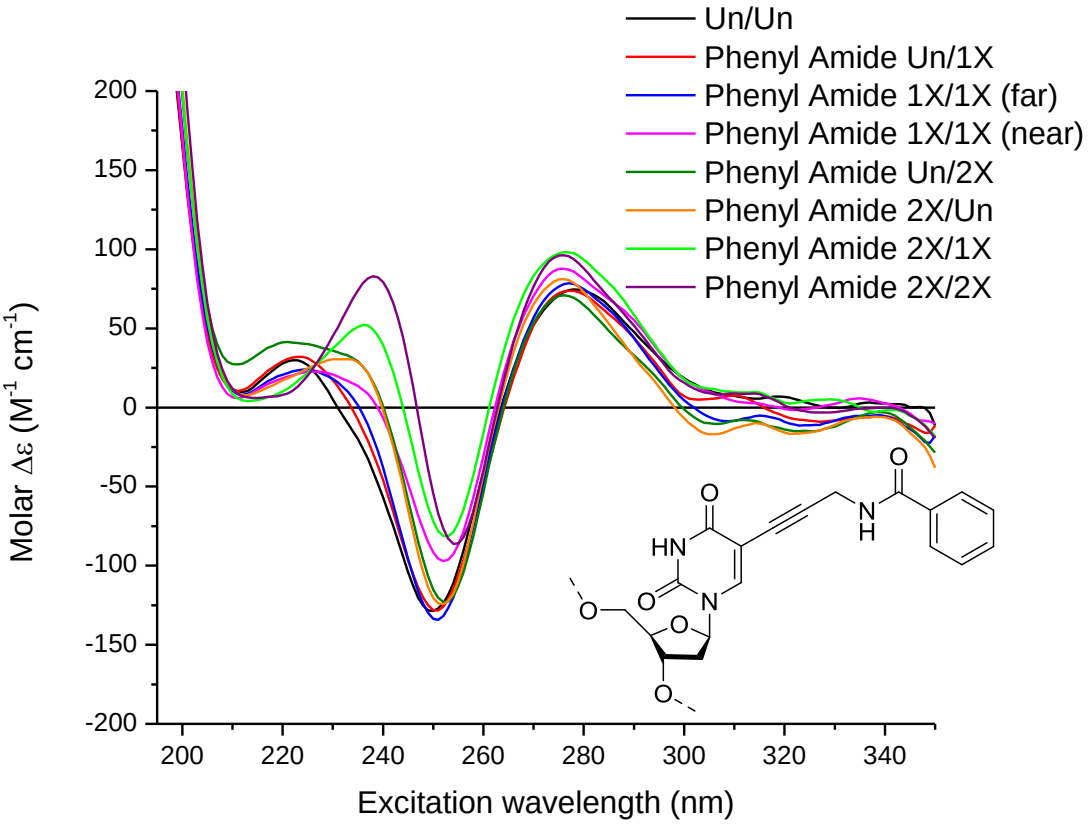

Figure 6.20 CD spectra of the duplexes containing the Phenyl Amide modified T base.

Once again the addition of the phenyl ring and amide linker has had a substantial effect on the spectra compared to just the acetylene modified T base. As ever, the trough at 250 nm becomes less intense with the addition of more modifications and a pronounced red shift in this peak of up to 5 nm can be seen. This shift in the peak occurs as the "shoulder" at 230 nm grows into a peak in its own right. The emergence of this shoulder/peak was noted in the

porphyrin amide spectra (Figure 6.8) and at the time attributed to the linker. Without the porphyrin attached, this peak becomes much more prominent especially when there are three or four modifications in the duplex. This shows that the amide linkage is responsible for this change in the spectra and the inclusion of the porphyrin perhaps overpowers this signal cancelling it out slightly.

The positive peak at 275 nm is also noteworthy. Peaks of varying sizes have been present in all of the spectra presented. However, no obvious trend has been seen to correlate the addition of modifications with a continual change in the spectra. All datasets have shown these peaks to have intensities in the region of 0 – 100 M^{-1} cm^{-1}. The Phenyl Amide spectra however, are a lot more consistent showing very little change in this area with increasing modification.

The three truncated nucleosides were designed to help decipher the CD spectra of the porphyrin-modified DNA. By building up the linker in stages before adding the porphyrin unit, it was hoped different aspects of the spectra could be assigned to certain parts of the modification. To a certain extent this has been achieved. The acetylene bond has been shown to have little impact on the spectra, but adding a phenyl ring, both with and without an amide linkage, does have an effect. Figure 6.21 combines the spectra for all the modifiers building up to the Porph Acet sample with the modifications in the same positions (2X/Un). The rest of the spectra have been compared in the same way and can be seen in the appendix.

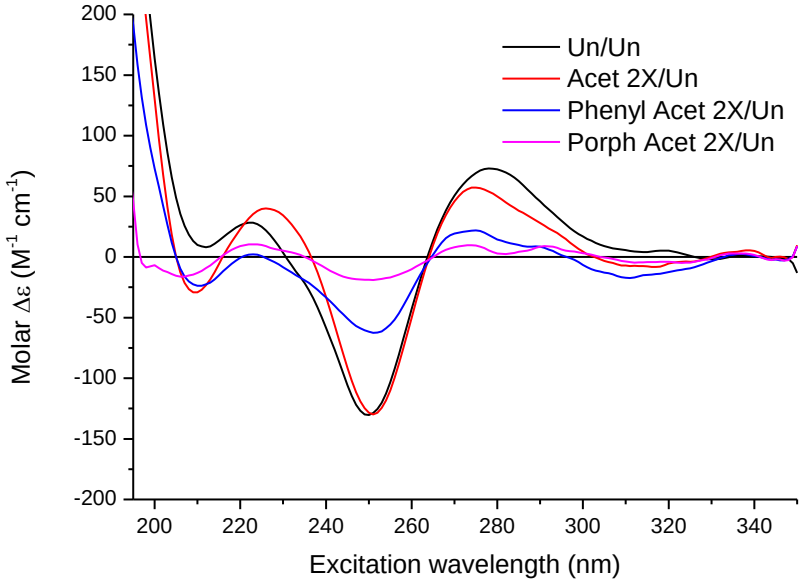

Figure 6.21 The changes in the spectra of the 2X/Un duplex when building up from the unmodified duplex to the porphyrin modification.

The spectra in Figure 6.21 and the appendix reiterate the increasing distortion of the spectra as the modifications get larger. The Phenyl Acet sample shows a reduction in the amplitude of the peaks in the same way as the Porph Acet sample, but just to a lesser extent. The linkers are clearly having a similar effect on the DNA structure, but as would be expected, the addition of the much larger porphyrin causes a significantly larger change in the spectra, and therefore a larger change to the structure of the of the DNA backbone.

6.7 Melting Studies of Modified DNA

The circular dichroism data described in sections 6.3 and 6.6 was acquired for the purposes of structural analysis of porphyrin-modified oligonucleotides. When assessing DNA duplexes, the stability of this duplex is an important property and is determined by its melting temperature (T_m). The T_m of a DNA duplex is defined as the temperature at which half of all molecules of a specific sequence are hybridised into a duplex, and the other half have dissociated into the single strands.[254] Heating a sample of duplex DNA breaks the hydrogen bonds in the Watson-Crick base pairs causing the two strands to dissociate. Therefore, the melting temperature of a DNA sequence is a measure of how stable a duplex is towards heat.

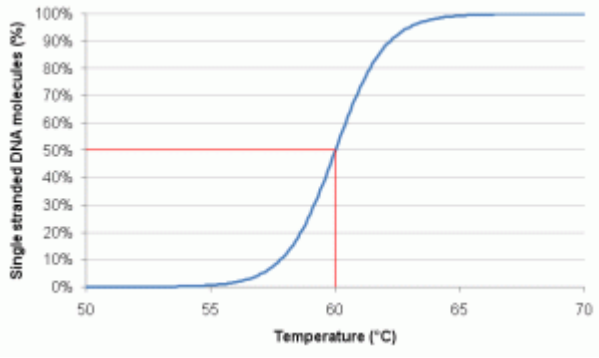

Figure 6.22 Graphical representation showing the melting temperature of a DNA duplex corresponds to the temperature where 50 % of DNA molecules are single stranded, and 50 % are hybridised.[255]

The melting temperatures of different sequences can vary quite widely even when only considering unmodified DNA. A short, ten base pair oligonucleotide, has a lot less hydrogen bond pairs than a five hundred base pair duplex and as such would be expected to be less stable. The sequence also plays an important role. A G-C base pairing forms three hydrogen bond pairs compared to two formed by an A-T pairing. A sequence rich with G-C pairs would therefore be expected to have a higher melting temperature.[256] The bases are also planar allowing neighbouring base pairs to π-stack, adding additional stabilising effects to the hydrogen bonding. This base stacking is

electrostatic and hydrophobic in nature and as such is more prevalent in the hydrophobic core of a duplex compared to the single strand. This desire to stack is a strong driving force in duplex formation.

Having the appropriate complementary strand is also important. The single strand AAAAA may be capable of forming a duplex with the strand TTCTT. Whilst the sequences are not fully complementary, there may be enough correct bases to overcome this mismatch. However, due to the reasons already mentioned, this duplex would not be as stable as the fully complementary duplex.

The other major factor of the sequence is the potential for a single strand to form an internal loop, binding to itself. Bases are capable of binding to their Watson-Crick pair in whatever strand they are in, including the same strand. This is something researchers need to be aware of when designing sequences. Three or four base pair self-binding sites will not be very stable, but longer complementary sections can cause a stable internal loop to form at the expense of the desired duplex.

The concentration of both the DNA and the ions in solution play a role in duplex stability and T_m. DNA duplex formation is a bimolecular process relying on two molecules interacting with each other. A higher DNA concentration gives more molecules in solution increasing the chances of a strand finding its complement and forming the duplex. This leads to a higher percentage of molecules forming a duplex at lower temperature resulting in an increase to the melting temperature.

Ion concentration, specifically the likes of Na^+, K^+ and Mg^{2+}, is a key factor in duplex stability due to the negative charge of DNA. Two negatively charged backbones coming into close proximity as a duplex is formed will raise the energy of the system. The presence of positive counter ions helps to stabilise the duplex and lower the energy of the system. Divalent cations, such as Mg^{2+}, are better than monovalent for stabilising the system due to their ability to counter two negative charges per ion.

Melting temperatures of unmodified oligonucleotides can be predicted using several different methods with varying degrees of accuracy. A quick and easy prediction can be made by the so called "2 + 4 rule".[257] This adds 2 °C for each

A-T pair and 4 °C for each G-C pair recognising the stronger G-C bonding. This method however, is very rough and only applicable to oligos in the region of 20 – 40 base pairs.

A more accurate, but far less easy to calculate method of predicting melting temperatures is the nearest neighbour method presented by Rhoads *et al.*[258] This considers the enthalpy of base pair formation as well as the stacking effect of adjacent base pairs. Values for the enthalpy and entropy of each pair along with the interaction with the previous pair are looked up in experimentally pre-calculated tables and combined to give the estimate of the melting temperature.[254]

Whilst these estimates are useful, they are approximate and provide values for unmodified oligonucleotides only. Accurate melting data can only be acquired experimentally. A common experimental technique used is UV melting. By slowly heating the sample at a controlled rate and measuring the absorbance (260 nm) at periodic intervals, a melting curve resembling that in Figure 6.23 is produced. As the duplexes dissociate into the single strands, an increase in absorbance (hyperchromicity) of up to 40 % can be seen.[256] This increase as the duplex breaks apart is a function of the base pairing. The hydrogen bonding and stacking interactions in a duplex limit the resonance of the bases and as such reduce the absorbance. The melting temperature of a duplex is measured at the inflection-point of the melting curve.

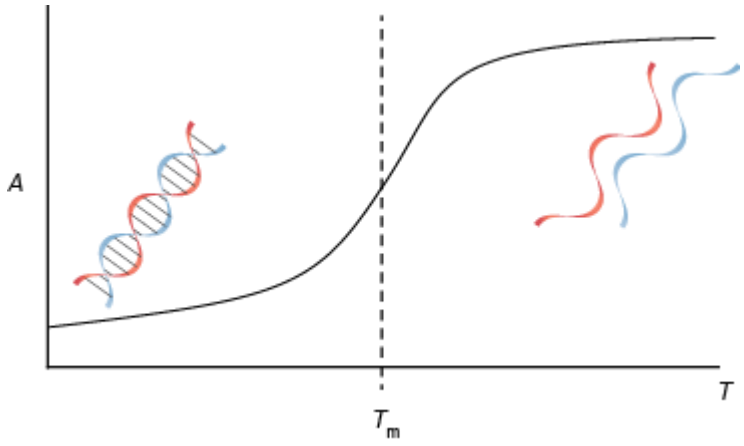

Figure 6.23 A typical melting curve showing the increased absorbance at 260 nm as the double stranded DNA is denatured. The T_m occurs at the inflection-point of this transition.[259]

Due to instrument issues in the lab which prevented accurate T_m measurements, a different method was initially used to measure the melting temperatures. Fluorescence melting follows the same gradual heating/cooling method as for a UV melting experiment, but fluorescence is measured instead of absorbance. To achieve this fluorescence, an intercalating dye is included in the sample. Sybr green II shows a higher fluorescence when in the presence of double stranded DNA compared to single stranded.[260] As such a fluorescence melting curve looks different to that of a UV melting curve, decreasing in emission as the temperature increases. The melting temperature however is still measured at the inflection-point of the melting curve.

Melting data was required for all duplexes discussed in the above sections. However, the porphyrins appeared to quench the fluorescence of the dye so that no clear transition could be seen in these samples. As such, an alternative way was needed to obtain this T_m data and will be discussed later. Fluorescence melting was successfully used to give melting temperature values for all the non-porphyrin samples and these are shown in Table 6.6 with the melting curves presented in the Figure 6.24.

	Melting temperature for each modification (˚C)		
Sample	**Acet**	**Phenyl Acet**	**Phenyl Amide**
Un/Un	47	47	47
Un/1X	52	47	48
1X/1X (far)	50	47	50
1X/1X (near)	51	45	49
Un/2X	52	44	50
2X/Un	50	39	49
2X/1X	51	41	50
2X/2X	53	44	49

Table 6.6 Melting temperatures of duplexes containing acetylene, phenyl acetylene or phenyl amide modifications. Data obtained using a Bio-Rad CFX Connect real time PCR system for fluorescence melting. 5 – 85 ˚C, 1 ˚C per min, average of 4 ramps. Buffer = 100 mM NaCl, 50 mM phosphate, pH = 7 with Sybr green II (1 in 10000). Sample concentration = 1.25 μM.

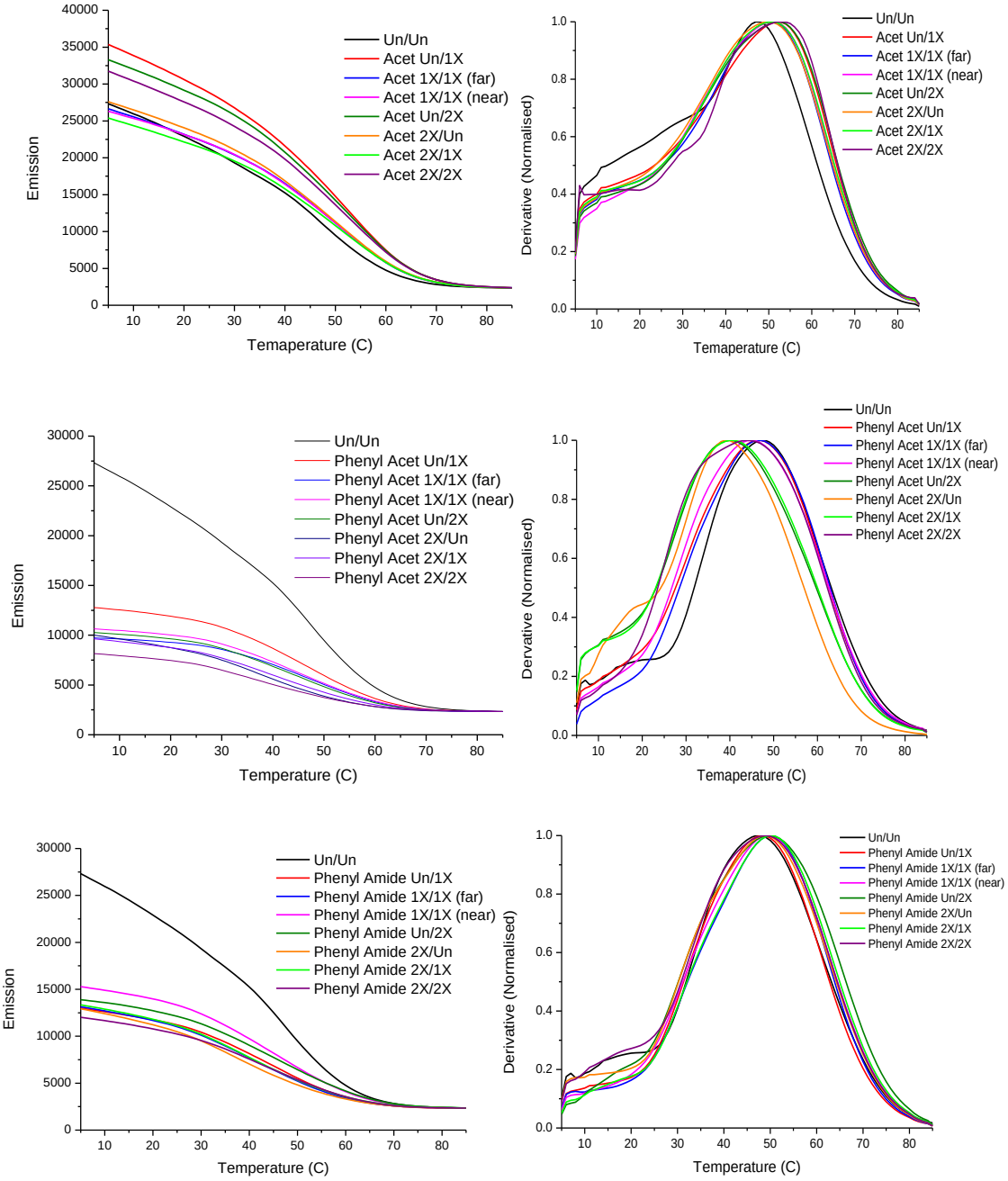

Figure 6.24 Left) Fluorescence melting curves for the Acet (top), Porph Acet (middle) and Porph Amide (bottom) duplex sets. Right) Derivatives of the corresponding melting curves.

The unmodified duplex has a measured melting temperature of 47 ˚C using a Bio-Rad CFX Connect real time PCR system for fluorescence melting. As mentioned above, DNA melting is concentration dependent and as such it was desirable to use the original 5 μM CD samples to measure the T_m's. However, after testing this, and other diluted samples, it was found the best data was

provided by samples diluted to 1.25 μM in the 100 mM NaCl, 50 mM phosphate, pH =7 buffer. Added to this was Sybr green II diluted by 1 in 10000 from the stock.

The smallest modification (Acet) produces a consistent set of melting temperatures, all at or just above 50 °C. This is a slight stabilisation from the unmodified duplex. The consistency matches well with the little change observed in the CD spectra (Figure 6.18). The slight stabilisation can also be explained by a π-interaction of the triple bond with the neighbouring bases.[261]

The T_m's for the duplexes containing the Phenyl Amide modification (Figure 6.24, bottom) are also consistently around 50 °C. A slight rise in melting temperature is seen in all samples compared to the unmodified duplex, and perhaps a slight decrease from the Acet duplexes. The fact that these values are consistent is surprising considering the increasing number of modifications and the changes that were seen in the CD spectra (Figure 6.20). Considering both sets of data would seem to suggest that whilst the structure of the duplex is changing, it is not being destabilised.

The measured Phenyl Acet T_m's are a bit more varied. The Un/1X and 1X/1X (far) samples have melting temperatures equal to that of the unmodified duplex. This suggests a modification on its own or two at a distance is having no effect on the stabilisation of the duplex. With increasing numbers of modifications, destabilisation to varying levels is seen. The sample which shows the most destabilisation is Phenyl Acet 2X/Un (-8 °C) which is consistent with the CD spectra (Figure 6.19) as the trace for this system (orange line) shows the most variation from the unmodified duplex. The rest of the data however do not appear to correlate in this way. 39 °C seems a little low for the 2X/Un sample compared to the rest, and certainly the Un/2X system, and may be an erroneous result. A repeat of the sample was run however, and produced the same result suggesting the spectroscopic data is in fact correct for the measured sample.

The data presented would suggest that these smaller modifications are not having a large effect on the stability of the duplex. However, the CD spectra clearly show changes to the structure of the DNA helix. Either these structural changes are not impacting the Watson-Crick base pairing, or positive

interactions between the modifications are off-setting the destabilisation caused by the structural changes.

As mentioned above, attempts at acquiring melting temperatures for the porphyrin-modified duplexes could not be achieved using fluorescence spectroscopy due to the quenching effect of the porphyrins. UV melting was also unsuccessful due to a fault with the heater. This data was therefore acquired at the University of Birmingham with the help of James Carr-Smith and Professor James Tucker.

The temperature ramp was slightly different to that used for the fluorescence melting experiments. Measurements were taken every 0.5 °C between 15 and 85 °C with heating/cooling at a rate of 0.5 °C per minute. An average over 3 melting experiments was taken to produce the melting curves. The curves produced by the Porph Amide duplexes are pictured in Figure 6.25. The samples did not need to be diluted as with fluorescence melting so are the same 5 μM concentration as used for CD spectroscopy. A Boltzmann fitting within Origin software was used to obtain the associated melting temperatures presented in Table 6.7, i.e. to calculate the point where the absorbance crosses the halfway point between the upper and lower baselines.

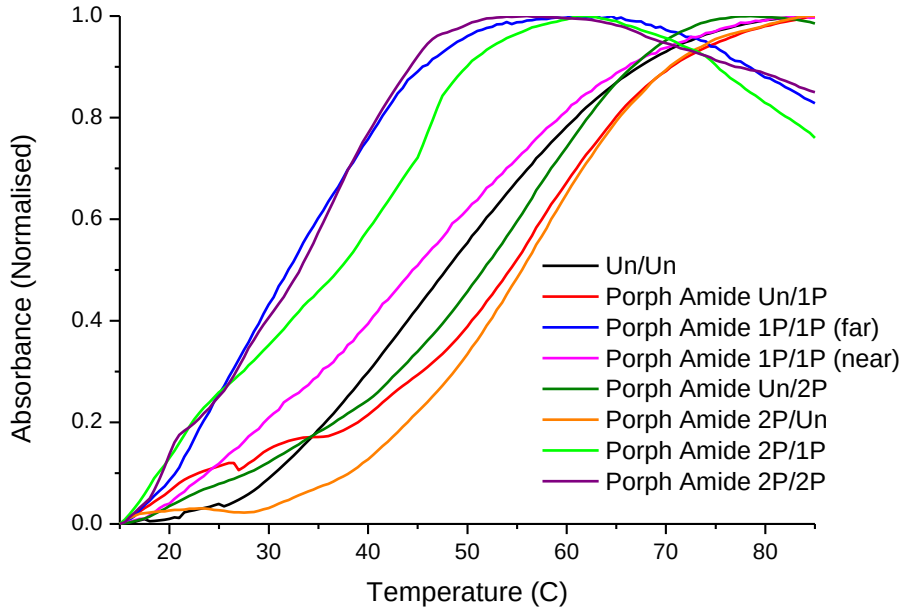

Figure 6.25 UV melting curves for the Porph Amide duplexes. Data acquired at a heating rate of 0.5 ˚C per minute. An average over 3 melting experiments was taken to produce the melting curves.

Sample	T_m of Porph Amide duplexes (˚C)	T_m of mixed Porph duplexes (˚C)
Un/Un	47.5	47.5
Un/1P	55.7	-
1P/1P (far)	30.8	30.4
1P/1P (near)	43.0	43.2
Un/2P	52.2	-
2P/Un	55.9	-
2P/1P	35.8	-
2P/2P	32.2	28.5

Table 6.7 Melting temperatures of the Porph Amide and mixed Porph duplexes as measured by UV melting.

From the acquired melting data, the first point of note is the measured melting temperature of the unmodified duplex. This value of 47.5 ˚C is consistent with that measured by fluorescence melting above. As such, the melting temperatures obtained by the two different techniques should be comparable.

The melting temperatures for the Porph Amide duplexes are a lot more varied than for any of the smaller modification systems. The previous data was mostly consistent with only slight stabilisation or destabilisation apparent. Perhaps the most surprising value is for the sample Porph Amide Un/1P which shows a stabilisation of 8 °C from the unmodified duplex. The previous data showed slight increases in melting temperature for the corresponding truncated samples but not by this much. With only one porphyrin in the system there are no porphyrin-porphyrin π-stacking interactions to add stability so it is hard to see what is causing this added stability.

The two 1P/1P samples also show a large variation with the 1P/1P (near) system destabilised by 4.5 °C and the 1P/1P (far) by 16.7 °C compared to the unmodified duplex. Little difference was seen in the corresponding small modification systems so it must be the porphyrins which are causing this destabilisation.

The Un/2P and 2P/Un samples, strangely, are both stabilised (4.7 °C and 8.4 °C respectively). The Zipper array was designed so porphyrins on opposite strands can π-stack with a stabilising effect on the duplex. The porphyrins in these systems however are on the same strand and so no inter-strand porphyrin interactions can be present. If this stabilisation is not an intramolecular effect then it is perhaps intermolecular. Establishing exactly what though will require enhanced modelling.

The final two samples, 2P/1P and 2P/2P, both show destabilisation from the unmodified system (11.7 °C and 15.3 °C respectively). This was surprising as with more porphyrins in closer proximity and on alternating strands, the discussed stabilising π-interactions were expected. The reasoning behind these expectations has however been very simplistic. Further intra- and intermolecular interactions must also be affecting the stability of these duplexes and influencing the observed melting temperatures.

The mixed Porph systems produced T_m values very similar to the corresponding Porph Amide samples. This suggests the mix between the amide flexibility and the acetylene rigidity is having no effect on the stability of the system. The consistency of these measured values seems at odds with the CD spectra (Figure 6.8 and 6.15) which show large differences between the two systems.

Unfortunately, the data for the Porph Acet systems acquired at Birmingham was corrupted and unusable. Melting data for these systems has been acquired in Southampton, but the quality of the data is such that no clear melting transition can be seen. As such no melting temperatures could be acquired for the Porph Acet samples. An example of the type of data obtained is presented in the appendix.

The lack of quality data has been attributed to the machine in Southampton rather than the state of the samples. It is possible however that the samples have degraded in the extended time between being made up for CD spectroscopy and UV melting.

When considering the CD spectra produced by the two sets of porphyrin-modified systems (Figure 6.8 and 6.12), the T_m's for the Porph Acet systems may be expected to be similar to the Porph Amide values. The CD spectra of sample Porph Acet 2P/2P (Figure 6.12) however, does not show a characteristic B-DNA signal and so it is conceivable that no double stranded DNA is present in this system.

If more time was available the samples could be re-made to ensure the quality, and the melting temperatures acquired on a spectrometer that is functioning correctly.

6.8 Conclusions: Structural Analysis of Porphyrin-Modified DNA

Circular dichroism spectroscopy has been used to investigate the ramifications of adding porphyrin modifications into a DNA duplex. This study has been supplemented with data obtained by UV/Vis and fluorescence spectroscopies along with molecular modelling.

Samples containing 0-4 modifications have all been investigated allowing the effect of increasing numbers of modifications to be analysed. The size of the modification has also been considered with the inclusion of smaller units before building up to the full porphyrin-modified systems.

A large amount of high quality spectra have been obtained and have shown that whilst the smaller modifications have a limited impact on the CD signal, the porphyrin modifications can drastically alter the spectra. Changes to the CD in the DNA region of the spectra correspond to changes in the molecule's structure. Attempts have been made to visualise these structural changes using molecular modelling, but the produced models require further work and expertise to fully reflect the actual structures.

The melting temperatures of the duplexes also reflect these structural changes further enforcing the impact that multiple porphyrins have on the 12-mer duplex. It is a great shame the melting temperatures for the acetylene-linked porphyrin modified samples could not be obtained in the allotted time. These data will prove interesting when comparing to the amide linked porphyrin units as the reduced flexibility of the acetylene linker could result in different melting temperatures. The extent of these differences in unclear however. The more rigid linker is designed to hold the porphyrins in a more defined position. As such the porphyrins may be less able to interact. The CD data however, suggests a lot more distortion is present in these duplexes and as such lower melting temperatures are expected for each corresponding sample.

A large number of excellent spectroscopic data has been acquired on these systems. With the addition of accurate models, a lot of insight can be gained into the structural characteristics of porphyrin-modified DNA.

7. Concluding Remarks

The main focus of this work has been the synthesis of the building blocks required to form a functional electronic wire from porphyrin-modified DNA. Three different porphyrin units were designed and synthesised with the aim of creating two porphyrin containing systems.

Porphyrins have been included in oligonucleotides using several different techniques. The Stulz group have used porphyrin-modified nucleotides in solid phase oligonucleotide synthesis for many years but this method remains far from perfect. The stability of the porphyrin nucleotides limits the number of porphyrins that can be included in an oligo if a reasonable yield is to be achieved. Synthesis of the six porphyrin Zipper strands proved tricky, but a small amount of product could be obtained. The purification method used for this system also requires work due to the nature of the porphyrins and the number present. There are many ways to address these problems however. Longer coupling times or more concentrated phosphoramidites could provide better coupling and a larger or different type of HPLC column may aid the purification.

Many hours were also dedicated to the synthesis of the di-acetylene porphyrin. Several synthetic pathways were attempted before the porphyrin was attached to an oligonucleotide. This work has led to a refined synthetic route allowing a porphyrin to be synthesised and attached to oligonucleotides post synthetically in a matter of weeks. This work will allow larger stocks of the porphyrins to be obtained in a much shorter time frame allowing any future work on this project to be focused on forming the DNA systems.

As a part of this work, three different methods, copper catalysed azide-alkyne cycloaddition, copper-free click chemistry and amide coupling were investigated as potential methods to couple porphyrins to oligonucleotides post synthetically. Single modification at the 5'-terminus of the oligo produced good results in all cases, but less promise was shown with internal modifications. Until further investigations can be carried out, it appears that, despite the shortcomings, the porphyrin-modified nucleosides are the best option for creating systems similar to the twelve porphyrin Zipper array. The possible challenger to this method would be copper-free click chemistry. This

technique has shown good coupling efficiencies with a single end-modification, but at the time the work was carried out was not available as an internal modifier. With one now becoming commercially available, it would be very interesting to test a multi-labelling reaction. Given the way these reactions are carried out on a small amount of DNA in an eppendorf tube, this technique (if successful) is likely to be more efficient, both in terms of time and money, than the modified solid phase oligonucleotide synthesis approach.

The aims of this project were designed to be ambitious and so a functional wire could not be made in the time allowed. Whilst the final aim could not be met, great strides have been taken and solid groundwork laid for ongoing work. Given sufficient time dedicated to each of the systems, there is no reason why the porphyrin-DNA wires cannot be realised and will hopefully display strong electron transfer properties.

A large amount of high quality spectroscopic data has also been obtained for the modified nucleotide samples building up from the natural DNA duplex, through the truncated systems to the full porphyrin modification. By following the changes to the circular dichroism, UV-Vis and fluorescence spectra with reference to molecular modelling, great insight has been gained into the structure and interactions of porphyrin-modified DNA. It was shown however, that the produced models do not fully agree with the data and a lot more complex interactions are occurring. To fully appreciate all that is going on within these systems, more in depth modelling is required. Understanding how the addition of modifications into duplex DNA affects the double helical structure will aid researchers in designing more elaborate DNA systems. Knowledge of the interactions between porphyrins can also be gained through this experimentation and will help the production of an efficient porphyrin based electronic wire.

The work carried out during this Ph.D project has been mainly in a preliminary capacity but has produced many encouraging results. Clear plans exist for continuing the projects and reaching the desired goals. Challenges still

remain, but the wire systems show great promise and the structural analysis has produced some excellent data on which to build.

8. General Experimental Methods

8.1 Suppliers

Reagents and solvents were supplied by Fisher Scientific, Sigma-Aldrich, Acros Organics, Glen Research and Link Technologies. These were used as directed by the supplier. Glen-Pak columns were provided by Glen Research and Fluoro-pak columns by Berry and Associates. Spin filters were provided by Costar. De-ionised water used was filtered by a Milli-Q Gradient A10 provided by Millipore.

8.2 Column Chromatography and Thin Layer Chromatography

Column chromatography was carried out using silica gel (40 – 60 μm particle size), silica gel type H (10 – 40 μm particle size) (both from Sigma-Aldrich) and basic aluminium oxide (50 – 200 μm, Brockmann activity I, from Acros Organics).

TLC plates used were TLC silica gel 60 F_{254} provided by Merck. Compounds on TLC plates were visualised using UV light of wavelengths 254 nm and 365 nm and/or anisaldehyde or ninhydrin stain.

8.3 Nuclear Magnetic Resonance Spectroscopy

NMR spectra were obtained using Bruker Advance DPX-300 and DPX-400 spectrometers with ^{1}H frequencies of 300.130 MHz and 400.132 MHz respectively. NMR tubes used were Wilmad-LabGlass 5 mm diameter.

8.4 Mass Spectrometry

Low resolution electrospray mass spectrometry was carried out on a Walters ZMD. LC-MS was carried out using a Bruker microTOF mass spectrometer with

a Dionex UltiMate 3000 HPLC system. MALDI-ToF was carried out on a Bruker UltrafleXtreme spectrometer.

8.5 Ultraviolet-Visible Spectroscopy

8.5.1 UV-Vis Scans

UV-Vis spectroscopy of both organic compounds and DNA samples were conducted using a Varian Cary 300 Bio spectrometer with quartz cells of 1 cm or 1mm path length (Hellma and Starna). Scans were carried out at room temperature over the region 200 – 800 nm.

8.5.2 UV Melting Experiments

Melting temperatures of porphyrin-modified oligonucleotides were determined at the University of Birmingham using a Varian Cary 500 spectrometer with quartz cells of 1 cm path length. Measurements at 260 nm were taken every 0.5 °C between 15 and 85 °C heating/cooling at a rate of 0.5 °C per minute. An average over 3 melts was taken to produce the melting curves with a Boltzmann fitting employed. The samples were made to a concentration of 5 μM in a 100 mM NaCl, 50 mM phosphate, pH = 7 buffer.

8.6 Fluorescence Spectroscopy

8.6.1 Fluorescence Scans

Fluorescence spectroscopy was conducted using a Varian Cary Eclipse spectrometer with quartz cells of 1 cm path length (Hellma and Starna). Scans were carried out at room temperature exciting at the absorption maximum.

8.6.2 Fluorescence Melting Experiments

Fluorescence melts were carried out using a Bio-Rad CFX Connect real time system. Emission measurements were taken every 1 °C between 5 and 85 °C heating/cooling at a rate of 1 °C per minute. An average over 4 ramps was taken to produce the melting curves. The samples were made to a concentration of 1.25 μM in a 100 mM NaCl, 50 mM phosphate, pH = 7 buffer with the addition of Sybr green II fluorescent dye (1 in 10000). 25 μL samples were placed in wells of a 96 well plate.

8.7 Solid Phase Oligonucleotide Synthesis

Solid phase DNA synthesis was carried out on a Applied Biosystems Expedite machine using CPG beads (500 or 1000 Å) on a 1 μmol scale.

De-blocking of the 5'-DMT protected nucleotide was achieved with 3 % TCA in DCM. Activation of the 3'-phosphoramidite used 'BTT Activator' 0.3 M Benzylthio-1 *H*-tetrazole in acetonitrile. Capping of unreacted 5'-hydroxyls was achieved using acetic anhydride in THF (Cap A) and 10 % N-methylimidazole in THF/pyridine (8:1) (Cap B). Oxidation used 0.02 M Iodine in THF/pridine/water. Washing steps used MeCN.

Cleavage of oligonucleotides from the solid supports was achieved by passing concentrated ammonium hydroxide (1 mL) back-and-forth though the column between two syringes (room temperature, 1 hour). Deprotection of the bases was carried out by heating to either 55 °C for 4 hours, or 40 °C for 18 hours. This process was carried out with agitation in an Eppendorf Thermomixer Compact or Eppendorf Thermomixer Comfort.

8.8 Purification of Oligonucleotides by Fluorous Affinity

Fluoro-Pak™ cartridges and associated solutions were provided by Berry and Associates. Instructions are provided and were followed. These are stated below.

Oligonucleotides are prepared by including a fluorous DMT (FDMT) monomer at the 5'-end of the oligonucleotide. After cleavage and deprotection, the oligonucleotide in ammonium hydroxide (1 mL) was diluted with 'Loading buffer' (equal volumes). Fluoro-Pak™ cartridges are conditioned with MeCN (2 mL), 0.1 M aqueous TEAA (2 mL) and 'Loading buffer' (2 mL) sequentially at a flow rate of 2 seconds per drop.

The fluorous tagged oligonucleotide solution was loaded onto the cartridge at a flow rate of 5 seconds per drop. Failure sequences were eluted with 10 % MeCN in 0.1 M aqueous TEAA (2 mL) followed by water (2 mL).

On-column de-tritylation was carried out with 3 % aqueous TFA (3 mL), 0.1 M aqueous TEAA (1 mL) and water (1 mL). Elution of the desired oligonucleotide was achieved with 50/50 MeCN/water. Removal of this solvent to dry the oligonucleotides was done in an Eppendorf Concentrator 5301.

8.9 Purification of Oligonucleotides by Glen-Pak™

Glen-Pak™ cartridges were provided by Glen Research. Instructions are provided and were followed. These are stated below using a flow rate of 1-2 drops per second throughout.

Oligonucleotides are prepared by standard solid phase DNA synthesis without removing the final 5'-DMT protecting group (DMT-ON). The oligonucleotide is then cleaved and the bases deprotected following section 8.7. The oligonucleotide in ammonium hydroxide was diluted with 100 mg mL^{-1} sodium chloride solution (equal volumes). Glen-Pak™ cartridges are conditioned with MeCN (0.5 mL) followed bt 1.0 M TEAA (1 mL).

The DMT-ON oligonucleotide solution was loaded onto the cartridge with all failure sequences not being retained due to a lack of the DMT group 'handle'. The cartridge is then washed with a 5 % MeCN in 100 mg mL^{-1} sodium chloride solution (salt wash solution, 2 X 1 mL), the DMT group cleaved with 2 % TFA (2 X 1 mL) and the cartridge washed again with water (2 X 1 mL). The purified oligonucleotide was then eluted with 50/50 MeCN/water (1 mL). Removal of this solvent to dry the oligonucleotides was done in an Eppendorf Concentrator 5301.

8.10 High Performance Liquid Chromatography

HPLC was carried out using a ThermoFisher HPLC or a Varian 920-LC with either a Waters XBridge OST C18 2.5 µm (4.8 X 50 mm or 10 X 50 mm) or a Polaris 3 C18-A 150 × 4.6 mm column. Eluents, gradients and column temperature varied between experiments so are stated in the relevant sections. A flow rate of 1 mL per minute was used in all cases.

8.11 Annealing DNA Duplexes

When annealing two complementary strands, an equal amount of the two strands was dissolved in water or an aqueous buffer and placed in an eppendorf tube. An Eppendorf Thermomixer Compact was pre-heated to 70 – 90 °C dependant on the length of the sequences, a higher temperature was used for longer sequences. The Eppendorf tube containing the DNA was sealed and mixed well by a pipette and/or vortex. The tube was placed in the hot Thermomixer for 1 minute without mixing. At this point the Thermomixer was turned off and the sample left in as the machine cooled naturally over a period of about 2 hours.

For example, to anneal samples for CD spectroscopy; 2.5 nmoles of the A strand and 2.5 nmoles of the appropriate B strand were combined and dissolved in 500 µL of 100 mM NaCl, 50 mM phosphate, pH = 7 buffer. The samples were then annealed in the Thermomixer as described.

8.12 Porphyrin-DNA Coupling Reactions

8.12.1 Copper Catalysed Azide-Alkyne Cycloaddition with the Baseclick Oligo-Click Kit

The Oligo-Click Kit was provided by Baseclick, Tutzing, Germany. This contained all required reagents except the porphyrin azides synthesised

during this project. Instructions were provided with the kit but were deviated from slightly.

The "activator" (ligand) solution (5 µL) was added to the copper catalyst in the "reactor" vial and thoroughly flushed with argon. To this was added the alkyne-modified oligonucleotide (5 nmoles, 1 equiv.) in water (5 µL) and the porphyrin azide (250 nmoles, 50 equiv.) in DMF (50 µL). The reactor vial was sealed under argon and the reaction mixture was heated to 25 - 30 °C with shaking and in the dark for 24 – 48 hours. After this time no progression in the reaction could be detected by HPLC.

When the reaction was deemed to be complete, water (100 µL) was added to the reaction mixture. This was washed sequentially with aliquots of ethyl acetate (200 µL) until the organic layer was colourless. This lack of colour suggested the majority of the free porphyrin had been removed from the vial.

The porphyrin-modified oligonucleotide in the aqueous layer was isolated by HPLC.

8.12.2 Copper-Free Click Chemistry

5'-cyclooctyne-modified DNA (10 nmoles, 1 equiv.) was dissolved in de-ionised water (10 µL) in an argon pursed eppendorf tube. To this was added a porphyrin azide (100 nmoles, 10 equiv.) in DMF (40 µL). The reaction mixture was maintained at 25 °C, under argon and shaken for 24 hours in a thermomixer.

After this time, water (100 µL) was added to the reaction mixture. This was washed sequentially with aliquots of ethyl acetate (200 µL) until all excess porphyrin had been removed. The porphyrin-modified oligonucleotide remained in the aqueous layer and was isolated by HPLC.

8.12.3 Post Synthetic Labelling of Carboxy Modified DNA with Amino-Modified Porphyrin

The desired oligonucleotide sequences were synthesised using a 1 μM solid phase oligonucleotide synthesis as described in section 8.7. The final base added (the 5'-end) was a Carboxy modifier C_{10} (Glen Research, pictured in Figure 5.3). This was given an extended 6 minute coupling time to ensure maximum coupling efficiency.

Upon completion of the synthesis, the CPG beads were cut out of the column and collected in an eppendorf tube. A solution of porphyrin (3 μmol, 3 equiv.) and DIPEA (6 μmol, 6 equiv.) in DMF (500 μL) was added to the beads before the tube was flushed with argon and sealed. The tube of carboxy-modified DNA and porphyrin solution was heated to 25 °C, with shaking, in a thermomixer for 18 hours in the dark.

The liquid was removed from the tube using a fine pipette to ensure the beads were left behind. These were then sequentially washed with aliquots of DMF (200 μL) until the washes became colourless showing a lack of porphyrin in solution. The porphyrin-modified strands were cleaved from the CPG beads by the addition of ammonium hydroxide (1 mL) and heating to 25 ° in a thermomixer for 2 hours whilst shaking in the dark.

The porphyrin coloured solution was transferred to a new eppendorf tube leaving the now white (or less intensely coloured) beads behind. The solution was heated to 40 °C with shaking and in the dark for 18 hours to deprotect the bases and remove the TMS groups.

The crude porphyrin-modified DNA was collected by removing the liquid in an eppendorf concentrator, and then purified by HPLC.

8.13 DNA Templated Glaser-Hay Reactions

DNA template Glaser-Hay couplings were attempted using many different reaction conditions as described in section 5.6. Reactions were all carried out using 33.3 pmoles per strand (2 × porphyrin, 1 × template) in a 1.5 mL eppendorf tube.

General Experimental Methods

For Gothelf type conditions:

The DNA was first dissolved in water (20.8 µL) with the addition of 100 mM CAPS buffer and 1 M $NaCl_{aq}$ (3.3 µL each) to anneal following the procedure in section 8.11. Once cooled, a pre-formed mixture of 6 mM $CuOAc_{aq}$ (0.6 µL), 60 mM $CuSO_{4aq}$ (0.6 µL) and 50 mM aqueous THPTA stabilising ligand (4.7 µL) was added to give a final volume of 33.3 µL. Samples were placed in a Thermomixer to agitate at the desired temperature (4, 25, 35 °C all tested) and for the desired time (24 – 48 hours). The reactions were followed by denaturing PAGE.

When including a base or another copper source, volumes were adjusted appropriately to always give a final volume of 33.3 µL.

For Hay type conditions:

The DNA was first dissolved in water to anneal. Once cool, TBA PF_6 (1.5 mg, 3.87 µmol, 0.5 equiv. to the number of phosphates) was added and the sample maintained at 25 °C until full dissolution. The water was removed *in vacuo* before the addition of a pre-formed mixture of 10 mM TMEDA (23.3 µL) and 10 mM CuCl (3.3 µL) both in DCE. The reaction mixture was topped up to a volume of 33.3 µL by adding DCE (6.7 µL).

The reaction was maintained at 25 °C for 24 hours and monitored by denaturing PAGE.

8.14 Gel Electrophoresis

<u>Native PAGE</u>

- For a 5 mL native PAGE stacking gel

0.375 M Tris-HCl (pH 8.8)	4.275 mL
Acrylamide / Bis-acrylimide (40 % w/v, 37.5 : 1)	0.67 mL

10 % (w/v) ammonium persulfate*	50 µL
TEMED*	5 µL

* Added just before use

- For a 10 mL native PAGE resolving gel

	20 %
0.375 M Tris-HCl (pH 8.8)	4.89 mL
Acrylamide / Bis-acrylimide (40 % w/v, 37.5 : 1)	5 mL
10 % (w/v) ammonium persulfate*	100 µL
TEMED*	10 L

* Added just before use

- Loading Buffer (100 mL)

62.5 mM Tris-HCl (pH 6.8)	757 mg
25 % Glycerol	2.5 g
1 % Bromophenol blue	100 mg
De-ionised water	To 100 mL

- Running buffer (1 L)

25 mM Tris-HCl	3.0 g
192 mM glycine	14.4 g
De-ionised water	To 1 L

Denaturing Urea PAGE

- For a 15 mL denaturing Urea PAGE gel

	10 %	15 %
Acrylamide / Bis-acrylimide (40 % w/v, 37.5 : 1)	3.8 mL	5.6 mL
Urea	6.3 g	6.3 g
10 × TBE	4.0 mL	3.0 mL
De-ionised water	4.0 mL	3.0 mL
10 % (w/v) ammonium persulfate*	100 µL	100 µL
TEMED*	5 µL	5 µL

* Added just before use

- 0.5 M EDTA (pH 8)

EDTA di-sodium di-hydrate	186.1 g
De-ionised water	To 1 L
	adjusted to pH 8 with 10 mM

NaOH

- 10 × TBE Running buffer

Tris base	108.0 g
Boric acid	55.0 g
0.5 M EDTA (pH 8)	40 mL
De-ionised water	To 1 L

- Loading buffer

Formamide	800 µL
Water	200 µL

8.15 Circular Dichroism Spectroscopy

CD spectroscopy data were acquired at the Diamond Light Source, Harwell Science and Innovation Campus, Didcot, Oxfordshire. The B23 Beamline was used with the assistance of Dr Giuliano Siligardi and Dr Rohanah Hussain.

Two CD spectrometers were used during this project. The B23 Beamline Module B was used to measure in the region 190 – 350 nm with a 1 nm

increment, a slit width of 1 mm and an integration time of 1 s. A circular cell with a volume of 350 µL and a pathlength of 1 mm was used with this machine.

An Applied Photophysics Chirascan was used to measure in the region 350 - 550 nm with a 1 nm increment, a slit width of 1 mm and an integration time of 1.5 s. A cuboid cell with a volume of 400 µL and a pathlength of 3 mm was used with this machine.

The CD spectrometers measure in units of millidegrees. This was then converted into the concentration independent units of Molar Δε using the equation below.

$$Molar\ \Delta\varepsilon = \frac{mdeg}{32980\ cL}$$

mdeg = measured difference in absorbance of left and right circularly polarised light

c = concentration (mol dm^{-3})

L = pathlength (cm)

9. Synthetic Procedures

9.1 Synthesis of 5-(*p*-methyl benzoate)-10, 15, 20-triphenyl porphyrin

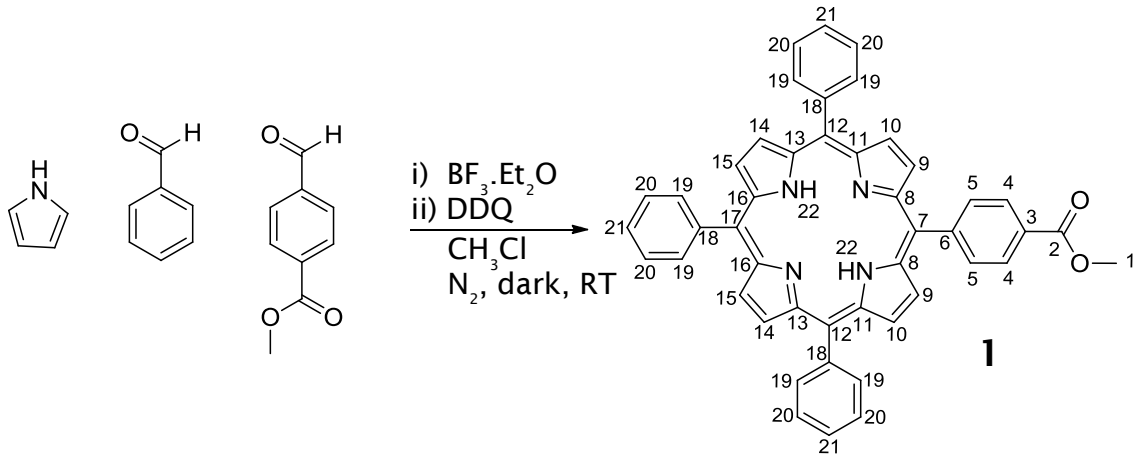

Chloroform (500 mL) was purged with Nitrogen (45 mins). To this was added Pyrrole (2.52 mL, 36 mmol, 6 equiv.), Benzaldehyde (3.64 mL, 36 mmol, 6 equiv.) and methyl-*p*-formylbenzoate (0.985 g, 6 mmol, 1 equiv.). The reaction proceeded for 45 mins in the dark and under nitrogen.

Boron trifluoride etherate (0.69 mL, 5.4 mmol, 0.9 equiv.) was added turning the reaction solution an orange colour. The nitrogen line was removed and the reaction remained in the dark at room temperature. Over time the solution darkened to a brown/black colour. After 1 hour 2, 3-dichloro-5, 6-dicyano-*p*-benzoquinone (DDQ) (8.14 g, 36 mmol, 6 equiv.) was added and the reaction left to stir overnight.

The crude product, a black sludge, was concentrated *in vacuo* before purification by two rounds of column chromatography. Firstly, silica/alumina, eluent – DCM, to separate the porphyrin compounds from the sludge. Second, silica/alumina, eluent – Toluene, to separate the different porphyrin's. This produced 386 mg (0.57 mmol, 10 %) of purple crystalline mono-substituted product **1**.

$\mathbf{R_f}$ (silica, DCM) = 0.89

LR-ESI (+ve) ($C_{46}H_{32}N_4O_2$): Monoisotopic mass = 672.3, observed m/z = 673.3 $[M + H]^+$

^{1}**H NMR** (CHLOROFORM-d ,400MHz): δ = 8.87 - 8.94 (m, 6 H, **H-10**, **H-14**, and **H-15**), 8.81 - 8.86 (m, *J*=5.1 Hz, 2 H, **H-9**), 8.47 (d, *J*=8.1 Hz, 2 H, **H-5**), 8.35 (d, *J*=8.1 Hz, 2 H, **H-4**), 8.23 - 8.28 (m, 6 H, **H-19**), 7.75 - 7.82 (m, 9 H, **H-20** and **H-21**), 4.14 (s, 3 H, **H-1**), -2.72 ppm (br. s, 2 H, **H-22**)

^{13}**C NMR** (CHLOROFORM-d ,75MHz): δ = 167.4 (C, **C-2**), 147.1 (C, **C-3**), 142.1 (C, **C-7**), 134.6 (CH, **C-19**), 129.7 (CH, **C-9**), 129.6 (C, **C-8**), 129.0 (CH, **C-10**), 127.9 (CH, **C-4** or**C-5**), 127.8 (CH, **C-4** or **C-5**), 126.7 (CH, **C-20** and **C-21**), 120.6 (C, **C-18**), 118.6 (C, **C-6**), 52.4 ppm (CH_3, **C-1**)

UV-Vis (DCM, 9.7 μM) *λ* (log ε) = 417 nm (4.91), 516 nm (3.51), 550 nm (3.14), 591 nm (2.99), 647 nm (2.83)

Emission (DCM, 9.7 μM, λ_{ex} = 417 nm) λ_{em} (relative intensity) = 651 nm (1), 717 nm (0.34)

9.2 Synthesis of 5-p-(benzoic acid)-10, 15, 20-triphenyl porphyrin

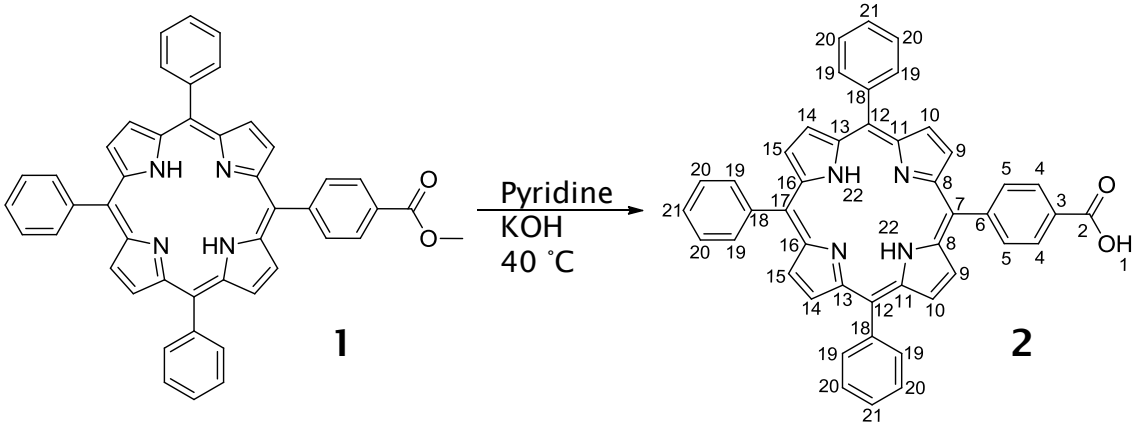

5-(*p*-methyl benzoate)-10, 15, 20-triphenyl porphyrin (**1**) (320 mg, 0.48 mmol, 1 equiv.) was dissolved in Pyridine (10 mL). Potassium hydroxide (1.35 g, 24 mmol, 50 equiv.) was dissolved in the minimum of de-ionised water and added to the reaction forming a purple organic layer on top a colourless aqueous layer. The reaction mixture was heated to 40 °C and left to stir overnight.

The Pyridine was removed *in vacuo* and the crude product separated between DCM (50 mL) and water (3 × 50 mL). 1 M HCl (10-15 mL) was added to the separating funnel to neutralise the solution and aid the separation. The aqueous layers were back extracted with more DCM and the organic fractions combined and dried (Na_2SO_4).

The crude product was purified by column chromatography (silica, eluent – DCM → 10 % MeOH in DCM). This gave 186 mg (0.28 mmol, 55 %) of purple crystalline **2**.

$\mathbf{R}_f$ (silica, 10 % MeOH in DCM) = 0.69

LR-ESI (+ve) ($C_{45}H_{30}N_4O_2$): Monoisotopic mass = 658.2, observed m/z = 659.5 $[M + H]^+$

^{1}**H NMR** (CHLOROFORM-d ,300MHz): δ = 8.85 - 8.93 (m, 6 H, **H-10**, **H-14**, and **H-15**), 8.78 - 8.84 (m, 2 H, **H-9**), 8.46 (d, *J*=8.1 Hz, 2 H, **H-4**), 8.32 (d, *J*=8.1 Hz, 2 H, **H-5**), 8.23 (dd, *J*=7.0, 1.5 Hz, 6 H, **H-19**), 7.70 - 7.85 (m, 9 H, **H-20** and **H-21**), -2.75 ppm (br. s, 2 H, **H-22**)

^{13}C NMR (DMSO-d_6 ,101MHz): δ = 147.0 (C, **C-3**), 141.6 (C, **C-7**), 134.8 (CH, **C-5**), 134.7 (CH, **C-19**), 130.9 (CH, **C-9**, **C-10**, **C-14** and **C-15**), 128.6 (CH, **C-4**), 127.6 (CH, **C-21**), 127.5 ppm (CH, **C-20)**

UV-Vis (DCM, 3.8 μM) λ (log ε) = 417 nm (5.26), 513 nm (3.86), 549 nm (3.52), 590 nm (3.36), 646 nm (3.22)

Emission (DCM, 3.8 μM, λ_{ex} = 417 nm) λ_{em} (relative intensity) = 650 nm (1), 716 nm (0.33)

9.3 Synthesis of 5'-DMT-5-Iodo-deoxyuridine

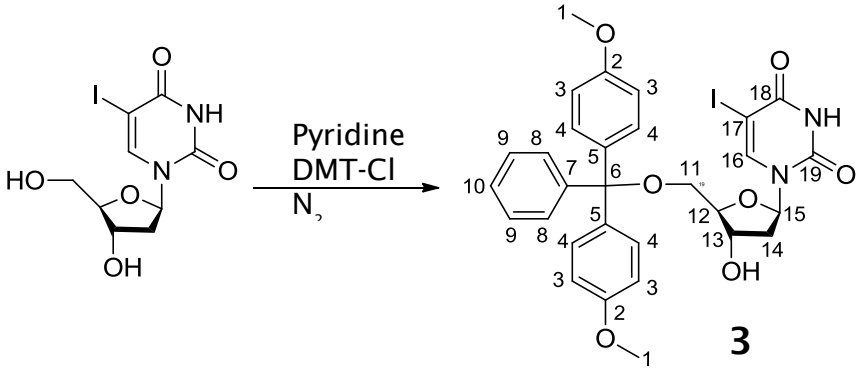

3

5-iodo-2'-deoxyuridine (5 g, 14.1 mmol, 1 equiv.) was dried by co-evaporation with Pyridine (3 × 10 mL) *in vacuo*. The solid was then dissolved in Pyridine (30 mL) and placed under Nitrogen. 4, 4' dimethyoxytrityl chloride (5.02 g, 14.8 mmol, 1.05 equiv.) was added in portions over 5 hours. Each added portion turned the solution a bright orange colour. This returned to the original yellow over 20/30 mins. Once all the DMT-Cl had been added the reaction was left for a further 15 mins. At this point MeOH : water (1:1, v:v, 5 mL) was added to quench the reaction. The solvent was removed *in vacuo* leaving a yellow oil.

The oil was dissolved in DCM (80 mL) and washed with water (2 × 100 mL), followed by sat. KCl (100 mL). The organic was collected, dried (Na_2SO_4), and concentrated before purification by column chromatography (silica (pre-treated with triethylamine), eluent – ethyl acetate : hexane 3:2 →6:1 (slow increase). The product containing fractions were collected and concentrated before co-evaporation with Toluene (3 × 20 mL) and Chloroform (3 × 20 mL) to remove any triethylamine. This produced 6.77 g (10.3 mmol, 73 %) of solid white product **3**.

R_f (silica, 10 % MeOH in DCM) = 0.66

ESI+ ($C_{30}H_{29}IN_2O_7$): Monoisotopic mass = 656.46, observed m/z = 679 $[M + Na]^+$

^{1}H NMR (CHLOROFORM-d ,300MHz): δ = 8.2 (s, 1 H, **H-16**), 7.4 (d, *J*=7.3 Hz, 2 H, **H-8**), 7.2 - 7.4 (m, 4 H, **H-4**), 7.2 (d, *J*=8.8 Hz, 3 H, **H-9** and **H-10**), 6.8 - 6.9

(m, 4 H, **H-3**), 6.3 (dd, *J*=6.6 Hz, 1 H, **H-15**), 4.6 (br. s., 1 H, **H-13**), 4.1 (d, *J*=2.2 Hz, 1 H, **H-12**), 3.8 (s, 3 H, **H-1**), 3.8 (s, 3 H, **H-1**), 3.42 (dd, *J*=6.2, 2.9 Hz, 2 H, **H-11**), 2.5 - 2.6 (m, 1 H, **H-14**), 2.2 ppm (m, 1 H, , **H-14**)

^{13}**C NMR** (CHLOROFORM-d ,75MHz): δ = 160.0 (C, **C-19**), 158.7 (C, **C-2**), 150.0 (C, **C-18**), 144.3 (CH, **C-16**), 135.5 (C, **C-5**), 135.4 (C, **C-5**), 130.1 (CH, **C-4**), 128.1 (CH, **C-8**), 128.1 (CH, **C-9**), 127.1 (CH, **C-10**), 113.4 (CH, **C-3**), 87.1 (C, **C-6**), 86.6 (CH, **C-12**), 85.7 (CH, **C-15**), 72.5 (CH, **C-13**), 68.6 (C, **C-17**), 63.5 (C, **CH_2-11**), 55.3 (CH_3, **C-1**), 41.5 ppm (CH_2, **C-14**)

UV-Vis (DCM, 15.2 μM) λ (log ε) = 229 nm (4.04), 281 nm (3.63)

Emission (DCM, 15.2 μM, λ_{ex} = 229 nm) λ_{em} (relative intensity) = No emission observed

9.4 Synthesis of 5'-DMT-5-propargylamine-deoxyuridine

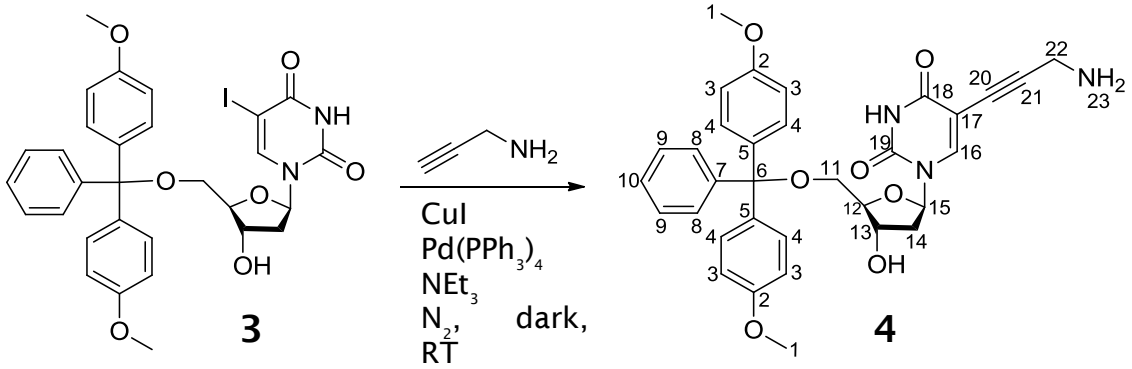

5'-DMT-5-Iodo-deoxyuridine (**3**) (500 mg, 0.76 mmol, 1 equiv.) dissolved in anhydrous DMF (5 mL) in oven dried glassware. 3 Å molecular sieves were added and the flask placed under nitrogen and in the dark. Propargylamine (100 µL, 1.52 mmol, 2 equiv.) and Copper iodide (35.8 mg, 0.19 mmol, 0. 25 equiv.) were added and the yellow solution stirred under nitrogen for 15 mins. At this point tetrakis (triphenylphosphine) Palladium (0) (90.3 mg, 0.076 mmol, 0.1 equiv.) and triethylamine (0.75 mL, 5.32 mmol, 7 equiv.) were added and the reaction stirred in the dark under nitrogen for 3 hours forming a dark brown solution.

The reaction mixture was diluted with ethyl acetate (50 mL) and separated with 5 % w:v EDTA (pH 9) (3 × 50 mL) followed by saturated potassium chloride (2 × 50 mL). The aqueous layers were back extracted and the combined organic layers dried (Na_2SO_4) and solvent removed *in vacuo*. A yellow/ orange oil remained which was co-evaporated with Toluene (3 × 20 mL) to attempt the removal of any remaining DMF.

The crude product was purified by column chromatography (silica (pre-treated with triethylamine), eluent – 5 % MeOH in DCM →10 % MeOH in DCM). Product fractions were combined and concentrated giving a fine yellow/ orange oil which became a yellow solid after co-evaporated with Toluene (3 × 20 mL) and neutralised Chloroform (3 × 20 mL). 265 mg (0.45 mmol, 60 %) of the solid yellow product **4** was obtained.

$\mathbf{R_f}$ (silica, 10 % MeOH in DCM) = 0.20

LR-ESI (+ve) ($C_{33}H_{33}N_3O_7$): Monoisotopic mass = 583.63, obserced m/z = 606 [M + Na^+]

^{1}H NMR (DMSO-d_6 ,300MHz): δ = 7.92 (s, 1 H, **H-16**), 7.41 (d, *J*=7.3 Hz, 2 H, **H-8**), 7.24 - 7.36 (m, 4 H, **H-4**), 7.13 - 7.21 (m, 3 H, **H-9** and **H-10**), 6.90 (d, *J*=8.8 Hz, 4 H, **H-3**), 6.11 (dd, *J*=6.6 Hz, 1 H, **H-15**), 4.24 - 4.30 (m, 1 H, **H-13**), 3.90 - 3.95 (m, 1 H, **H-12**), 3.74 (s, 6 H, **H-1**), 3.35 (s, 2 H, **H-22**), 3.20 - 3.27 (m, 1 H, **H-11**), 3.08 - 3.16 (m, 1 H, **H-11**), 2.19 - 2.26 ppm (m, 2 H, **H-14**)

^{13}C NMR (CHLOROFORM-d ,101MHz): δ = 158.7 (C, **C-2**), 135.6 (C, **C-5**), 130.0 (CH, **C-4**), 128.1 (CH, **C-8**), 127.9 (CH, **C-9**), 127.0 (CH, **C-10**), 113.4 (CH, **C-3**), 87.0 (C, **C-6**), 86.6 (CH, **C-12**), 85.6 (CH, **C-15**), 72.0 (CH, **C-13**), 63.5 (CH_2, **C-11**), 55.3 (CH_3, **C-1**), 41.6 (CH_2, **C-14**), 31.8 ppm (CH_2, **C-22**)

UV-Vis (DCM, 17.1 μM) λ (log ε) = 228 nm (4.24), 286 nm (3.71)

Emission (DCM, 17.1 μM, λ_{ex} = 228 nm) λ_{em} (relative intensity) = No emission observed

9.5 Synthesis of 5'-DMT-5-propargyl-dU-10", 15", 20"-triphenyl-5"-(P-benzamide)- porphyrin

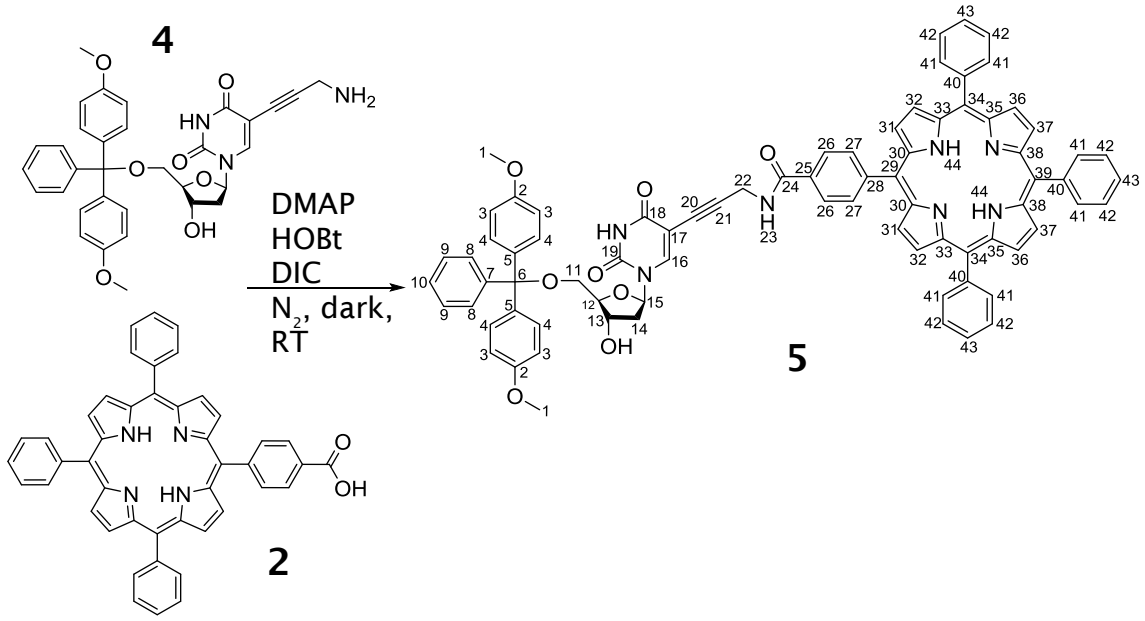

5-*p*-(benzoic acid)-10, 15, 20-triphenyl porphyrin (**2**) (60.0 mg, 0.092 mmol, 1 equiv.) was dissolved in anhydrous DCM (8 mL) in oven dried glassware containing 3 Å molecular sieves. To this was added DMAP (22.5 mg, 0.184 mmol, 2 equiv.), HOBt (13 mg, 0.096 mmol, 1.05 equiv.) and DIC (30 µL, 0.184 mmol, 2 equiv.). After 10 mins stirring in the dark and under nitrogen, 5'-DMT-5-propargylamine-dU) (**5**) (70.0 mg, 0.120 mmol, 1.3 equiv.) was added. The reaction mixture was stirred under these conditions for 2 hours.

The reaction mixture was diluted in DCM (30 mL) and washed with water (3 × 30 mL). The water was back extracted with DCM and the organic collected and combined. This was dried with Na_2SO_4 and concentrated *in vacuo*. The crude product was stored at 4 ˚C.

Purification was achieved by column chromatography (silica (pre-treated with triethylamine), eluent – 1 % MeOH in DCM → 1.5 % MeOH in DCM). Co-evaporation with Toluene (3 × 20 mL) and neutralised chloroform (3 × 20 mL) was used to remove the triethylamine.

88.5 mg (78 %) of purple crystalline product **5** was produced.

Synthetic Procedures

R_f (silica, 10 % MeOH in DCM) = 0.66

^{1}H NMR (CHLOROFORM-d ,300MHz): δ = 8.81 - 8.87 (m, 6 H, **H-32**, **H-36** and **H-37**), 8.75 (d, *J*=4.8 Hz, 2 H, **H-31**), 8.26 (s, 1 H, **H-16**), 8.16 - 8.23 (m, 8 H, **H-26** and **H-41**), 7.94 (d, *J*=8.4 Hz, 2 H, **H-27**), 7.69 - 7.78 (m, 9 H, **H-42** and **H-43**), 7.45 (d, *J*=7.3 Hz, 2 H, **H-8**), 7.35 (d, *J*=8.8 Hz, 4 H, **H-4**), 7.22 - 7.28 (m, 2 H, **H-9**), 7.18 (t, *J*=7.3 Hz, 1 H, **H-10**), 6.83 (d, *J*=7.7 Hz, 4 H, **H-3**), 6.62 - 6.71 (m, 1 H, **H-23**), 6.32 (t, *J*=6.4 Hz, 1 H, **H-15**), 4.51 - 4.58 (m, 1 H, **H-13**), 4.32 (dd, *J*=17.9, 4.8 Hz, 1 H, **H-22**), 4.29 (dd, *J*=17.9, 4.8 Hz, 1 H, **H-22**), 4.08 (d, *J*=2.6 Hz, 1 H, **H-12**), 3.72 (s, 6 H, **H-1**), 3.39 (dd, *J*=11.0, 2.2 Hz, 1 H, **H-11**), 3.36 (dd, *J*=11.0, 3.3 Hz, 1 H, **H-11**), 2.47 - 2.57 (m, *J*=3.3 Hz, 1 H, **H-14**), 2.31 (dd, *J*=1.0 Hz, 1 H, **H-14**), -2.79 ppm (s, 2 H, **H-44**)

^{13}C NMR (CHLOROFORM-d ,101MHz): δ = 167.0 (C, **C-24**), 158.7 (C, **C-2**), 158.7 (C, **C-2**), 145.6 (C, **C-28**), 143.3 (CH, **C-16**), 135.6 (C, **C-5**), 135.5 (C, **C-5**), 134.6 (CH, **C-26**), 134.5 (CH, **C-41**), 131.4 (CH, **C-31**, **C-31**, **C-36** and **C-37**), 130.0 (CH, **C-4**), 130.0 (CH, **C-4**), 128.2 (CH, **C-9**), 127.9 (CH, **C-8**), 127.8 (CH, **C-43**), 127.1 (CH, **C-10**), 126.7 (CH, **C-42**), 125.5 (CH, **C-27**), 120.4 (C, **C-40**), 118.6 (C, **C-25**), 113.5 (CH, **C-3**), 99.5 (C, **C-20**), 89.6 (C, **C-21**), 87.2 (C, **C-6**), 86.7 (CH, **C-12**), 85.9 (CH, **C-15**), 72.2 (CH, **C-13**), 63.5 (CH_2, **C-11**), 55.3 (CH_3, **C-1**), 41.7 (CH_2, **C-14**), 30.8 ppm (CH_2, **C-22**)

UV-Vis (DCM, 2.0 μM) λ (log ε) =227 nm (4.85), 289 nm (4.11), 417 nm (5.21), 515 nm (3.88), 551 nm (3.62), 592 nm (3.52), 647 nm (3.46)

Emission (DCM, 2.0 μM, λ_{ex} = 227 nm) λ_{em} (relative intensity) = 650 nm (1), 715 nm (0.33)

9.6 Synthesis of 5'-DMT-(5-propargyl-dU)-10", 15",20"-triphenyl-5"-(P- benzamide)-porphyrin-3' amidite

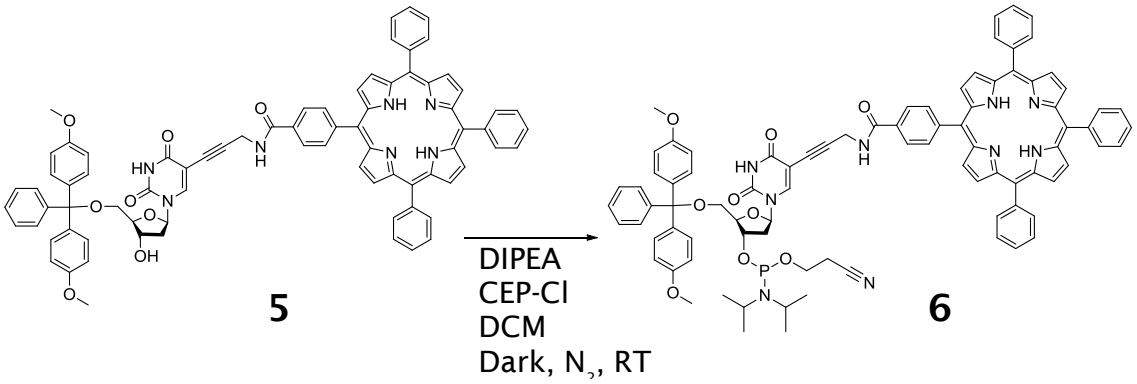

5'-DMT-5-propargyl-dU-10'', 15'',20''-triphenyl-5''-(*P*-benzamide)-porphyrin (**5**) (120 mg, 0.098 mmol, 1 equiv.) was placed in oven dried glassware with 3 Å molecular sieves. The flask was left under vacuum overnight. The porphyrin nucleoside was then dissolved in anhydrous DCM (5 mL) and had added to it DIPEA (68.3 µL, 0.392 mmol, 4 equiv.) and CEP-Cl (65.6 µL, 0.294 mmol, 3 equiv.). The flask was kept under nitrogen, in the dark and was stirred for 1.5 hours. TLC analysis showed formation of product.

The reaction mixture was transferred to a new oven dried, nitrogen purged flask *via* a cannula. The mixture was concentrated to approximately 1 mL using nitrogen flow through this flask. De-gassed hexane (5 – 10 mL) was added and the flask placed on ice to precipitate the product. The solvent was removed by filtration through a cannula.

Due to air sensitivity and instability of the compound no spectroscopic data were acquired.

9.7 Synthesis of 4-(3-hydroxy-3-methylbut-1-ynyl)benzaldehyde

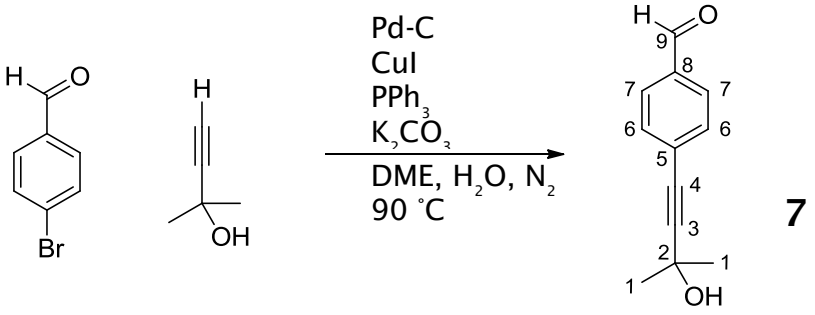

7

P-bromobenzaldehyde (6.0 g, 30.0 mmol, 1 equiv.), 10 % palladium on carbon (1.26 g, 12.0 mmol, 0.40 equiv.), triphenylphosphine (1.28 g, 4.8 mmol, 0.16 equiv.), copper iodide (0.46 g, 2.4 mmol, 0.08 equiv.) and potassium carbonate (20.58 g, 150.0 mmol, 5 equiv.) were dissolved in DME:H_2O (1:1, 120 mL). This was purged with nitrogen for 30 mins before 2-methyl-3-butyn-2-ol (14.7 mL, 150.0 mmol, 5 equiv.) was added and the reaction mixture heated (90 °C) for 18 hours.

Upon completion the reaction mixture was filtered through celite and separated between ethyl acetate (400 mL) and brine (3 × 50 mL). The organic phase was collected, dried (Na_2SO_4) and concentrated *in vacuo*.

The crude product was purified with two rounds of column chromatography. Firstly, (silica, eluent – 12.5 % EtOAc in petroleum ether → 20 % EtOAc in petroleum ether). Secondly, (silica, eluent – DCM → 30 % EtOAc in DCM). The product **7** was concentrated and collected as a yellow/orange oil of mass 4.96 g (26.4 mmol, 88 %)

R_f (silica, 20 % EtOAc in pet. Ether): 0.24

LR-ESI (+ve) ($C_{12}H_{12}O_2$) Monoisotopic mass = 188.08, observed m/z = 173.1 [M – CH_3]$^+$

^{1}**H NMR** (CHLOROFORM-d ,300MHz): δ = 9.98 (s, 1 H, **H-9**), 7.80 (d, *J*=8.4 Hz, 2 H, **H-7**), 7.53 (d, *J*=8.1 Hz, 2 H, **H-6**), 1.64 ppm (s, 6 H, **H-1**)

^{13}**C NMR** (CHLOROFORM-d ,75MHz): δ = 191.6 (CH, **C-9**), 135.4 (C, **C-8**), 132.1 (CH, **C-6**), 129.5 (CH, **C-7**), 129.1 (C, **C-5**), 98.0 (C, **C-3**), 81.3 (C, **C-4**), 65.6 (C, **C-2**), 31.3 ppm (CH_3, **C-1**)

UV-Vis (DCM, 53.0 μM) λ (log ε) = 228 nm (3.67), 277 nm (4.15)

Emission (DCM, 53.0 μM, λ_{ex} = 228 nm) λ_{em} (relative intensity) = No emission observed

9.8 Synthesis of 5-P-(3-methyl-3-hydroxyl-1-butynl) phenyl – 10, 15, 20-triphenyl porphyrin

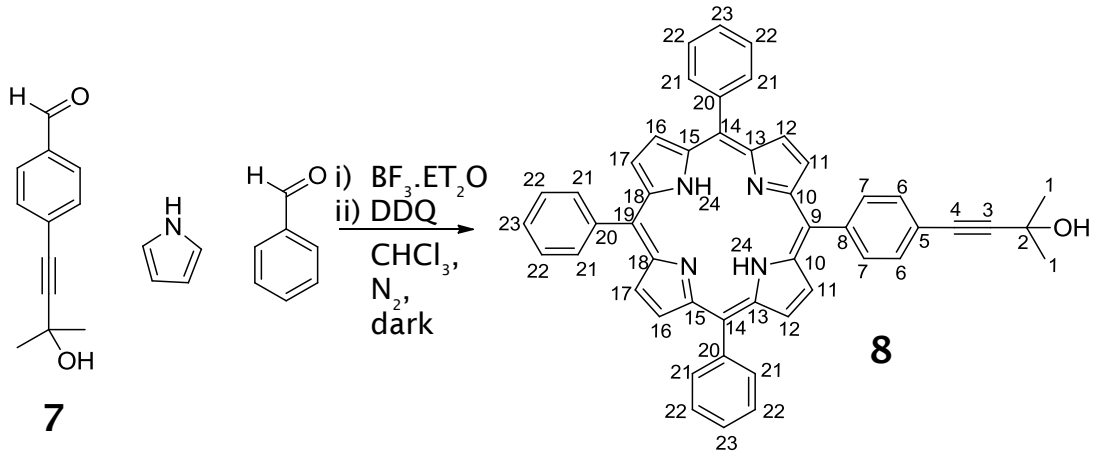

Chloroform (500 mL) was de-gassed for 15 mins. To this was added pyrrole (2.1 mL, 30.0 mmol, 6 equiv.), benzaldehyde (3.05 mL, 30.0 mmol, 6 equiv.) and 4-(3-hydroxy-3-methylbut-1-ynyl)benzaldehyde (7) (0.94 g, 5.0 mmol, 1 equiv.) and the mixture stirred under nitrogen and in the dark for 30 mins. Boron trifluoride etherate (0.57 mL, 4.5 mmol, 0.9 equiv.) was added and the reaction left to stir at room temperature under nitrogen and in the dark. After 1 hour DDQ (6.81 g, 30.0 mmol, 6 equiv.) was added and the nitrogen removed. The reaction was left at room temperature in the dark for 18 hours.

The reaction mixture was then concentrated *in vacuo* and re-dissolved in DCM (200 mL). This was purified by column chromatography. Firstly, to remove the polypyrrole side products and tetraphenyl porphyrin, (silica/alumina, eluent – DCM → 5 % MeOH in DCM). Further column chromatography was carried out (silica/alumina, eluent – DCM → 0.5 % MeOH in DCM) giving 361 mg (0.52 mmol, 10 %) of dark purple crystalline **8**.

R_f (silica, DCM) = 0.33

LR-ESI (+ve) ($C_{49}H_{36}IN_4O$): Monoisotopic mass = 696.29, observed m/z = 697.0 $[M + H]^+$

^{1}H NMR (CHLOROFORM-d ,300MHz): δ = 8.89 - 8.93 (m, 6 H, **H-12/H-16/H-17**), 8.87 (m, 2 H, **H-11**), 8.24 - 8.29 (m, 6 H, **H-21**), 8.22 (d, *J*=8.1 Hz, 2 H, **H-7**),

7.87 (d, *J*=8.1 Hz, 2 H, **H-6**), 7.75 - 7.83 (m, 9 H, **H-22/H-23**), 1.81 (s, 6 H, **H-1**), -2.72 ppm (br. s, 2 H, **H-24**)

^{13}**C NMR** (CHLOROFORM-d ,75MHz): δ = 142.3 (C, **C-8**), 142.1 (C, **C-20**), 134.6 (CH, **C-21**), 134.5 (CH, **C-7**), 130.1 (CH, **C-6**), 127.8 (CH, **C-23**), 126.7 (CH, **C-22**), 122.2 (C, **C-18**), 120.4 (C, **C-13 or C-15**), 120.3 (C, **C-13 or C-15**), 119.1 (C, **C-10**), 95.0 (C, **C-3**), 82.2 (C, **C-4**), 65.8 (C, **C-2**), 31.7 ppm (CH_3, **C-1**)

UV-Vis (DCM, 3.6 µM) λ (log ε) = 418 nm (5.31), 515 nm (3.90), 549 nm (3.55), 592 nm (3.36), 647 nm (3.22)

Emission (DCM, 3.6 µM, λ_{ex} = 418 nm) λ_{em} (relative intensity) = 650 nm (1), 718 nm (0.32)

9.9 Synthesis of Zn(II)-5-P-(3-methyl-3-hydroxyl-1-butynyl)-10,15,20 triphenyl porphyrin

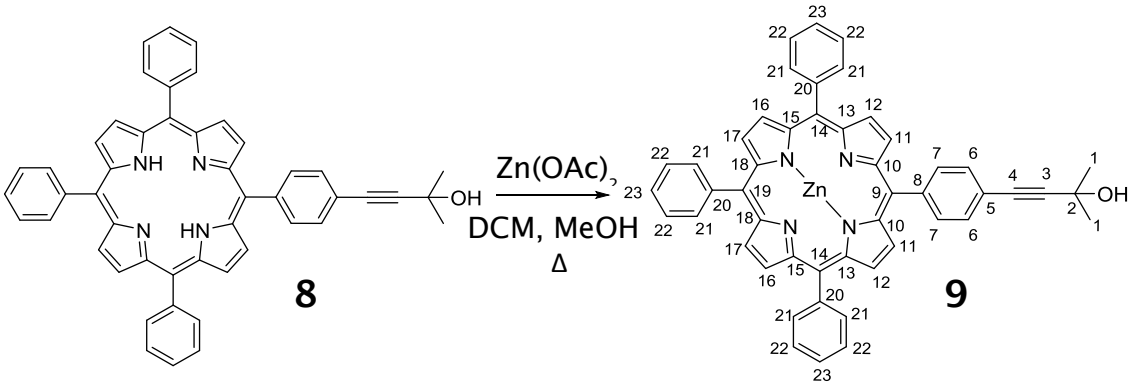

5-*P*-(3-methyl-3-hydroxyl-1-butynl) phenyl – 10, 15, 20-triphenyl porphyrin (**8**) (350 mg, 0.502 mmol, 1 equiv.) and zinc acetate dehydrate (4.4 g, 20 mmol, 40 equiv.) were dissolved in DCM:MeOH (80 mL : 10 mL). The reaction mixture was heated gently with a heat gun whilst swirling for 5 minutes. The solvent was removed *in vacuo* and the product re-dissolved in DCM (20 mL). The insoluble zinc was removed by filtration and solvent removed *in vacuo*.

The crude product was purified by column chromatography (silica, eluent – DCM) giving 277 mg (0.365 mmol, 73 %) of purple powder **9**.

R_f (silica, 10 % MeOH in DCM) = 0.77

^{1}H NMR (CHLOROFORM-d ,400MHz): δ = 8.96 - 9.00 (m, 6 H, **H-12, H-16** and **H-17**), 8.94 (d, *J*=5.1 Hz, 2 H, **H-11**), 8.24 (d, *J*=6.7 Hz, 6 H, **H-21**), 8.20 (d, *J*=7.8 Hz, 2 H, **H-7**), 7.83 (d, *J*=7.8 Hz, 2 H, **H-6**), 7.74 - 7.80 (m, 9 H, **H-22** and **H-23**), 1.71 ppm (s, 6 H, **H-1**)

^{13}C NMR (CHLOROFORM-d ,101MHz): δ = 143.1 (C, **C-8**), 142.8 (C, **C-20**), 134.5 (CH, **C-21**), 134.4 (CH, **C-7**), 132.2 (C, **C-12**, **C-16**, or **C-17**), 132.1 (C, **C-12**, **C-16**, or **C-17**), 132.1 (C, **C-12**, **C-16**, or **C-17**), 131.7 (C, **C-11**), 129.9 (CH, **C-6**), 127.5 (CH, **C-23**), 126.6 (CH, **C-22**), 121.9 (C, **C-18**), 121.4 (C, **C-13 or C-15**), 121.3 (C, **C-13 or C-15**), 120.1 (C, **C-10**), 94.7 (C, **C-3**), 82.3 (C, **C-4**), 65.8 (C, **C-2**), 31.5 ppm (CH_3, **C-1**)

UV-Vis (DCM, 3.3 μM) λ (log ε) = 419 nm (5.36), 548 nm (3.94), 585 nm (3.16)

Emission (DCM, 3.3 μM, λ_{ex} = 419 nm) λ_{em} (relative intensity) = 597 nm (0.94), 645 nm (1)

9.10 Synthesis of 5-P-ethynylphenyl-10, 15, 20-triphenyl porphyrin

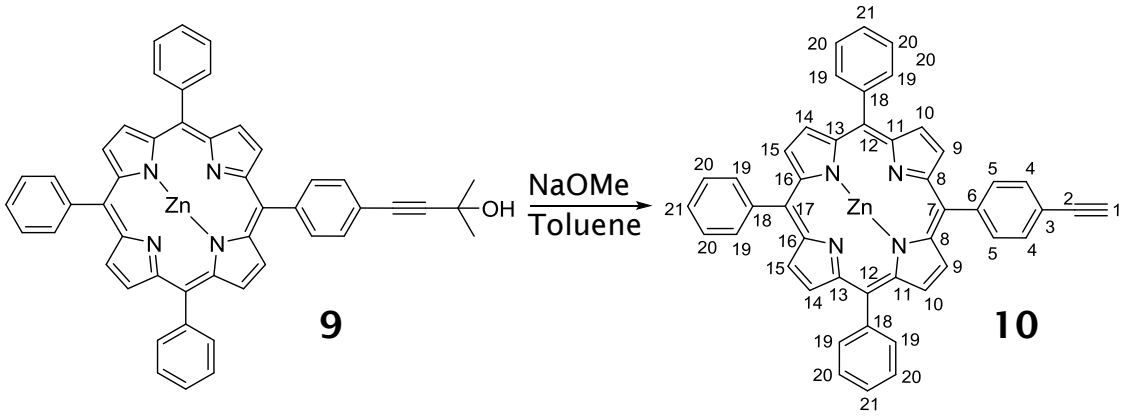

Zn(II)-5-*P*-(3-methyl-3-hydroxyl-1-butynyl)-10,15,20 triphenyl porphyrin (**9**) (260 mg, 0.342 mmol, 1 equiv.) and NaOMe (556 mg, 10.3 mmol, 30 equiv.) were dissolved in toluene (100 mL) and purged with nitrogen for 10 mins. The reaction was heated to reflux (125 ˚C) for 14 hours.

At this time no starting material remained. The solvent was removed *in vacuo* and the product re-dissolved in DCM (50 mL). This was washed with brine (3 × 50 mL) and dried with sodium Na_2SO_4. The product was obtained by filtration and concentration *in vacuo*. This produced 216 mg (0.307 mmol, 90 %) of purple powder **10**.

R_f (silica, 10 % MeOH in DCM) = 0.97

LR-ESI (+ve) ($C_{46}H_{28}N_4Zn$): Monoisotopic mass = 700.16, observed m/z = 701.0 $[M + H]^+$

^{1}**H NMR** (CHLOROFORM-d ,300MHz): δ = 8.85 - 8.89 (m, 6 H, **H-10, H-14** and **H-15**), 8.84 (d, *J*=5.1 Hz, 2 H, **H-9**), 8.08 - 8.17 (m, 10 H, **H-4** or **H-5** and **H-19**), 7.79 (d, 2 H, **H**-4 or **H**-5), 7.63 - 7.70 (m, 9 H, **H-20** and **H-21**), 3.21 ppm (s, 1 H, **H-1**)

^{13}**C NMR** (CHLOROFORM-d ,75MHz): δ = 150.3 (C, **C-12**), 150.3 (C, **C-12**), 150.2 (C, **C-17**), 149.8 (C, **C-7**), 143.6 (C, **C-6**), 142.8 (C, **C-18**), 134.4 (CH, **C-19**), 134.4 (CH, **C-5**), 132.2 (CH, **C-9**/**C-10**), 132.1 (CH, **C-14**/**C-15**), 132.1 (CH, **C-14**/**C-15**), 131.6 (CH, **C-9**/**C-10**), 130.4 (CH, **C-4**), 127.5 (CH, **C-21**), 126.6 (CH,

C-20), 121.4 (C, **C-16**), 121.3 (C, **C-11** and **C-13**), 120.0 (C, **C-8**), 83.8 (CH, **C-1**), 78.1 ppm (C, **C-2**)

UV-Vis (DCM, 3.1 µM) λ (log ε) = 419 nm (5.45), 549 nm (4.01), 587 nm (3.26)

Emission (DCM, 3.1 µM, λ_{ex} = 419 nm) λ_{em} (relative intensity) = 596 nm (0.88), 644 nm (1)

9.11 Synthesis of 5'-DMT-(5"-P-ethynylphenyl)-10", 15", 20"-triphenyl-Zn (II)-porphyrin-dU

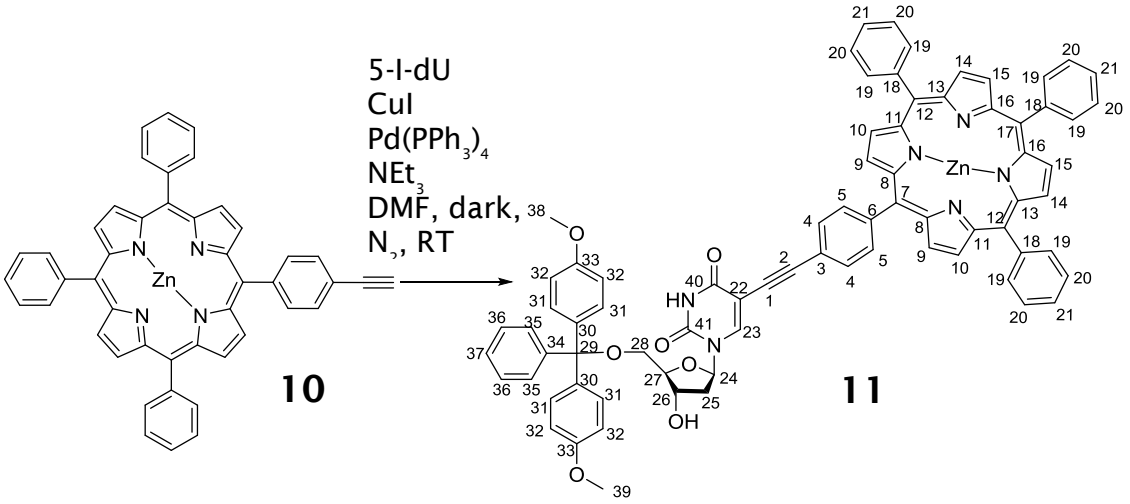

Zn (II)-5-*P*-ethynylphenyl-10, 15, 20-triphenyl porphyrin (**10**) (100 mg, 0.142 mmol, 1 equiv.), 5'-DMT-5-

Iodo-deoxyuridine (120 mg, 0.185 mmol, 1.3 equiv.), CuI (8.95 mg, 0.047 mmol, 0.33 equiv.) and triethylamine (35 µL) were dissolved in DMF (5 mL) in an oven dry, nitrogen purged flask containing molecular sieves. The reaction mixture was purged with nitrogen for 20 mins before tetrakis triphenyl phosphine palladium (0) (41.6 mg, 0.036 mmol, 0.25 eq) was added. The reaction was stirred in the dark, under nitrogen for 24 hours.

TLC analysis after 24 hours showed starting material remained. CuI (5 mg) and $Pd(PPh_3)_4$ (20 mg) were added and the reaction left for a further 5 hours.

After this time the reaction mixture was diluted with ethyl acetate (50 mL) and washed with brine (3 × 50 mL). The organic layer was dried (Na_2SO_4) and the solvent removed *in vacuo*.

The crude product was purified three times by column chromatography. Firstly, (Silica/10 % silica H + NEt_3, eluent – DCM : MeOH : EtOAc, 100:0.5:0.5 → 100:2:2). NMR showed the presence of starting nucleoside mixed with porphyrin nucleoside product. This was due to the starting nucleoside and product having near identical R_f values.

Second column, (Silica/10 % silica H + NEt_3, eluent – DCM : MeOH : EtOAc, 100:1:1). Each fraction was checked by NMR. Fractions clear of starting

nucleoside were kept separate. Mixed fractions were purified again to maximise yield.

Third column, (Silica/10 % silica H + NEt_3, eluent – DCM : MeOH : EtOAc, 100:1:1). All clean fractions were combined and co-evaporation with toluene (X 3) followed by neutralised chloroform (X 3) carried out to remove residual NEt_3. 101.4 mg (0.083 mmol, 58 %) of purple solid **11** was produced.

R_f (silica, 10 % MeOH in DCM) = 0.61

ESI- ($C_{76}H_{56}N_6O_7Zn$): Monoisotopic mass = 1228.35, observed m/z = 1229.7 $[M + H]^+$

^{1}**H NMR** (CHLOROFORM-d ,400MHz): δ = 8.86 (d, *J*=4.6 Hz, 2 H, **H-10**), 8.84 (s, 4 H, **H-14** and**H-15**), 8.79 (d, *J*=4.5 Hz, 2 H, **H-9**), 8.13 (d, *J*=6.6 Hz, 6 H, **H-19**), 7.92 (d, *J*=8.1 Hz, 2 H, **H-5**), 7.77 (s, 1 H, **H-23**), 7.61 - 7.69 (m, 9 H, **H-20** and **H-21**), 7.30 (d, *J*=7.6 Hz, 2 H, **H-35**), 7.20 - 7.24 (m, 4 H, **H-31**), 7.18 - 7.20 (m, 4 H, **H-4** and **H-36**), 7.08 - 7.14 (m, 1 H, **H-37**), 6.71 (d, *J*=7.6 Hz, 4 H, **H-32**), 5.50 (dd, *J*=6.6 Hz, 1 H, **H-24**), 4.10 (br. s., 1 H, **H-26**), 3.60 (s, 3 H, **H-38** or **H-39**), 3.59 (s, 3 H, **H-38** or **H-39**), 3.27 (br. s., 1 H, **H-27**), 2.93 - 3.02 (m, 2 H, **H-28**), 2.02 - 2.10 (m, 1 H, **H-25**), 1.84 - 1.93 ppm (m, 1 H, **H-25**)

^{13}**C NMR** (CHLOROFORM-d ,101MHz): δ = 160.9 (C, **C-40**), 158.6 (C, **C-33**), 150.2 (C, **C-17**), 150.1 (C, **C-12**), 149.8 (C, **C-7**), 148.6 (C, **C-41**), 144.3 (C, **C-3**), 143.1 (C, **C-34**), 142.9 (C, **C-18**), 141.7 (CH, **C-23**), 135.5 (C, **C-6** and **C-30**), 134.5 (C, **C-19**), 134.2 (CH, **C-5**), 132.1 (CH, **C-10**), 132.0 (CH, **C-14**), 132.0 (CH, **C-15**), 131.6 (CH, **C-9**), 129.9 (CH, **C-36**), 129.9 (CH, **C-31**), 129.8 (CH, **C-31**), 128.1 (CH, **C-32**), 128.0 (CH, **C-21**), 127.5 (CH, **C-35**), 127.1 (CH, **C-37**), 126.6 (CH, **C-20**), 121.5 (C, **C-11**), 121.2 (C, **C-13**), 121.1 (C, **C-16**), 120.1 (C, **C-8**), 113.4 (CH, **C-32**), 100.3 (C, **C-1**), 94.0 (C, **C-2**), 87.1 (C, **C-29**), 86.3 (CH_2, **C-27**), 85.4 (CH, **C-24**), 80.7 (C, **C-22**), 71.9 (CH, **C-26**), 63.1 (CH_2, **C-28**), 55.2 (CH_3, **C-38** and **C-39**), 41.3 ppm (CH_2, **C-25**)

UV-Vis (DCM, 2.0 μM) λ (log ε) = 228 nm (4.92), 420 nm (5.30), 548 nm (3.88), 587 nm (3.09)

Emission (DCM, 2.0 μM, λ_{ex} = 420 nm) λ_{em} (relative intensity) = 598 nm (1), 644 nm (0.94)

9.12 Synthesis of 5'-DMT-5-(5"-p-ethynylphenyl)-10", 15",20"-triphenyl-Zn(II)- porphyrin-dU-3' amidite

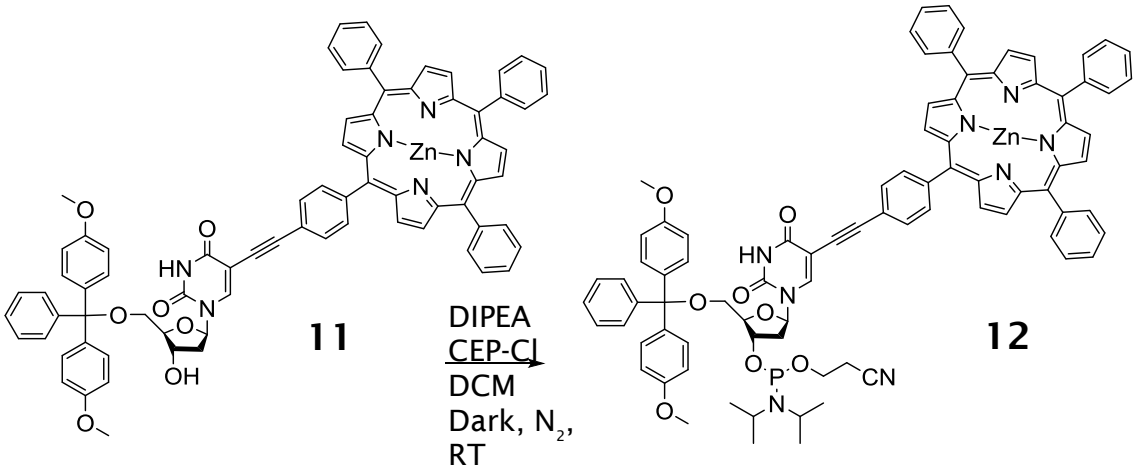

5'-DMT-(5''-*P*-ethynylphenyl)-10'', 15'', 20''-triphenyl-Zn (II)-porphyrin-dU (**11**) (120 mg, 0.098 mmol, 1 equiv.) was dissolved in anhydrous DCM and transferred to an oven dried, nitrogen purged flask containing 3 Å molecular sieves and stirrer bar. The solvent was removed and the flask left *in vacuo* overnight.

The starting porphyrin nucleotide was re-dissolved in anhydrous DCM (3 mL) and placed under nitrogen in the dark. To this was added DIPEA (67.4 µL, 0.392 mmol, 4 equiv.) and the solution purged with nitrogen for 10 mins. CEP-Cl (65.6 µL, 0.294 mmol, 3 equiv.) was added and the reaction left in the dark, under nitrogen for 2 hours (monitored by TLC).

The stirrer bar and molecular sieves were removed by filtration through a cannula to a new oven dried, nitrogen purged flask. The cannula was used to avoid opening the flask to the atmosphere and oxidising the product. Nitrogen was passed through the flask and exhausted to reduce the volume of the solvent to approximately 1 mL. De-gassed hexane (5 mL) was added and the flask placed on ice to precipitate the purple product. Filtration *via* the cannula was used to remove the hexane before drying *in vacuo* for 10 mins.

The product was dissolved in anhydrous DCM (0.5 mL) and transferred to an oven dried, nitrogen purged DNA synthesiser vile. The flask was washed with MeCN:DCM (1:1, 1.5 mL), then MeCN (1 mL) making the total volume 3 mL in

the DNA synthesiser vile. This was transferred straight onto the DNA synthesiser and used in DNA synthesis immediately.

$\mathbf{R}_f$ (silica, 5 % MeOH in DCM) = 0.59 and 0.56 (product diastereomers)

No further characterisation data was obtained due to the instability / air sensitivity of the product meaning it had to be used immediately for DNA synthesis.

9.13 Synthesis of 1-amino-3-propylazide

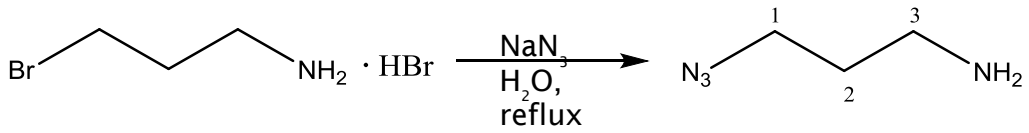

13

3-bromoproylamine hydrobromide (1.0 g, 4.57 mmol, 1 equiv.) was dissolved in water (5 mL). To this was added sodium azide (988 mg, 15.2 mmol, 3.33 equiv) in water (7 mL). The reaction mixture was heated under reflux conditions for 18 hours.

The amount of solvent was reduced by approximately 2/3 *in vacuo*. The remainder of the reaction mixture was cooled on ice with the addition of Ice cold diethyl ether (15 mL). KOH (1.22 g) was added in portions to keep the temperature of the solution down. The organic layer was removed and the aqueous layer extracted twice with more diethyl ether. The combined organic layers were dried with potassium carbonate and the solvent removed *in vacuo*.

A clear, yellow oil of mass 396.5 mg (3.96 mmol, 87 %) was collected with no further purification required.

R_f (silica, 10 % MeOH in DCM) = 0.18

LR-ESI (+ve) ($C_3H_8N_4$): Monoisotopic mass = 100.07, observed m/z = 101.1

^{1}**H NMR** (CHLOROFORM-d ,400MHz): δ = 3.37 (t, *J*=6.7 Hz, 2 H, **H-1**), 2.80 (t, *J*=6.8 Hz, 2 H, **H-3**), 1.73 ppm (quin, *J*=6.8 Hz, 2 H, **H-2**)

^{13}**C NMR** (CHLOROFORM-d ,101MHz): δ = 49.2 (CH_2, **C-1**), 39.4 (CH_2, **C-3**), 32.5 ppm (CH_2, **C-2**)

9.14 Synthesis of dipyrromethane

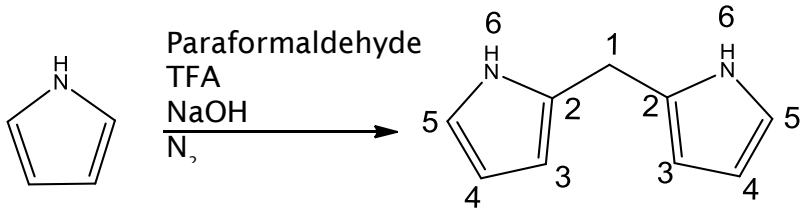

14

Freshly distilled pyrrole (400 mL) was purged with nitrogen for 30 mins prior to the addition of paraformaldehyde (1.70 g, 18.9 mmol). The flask was kept under nitrogen and the reaction mixture heated to 50 °C until complete dissolution when it was then cooled.

TFA (0.42 mL) was added dropwise and the reaction left under nitrogen for 6 hours turning a dark brown over time. NaOH (0.60 g) was then added to neutralise the reaction and this left for 14 hours.

The excess pyrrole was removed *in vacuo* leaving a dark sludge. This was purified by column chromatography (silica, eluent – 5 % EtOAc in hexane) giving 1.52 g (10.4 mmol, 55 %) of white solid product **14**.

R_f (silica, DCM) = 0.65

ESI- ($C_9H_{10}N_2$): Monoisotopic mass = 146.08 , observed m/z = 145.1 $[M - H]^+$

^{1}H NMR (CHLOROFORM-d ,300MHz): δ = 7.73 (br. s, 2 H, **H-6**), 6.65 (d, *J*=1.8 Hz, 2 H, **H-5**), 6.19 (dd, *J*=2.6 Hz, 2 H, **H-4**), 6.08 (br. s., 2 H, **H-3**), 3.97 ppm (s, 2 H, **H-1**)

^{13}C NMR (CHLOROFORM-d ,75MHz): δ = 129.2 (C, **C-2**), 117.5 (CH, **C-5**), 108.3 (CH, **C-4**), 106.6 (CH, **C-3**), 26.3 ppm (CH_2, **C-1**)

9.15 Synthesis of 5-(p-methyl benzoate)-15-phenyl porphyrin

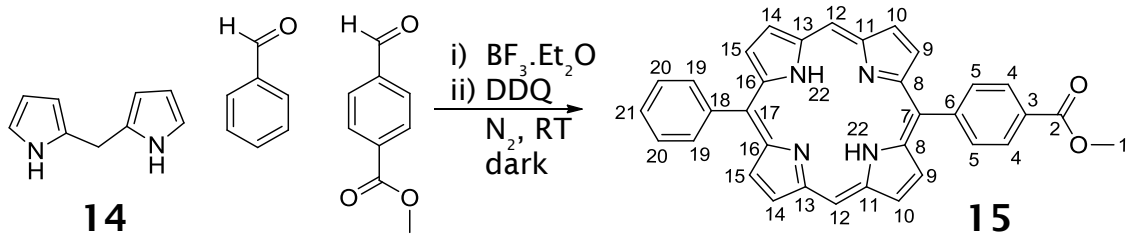

DCM (400 mL) was purged with nitrogen for 45 mins. Dipyrromethane (**14**) (500 mg, 3.42 mmol, 1 equiv.), benzaldehyde (0.35 mL, 3.42 mmol, 1 equiv.) and methyl-4-formylbenzoate (560 mg, 3.42 mmol, 1 equiv.) were added and the solution further purged with nitrogen for 15 mins with the reaction flask shielded from the light.

Boron trifluoride etherate (40 µL, 0.342 mmol, 0.1 equiv.) was added and the reaction left to stir in the dark, under nitrogen for 3 hours. The flask was then opened to the air and the oxidiser DDQ (1.16 g, 5.13 mmol, 1.5 equiv.) was added. The reaction was left in the dark overnight.

The solvent was removed *in vacuo* and the crude mono-ester porphyrin product separated from the side products (porphyrins and polypyrroles) by column chromatography (Silica/Alumina, eluent – DCM).

127 mg (0.244 mmol, 7 %) of the product **15** was collected as a purple/copper coloured solid.

$\mathbf{R_f}$ (silica, DCM) = 0.67

ESI+ ($C_{34}H_{24}N_4O_2$): Monoisotopic mass = 520.19 , observed m/z = 521.3 $[M + H]^+$

^{1}**H NMR** (CHLOROFORM-d ,300MHz): δ = 10.20 (s, 2 H, **H-12**), 9.28 (d, *J*=4.4 Hz, 4 H, **H-10 and H-14**), 8.99 (d, *J*=4.8 Hz, 2 H, **H-15**), 8.92 (d, *J*=4.4 Hz, 2 H, **H-9**), 8.40 (d, *J*=8.1 Hz, 2 H, **H-4**), 8.26 (d, *J*=8.1 Hz, 2 H, **H-5**), 8.13 - 8.21 (m, 2 H, **H-19**), 7.66 - 7.77 (m, 3 H, **H-20 and H-21**), 4.05 (s, 3 H, **H-1**), -3.22 ppm (br. s., 2 H, **H-22**)

^{13}**C NMR** (CHLOROFORM-d ,75MHz): δ = 167.4 (C, **C-2**), 134.9 (CH, **C-5** and **C-19**), 131.9 (CH, **C-10** or **C-14**), 131.7 (CH, **C-10** or **C-14**), 131.2 (CH, **C-15**), 130.6 (CH, **C-9**), 128.2 (CH, **C-4**), 127.8 (CH, **C-21**), 127.0 (CH, **C-20**), 105.5 (CH, **C-12**), 52.5 ppm (CH_3, **C-1**)

UV-Vis (DCM, 4.8 μM) λ (log ε) = 406 nm (5.31), 502 nm (4.01), 537 nm (3.62), 575 nm (3.57), 629 nm (3.22)

Emission (DCM, 4.8 μM, λ_{ex} = 406) λ_{em} (relative intensity) = 633 nm (1), 699 nm (0.48)

9.16 Synthesis of 5-(p-methyl benzoate)-15-phenyl, 10, 20-dibromo porphyrin

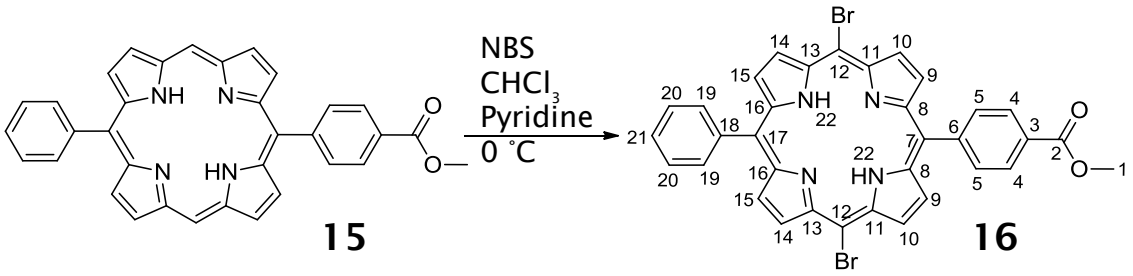

5-(*p*-methyl benzoate)-15-phenyl porphyrin (**15**) (100 mg, 0.192 mmol, 1 equiv.) was dissolved in chloroform (25 mL) and cooled to 0 °C on ice. To this was added pyridine (170 µL, 2.11 mmol, 11 equiv.) followed by N-bromosuccinimide (71.7 mg, 0.403 mmol, 2.1 equiv.). The reaction mixture was left on ice for 30 minutes.

At completion, acetone (4.5 mL) was added. The solvent was removed *in vacuo*, before co-evaporating with methanol (3 × 10 mL).

Purification was carried out by column chromatography (silica, eluent – DCM : hexane (1:1)) producing 111.7 mg (0.165 mmol, 86 %) of purple solid product **16**.

R_f (silica, DCM : hexane (2:1)) = 0.58

ESI+ ($C_{34}H_{22}N_4O_2Br_2$): Monoisotopic mass = 678.37 , observed m/z = 678.8 $[M + H]^+$

^{1}H NMR (CHLOROFORM-d ,300MHz): δ = 9.47 (d, *J*=4.9 Hz, 4 H, **H-10 and H-14**), 8.71 (d, *J*=4.9 Hz, 2 H, **H-15**), 8.62 (d, *J*=4.5 Hz, 2 H, **H-9**), 8.34 (d, *J*=8.3 Hz, 2 H, **H-4**), 8.09 (d, *J*=8.3 Hz, 2 H, **H-5**), 7.98 - 8.06 (m, 2 H, **H-19**), 7.60 - 7.76 (m, 3 H, **H-20 and H-21**), 4.04 (s, 3 H, **H-1**), -2.92 ppm (br. s., 2 H, **H-22**)

^{13}C NMR (CHLOROFORM-d,101MHz): δ = 167.2 (C, **C-2**), 146.1 (C, **C-3**), 141.3 (C), 134.5 (CH, **C-5** and **C-19**), 132.5 (br., CH, **C-9**, **C-10**, **C-14** and **C-15**), 129.9 (C), 128.1(CH, **C-21**), 128.0 (CH, **C-4**), 126.8 (CH, **C-20**), 121.8 (C, **C-18**), 119.7 (C, **C-6**), 103.9 (C, **C-12**), 52.5 ppm (CH_3, **C-1**)

UV-Vis (DCM, 6.6 μM) λ (log ε) = 420 nm (5.01), 520 nm (3.81), 555 nm (3.64), 600 nm (3.33), 658 nm (3.29)

Emission (DCM, 6.6 μM, λ_{ex} = 420 nm) λ_{em} (relative intensity) = No emission observed

9.17 Synthesis of Zn(II)-5-(P-methylbenzoate)-15-phenyl-10,20 dibromo porphyrin

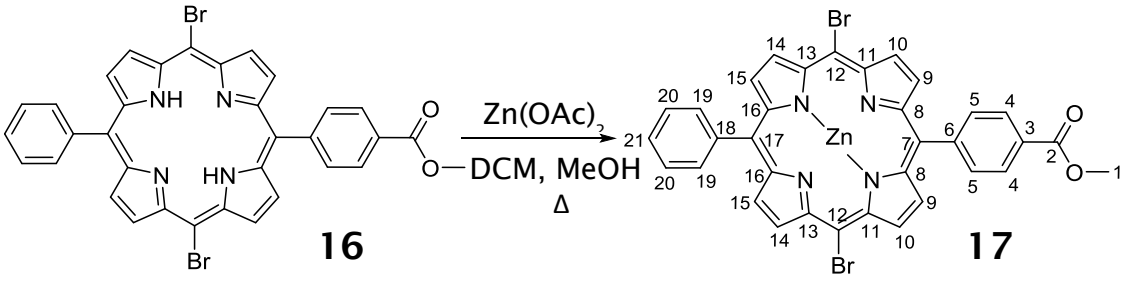

5-(*P*-methylbenzoate)-15-phenyl-10, 20 dibromo porphyrin (**16**) (430 mg, 0.636 mmol, 1 equiv.) and zinc acetate dehydrate (large excess) were dissolved in DCM:MeOH (20 mL : 4 mL). The reaction mixture was heated gently with a heat gun whilst swirling for 5 minutes. The solvent was removed *in vacuo* and the product re-dissolved in ethyl acetate (20 mL). This was thoroughly washed with water (5 × 30 mL) to remove the excess zinc acetate. The solvent and residual water were removed *in vacuo*.

This produced 474.4 mg (> 100 %) of crude purple, solid product **17**. The product was carried through to the next reaction without further purification.

R_f (silica, DCM) = 0.65

ESI+ ($C_{34}H_{20}N_4O_2Br_2Zn$): Monoisotopic mass = 741.74 , observed m/z = 742.6 $[M + H]^+$

^{1}H NMR (CHLOROFORM-d ,300MHz): δ = 9.58 (m, 4 H, **H-10 and H-14**), 8.79 (d, *J*=4.5 Hz, 2 H, **H-15**), 8.72 (d, *J*=4.5 Hz, 2 H, **H-9**), 8.35 (d, *J*=7.9 Hz, 2 H, **H-4**), 8.17 (d, *J*=7.9 Hz, 2 H, **H-5**), 8.08 (d, *J*=6.4 Hz, 2 H, **H-19**), 7.61 - 7.74 (m, 3 H, **H-20 and H-21**), 4.05 ppm (s, 3 H, **H-1**)

^{13}C NMR (CHLOROFORM-d, 101MHz): δ = 167.4 (C, **C-2**), 150.8 (C, **C-3**), 150.2 (C), 150.1 (C), 150.1 (C), 134.5 (CH, **C-5** and **C-19**), 133.5 (CH, **C-10** or **C-14**), 133.3 (CH, **C-10** or **C-14**), 133.0 (CH, **C-15**), 132.8 (CH, **C-9**), 127.7 (CH, **C-4**), 127.6 (CH, **C-21**), 126.5 (CH, **C-15**), 122.3 (C, **C-18**), 120.3 (C, **C-6**), 105.0 (C, **C-12**), 52.4 ppm (CH_3, **C-1**)

UV-Vis (DCM, 3.4 μM) λ (log ε) = 423 nm (5.29), 556 nm (3.95), 596 nm (3.47)

Emission (DCM, 3.4 μM, λ_{ex} = 423 nm) λ_{em} (relative intensity) = No emission observed

9.18 Synthesis of Zn(II)-5-(P-methylbenzoate)-15-phenyl-10,20 di-(trimethylsilyl) acetylene porphyrin

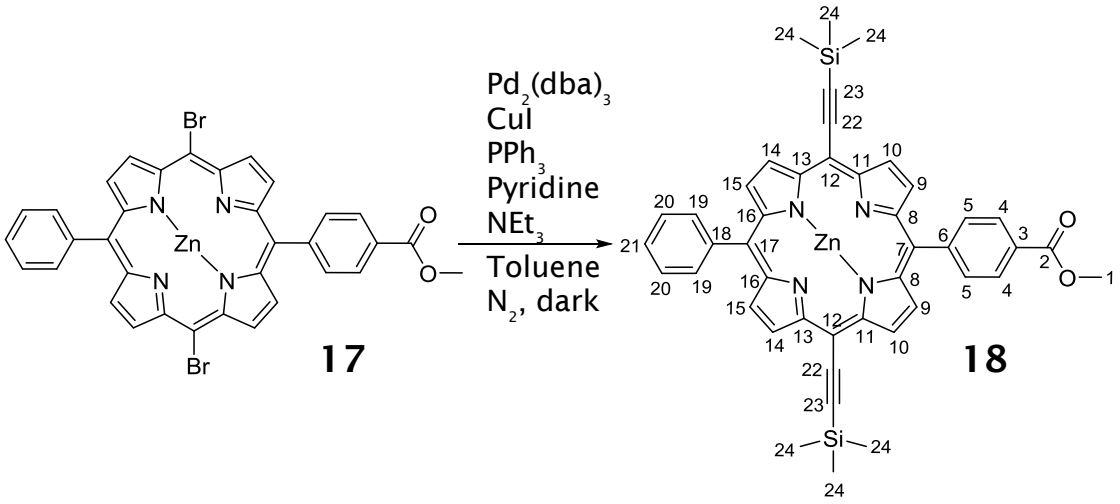

Toluene (30mL) was degassed for 30 mins with nitrogen. To this was added Zn(II)-5-(*P*-methylbenzoate)-15-phenyl-10,20 dibromo porphyrin (**17**) (100 mg, 0.135 mmol, 1 equiv.), $Pd_2(dba)_3$ (8.65 mg, 9.45 µmol, 0.07 equiv.), CuI (6.48 mg, 0.034 mmol, 0.25 equiv.), PPh_3 (17.8 mg, 0.068 mmol, 0.5 equiv.), pyridine (1.90 mL) and NEt_3 (2.75 mL). The solution was bubbled with N_2 for 10 mins before the addition of trimethylsilylacetylene (85 µL, 0.608 mmol, 4.5 equiv.). The reaction was heated to 45 ˚C and kept under nitrogen for 15 hours.

At completion the reaction mixture was separated with EtOAc and water (3 × 50 mL) and dried with sodium sulfate. Co-evaporation with toluene (3 × 20 mL) was used to remove pyridine followed by chloroform (3 × 20 mL) to remove the toluene. The solvent was removed *in vacuo* before purification by column chromatography (silica, eluent – 10 % ethyl acetate in petroleum ether 40 – 60 ˚C). This gave 99.3 mg (0.128 mmol, 95 %) of blue / green solid **18.**

$\mathbf{R}_f$ (silica, 10 % EA in Pet.) = 0.73

^{1}**H NMR** (CHLOROFORM-d ,300MHz): δ = 9.62 (d, *J*=1.9 Hz, 2 H, **H-10/H-14**), 9.60 (d, *J*=1.9 Hz, 2 H, **H-10/H-14**), 8.83 (d, *J*=4.5 Hz, 2 H, **H-15**), 8.75 (d, *J*=4.5 Hz, 2 H, **H-9**), 8.32 (d, *J*=8.3 Hz, 2 H, **H-4**), 8.17 (d, *J*=8.3 Hz, 2 H, **H-5**),

8.06 - 8.11 (m, 2 H, **H-19**), 7.66 - 7.74 (m, 3 H, **H-20 and H-21**), 4.00 (s, 3 H, **H-1**), 0.53 ppm (s, 18 H, **H-24**)

^{13}**C NMR** (CHLOROFORM-d ,101MHz): δ = 167.3 (C, **C-2**), 151.9 (C, **C-11** or **C-13**), 151.8 (C, **C-11** or **C-13**), 149.9 (C, **C-16**), 149.1 (C, **C-8**), 147.2 (C, **C-3**), 134.4 (CH, **C-5**), 134.1 (CH, **C-19**), 132.2 (CH, **C-15**), 131.6 (CH, **C-9**), 130.9 (CH, **C-10** or **C-14**), 130.7 (CH, **C-10** or **C-14**), 127.3 (CH, **C-4**), 127.1 (CH, **C-21**), 126.1 (CH, **C-20**), 121.6 (C, **C-18**), 120.4 (C, **C-6**), 100.9 (C, **C-22**), 100.6 (C, **C-23**), 52.0 (CH_3, **C-1**), 0.0 ppm (CH_3, **C-24**)

UV-Vis (DCM, 3.2 µM) λ (log ε) = 434 nm (4.97), 575 nm (4.11), 618 nm (4.32)

Emission (DCM, 3.2 µM, λ_{ex} = 434 nm) λ_{em} (relative intensity) = 625 nm (1), 680 nm (0.18)

9.19 Synthesis of Zn(II)-5-(P-methylbenzoate)-15-phenyl-10,20 di-acetylene porphyrin

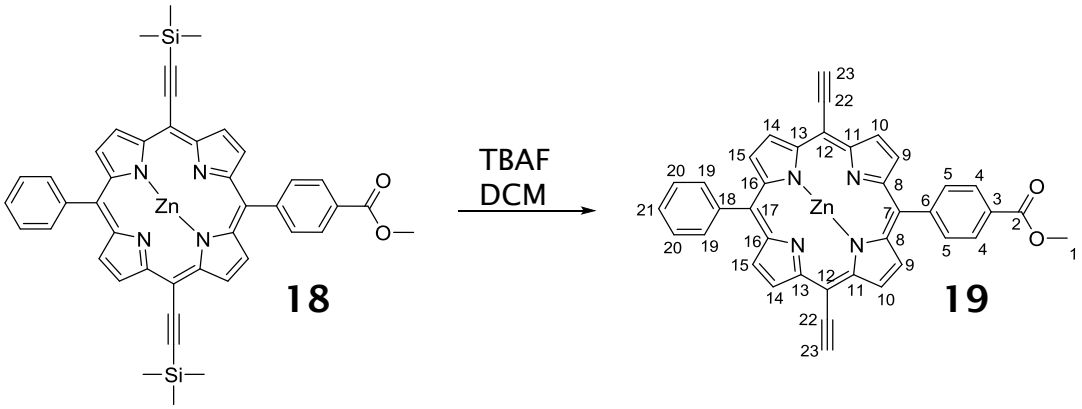

18 **19**

Zn(II)-5-(*P*-methylbenzoate)-15-phenyl-10, 20 di-trimethylsilylacetylene porphyrin (**18**) (100 mg, 0.129 mmol, 1 equiv.) was dissolved in anhydrous DCM (15 mL). To this was added TBAF (1 M in THF) (205 µL, 0.710 mmol, 5.5 equiv.) and the reaction stirred at room temperature for 1 hour.

At completion acetic acid (1 pipette full) was added. The reaction mixture was separated between water and DCM (x5) to ensure full removal of the TBAF. The organic phase was dried (Na_2SO_4), filtered and and the solvent removed *in vacuo*. This gave 85.1 mg (0.135 mmol, > 100 %) of blue / green solid crude product **19**. No further purification was carried out and the crude product was used straight in the next step.

R_f (silica, DCM) = 0.54

ESI+ ($C_{38}H_{22}N_4O_2Zn$): Monoisotopic mass = 630.10, observed m/z = 631.1 $[M + H]^+$

^{1}H NMR (Pyr ,300MHz): δ = 10.07 (d, *J*=4.8 Hz, 2 H, **H-10** or **H-14**), 10.04 (d, *J*=4.8 Hz, 2 H, **H-10** or **H-14**), 9.11 (d, *J*=4.8 Hz, 2 H, **H-9** or **H-15**), 9.07 (d, *J*=4.4 Hz, 2 H, **H-9** or **H-15**), 8.54 (d, *J*=8.1 Hz, 2 H, **H-4**), 8.36 (d, *J*=8.0 Hz, 2 H, **H-5**), 8.27 - 8.33 (m, 2 H, **H-19**), 7.77 - 7.87 (m, 3 H, **H-20** and **H-21**), 5.21 (s, 2 H, **H-23**), 4.09 ppm (s, 3 H, **H-1**)

UV-Vis (DCM, 7.9 µM) λ (log ε) = 430 nm (4.56), 575 nm (3.18), 620 nm (3.22)

Emission (DCM, 7.9 μM, λ_{ex} = 430 nm) λ_{em} (relative intensity) = 625 nm (1), 672 nm (0.25)

9.20 Synthesis of Zn(II)-5-(P-benzoic acid)-15-phenyl-10,20 di-acetylene porphyrin

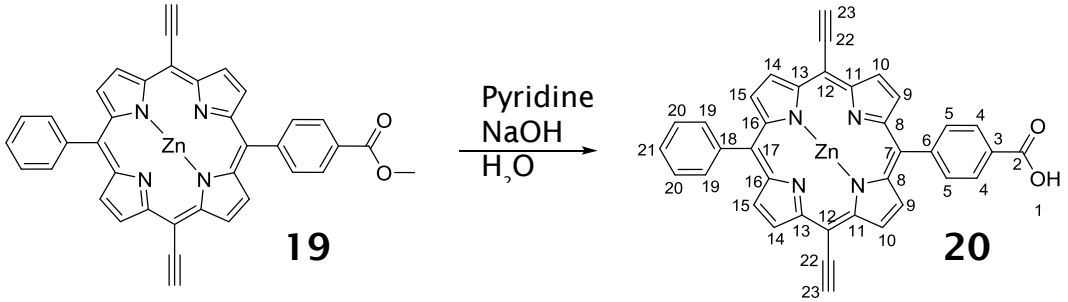

Zn(II)-5-(*P*-benzoic acid)-15-phenyl-10,20 di-acetylene porphyrin (**19**) (67.0 mg, 0.106 mmol, 1equiv.) was dissolved in pyridine (10 mL). NaOH (25.0 mg, 0.600 mmol, 6 equiv.) was dissolved in water (4 mL). The aqueous NaOH was added to the reaction mixture and the reaction stirred at room temperature for 24 hours.

At completion, the reaction mixture was added to DCM (20 mL) and separated with water (20 mL × 3) using 0.5 M HCl to neutralise, then dried (Na_2SO_4), filtered and solvent removed *in vacuo*. Co-evaporation with toluene (20 mL × 3) followed by chloroform (20 mL × 3) removed the excess pyridine with the solvents removed *in vacuo*. 52.9 mg (0.086 mmol, 81 %) of green solid product **20** was produced.

R_f (silica, 10 % MeOH in DCM) = 0.65

ESI+ ($C_{37}H_{20}N_4O_2Zn$): Monoisotopic mass = 616.09, observed m/z = 617.09 $[M + H]^+$

^{1}H NMR (DMSO-d_6 ,400MHz): δ = 9.67 (d, *J*=3.0 Hz, 2 H, **H-10** or **H-14**), 9.66 (d, *J*=3.0 Hz, 2 H, **H-10** or **H-14**), 8.85 (d, *J*=2.0 Hz, 2 H, **H-9** or **H-15**), 8.84 (d, *J*=2.0 Hz, 2 H, **H-9** or **H-15**), 8.45 (d, *J*=8.1 Hz, 2 H, **H-4**), 8.35 (d, *J*=8.1 Hz, 2 H, **H-5**), 8.20 - 8.24 (m, 2 H, **H-19**), 7.86 - 7.91 (m, 3 H, **H-20** and **H-21**), 5.32 ppm (s, 2 H, **H-23**)

UV-Vis (DCM, 16.2 μM) λ (log ε) = 429 nm (4.07), 570 nm (2.92), 610 nm (2.89)

Emission (DCM, 16.2 μM, λ_{ex} = 429 nm) λ_{em} (relative intensity) = 617 nm (1), 672 nm (0.36)

9.21 Synthesis of 5-p-(benzoic acid NHS-ester)-10, 15, 20-triphenyl porphyrin

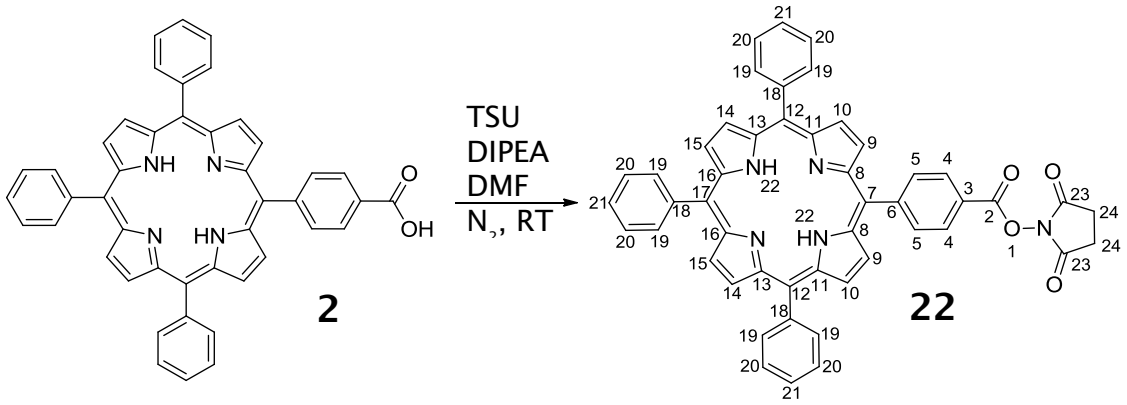

5-*p*-(benzoic acid)-10, 15, 20-triphenyl porphyrin (**2**) (30 mg, 0.046 mmol, 1 equiv.) was dissolved in DMF (3 mL). To this was added DIPEA (8 µL, 0.046 mmol, 1 equiv.) and TSU (27.7 mg, 0.092 mmol, 2 equiv.). The reaction was stirred under nitrogen at room temperature for 2 hours.

The reaction mixture was diluted with DCM (10 mL) and separated with water (3 × 15 mL). The organic layer was collected, dried (Na_2SO_4) and the solvent removed *in vacuo*. The crude product was purified by column chromatography (Silica, eluent – DCM) producing 26.9 mg (0.036 mmol, 78 %) of solid purple product.

$\mathbf{R}_f$ (silica, DCM) = 0.52

LR-ESI (+ve) ($C_{49}H_{33}N_5O_4$): Monoisotopic mass = 755.2, observed m/z = 756.2 $[M + H]^+$

^{1}**H NMR** (CHLOROFORM-d ,300MHz): δ = 8.93 (d, *J*=4.9 Hz, 2 H, **H-15**), 8.89 (br. s, 4 H, **H-10** and **H-14**), 8.80 (d, *J*=4.9 Hz, 2 H, **H-9**), 8.57 (d, *J*=8.3 Hz, 2 H, **H-4**), 8.41 (d, *J*=8.3 Hz, 2 H, **H-5**), 8.21 - 8.28 (m, 6 H, **H-19**), 7.73 - 7.85 (m, 9 H, **H-20** and **H-21**), 3.01 (br. s., 4 H, **H-24**), -2.74 ppm (br. s, 2 H, **H-22**)

^{13}**C NMR** (CHLOROFORM-d ,101MHz): δ = 169.4 (C, **C-23**), 162.1 (C, **C-2**), 149.4 (C, **C-3**), 134.9 (CH, **C-5**), 134.6 (CH, **C-19**), 131.3 (CH, **C-10**, **C-14** and **C-15**), 129.0 (CH, **C-9**), 127.9 (CH, **C-4**), 126.8 (CH, **C-20**), 126.7 (CH, **C-21**), 120.6 (C, **C-18**), 117.6 (C, **C-6**), 25.8 ppm (CH_2, **C-24**)

UV-Vis (DCM, 1.65 μM) λ (log ε) = 418 nm (5.78), 515 nm (4.38), 550 nm (3.99), 591 nm (3.78), 646 nm (3.63)

Emission (DCM, 1.65 μM, λ_{ex} = 418 nm) λ_{em} (relative intensity) = 651 nm (1), 717 nm (0.34)

9.22 Synthesis of Zn (II)-5-(P-benzoic acid)-15-phenyl-10, 20-dibromo porphyrin

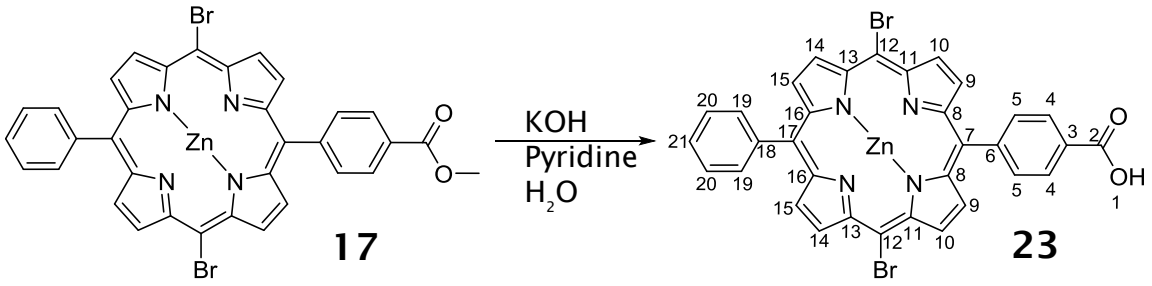

Zn(II)-5-(*P*-methylbenzoate)-15-phenyl-10,20 dibromo porphyrin (**17**) (100 mg, 0.134 mmol, 1 equiv.) was dissolved in pyridine (3 mL). KOH (380 mg, 6.70 mmol, 50 equiv.) was dissolved in de-ionised water (1 mL) and added to the porphyrin solution. The reaction mixture was heated to 40 °C for 15 hours.

Upon completion the reaction mixture was diluted with ethyl acetate (10 mL). This was washed with sat. KCl (5 × 20 mL). The organic phase was collected and the solvent removed *in vacuo*.

Purification was carried out by re-crystallisation with hot chloroform and ice cold hexane resulting in 68.3 mg (0.094 mmol, 70 %) of green / blue solid product.

$\mathbf{R}_f$ (silica, 2 % MeOH inDCM) = 0.10

LR-ESI (+ve) ($C_{33}H_{18}Br_2N_4O_2Zn$): Monoisotopic mass = 723.91, observed m/z = 724.8 $[M + H]^+$

^{1}**H NMR** (Pyr ,300MHz): δ = 9.92 (d, *J*=4.5 Hz, 2 H, **H-10** or **H-15**), 9.89 (d, *J*=4.9 Hz, 2 H, **H-10** or **H-15**), 9.06 (d, *J*=4.5 Hz, 4 H, **H-9** and **H-15**), 8.87 (d, *J*=7.2 Hz, 2 H, **H-4**), 8.41 (d, *J*=8.3 Hz, 2 H, **H-5**), 8.30 (d, *J*=6.4 Hz, 2 H, **H-19**), 7.75 - 7.87 ppm (m, 3 H **H-20** or **H-21**)

^{13}**C NMR** (Pyr ,101MHz): δ = 151.6 (CH, **C-4**), 136.3 (CH, **C-19**), 136.1 (CH, **C-5**), 135.2 (CH, **C-9** or **C-15**), 135.1 (CH, **C-9** or **C-15**), 134.9 (CH, **C-10** or **C-14**), 134.8 (CH, **C-10** or **C-14**), 129.3 (CH, **C-21**), 128.3 (CH, **C-20**), 124.1 (CH, **C-18**), 123.5 ppm (CH, **C-6**)

UV-Vis (MeOH, 2.75 μM) λ (log ε) = 426 nm (5.41), 563 nm (4.04), 604 nm (3.84)

Emission (MeOH, 2.75 μM, λ_{ex} = 426 nm) λ_{em} (relative intensity) = No emission observed

9.23 Synthesis of Zn (II)-5-(P-benzoic acid)-15-phenyl-10, 20-di-(trimethylsilyl) acetylene porphyrin

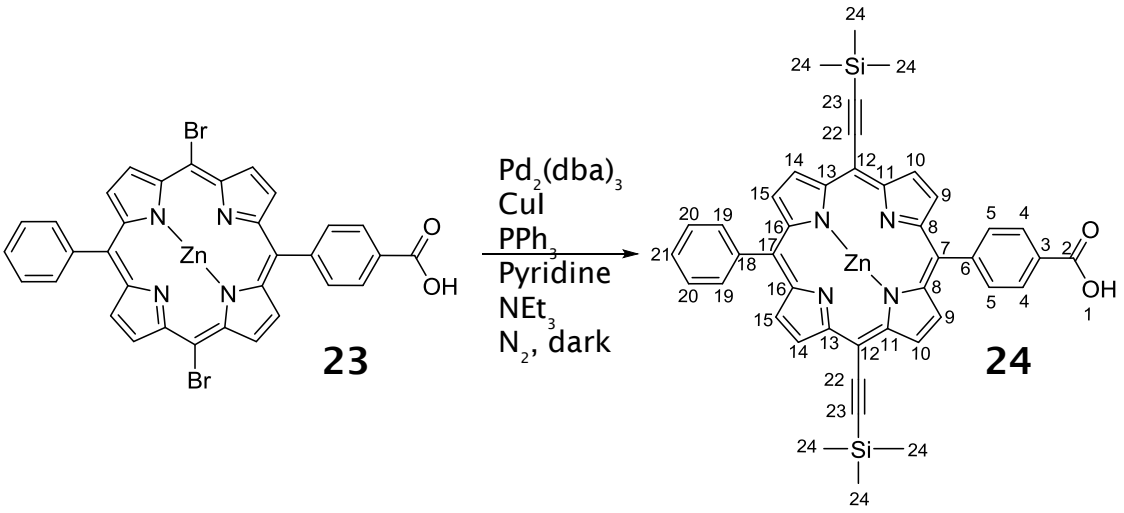

Zn (II)-5-(*P*-benzoic acid)-15-phenyl-10, 20-dibromo porphyrin (**23**) (120 mg, 0.165 mmol, 1 equiv.) was dissolved in dry toluene (10 mL) and triethylamine (3.5 mL, 24.8 mmol, 150 equiv.) with the addition of 3 Å molecular sieves. CuI(15.8 mg, 0.083 mmol, 0.5 equiv.), PPh_3 (21.8 mg, 0.083 mmol, 0.5 equiv.), $Pd_2(dba)_3$ (76.0 mg, 0.083 mmol, 0.5 equiv.) and pyridine (2.0 mL, 24.8 mmol, 150 equiv.) were added to the reaction mixture. This was flushed with argon for 10 mins before the addition of TMS acetylene (93.0 µL, 0.660 mmol, 4 equiv.). The reaction was heated to 45 ˚C and kept under argon and in the dark for 24 hours.

Upon completion the reaction mixture was diluted with ethyl acetate (20 mL) and washed with sat. KCl (5 × 30 mL). The organic layer was collected and the solvent removed *in vacuo* before co-evaporation with toluene and chloroform (3 times each). Purification was achieved by column chromatography (silica + 10 % silica H, eluent – 1 % MeOH in DCM →5 % MeOH in DCM). This gave 87.0 mg (0.114 mmol, 69 %) of solid green product.

R_f (silica, 2 % MeOH inDCM) = 0.11

LR-ESI (-ve) ($C_{43}H_{36}N_4O_2Si_2Zn$): Monoisotopic mass = 760.17, observed m/z = 759.2 $[M-H]^-$

^{1}H NMR (CHLOROFORM-d ,300MHz): δ = 9.55 (d, *J*=1.5 Hz, 2 H, **H-10** or **H-14**), 9.53 (d, *J*=1.5 Hz, 2 H, **H-10** or **H-14**), 8.72 - 8.81 (m, 4 H, **H-9** and **H-15**), 8.28 (br. s., 2 H, **H-4**), 8.09 (br. s., 2 H, **H-19**), 8.07 (br. s., 2 H, **H-5**) , 7.60 - 7.73 (m, 3 H), 0.51 ppm (s, 18 H, **H-24**)

^{13}C NMR (CHLOROFORM-d ,101MHz): δ = 151.8 (C, **C-8** or **C-16**), 151.7 (C, **C-8** or **C-16**), 149.7 (C, **C-11** or **C-13**), 149.7 (C, **C-11** or **C-13**), 134.2 (CH, **C-19**), 133.8 (CH, **C-5**), 132.1 (CH, **C-9** or **C-15**), 132.0 (CH, **C-9** or **C-15**), 130.6 (CH, **C-10** or **C-14**), 130.5 (CH, **C-10** or **C-14**), 128.6 (CH, **C-21**), 127.0 (CH, **C-20**), 126.0 (CH, **C-4**), 100.5 (C, **C**-22), 100.2 (C, **C**-23), 0.0 ppm (CH_3, **C**-24)

UV-Vis (DCM, 1.31 μM) λ (log ε) = 434 nm (5.64), 575 nm (4.37), 620 nm (4.57)

Emission (DCM, 1.31 μM, λ_{ex} = 434 nm) λ_{em} (relative intensity) = 626 nm (1), 682 nm (0.17)

9.24 Synthesis of Zn (II)-5- *p*-(*N*-(3-azidopropyl) benzamide)-15-phenyl-10, 20-di-(trimethylsilyl) acetylene porphyrin

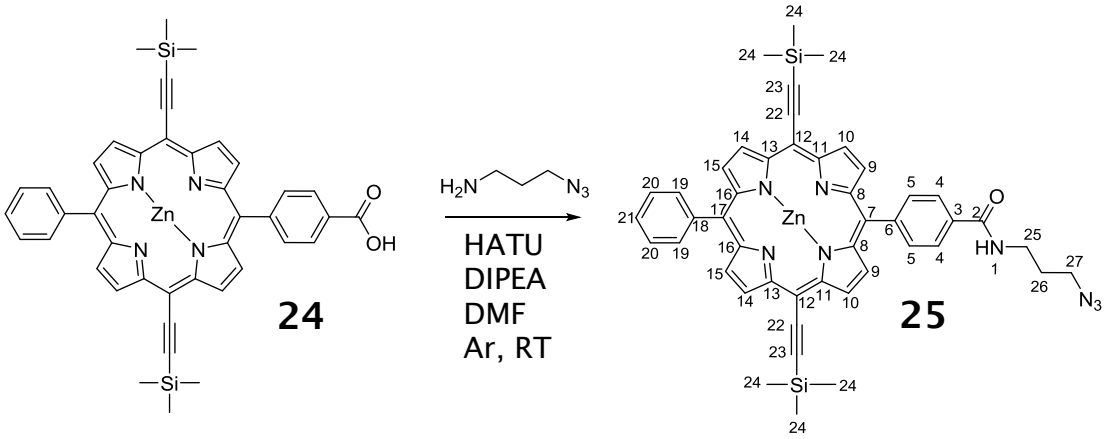

Zn (II)-5-(*P*-benzoic acid)-15-phenyl-10, 20-di-(trimethylsilyl) acetylene porphyrin (**24**) (8.5 mg, 0.011 mmol, 1 equiv.) was dissolved in anhydrous DMF (2 mL), and added to oven dried glassware containing 3 Å molecular sieves. This was purged with argon for 10 mins before the addition of HATU (8.4 mg, 0.022 mmol, 2 equiv.) and DIPEA (3.8 µL, 0.022 mmol, 2 equiv.). This was purged with argon for a further 10 mins. 1-amino-3-propylazide (2.2 mg, 0.022 mmol, 2 equiv.) was then added and the reaction kept under argon, at room temperature for 1 hour.

At completion, the reaction mixture was diluted with ethyl acetate (10 mL) and washed with sat. KCl (5 × 20 mL). The organic was collected and the solvent removed *in vacuo*. Purification was achieved by colimn chromatography (silica, eluent – 0.5 % MeOH in DCM) producing 4.7 mg (0.006 mmol, 55 %) of green solid product.

R$_f$ (silica, 2 % MeOH in DCM) = 0.37

CCMS (+ve) ($C_{46}H_{42}N_8OSi_2Zn$): Monoisotopic mass = 842.2, observed m/z = 843.1 $[M + H]^+$

^{1}**H NMR** (Pyr ,400MHz): δ = 10.08 (d, *J*=4.5 Hz, 2 H, **H-10** or **H-14**), 10.05 (d, *J*=4.6 Hz, 2 H, **H-10** or **H-14**), 9.54 (t, *J*=5.8 Hz, 1 H, **H-1**), 9.07 (d, *J*=4.4 Hz, 2 H, **H-9** or **H-15**), 9.03 (d, *J*=4.5 Hz, 2 H, **H-9** or **H-15**), 8.65 (d, *J*=7.7 Hz, 2 H, **H-4**), 8.34 (d, *J*=7.7 Hz, 2 H, **H-5**), 8.29 (d, *J*=6.6 Hz, 2 H, **H-19**), 7.74 - 7.86 (m, 3

H, **H-20** and **H-21**), 4.76 (m, 2 H, **H-27**), 4.00 (m, 2 H, **H-25**), 2.39 (tt, *J*=6.2 Hz, 2 H, **H-26**), 0.66 ppm (s, 18 H, **H-24**)

^{13}C NMR (Pyr ,101MHz): δ = 168.6 (C, **C-2**), 153.4 (C, **C-8** or **C-16**), 153.3 (C, **C-8** or **C-16**), 151.4 (C, **C-11** or **C-13**), 151.0 (C, **C-11** or **C-13**), 146.3 (C, **C-3**), 135.6 (CH, **C-19**), 135.5 (CH, **C-5**), 132.4 (CH, **C-9** or **C-15**), 132.2 (CH, **C-9** or **C-15**), 131.0 (CH, **C-10** and **C-14**), 128.6 (CH, **C-21**), 127.7 (CH, **C-20**), 126.9 (CH, **C-4**), 123.6 (C, **C-18**), 122.9 (C, **C-6**), 102.7 (C, **C-22**), 102.0 (C, **C-23**), 68.5 (CH_2, **C-27**), 37.4 (CH_2, **C-25**), 31.6 (CH_2, **C-26**), 0.9 ppm (CH_3, **C-24**)

UV-Vis (DCM, 1.18 µM) λ (log ε) = 434 nm (5.88), 574 nm (4.47), 619 nm (4.72)

Emission (DCM, 1.18 µM, λ_{ex} = 434 nm) λ_{em} (relative intensity) = 626 nm (1), 682 nm (0.17)

9.25 Synthesis of Zn (II)-5-p-(N-(3-Fmoc-aminopropyl)benzamide-15-phenyl-10, 20-di-(trimethylsilyl) acetylene porphyrin

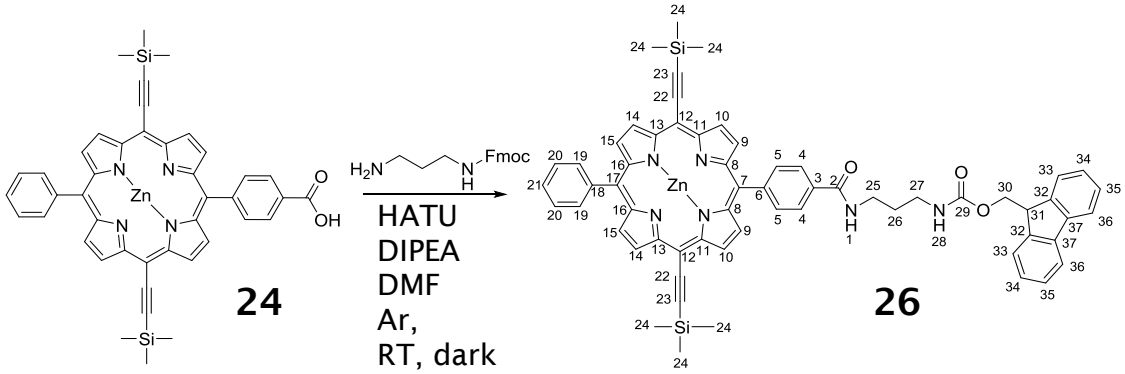

Zn (II)-5-(*P*-benzoic acid)-15-phenyl-10, 20-di-(trimethylsilyl) acetylene porphyrin (**24**) (30.0 mg, 0.039 mmol, 1 equiv.) was dissolved in DMF (2 mL) in oven dried glassware with the addition of 3 Å molecular sieves. The solution was purged with argon for 10 minutes before the addition of HATU (29.7 mg, 0.078 mmol, 2 equiv.) and DIPEA (13.6 µL, 0.078 mmol, 2 equiv.) in DMF (1 mL). This was purged with argon for a further 10 minutes before the addition of Fmoc-diaminopropane.HCl (26.0 mg, 0.078 mmol, 2 equiv.). The reaction was kept under argon, in the dark, for 2 hours.

The reaction mixture was diluted with ethyl acetate (10 mL) and extracted with sat. KCl (5 × 20 mL). The organic layer was taken and the solvent removed *in vacuo*. Purification was achieved by column chromatography (silica, eluent – 0.5 % MeOH in DCM) giving 24.0 mg (0.023 mmol, 59 %) of blue/green solid product.

R_f (silica, 2 % MeOH in DCM) = 0.16

CCMS (+ve) ($C_{61}H_{54}N_6O_3Si_2Zn$): Monoisotopic mass = 1038.3, observed m/z = 1039.1 [M + H^+]

^{1}H NMR (CHLOROFORM-d ,400MHz): δ = 9.65 (t, *J*=4.2 Hz, 4 H, **H-10** and **H-14**), 8.87 (d, *J*=4.6 Hz, 2 H, **H-9** or **H-15**), 8.74 (d, *J*=4.5 Hz, 2 H, **H-9** or **H-15**), 8.15 - 8.20 (m, 2 H, **H-19**), 8.10 (d, *J*=7.9 Hz, 2 H, **H-5**), 7.73 - 7.81 (m, 3 H, **H-20** and **H-21**), 7.70 (d, *J*=7.3 Hz, 2 H, **H-36**), 7.60 (d, *J*=7.9 Hz, 2 H, **H-4**), 7.51 (d,

J=7.3 Hz, 2 H, **H-33**), 7.31 - 7.38 (m, 4 H, **H-34** and **H-35**), 6.97 - 7.05 (m, 1 H, **H-1**), 5.14 - 5.21 (m, 1 H, **H-28**), 4.16 - 4.25 (m, 2 H, **H-30**), 4.03 - 4.13 (m, 1 H, **H-31**), 2.97 - 3.10 (m, 4 H, **H-25** and **H-27**), 1.39 - 1.49 (m, 2 H, **H-26**), 0.60 ppm (s, 18 H, **H-24**)

^{13}C NMR (CHLOROFORM-d ,101MHz): δ = 166.7 (C, **C-2**), 156.8 (C, **C-29**), 151.8 (C, **C-8** or **C-16**), 151.7 (C, **C-8** or **C-16**), 149.8 (C, **C11** or **C-13**), 149.2 (C, **C-11** or **C-13**), 144.5 (C, **C-3**), 143.3 (C), 142.1 (C, **C-37**), 140.8 (C, **C-32**), 134.1 (CH, **C-5** and **C-19**), 132.2 (CH, **C-9** or **C-15**), 131.7 (CH, **C-9** or **C-15**), 130.8 (CH, **C-10** or **C-14**), 130.7 (CH, **C-10** or **C-14**), 127.3 (CH, **C-35**), 127.1 (CH, **C-21**), 126.6 (CH, **C-34**), 126.2 (CH, **C-20**), 124.5 (CH, **C-33**), 124.5 (CH, **C-4**), 119.5 (CH, **C-36**), 101.0 (C, **C-22**), 100.5 (C, **C-23**), 66.1 (CH_2, **C-30**), 46.8 (C, **C-31**), 37.0 (CH_2, **C-27**), 35.4 (CH_2, **C-25**), 29.2 (CH_2, **C-26**), 0.0 ppm (CH_3, **C-24**)

UV-Vis (DCM, 0.96 μM) λ (log ε) = 434 nm (5.64), 572 nm (4.25), 619 nm (4.49)

Emission (DCM, 0.96 μM, λ_{ex} = 434 nm) λ_{em} (relative intensity) = 625 nm (1), 679 nm (0.17)

9.26 Synthesis of Zn (II)-5-p-(3-aminopropyl)benzamide-15-phenyl-10, 20-di-(trimethylsilyl) acetylene porphyrin

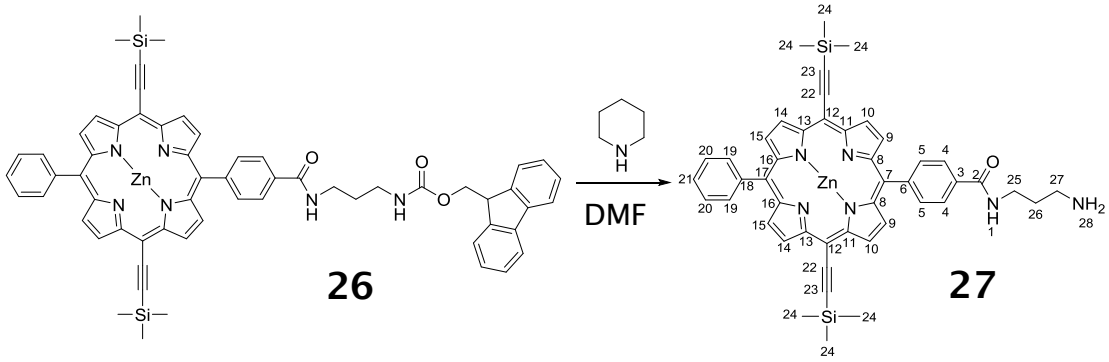

26 **27**

Zn (II)-5-*p*-(*N*-(3-Fmoc-aminopropyl)benzamide-15-phenyl-10, 20-di-(trimethylsilyl) acetylene porphyrin (**26**) (23 mg, 0.022 mmol) was dissolved in a solution of 20 % piperidine in DMF (2 mL). The solution was stirred at room temperature and in the dark for 1 hour.

Upon completion the reaction mixture was diluted with ethyl acetate (20 mL) and extracted with sat. KCl (5 × 20 mL). The organic layer was taken and the solvent removed *in vacuo*. Purification was achieved by column chromatography (silica, eluent – 2 % MeOH in DCM → 10 % MeOH in DCM) giving 11.5 mg (0.014 mmol, 64 %) of solid green product.

R_f (silica, 10 % MeOH in DCM) = 0.07

CCMS (+ve) ($C_{46}H_{44}N_6OSi_2Zn$): Monoisotopic mass = 816.2, observed m/z = 817.2 $[M + H]^+$

^{1}H NMR (Pyr ,400MHz): δ = 10.31 (br. s., 1 H, **H-1**), 10.05 (t, *J*=4.3 Hz, 4 H, **H-10** and **H-14**), 9.07 (d, *J*=4.5 Hz, 2 H, **H-9** or **H-15**), 9.02 (d, *J*=4.5 Hz, 2 H, **H-9** or **H-15**), 8.94 (d, *J*=7.8 Hz, 2 H, **H-4**), 8.35 (d, *J*=7.8 Hz, 2 H, **H-5**), 8.29 (d, *J*=6.6 Hz, 2 H, **H-19**), 7.73 - 7.87 (m, 3 H, **H-20** and **H-21**), 4.18 (m, 2 H, **H-25**), 3.64 - 3.72 (m, 2 H, **H-27**), 2.58 (br. s., 2 H, **H-26**), 0.65 ppm (s, 18 H, **H-24**)

^{13}C NMR (Pyr ,101MHz): δ = 168.5 (C, **C-2**), 153.4 (C, **C-11** or **C-13**), 153.3 (C, **C-11** or **C-13**), 151.4 (C, **C-8** or **C-16**), 151.0 (C, **C-8** or **C-16**), 135.6 (CH, **C-5** and **C-19**), 133.9 (CH, **C-9** or **C-15**), 133.6 (CH, **C-9** or **C-15**), 132.4 (CH, **C-10** or **C-14**), 132.2 (CH, **C-10** or **C-14**), 127.8 (CH, **C-21**), 127.7 (CH, **C-20**), 127.2

(CH, **C-4**), 102.8 (C, **C-22**), 102.0 (C, **C-23**), 38.0 (CH_2, **C-27**), 37.5 (CH_2, **C-25**), 28.9 (CH_2, **C-26**), 0.9 ppm (CH_2, **C**-24)

UV-Vis (DCM, 1.83 µM) λ (log ε) = 439 nm (5.36), 458 nm (5.17), 593 nm (4.00), 643 nm (4.38)

Emission (DCM, 1.83 µM, λ_{ex} = 439 nm) λ_{em} (relative intensity) = 646 (1), 695 nm (0.15)

9.27 Synthesis of 5-p-(N-(3-hydroxypropyl)benzamide)-10, 15, 20-triphenyl porphyrin

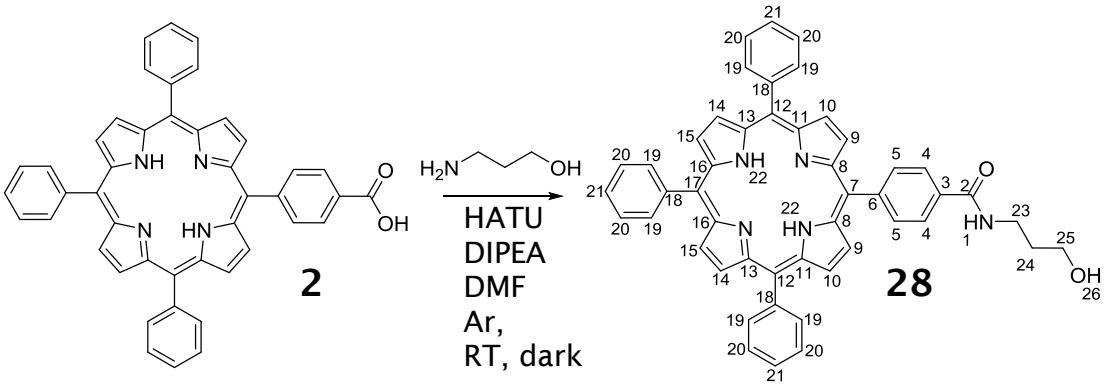

5-*p*-(benzoic acid)-10, 15, 20-triphenyl porphyrin (**2**) (100 mg, 0.152 mmol, 1 equiv.) was dissolved in DMF (10 mL) in oven dried glassware with 3 Å molecular sieves. The solution was purged with nitrogen for 15 min before the addition of HATU (116 mg, 0.304 mmol, 2 equiv.) and DIPEA (55 µL, 0.304 mmol, 2 equiv.). The solution was purged with nitrogen for a further 15 min before 3-aminopropan-1-ol (25 µL, 0.304 mmol, 2 equiv.) was added. The reaction was stirred under nitrogen, in the dark and at room temperature for 1 hour.

The reaction mixture was diluted with DCM (30 mL) and extracted with de-ionised water (5 × 30 mL). The organic phase was dried with Na_2SO_4 and filtered before the solvent was removed. The crude product was purified by column chromatography (silica, eluent – 2 % MeOH in DCM) to give 105.9 mg (0.148 mmol, 97 %) of purple solid product.

R_f (silica, 10 % MeOH in DCM) = 0.69

LR-ESI (+ve) ($C_{48}H_{37}N_5O_2$): Monoisotopic mass = 715.8, observed m/z = 716.6 $[M + H]^+$

^{1}H NMR (CHLOROFORM-d, 300MHz): δ = 8.84 - 8.92 (m, 6 H, **H-10**, **H-14** and **H-15**), 8.79 (d, *J*=4.9 Hz, 2 H, **H-9**), 8.19 - 8.30 (m, 8 H, **H-5** and **H-19**), 8.11 (d, *J*=8.3 Hz, 2 H, **H-4**), 7.69 - 7.84 (m, 9 H, **H-20** and **H-21**), 6.94 (t, *J*=5.8 Hz, 1 H, **H-1**), 3.85 (t, *J*=5.3 Hz, 2 H, **H-25**), 3.78 (q, *J*=6.0 Hz, 2 H, **H-23**), 1.91 ppm (quin, *J*=5.7 Hz, 2 H, **H-24**), -2.74 ppm (br. s, 2 H, **H-22**)

^{13}**C NMR** (CHLOROFORM-d, 101MHz): δ = 168.5 (C, **C-2**), 145.7 (C, **C-3**), 142.1 (C), 142.0 (C), 134.7 (CH, **C-5**), 134.5 (CH, **C-19**), 133.5 (C), 131.4 (br., CH, **C-9**, **C-10**, **C-14** and **C-15**), 127.8 (CH, **C-21**), 126.7 (CH, **C-20**), 125.3 (CH, **C-4**), 120.6 (C), 120.4 (C, **C-18**), 118.5 (C, **C-6**), 60.1 (CH_2, **C-25**), 37.5 (CH_2, **C-23**), 32.3 ppm (CH_2, **C-24**)

UV-Vis (DCM, 4.2 µM) λ (log ε) = 417 nm (5.22), 513 nm (3.81), 548 nm (3.42), 591 nm (3.26), 647 nm (3.08)

Emission (DCM, 4.2 µM, λ_{ex} = 417 nm) λ_{em} (relative intensity) = 650 nm (1), 716 nm (0.33)

9.28 Synthesis of 5-*p*-(*N*-(3-Bromopropyl)benzamide)-10, 15, 20-triphenyl porphyrin

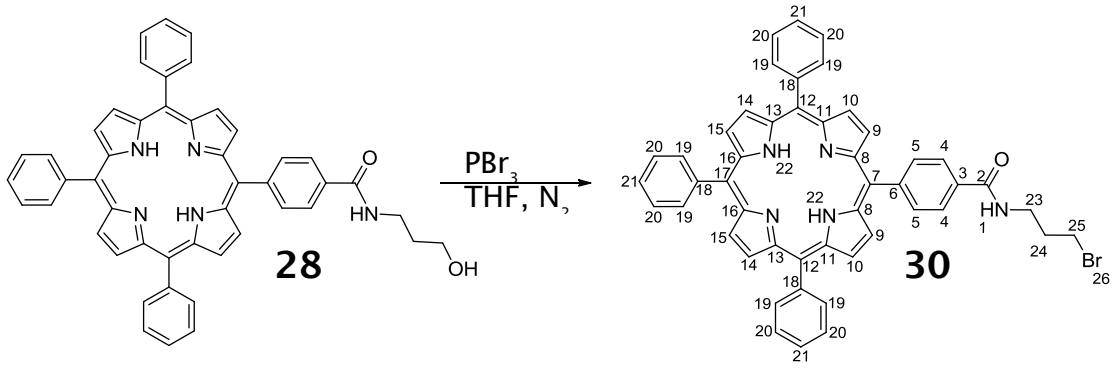

5-*p*-(*N*-(3-hydroxypropyl)benzamide)-10, 15, 20-triphenyl porphyrin (**28**) (50 mg, 0.070 mmol, 1 equiv.) was dissolved in THF (10 mL) in a flask with 3 Å molecular sieves. PBr_3 (7.25 µL, 0.077 mmol, 1.1 equiv.) was added to the solution and stirred under nitrogen in the dark for 3 hours. TLC analysis showed the reaction was incomplete so a further 5 µL (0.053 mmol, 0.75 equiv.) was added and the reaction left for a further 16 hours.

Whilst the reaction still had not reached completion it was decided to isolate the product that had been produced. The reaction mixture was diluted with ethyl acetate and washed with water (5 × 20 mL), dried (Na_2SO_4) and the solvent removed *in vacuo*. The pure product was isolated by column chromatography (silica, eluent – DCM) giving 16.1 mg (0.021 mmol, 30 %) of purple solid product.

R_f (silica, DCM) = 0.39

LR-ESI (+ve) ($C_{48}H_{36}N_5OBr$): Monoisotopic mass = 777.21, observed m/z = 778.2 $[M + H]^+$, 780.0 $[M + H + Br^{81}]^+$

^{1}H NMR (CHLOROFORM-d ,300MHz): δ = 8.85 - 8.92 (m, 6 H, **H-10**, **H-14** and **H-15**), 8.80 (d, *J*=4.5 Hz, 2 H, **H-9**), 8.31 (d, *J*=7.9 Hz, 2 H, **H-5**), 8.20 - 8.26 (m, 6 H, **H-19**), 8.15 (d, *J*=7.9 Hz, 2 H, **H-4**), 7.72 - 7.84 (m, 9 H, **H-20** and **H-21**), 6.66 (t, *J*=5.8 Hz, 1 H, **H-1**), 3.81 (q, *J*=6.4 Hz, 2 H, **H-23**), 3.64 (t, *J*=6.4 Hz, 2 H, **H-25**), 2.37 (tt, *J*=6.5 Hz, 2 H, **H-24**), -2.76 ppm (s, 2 H, **H-22**)

UV-Vis (DCM, 3.2 μM) λ (log ε) = 417 nm (5.33), 514 nm (3.93), 550 nm (3.57), 590 nm (3.45), 645 nm (3.40)

Emission (DCM, 3.2 μM, λ_{ex} = 417 nm) λ_{em} (relative intensity) = 650 nm (1), 716 nm (0.34)

9.29 Synthesis of 5-*p*-(*N*-(3-azidopropyl)benzamide)-10, 15, 20-triphenyl porphyrin

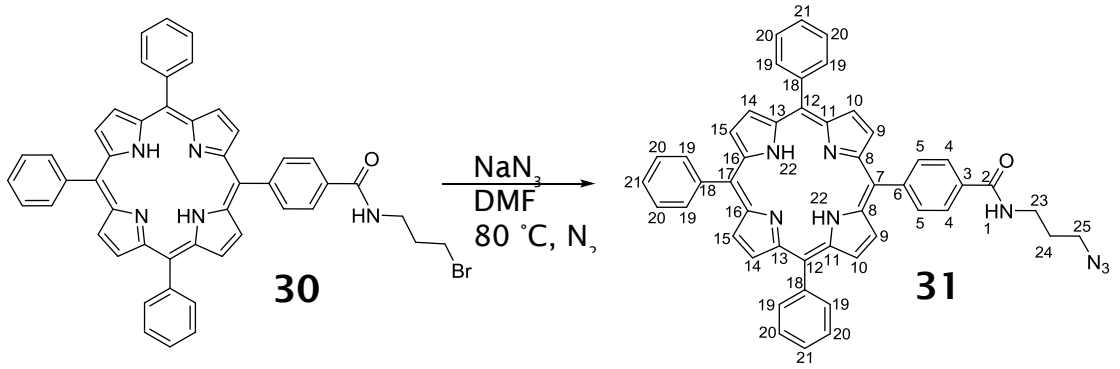

5-*p*-(*N*-(3-Bromoxypropyl)benzamide)-10, 15, 20-triphenyl porphyrin (**30**) (15 mg, 0.019 mmol, 1 equiv.) was dissolved in DMF (5 mL) in a flask with 3 Å molecular sieves. Sodium azide (2.5 mg, 0.038 mmol, 2 equiv.) was added and the reaction heated to 80 °C and stirred under nitrogen atmosphere for 3 hours.

At completion the reaction mixture was diluted with ethyl acetate (20 mL) and washed with de-ionised water (5 × 20 mL). The organic layer was dried (Na_2SO_4) and the solvent removed *in vacuo*. The crude was purified by column chromatography (silica, eluent –DCM). 10.3 mg (74 %) of purple solid product was collected.

R_f (silica, 5 % MeOH inDCM) = 0.81

LR-ESI (+ve) ($C_{48}H_{36}N_8O$): Monoisotopic mass = 740.30, observed m/z = 741.2 $[M + H]^+$

^{1}H NMR (CHLOROFORM-d, 400MHz): δ = 8.84 - 8.91 (m, 6 H, **H-10**, **H-14** and **H-15**), 8.80 (d, *J*=5.1 Hz, 2 H, **H-9**), 8.31 (d, *J*=8.1 Hz, 2 H, **H-5**), 8.20 - 8.26 (m, 6 H, **H-19**), 8.16 (d, *J*=8.1 Hz, 2 H, **H-4**), 7.73 - 7.84 (m, 9 H, **H-20** and **H-21**), 6.68 (t, *J*=5.8 Hz, 1 H, **H-1**), 3.75 (q, *J*=6.6 Hz, 2 H, **H-23**), 3.60 (t, *J*=6.6 Hz, 2 H, **H-25**), 2.08 (quin, *J*=6.6 Hz, 2 H, **H-24**), -2.75 ppm (br. s, 2 H, **H-22**)

^{13}C NMR (CHLOROFORM-d, 101MHz): δ = 166.2 (C, **C-2**), 144.2 (C, **C-3**), 140.5 (C), 133.2 (CH, **C-5**), 133.0 (CH, **C-19**), 132.2 (C), 129.5 (br., CH, **C-9**, **C-10**, **C-14** and **C-15**), 126.3 (CH, **C-21**), 125.2 (CH, **C-20**), 123.7 (CH, **C-4**), 119.1 (C),

118.9 (C, **C-18**), 117.0 (C, **C-6**), 48.2 (CH_2, **C-25**), 36.6 (CH_2, **C-23**), 27.4 ppm (CH_2, **C-24**)

UV-Vis (DCM, 8.1 µM) λ (log ε) = 417 nm (4.86), 514 nm (3.47), 550 nm (3.01), 592 nm (2.92), 645 nm (2.81)

Emission (DCM, 8.1 µM, λ_{ex} = 417 nm) λ_{em} (relative intensity) = 650 nm (1), 716 nm (0.35)

9.30 Synthesis of 5-*p*-(*N*-(3-Fmoc-aminopropyl)benzamide)-10, 15, 20-triphenyl porphyrin

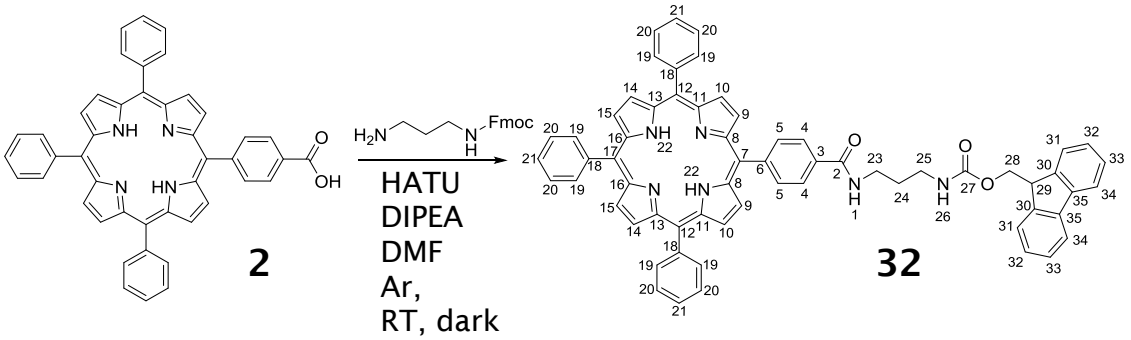

5-*p*-(benzoic acid)-10, 15, 20-triphenyl porphyrin (**2**) (30.0 mg, 0.045 mmol, 1 equiv.) was dissolved in DMF (2 mL) in oven dried glassware with the addition of 3 Å molecular sieves. The solution was purged with argon for 10 minutes before the addition of HATU (34.2 mg, 0.090 mmol, 2 equiv.) and DIPEA (15.7 µL, 0.090 mmol, 2 equiv.) in DMF (1 mL). This was purged with argon for a further 10 minutes before the addition of Fmoc-diaminopropane.HCl (30.3 mg, 0.090 mmol, 2 equiv.). The reaction was kept under argon, in the dark, for 2 hours.

The reaction mixture was diluted with ethyl acetate (10 mL) and extracted with sat. KCl (5 × 20 mL). The organic layer was taken and the solvent removed *in vacuo*. Purification was achieved by column chromatography (silica, eluent – 0.5 % MeOH in DCM) giving 40.3 mg (0.043 mmol, 93 %) of purple solid product.

R_f (silica, 2 % MeOH in DCM) = 0.18

RP-LCMS (+ve) ($C_{63}H_{48}N_6O_3$): Monoisotopic mass = 936.38, observed m/z = 937.20

^{1}H NMR (CHLOROFORM-d ,400MHz): δ = 8.88 (br. s., 6 H, **H-10**, **H-14**, and **H-15**), 8.83 (br. s., 2 H, **H-9**), 8.29 - 8.35 (m, 2 H, **H-4**), 8.20 - 8.28 (m, 8 H, **H-5** and **H-19**), 7.73 - 7.84 (m, 11 H, **H-20**, **H-21** and **H-34**), 7.65 (d, *J*=7.5 Hz, 2 H, **H-31**), 7.43 (br. s., 1 H, **H-1**), 7.40 (dd, *J*=7.4 Hz, 2 H, **H-33**), 7.32 (dd, *J*=7.4 Hz, 2 H, **H-32**), 5.33 (br. s., 1 H, **H-26**), 4.53 (d, *J*=6.7 Hz, 2 H, **H-28**), 4.24 -

4.27 (m, 1 H, **H-29**), 3.64 (d, *J*=5.5 Hz, 2 H, **H-23**), 3.46 (d, *J*=5.1 Hz, 2 H, **H-25**), 1.88 (br. s., 2 H, **H-24**), -2.74 ppm (br. s., 2 H, **H-22**)

^{13}**C NMR** (CHLOROFORM-d ,101MHz): δ = 167.7 (C, **C-2**), 157.5 (C, **C-27**), 145.5 (C, **C-3**), 143.9 (C), 142.1 (C), 142.1 (C, **C-35**), 141.4 (C, **C-30**), 134.7 (CH, **C-5**), 134.6 (CH, **C-19**), 133.8 (C), 131.2 (CH, **C-9**, **C-10**, **C-14** and **C-15**), 127.8 (CH, **C-32**), 127.7 (CH, **C33**), 127.1 (CH, **C-21**), 126.7 (CH, **C-20**), 125.4 (CH, **C-4**), 125.0 (CH, **C-31**), 120.4 (C), 120.0 (CH, **C-34**), 66.8 (CH_2, **C-28**), 47.4 (CH, **C-29**), 37.6 (CH_2, **C-25**), 36.2 (CH_2, **C-23**), 30.2 ppm (CH_2, **C-24**)

UV-Vis (DCM, 0.53 μM) λ (log ε) = 417 nm (6.21), 514 nm (4.85), 550 nm (4.50), 588 nm (4.35), 645 (4.22)

Emission (DCM, 0.53 μM, λ_{ex} = 417 nm) λ_{em} (relative intensity) = 650 nm (1), 715 nm (0.32)

9.31 Synthesis of 5-p-(N-(3-aminopropyl)benzamide)-10, 15, 20-triphenyl porphyrin

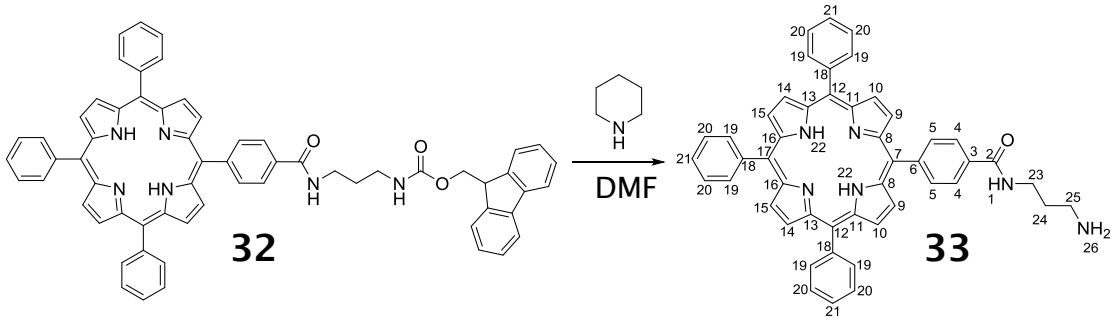

5-*p*-(*N*-(3-Fmoc-aminopropyl)benzamide)-10, 15, 20-triphenyl porphyrin (**32**) (40 mg, 0.043 mmol) was dissolved in a solution of 20 % piperidine in DMF (3 mL). The solution was stirred at room temperature and in the dark for 1 hour.

Upon completion the reaction mixture was diluted with ethyl acetate (20 mL) and extracted with sat. KCl (5 × 20 mL). The organic layer was taken and the solvent removed *in vacuo*. Purification was achieved by column chromatography (silica, eluent – 2 % MeOH in DCM → 10 % MeOH in DCM) giving 15.2 mg (0.021 mmol, 49 %) of solid purple product.

R_f (silica, 10 % MeOH in DCM) = 0.20

RP-LCMS (+ve) ($C_{48}H_{38}N_6O$): Monoisotopic mass = 714.31, observed m/z = 715.10

^{1}H NMR (Pyr ,400MHz): δ = 9.66 (t, *J*=5.3 Hz, 1 H, **H-1**), 9.08 - 9.12 (m, 2 H, **H-9**), 9.03 - 9.07 (m, 6 H, **H-10**, **H-14** and **H-15**), 8.70 (d, *J*=8.1 Hz, 2 H, **H-4**), 8.44 (d, *J*=7.9 Hz, 2 H, **H-5**), 8.35 - 8.41 (m, 6 H, **H-19**), 7.77 - 7.85 (m, 9 H, **H-20**, and **H-21**), 4.05 - 4.12 (m, 2 H, **H-26**), 3.99 - 4.04 (m, 2 H, **H-23**), 3.07 (br. s., 2 H, **H-25**), 2.01 - 2.06 (m, 2 H, **H-24**) , 2.01 - 2.06 (m, 2 H), -2.38 ppm (br. s., 2 H, **H-22**)

^{13}C NMR (Pyr ,101MHz): δ = 167.4 (C, **C-2**), 144.8 (C, **C-3**), 134.7 (CH, **C-19**), 131.6 (CH, **C-9**, **C-10**, **C-14** and **C-15**), 128.1 (CH, **C-21**), 127.1 (CH, **C-20**), 126.3 (CH, **C-4**), 120.7 (C), 40.3 (CH_2, **C-25**), 38.5 (CH_2, **C-23**), 33.0 ppm (CH_2, **C-22**)

UV-Vis (DCM, 2.80 μM) λ (log ε) = 417 nm (5.46), 515 nm (4.09), 549 nm (3.75), 589 nm (3.59), 644 nm (3.47)

Emission (DCM, 2.80 μM, λ_{ex} = 417 nm) λ_{em} (relative intensity) = 649 nm (1), 716 nm (0.34)

9.32 Synthesis of 5-*p*-(*N*-(3-azidopropyl)benzamide)-10, 15, 20-triphenyl porphyrin

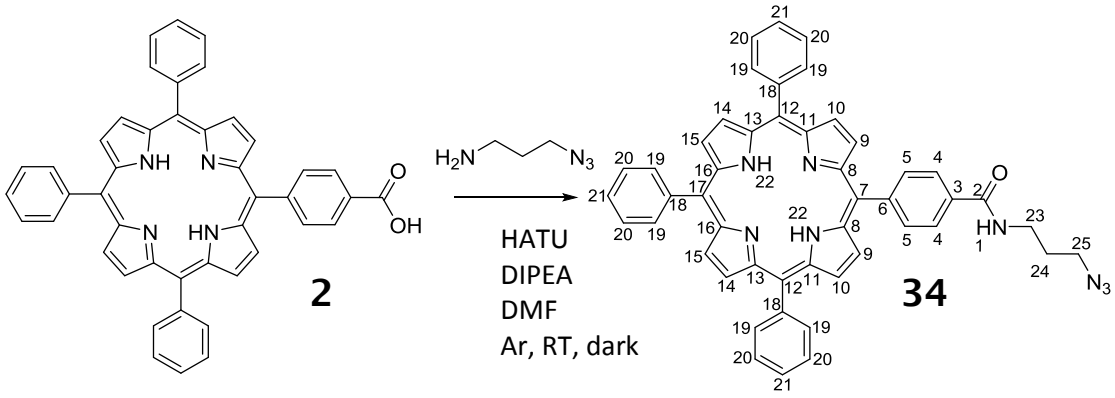

5-*p*-(benzoic acid)-10, 15, 20-triphenyl porphyrin (25.0 mg, 0.038 mmol, 1 equiv.) was dissolved in DMF (2 mL) in oven dried glassware with the addition of 3 Å molecular sieves. The solution was purged with argon for 10 minutes before the addition of HATU (28.9 mg, 0.076 mmol, 2 equiv.) and DIPEA (13.3 µL, 0.076 mmol, 2 equiv.) in DMF (1 mL). This was purged with argon for a further 10 minutes before the addition of 1-amino-3-propylazide (7.6 mg, 0.076 mmol, 2 equiv.) in DMF (1 ml). The reaction was kept under argon, in the dark, for 1 hour.

The reaction mixture was diluted with ethyl acetate (10 mL) and extracted with sat. KCl (5 × 20 mL). The organic layer was taken and the solvent removed *in vacuo*. Purification was achieved by column chromatography (silica, eluent – DCM) giving 26.9 mg (0.036 mmol, 95 %) of purple solid product.

R_f (silica, 5 % MeOH in DCM) = 0.81

RP-LC ESI (+ve) ($C_{48}H_{36}N_8O$): Monoisotopic mass = 740.30, observed m/z = 741.3

^{1}H NMR (CHLOROFORM-d ,400MHz): δ = 8.85 - 8.91 (m, 6 H, **H-10**, **H-14** and **H-15**), 8.80 (d, *J*=4.8 Hz, 2 H, **H-9**), 8.31 (d, *J*=8.2 Hz, 2 H, **H-5**), 8.20 - 8.25 (m, 6 H, **H-19**), 8.16 (d, *J*=8.2 Hz, 2 H, **H-4**), 7.73 - 7.83 (m, 9 H, **H-20** and **H-21**), 6.68 (t, *J*=5.7 Hz, 1 H, **H-1**), 3.75 (q, *J*=6.5 Hz, 2 H, **H-23**), 3.60 (t, *J*=6.5 Hz, 2 H, **H-25**), 2.08 (quin, *J*=6.6 Hz, 2 H, **H-24**), -2.76 ppm (br. s, 2 H, **H-22**)

^{13}**C NMR** (CHLOROFORM-d ,101MHz): δ = 167.8 (C, **C-2**), 145.7 (C, **C-3**), 142.1 (C), 134.7 (CH, **C-5**), 134.5 (CH, **C-19**), 133.7 (C), 127.8 (CH, **C-21**), 126.7 (CH, **C-20**), 125.3 (CH, **C-4**), 120.6 (C), 120.4 (C, **C-18**), 118.5 (C, **C-6**), 49.8 (CH_2, **C-25**), 38.1 (CH_2, **C-23**), 29.0 ppm (CH_2, **C-24**)

UV-Vis (DCM, 1.35 μM) λ (log ε) = 417 nm (5.68), 515 nm (4.27), 548 nm (3.95), 590 nm (3.77), 644 nm (3.65)

Emission (DCM, 1.35 μM, λ_{ex} = 417 nm) λ_{em} (relative intensity) = 651 nm (1), 716 nm (0.34)

9.33 Synthesis of 5'-DMT-5-trimethylsilylacetylene-deoxyuridine

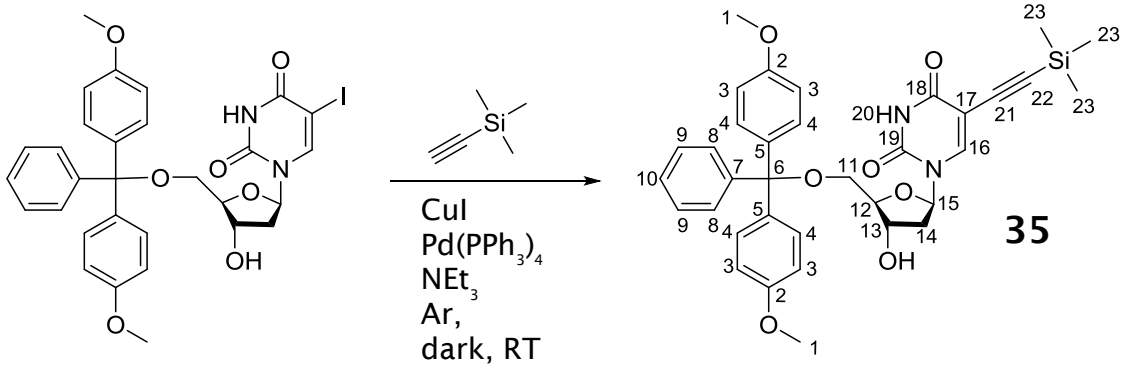

5'-DMT-5-Iodo-deoxyuridine (100 mg, 0.152 mmol, 1 eq.) was dissolved in anhydrous DMF (1 mL) in oven dried glassware containing 3 Å molecular sieves. This was purged with argon for 10 minutes before copper iodide (8.8 mg, 0.046 mmol, 0.3 eq.), trimethylsilylacetylene (43.0 µL, 0.304 mmol, 2 eq.) and triethylamine (52 µL, 0.380 mmol, 2.5 eq.) in DMF (1 mL) were added. After a further 5 minutes purging, tetrakis (triphenylphosphine) Palladium (0) (53.2 mg, 0.046 mmol, 0.3 eq.) and triethylamine (52 µL, 0.380 mmol, 2.5 eq.) in DMF (1 mL) were added. The reaction was stirred at room temperature, in the dark and under argon for 24 hours.

Upon completion the reaction mixture was diluted with ethyl acetate (20 mL) and washed with saturated KCl (5 X 20 mL). The aqueous layers were back extracted, the organic layers combined, and the solvent removed *in vacuo*.

The crude product was purified by column chromatography (silica + 10 % silica H (pre-treated with triethylamine), eluent – 50:50 ethyl acetate and hexane). Co-evaporation with Toluene (3 × 10 mL) and neutralised chloroform (3 × 10 mL) yielded 60.7 mg (0.097 mmol, 64 %) of an orange oily product.

R_f (silica, 2 % MeOH in DCM) = 0.16

LR-ESI (+ve) ($C_{35}H_{38}N_2O_7Si$): Monoisotopic mass = 626.24, observed m/z = 627.4

^{1}H NMR (CHLOROFORM-d ,400MHz): δ = 8.01 (s, 1 H, **H-16**), 7.44 (d, *J*=7.3 Hz, 2 H, **H-8**), 7.35 (dd, *J*=8.9, 1.5 Hz, 4 H, **H-4**), 7.29 - 7.32 (m, 2 H, **H-9**), 7.16 - 7.26 (m, 1 H, **H-10**), 6.86 (d, *J*=8.8 Hz, 4 H, **H-3**), 6.28 (dd, *J*=7.5, 5.5 Hz, 1 H,

H-15), 4.43 - 4.49 (m, 1 H, **H-13**), 4.06 - 4.11 (m, 1 H, **H-12**), 3.80 (s, 6 H, **H-1**), 3.42 (d, *J*=3.3 Hz, 1 H, **H-11**), 3.33 (d, *J*=3.7 Hz, 1 H, **H-11**), 2.44 - 2.54 (m, 1 H, **H-14**), 2.20 - 2.28 (m, 1 H, **H-14**), 0.02 ppm (s, 9 H, **H-23**)

^{13}**C NMR** (CHLOROFORM-d ,101MHz): δ = 161.5 (C, **C-19**), 159.0 (C, **C-2**), 149.4 (C, **C-18**), 143.0(CH, **C-16**), 130.4 (CH, **C-4**), 130.3 (CH, **C-4**), 128.4 (CH, **C-9**), 128.3 (CH, **C-8**), 127.3 (CH, **C-10**), 113.7 (CH, **C-3**), 100.9 (C, **C-22**), 95.1 (C, **C-21**), 87.4, 87.3 (C, **C-5** and **C-7**), 86.8 (CH, **C-12**), 86.1 (CH, **C-15**), 77.6 (C, **C-17**), 72.8 (CH, **C-13**), 63.8 (CH_2, **C-11**), 55.6 (CH_3, **C-1**), 41.7(CH_2, **C-14**), 0.0 ppm (CH_3, **C-23**)

9.34 Synthesis of 5'-DMT-5-phenylacetylene-deoxyuridine

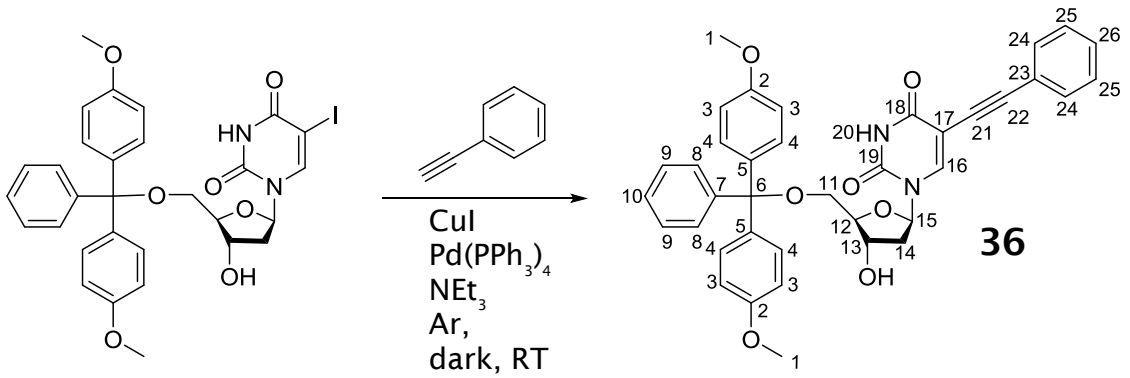

5'-DMT-5-Iodo-deoxyuridine (200 mg, 0.304 mmol, 1 eq.) was dissolved in anhydrous DMF (1 mL) in oven dried glassware containing 3 Å molecular sieves. This was purged with argon for 10 minutes before copper iodide (17.6 mg, 0.092 mmol, 0.3 eq.), phenylacetylene (66.8 µL, 0.608 mmol, 2 eq.) and triethylamine (105 µL, 0.760 mmol, 2.5 eq.) in DMF (1 mL) were added. After a further 5 minutes purging, tetrakis (triphenylphosphine) Palladium (0) (106.4 mg, 0.092 mmol, 0.3 eq.) and triethylamine (105 µL, 0.760 mmol, 2.5 eq.) in DMF (1 mL) were added. The reaction was stirred at room temperature, in the dark and under argon for 24 hours.

Upon completion the reaction mixture was diluted with ethyl acetate (20 mL) and washed with saturated KCl (5 X 20 mL). The aqueous layers were back extracted, the organic layers combined, and the solvent removed *in vacuo*.

The crude product was purified by column chromatography (silica + 10 % silica H (pre-treated with triethylamine), eluent – 1 % MeOH in DCM). Co-evaporation with Toluene (3 × 10 mL) and neutralised chloroform (3 × 10 mL) yielded 130.4 mg (0.207 mmol, 68 %) of an orange oily product.

R_f (silica, 2 % MeOH in DCM) = 0.14

LR-ESI (+ve) ($C_{38}H_{34}N_2O_7$): Monoisotopic mass = 630.24, observed m/z = 631.5

^{1}H NMR (CHLOROFORM-d ,400MHz): δ = 8.09 (s, 1 H, **H-20**), 8.07 (s, 1 H, **H-16**), 7.37 (d, *J*=7.5 Hz, 2 H, **H-8**), 7.27 (dd, *J*=8.7, 1.3 Hz, 4 H, **H-4**), 7.14 - 7.21 (m, 3 H, **H-9** and **H-10**), 7.05 - 7.12 (m, 3 H, **H-24** and **H-25**), 6.95 - 7.01 (m, 2 H, **H-23**), 6.70 (dd, *J*=8.7, 6.9 Hz, 4 H, **H-3**), 6.29 (dd, *J*=7.8, 5.8 Hz, 1 H, **H-**

15), 4.48 - 4.55 (m, 1 H, **H-13**), 4.07 - 4.13 (m, 1 H, **H-12**), 3.61 (s, 3 H, **H-1**), 3.59 (s, 3 H, **H-1**), 3.31 - 3.38 (m, 1 H, **H-11**), 3.23 - 3.30 (m, 1 H, **H-11**), 2.47 - 2.55 (m, 1 H, **H-14**), 2.19 - 2.25 ppm (m, 1 H, **H-14**)

^{13}**C NMR** (CHLOROFORM-d ,101MHz): δ = 161.4 (C, **C-19**), 158.6 (C, **C-2**), 158.6 (C, **C-2**), 149.3 (C, **C-19**), 142.2 (CH, **C-16**), 131.7 (CH, **C-24**), 130.0 (CH, **C-4**), 129.9 (C, **C-4**), 128.0 (CH, **C-9**), 128.0 (CH, **C-8**), 127.9 (CH, **C-25**), 127.0 (CH, **C-10**), 125.3 (CH, **C-26**), 113.3 (CH, **C-3**), 100.5 (C, **C-22**), 93.7 (C, **C-21**), 87.0 (C, **C-5** and **C-7**), 86.8 (CH, **C-12**), 85.9 (CH, **C-15**), 79.9 (C, **C-17**), 72.4 (CH, **C-13**), 63.7 (CH_2, **C-11**), 55.2 (CH_3, **C-1**), 41.7 ppm (CH_2, **C-14**)

UV-Vis (DCM, 20 µM) λ (log ε) = 233 nm (4.22), 264 nm (3.92), 277 nm (3.89), 309 nm (3.95)

9.35 Synthesis of 5'-DMT-5-propargylbenzamide-dU

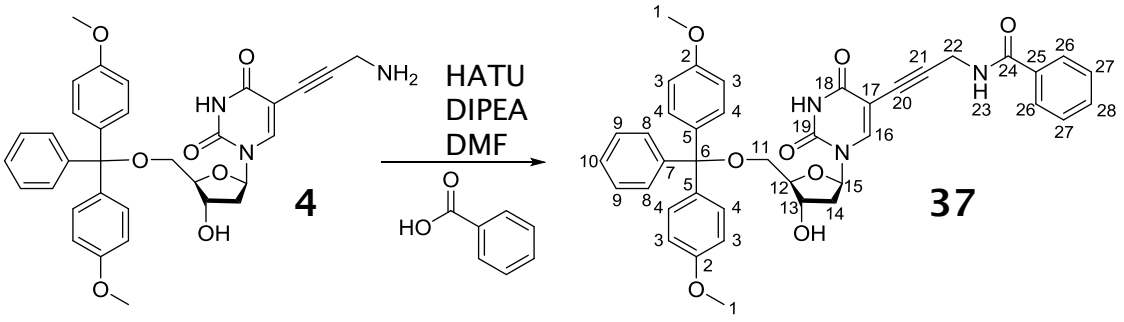

Benzoic acid (12.7 mg, 0.104 mmol, 1.2 equiv.) was dissolved in DMF (1 mL) in oven dried glassware with the addition of 3 Å molecular sieves. This was purged with argon for 10 minutes before HATU (39.5 mg, 0.104 mmol, 1.2 equiv.) and DIPEA (18.1 µL, 0. 104 mmol, 1.2 equiv.) in DMF (0.5 mL) was added and the solution purged for a further 10 minutes. Finally 5'-DMT-5-propargylamine-deoxyuridine (**4**) (50 mg, 0.087 mmol, 1 equiv.) in DMF (0.5 mL) was added and the reaction kept under argon for 1 hour.

At completion the reaction mixture was diluted with ethyl acetate (20 mL) and washed with saturated KCl solution (5 × 20 mL). The organic layer was collected and the solvent removed *in vacuo*. Purification was achieved by column chromatography (silica, eluent – 3 % MeOH in DCM) giving 46.8 mg (0.068 mmol, 78 %) of a golden solid.

R_f (silica, 5 % MeOH in DCM) = 0.50

LR-ESI (+ve) ($C_{38}H_{34}N_2O_7$): Monoisotopic mass = 687.26, observed m/z = 688.4

^{1}H NMR (CHLOROFORM-d ,400MHz): δ = 8.29 (s, 1 H, **H-16**), 8.18 (d, *J*=2.4 Hz, 2 H, **H-26**), 7.60 (d, *J*=7.5 Hz, 2 H, **H-27**), 7.40 (d, *J*=8.2 Hz, 2 H, **H-8**), 7.32 (d, *J*=7.8 Hz, 4 H, **H-4**), 7.16 (d, *J*=8.2 Hz, 3 H, **H-9** and **H-10**), 6.81 (d, *J*=7.7 Hz, 4 H, **H-3**), 6.51 - 6.64 (m, 1 H, **H-23**), 6.27 - 6.34 (m, 1 H, **H-15**), 4.56 (br. s., 1 H, **H-13**), 4.08 - 4.14 (m, 2 H, **H-22**), 4.07 (br. s, 1 H, **H-12**), 3.71 (s, 6 H, **H-1**), 3.38 - 3.47 (m, 2 H, **H-11**), 2.49 - 2.60 (m, 1 H, **H-14**), 2.21 - 2.31 ppm (m, 1 H, **H-14**)

^{13}C NMR (CHLOROFORM-d ,101MHz): δ = 158.6 (C, **C-2**), 144.6 (CH, **C-16**), 135.6 (C, **C-5**), 135.6 (C, **C-5**), 130.0 (CH, **C-4**), 129.1 (CH, **C-26**), 128.4 (CH, **C-**

27), 128.0 (CH, **C-8**), 127.9 (CH, **C-9**), 127.1 (CH, **C-10**), 113.4 (CH, **C-3**), 99.3 (C, **C-20**), 89.4 (C, **C-21**), 87.0 (C, **C-6**), 86.7 (C, **CH-12**), 85.9 (CH, **C-15**), 72.1 (CH, **C-13**), 63.7 (CH_2, **C-11**), 55.3 (CH_3, **C-1**), 41.7 (CH_2, **C-14**), 30.5 ppm (CH_2, **C-22**)

UV-Vis (DCM, 20 µM) λ (log ε) = 233 nm (4.26), 283 nm (3.79)

9.36 Synthesis of 5'-DMT-5-trimethylsilylacetylene-deoxyuridine -3' amidite

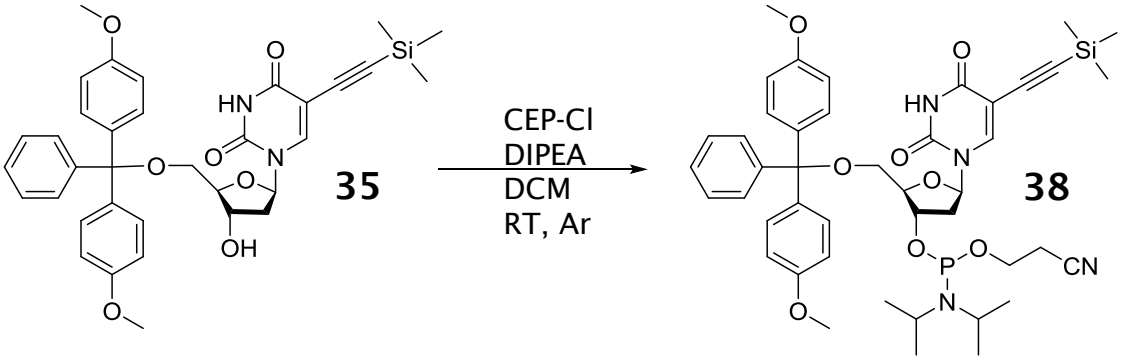

5'-DMT-5-trimethylsilylacetylene-deoxyuridine (**34**) (100mg, 0.160 mmol, 1 equiv.) was dissolved in anhydrous DCM (3 mL) in oven dried glassware with molecular sieves. This was purged with argon for 10 minutes. DIPEA (113 µL, 0.640 mmol, 4 equiv.) and CEP-Cl (152 µL, 0.480 mmol, 3 equiv.) were added and the reaction kept under argon at room temperature for 2 hours.

The reaction mixture was transferred to a new flask and the solvent reduced to approximately 1 mL using a flow of argon. Ice cold hexane (5 mL) was added and the flask placed on ice for 30 minutes to precipitate. The hexane was removed and the product dissolved in anhydrous MeCN (1.6 mL) to make up a solution of concentration 100 mM (assuming 100 % reaction yield). The solution was transferred to a DNA synthesiser vial and placed onto the synthesiser.

$\mathbf{R}_f$ (silica, 1 : 1 hexane : ethyl acetate) = 0.40

No further characterisation data was obtained due to the instability/air sensitivity of the product meaning it had to be used immediately for DNA synthesis.

9.37 Synthesis of 5'-DMT-5-phenylacetylene-deoxyuridine-3' amidite

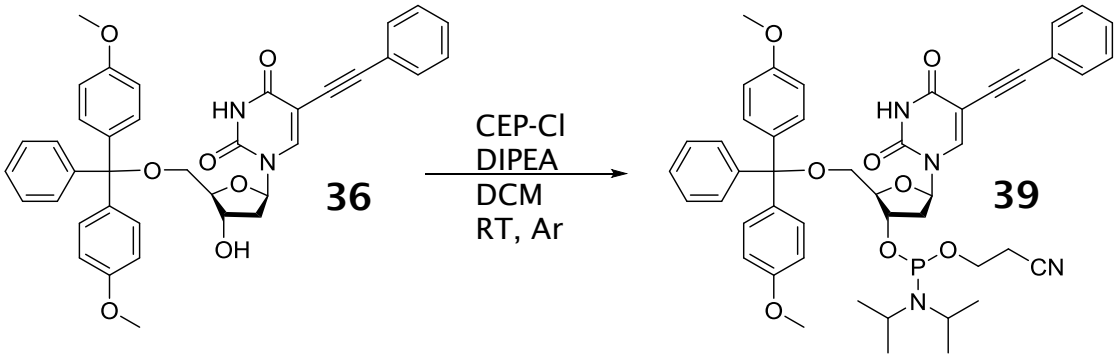

5'-DMT-5-phenylacetylene-deoxyuridine (**36**) (100mg, 0.159 mmol, 1 equiv.) was dissolved in anhydrous DCM (3 mL) in oven dried glassware with molecular sieves. This was purged with argon for 10 minutes. DIPEA (111 µL, 0.636 mmol, 4 equiv.) and CEP-Cl (151 µL, 0.477 mmol, 3 equiv.) were added and the reaction kept under argon at room temperature for 2 hours.

The reaction mixture was transferred to a new flask and the solvent reduced to approximately 1 mL using a flow of argon. Ice cold hexane (5 mL) was added and the flask placed on ice for 30 minutes to precipitate. The hexane was removed and the product dissolved in anhydrous MeCN (1.6 mL) to make up a solution of concentration 100 mM (assuming 100 % reaction yield). The solution was transferred to a DNA synthesiser vial and placed onto the synthesiser.

$\mathbf{R}_f$ (silica, 1 : 1 hexane : ethyl acetate) = 0.30

No further characterisation data was obtained due to the instability / air sensitivity of the product meaning it had to be used immediately for DNA synthesis.

9.38 Synthesis of 5'-DMT-5-propargylbenzamide-deoxyuridine-3' amidite

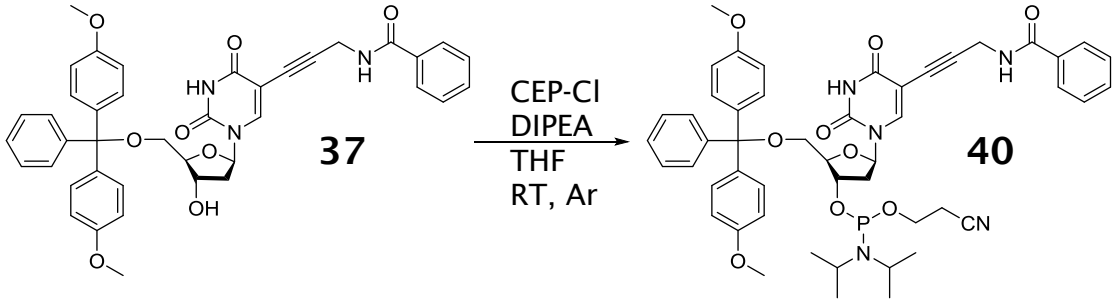

5'-DMT-5-propargylbenzamide-deoxyuridine (110mg, 0.160 mmol, 1 equiv.) was dissolved in anhydrous THF (3 mL) in oven dried glassware with molecular sieves. This was purged with argon for 10 minutes. DIPEA (112 µL, 0.640 mmol, 4 equiv.) and CEP-Cl (152 µL, 0.480 mmol, 3 equiv.) were added and the reaction kept under argon at room temperature for 2 hours.

The reaction mixture was transferred to a new flask and the solvent reduced to approximately 1 mL *in vacuo*. Ice cold hexane (5 mL) was added and the flask placed on ice for 30 minutes to precipitate. The hexane was removed and the product dissolved in anhydrous MeCN (1.6 mL) to make up a solution of concentration 100 mM (assuming 100 % reaction yield). The solution was transferred to a DNA synthesiser vial and placed onto the synthesiser.

Appendix

Carboxy di-acetylene aA

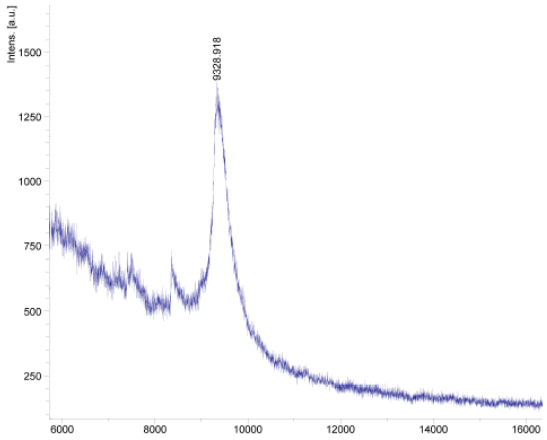

Carboxy di-acetylene bB

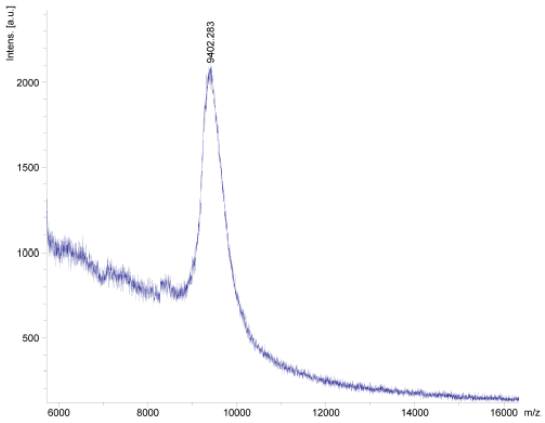

Carboxy di-acetylene cC

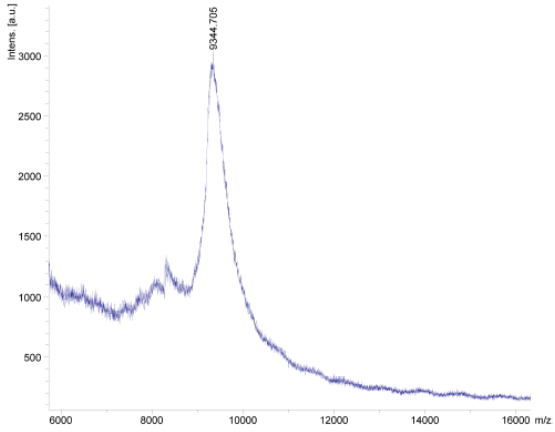

Carboxy di-acetylene dD

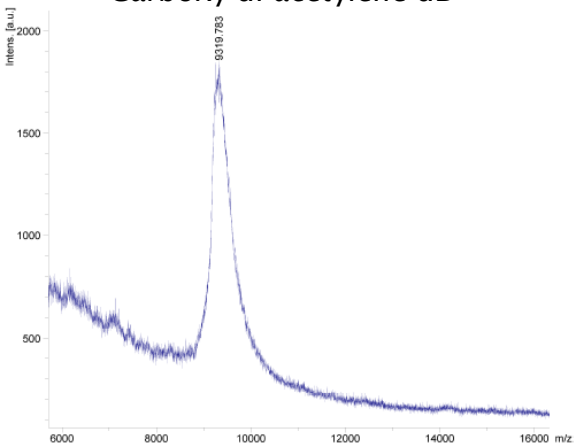

MALDI-ToF mass spectra for the di-acetylene-modified porphyrin DNA samples connected with the 5'-carboxy C10 linker. Calculated molecular masses and measured values displayed in figure 5.3.

Cu-free di-acetylene aA TMS ON

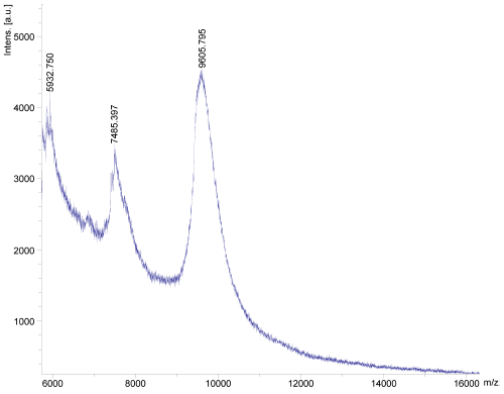

Cu-free di-acetylene aA TMS OFF

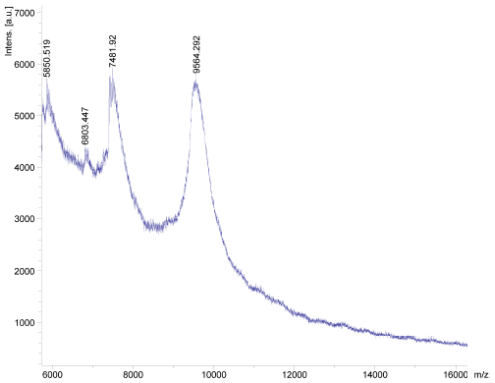

Cu-free di-acetylene bB TMS ON

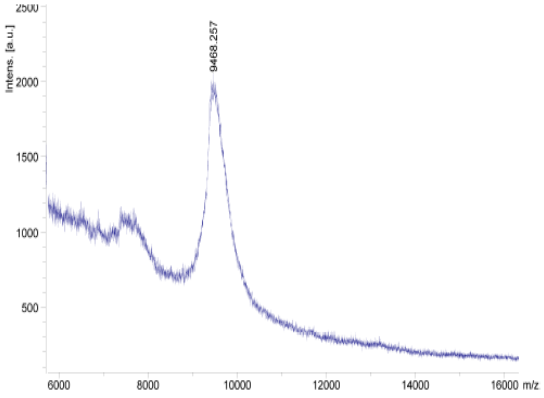

Cu-free di-acetylene bB TMS OFF

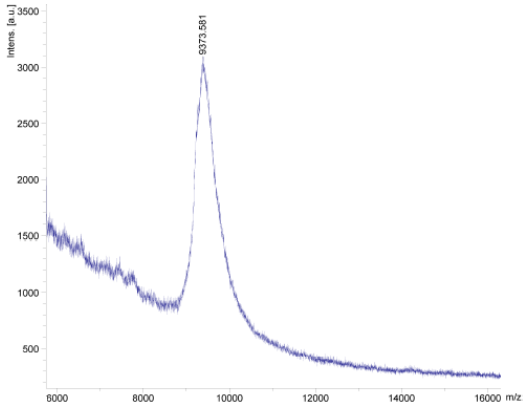

MALDI-ToF mass spectra for the di-acetylene-modified porphyrin DNA samples connected with the strained alkyne linker. Calculated molecular masses and measured values displayed in figure 5.4.

Porph Amide Un/1P

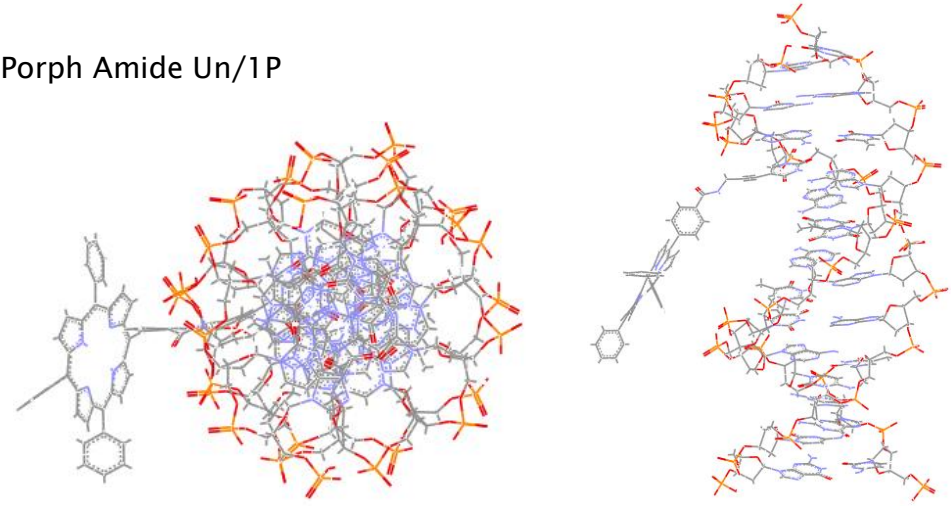

Porph Amide 1P/1P (far)

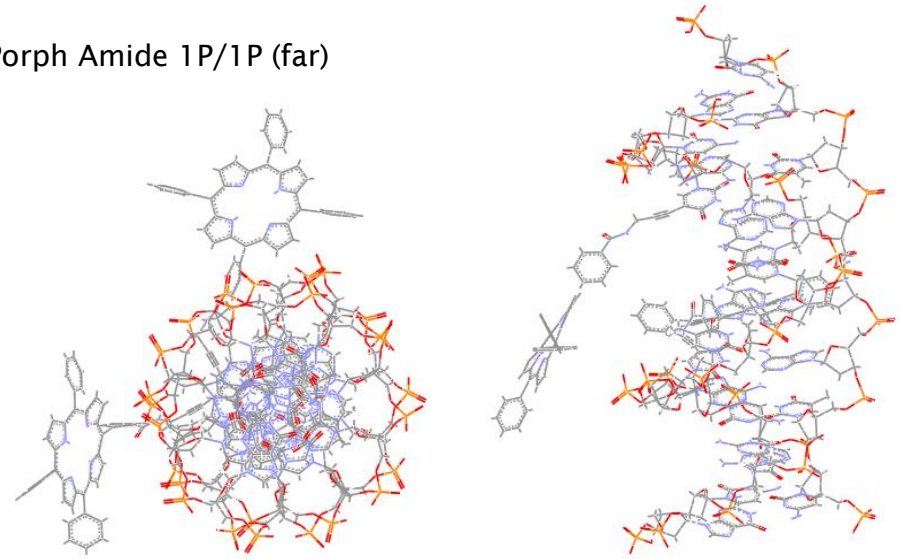

Porph Amide 1P/1P (near)

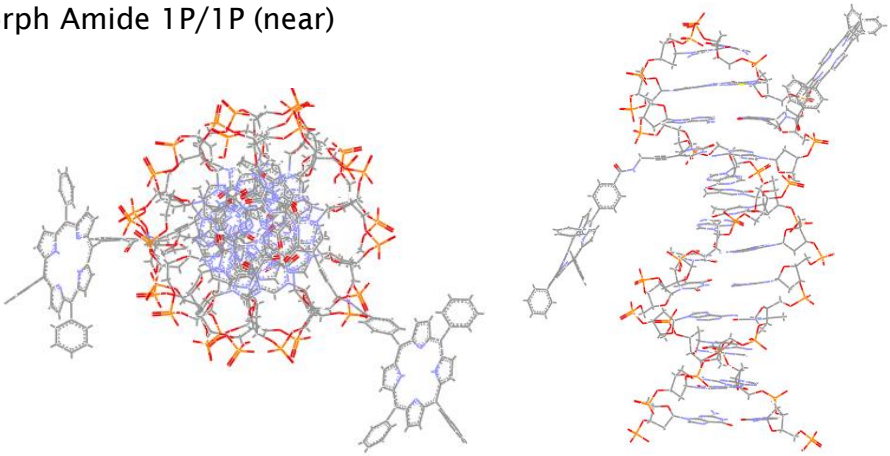

Porph Amide Un/2P

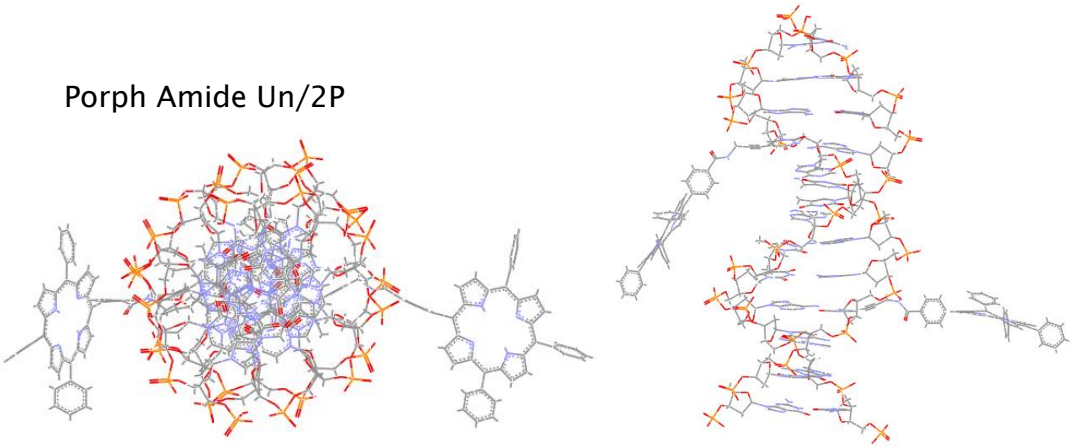

Porph Amide 2P/Un

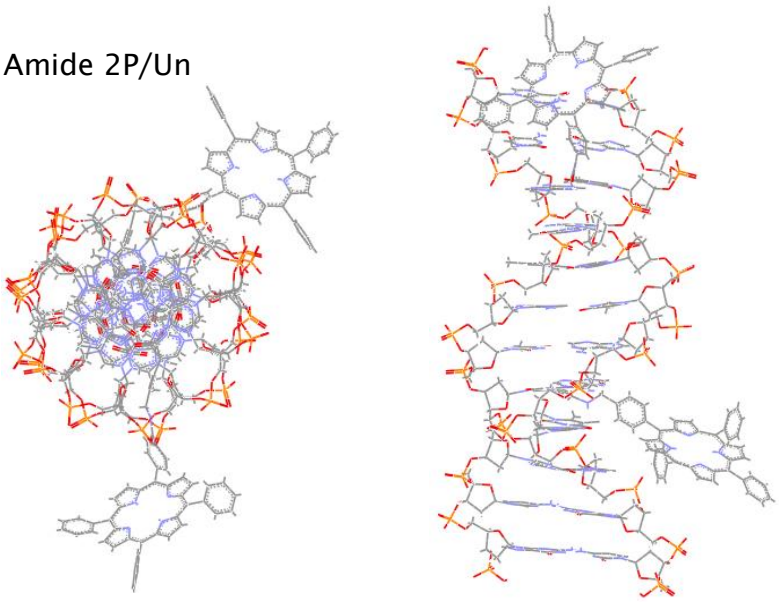

Porph Amide 2P/1P

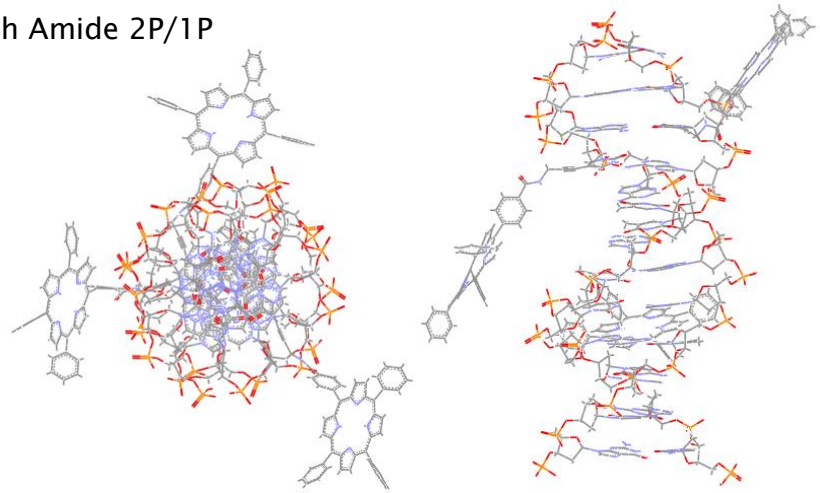

Porph Amide 2P/2P

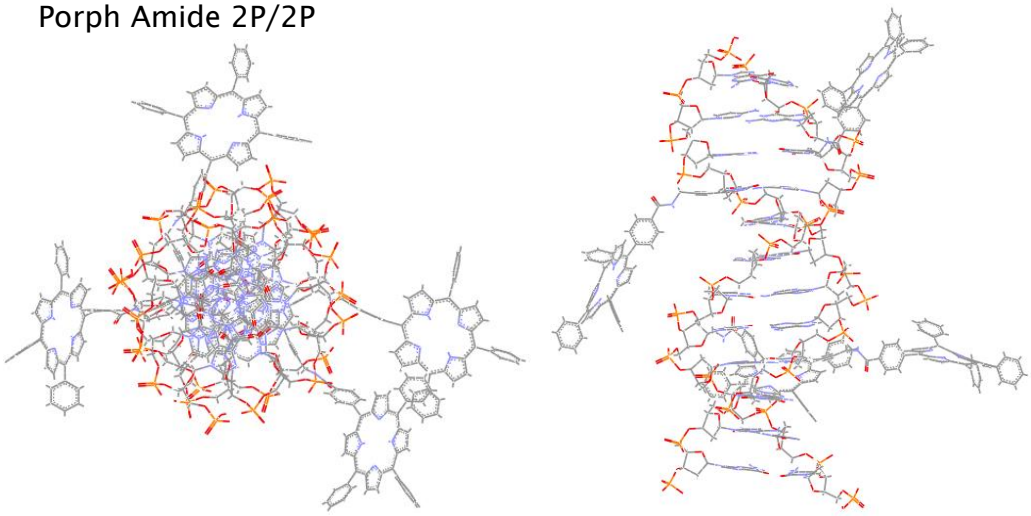

Porph Acet Un/1P

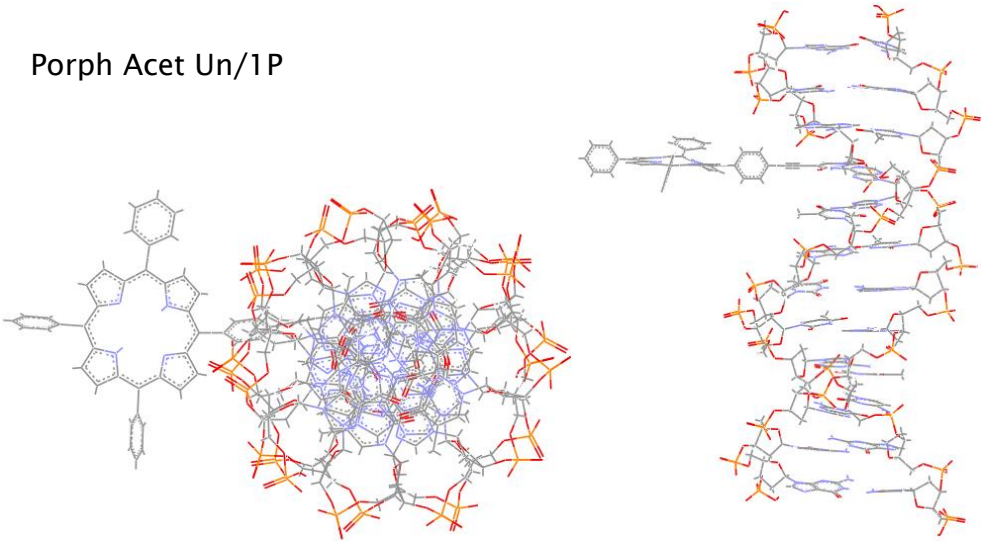

Porph Acet 1P/1P (far)

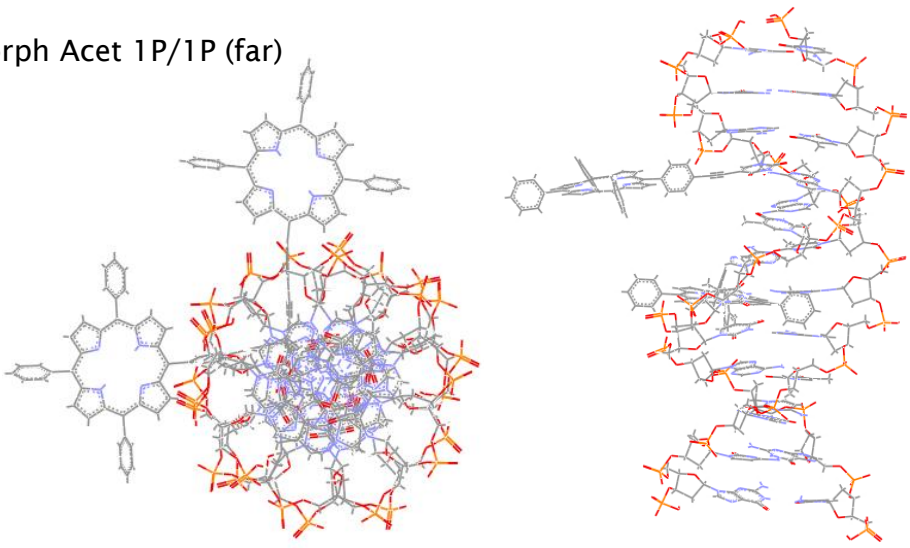

Porph Acet 1P/1P (near)

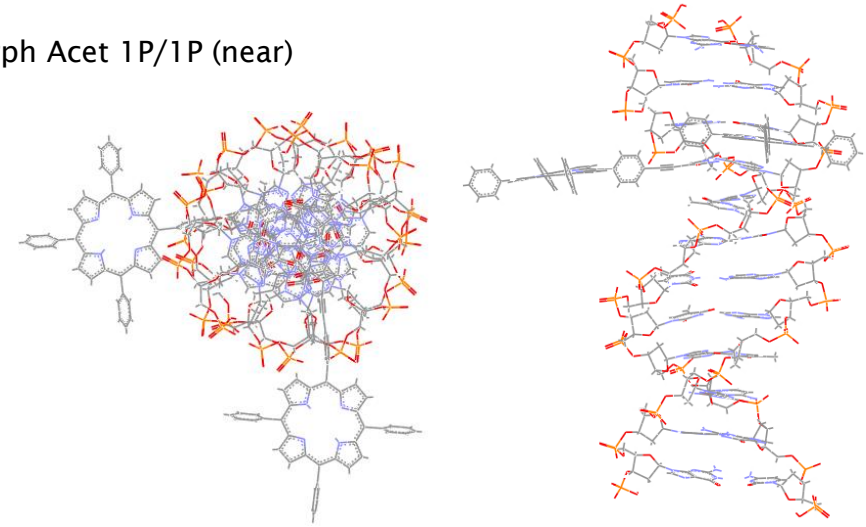

Porph Acet Un/2P

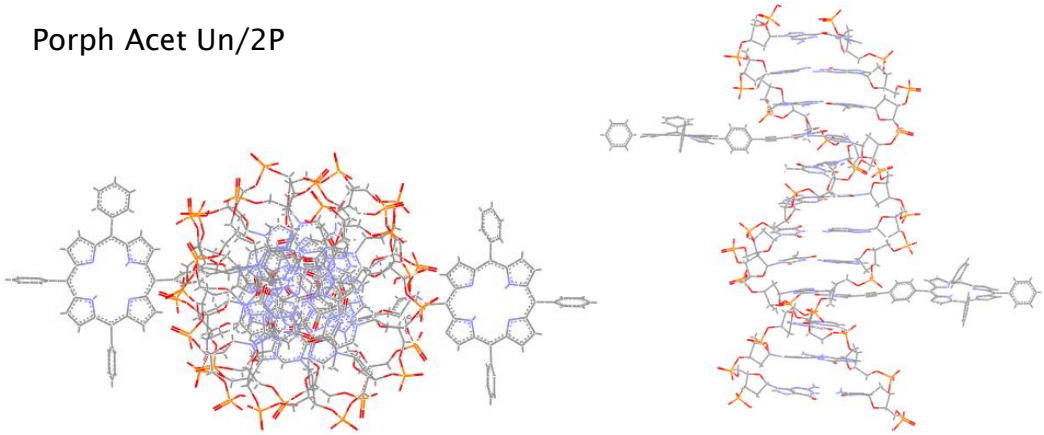

Porph Acet 2P/Un

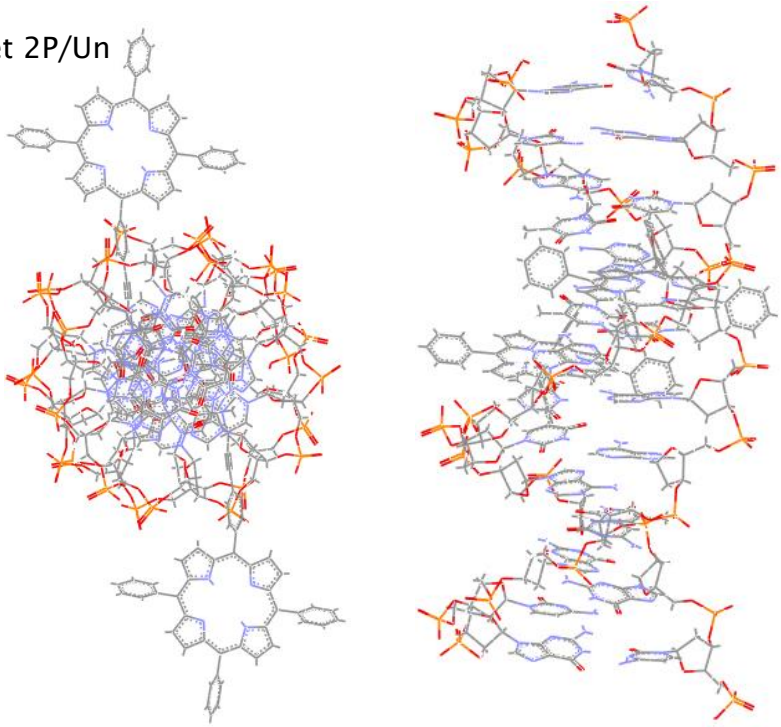

Porph Acet 2P/1P

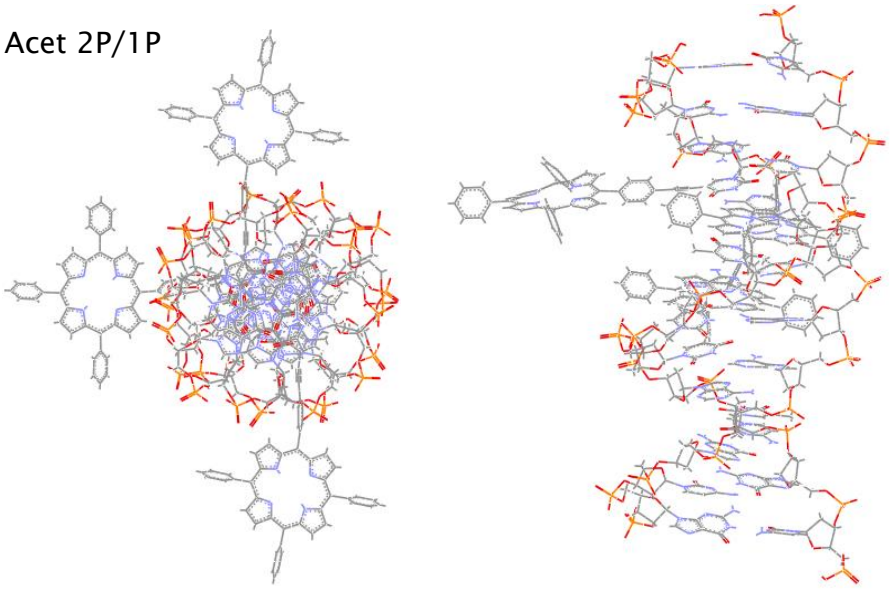

Porph Acet 2P/2P

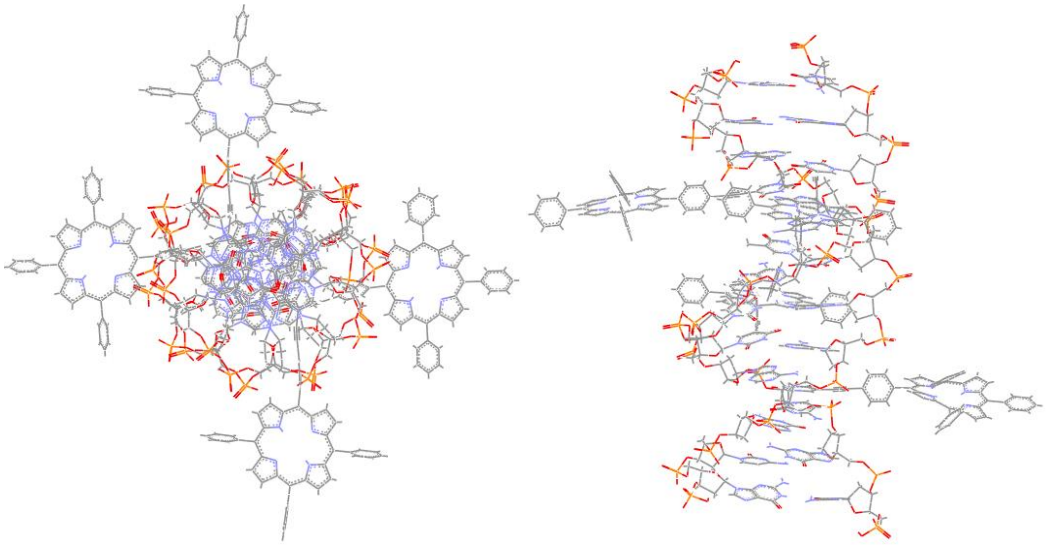

All models are displayed in the same orientation.

Appendix

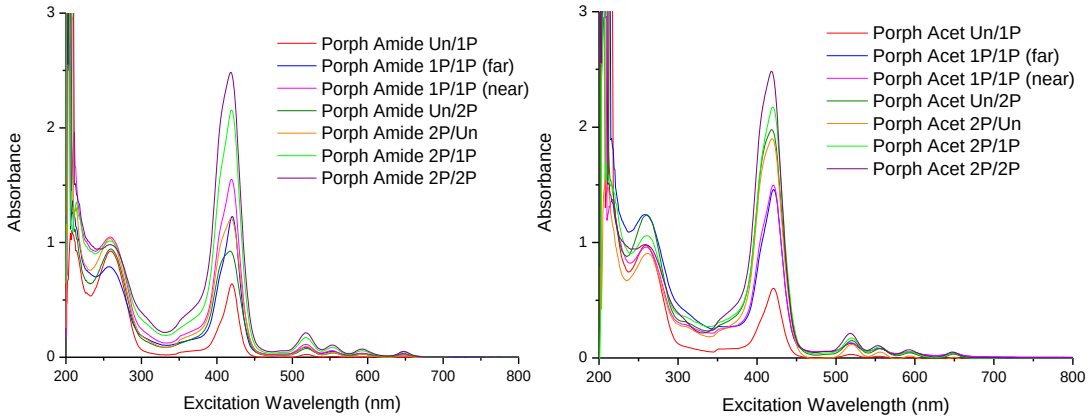

UV/Vis spectra for the Poprh Amide (left) and Porph Acet (right) duplex samples. Sample concentration = 5 μM. Path length = 1 cm.

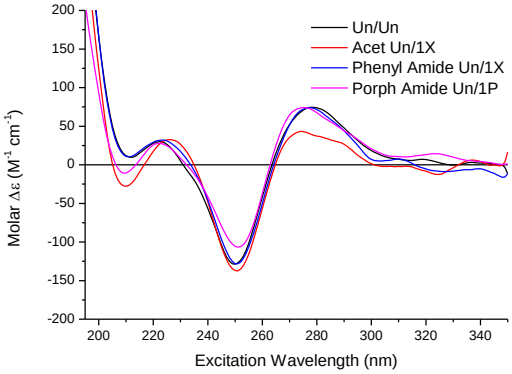

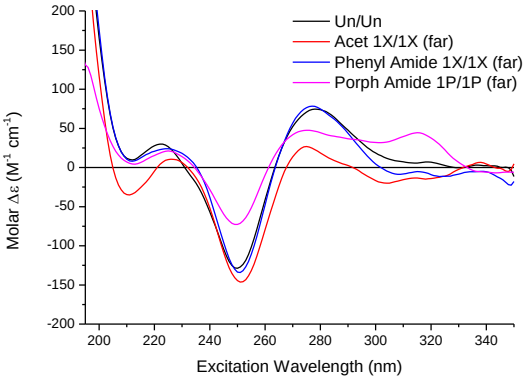

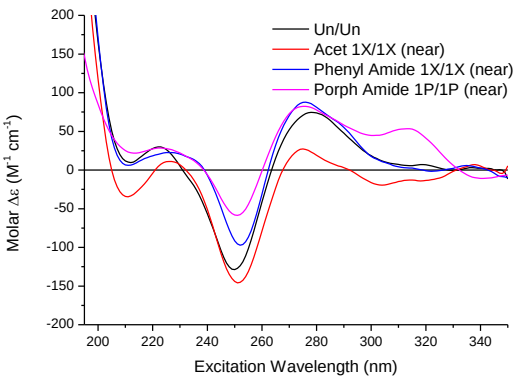

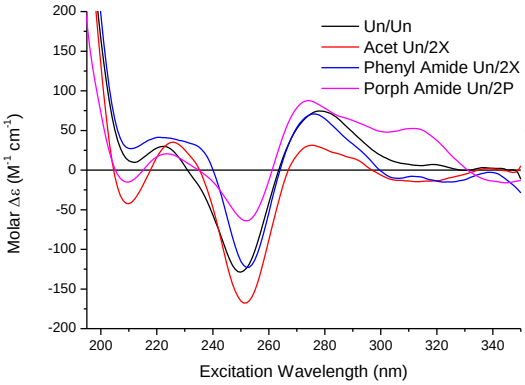

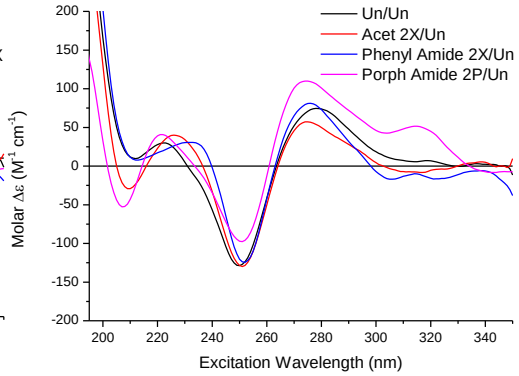

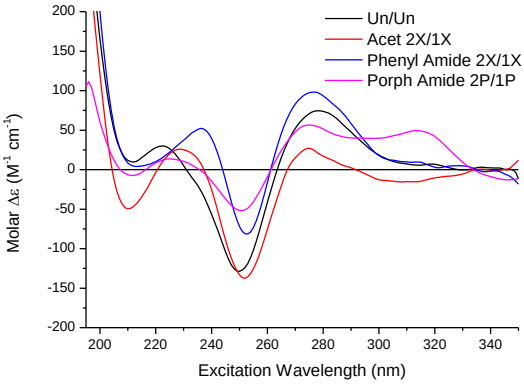

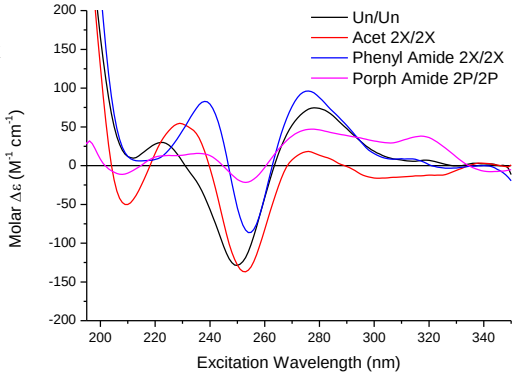

Comparisons between duplexes containing the same number of Acet, Phenyl Amide and Porph Amide modifications.

Appendix

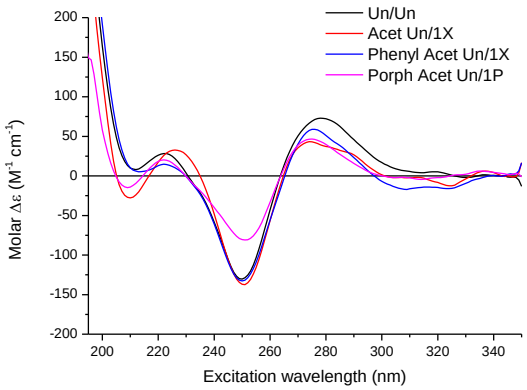

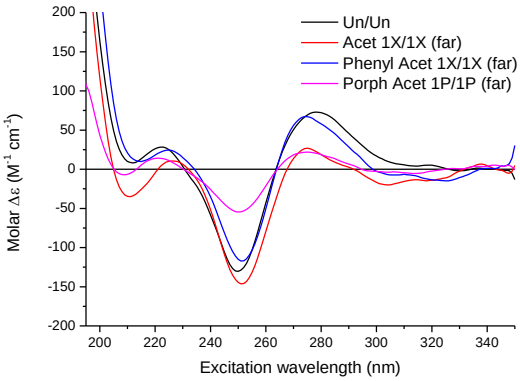

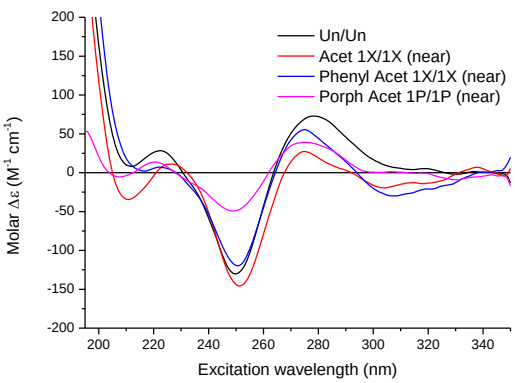

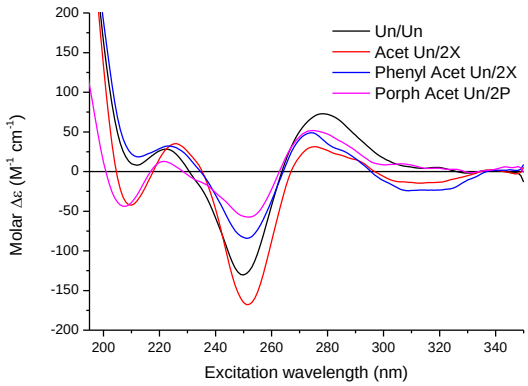

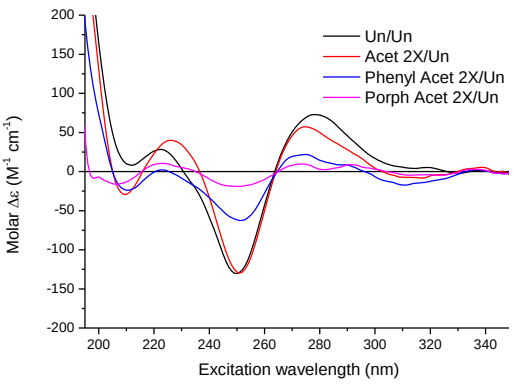

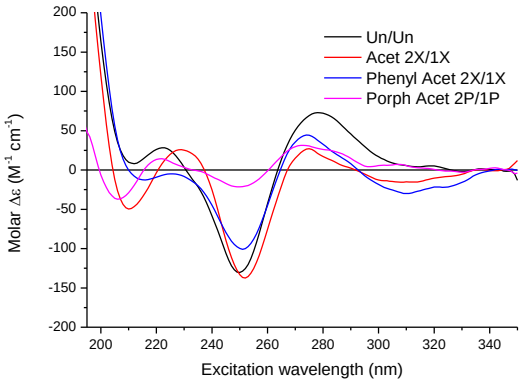

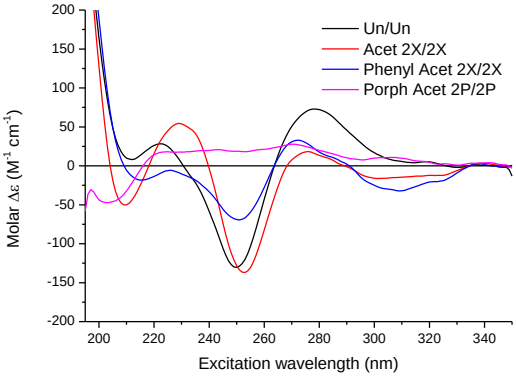

Comparisons between duplexes containing the same number of Acet, Phenyl Acet and Porph Acet modifications.

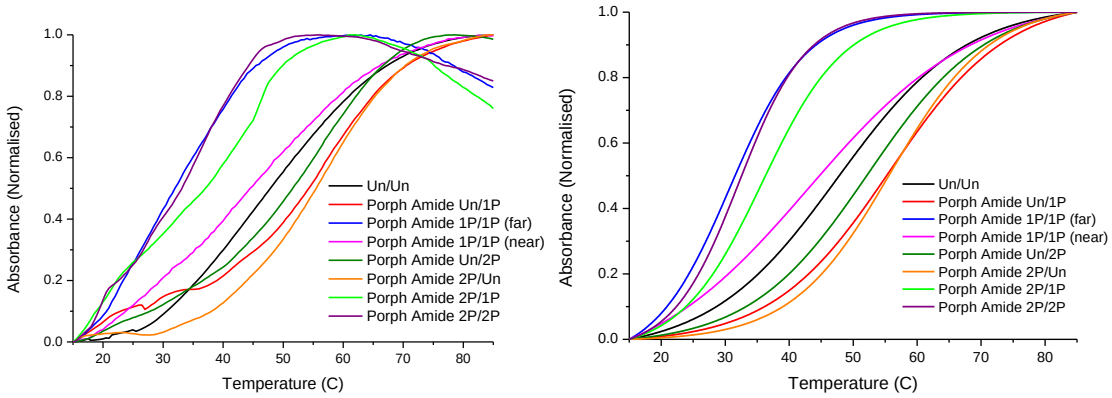

Crude melting curve (left) and data with a Boltzmann fitting (right) used to acquire T_m's for the Porph Amide duplex systems.

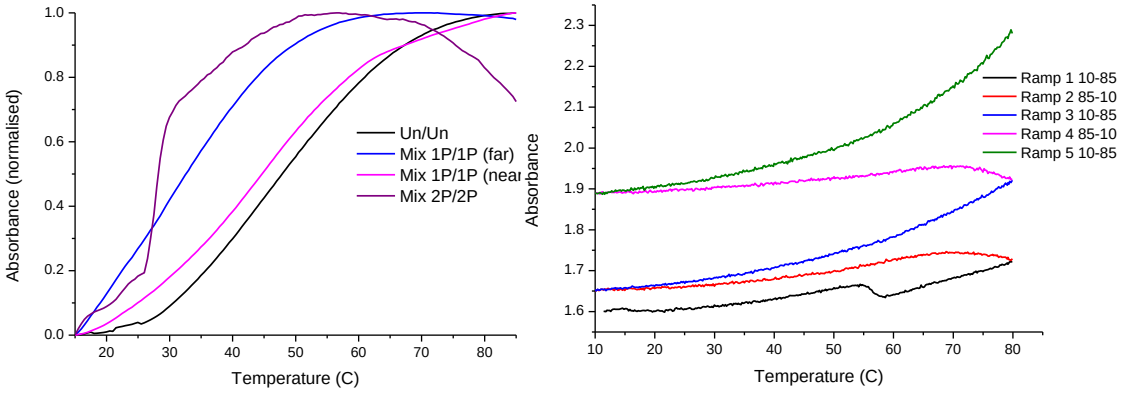

Left) Crude melting curve for the mixed Porph duplexes. Right) Example melting data produced at the University of Southampton. The presented data is from the sample Porph Acet 1P/1P (near)

Bibliography

1. E. Rabinowitch, *Rev. Mod. Phys.*, 1944, **16**, 226-235.
2. S. W. Ryter and R. M. Tyrrell, *Free Radic. Biol. Med.*, 2000, **28**, 289-309.
3. X. C. Hu, A. Damjanovic, T. Ritz and K. Schulten, *Proc. Natl. Acad. Sci. U. S. A.*, 1998, **95**, 5935-5941.
4. D. A. Bryant and N. U. Frigaard, *Trends Microbiol.*, 2006, **14**, 488-496.
5. D. Ostfeld and M. Tsutsui, *Accounts of Chemical Research*, 1974, **7**, 52-58.
6. M. John Plater, S. Aiken and G. Bourhill, *Tetrahedron*, 2002, **58**, 2415-2422.
7. S. Ryu, J. Kim, H. Yeo and K. Kim, *Inorg. Chim. Acta*, 1995, **228**, 233-236.
8. E. B. Fleischer and J. H. Wang, *J. Am. Chem. Soc.*, 1960, **82**, 3498-3502.
9. G. Ricciardi, A. Rosa, E. J. Baerends and S. A. J. van Gisbergen, *J. Am. Chem. Soc.*, 2002, **124**, 12319-12334.
10. D. Koszelewski, A. Nowak-Krol, M. Drobizhev, C. J. Wilson, J. E. Haley, T. M. Cooper, J. Romiszewski, E. Gorecka, H. L. Anderson, A. Rebane and D. T. Gryko, *J. Mater. Chem. C*, 2013, **1**, 2044-2053.
11. M. Y. R. Wang and B. M. Hoffman, *J. Am. Chem. Soc.*, 1984, **106**, 4235-4240.
12. H. Jiang, X. F. Huang, K. Nakanishi and N. Berova, *Tetrahedron Lett.*, 1999, **40**, 7645-7649.
13. G. Pescitelli, S. Gabriel, Y. K. Wang, J. Fleischhauer, R. W. Woody and N. Berova, *J. Am. Chem. Soc.*, 2003, **125**, 7613-7628.
14. L. A. Fendt, I. Bouamaied, S. Thoni, N. Amiot and E. Stulz, *J. Am. Chem. Soc.*, 2007, **129**, 15319-15329.
15. N. Thao-Nguyen, A. Brewer and E. Stulz, *Angew. Chem., Int. Ed.*, 2009, **48**, 1974-1977.
16. X. F. Huang, K. Nakanishi and N. Berova, *Chirality*, 2000, **12**, 237-255.
17. M. J. Gouterman, *Chem. Phys.* , 1959, **30**, 1139-1161.
18. M. Gouterman, *Journal of Molecular Spectroscopy*, 1961, **6**, 138-163.
19. P. J. Spellane, M. Gouterman, A. Antipas, S. Kim and Y. C. Liu, *Inorg. Chem.*, 1980, **19**, 386-391.
20. A. Ceulemans, W. Oldenhof, C. Gorllerwalrand and L. G. Vanquickenborne, *J. Am. Chem. Soc.*, 1986, **108**, 1155-1163.
21. V. N. Nemykin and R. G. Hadt, *J. Phys. Chem. A*, 2010, **114**, 12062-12066.
22. H. Fischer and K. Zeile, *Liebigs Ann. Chem.*, 1929, **468**, 98.
23. P. Rothemund, *J. Am. Chem. Soc.*, 1935, **57**, 2010-2011.
24. P. Rothemund, *J. Am. Chem. Soc.*, 1936, **58**, 625-627.
25. A. D. Adler, F. R. Longo, J. D. Finarelli, J. Goldmacher, J. Assour and L. Korsakoff, *The Journal of Organic Chemistry*, 1967, **32**, 476-476.
26. H. Fischer and W. Gleim, *Liebigs Ann. Chem.*, 1935, **521**, 157.
27. J. S. Lindsey, I. C. Schreiman, H. C. Hsu, P. C. Kearney and A. M. Marguerettaz, *J. Org. Chem.*, 1987, **52**, 827-836.
28. R. W. Wagner, T. E. Johnson and J. S. Lindsey, *J. Am. Chem. Soc.*, 1996, **118**, 11166-11180.
29. H. Fischer and H. Orth, *Die Chemie des Pyrrols*, Akademische Verlagsgesellschaft M.B.H. Leipzig, 1934.
30. C. H. Lee and J. S. Lindsey, *Tetrahedron*, 1994, **50**, 11427-11440.
31. B. J. Littler, M. A. Miller, C. H. Hung, R. W. Wagner, D. F. O'Shea, P. D. Boyle and J. S. Lindsey, *J. Org. Chem.*, 1999, **64**, 1391-1396.

32. K. M. Kadish, K. M. Smith and R. Guilard, *The Porphyrin Handbook Volume 1*, Elsevier Science Publishing Co Inc, 1999.
33. C. Bruckner, J. J. Posakony, C. K. Johnson, R. W. Boyle, B. R. James and D. Dolphin, *J. Porphyr. Phthalocyanines*, 1998, **2**, 455-465.
34. J. D. Watson and F. H. Crick, *Nature*, 1953, **171**, 964-967.
35. E. Chargaff, *Experientia*, 1950, **6**, 201-209.
36. J. D. Watson and F. H. C. Crick, *Nature*, 1953, **171**, 737-738.
37. M. H. F. Wilkins, A. R. Stokes and H. R. Wilson, *Nature*, 1953, **171**, 738-740.
38. R. E. Franklin and R. G. Gosling, *Nature*, 1953, **171**, 740-741.
39. Y. G. Gao, H. Robinson and A. H. J. Wang, *Eur. J. Biochem.*, 1999, **261**, 413-420.
40. R. Wing, H. Drew, T. Takano, C. Broka, S. Tanaka, K. Itakura and R. E. Dickerson, *Nature*, 1980, **287**, 755-758.
41. A. H. J. Wang, G. J. Quigley, F. J. Kolpak, J. L. Crawford, J. H. Vanboom, G. Vandermarel and A. Rich, *Nature*, 1979, **282**, 680-686.
42. S. Arnott, *Trends Biochem.Sci.*, 2006, **31**, 349-354.
43. G. M. Blackburn, M. J. Gait and Loakes, *Nucleic Acids in Chemistry and Biology* 2006.
44. *http://www.mun.ca/biology/scarr/MGA2_02-07.html*, Accessed on 2.3.15.
45. E. T. Kool, *Chem. Rev.*, 1997, **97**, 1473-1487.
46. M. Egli, V. Tereshko, M. Teplova, G. Minasov, A. Joachimiak, R. Sanishvili, C. M. Weeks, R. Miller, M. A. Maier, H. An, P. Dan Cook and M. Manoharan, *Biopolymers*, 1998, **48**, 234-252.
47. H. R. Drew and R. E. Dickerson, *J. Mol. Biol.*, 1981, **151**, 535-556.
48. M. L. Kopka, A. V. Fratini, H. R. Drew and R. E. Dickerson, *J. Mol. Biol.*, 1983, **163**, 129-146.
49. V. Tereshko, G. Minasov and M. Egli, *J. Am. Chem. Soc.*, 1999, **121**, 3590-3595.
50. S. L. Beaucage and M. H. Caruthers, *Tetrahedron Lett.*, 1981, **22**, 1859-1862.
51. J. A. Richardson, T. Morgan, M. Andreou and T. Brown, *Analyst*, 2013, **138**, 3626-3628.
52. N. Venkatesan, Y. J. Seo and B. H. Kim, *Chem. Soc. Rev.*, 2008, **37**, 648-663.
53. Y. Xiao, X. H. Lou, T. Uzawa, K. J. I. Plakos, K. W. Plaxco and H. T. Soh, *J. Am. Chem. Soc.*, 2009, **131**, 15311-15316.
54. T. J. Bandy, A. Brewer, J. R. Burns, G. Marth, T. Nguyen and E. Stulz, *Chem. Soc. Rev.*, 2011, **40**, 138-148.
55. K. Sonogashira, Y. Tohda and N. Hagihara, *Tetrahedron Lett.*, 1975, 4467-4470.
56. M. Rist, N. Amann and H. A. Wagenknecht, *Eur. J. Org. Chem.*, 2003, 2498-2504.
57. T. Kottysch, C. Ahlborn, F. Brotzel and C. Richert, *Chem.-Eur. J.*, 2004, **10**, 4017-4028.
58. I. Bouamaied and E. Stulz, *Synlett*, 2004, 1579-1583.
59. K. C. Schneider and S. A. Benner, *J. Am. Chem. Soc.*, 1990, **112**, 453-455.
60. W. Schmucker and H. A. Wagenknecht, *Synlett*, 2012, 2435-2448.
61. C. Brotschi, A. Haberli and C. J. Leumann, *Angew. Chem.-Int. Edit.*, 2001, **40**, 3012-3014.
62. A. T. Krueger and E. T. Kool, *Chem. Biol.*, 2009, **16**, 242-248.

63. L. L. Zhang and E. Meggers, *J. Am. Chem. Soc.*, 2005, **127**, 74-75.
64. E. Mayer-Enthart and H. A. Wagenknecht, *Angew. Chem.-Int. Edit.*, 2006, **45**, 3372-3375.
65. J. N. Wilson, Y. J. Cho, S. Tan, A. Cuppoletti and E. T. Kool, *ChemBioChem*, 2008, **9**, 279-285.
66. Y. Doi, J. Chiba, T. Morikawa and M. Inouye, *J. Am. Chem. Soc.*, 2008, **130**, 8762-8768.
67. K. Tanaka, M. Tasaka, H. H. Cao and M. Shionoya, *Eur. J. Pharm. Sci.*, 2001, **13**, 77-83.
68. G. H. Clever and M. Shionoya, *Coord. Chem. Rev.*, 2010, **254**, 2391-2402.
69. J. A. Richardson, M. Gerowska, M. Shelbourne, D. French and T. Brown, *ChemBioChem*, 2010, **11**, 2530-2533.
70. S. X. Jin, C. V. Miduturu, D. C. McKinney and S. K. Silverman, *J. Org. Chem.*, 2005, **70**, 4284-4299.
71. M. Gerowska, L. Hall, J. Richardson, M. Shelbourne and T. Brown, *Tetrahedron*, 2012, **68**, 857-864.
72. S. Obika, D. Nanbu, Y. Hari, K. Morio, Y. In, T. Ishida and T. Imanishi, *Tetrahedron Lett.*, 1997, **38**, 8735-8738.
73. A. A. Koshkin, S. K. Singh, P. Nielsen, V. K. Rajwanshi, R. Kumar, M. Meldgaard, C. E. Olsen and J. Wengel, *Tetrahedron*, 1998, **54**, 3607-3630.
74. H. Kaur, B. R. Babu and S. Maiti, *Chem. Rev.*, 2007, **107**, 4672-4697.
75. M. A. Campbell and J. Wengel, *Chem. Soc. Rev.*, 2011, **40**, 5680-5689.
76. F. Garo and R. Haner, *Eur. J. Org. Chem.*, 2012, 2801-2808.
77. P. E. Nielsen, M. Egholm, R. H. Berg and O. Buchardt, *Science*, 1991, **254**, 1497-1500.
78. L. Moggio, L. De Napoli, E. Di Blasio, G. Di Fabio, J. D'Onofrio, D. Montesarchio and A. Messere, *Org. Lett.*, 2006, **8**, 2015-2018.
79. V. L. Malinovskii, F. Samain and R. Haner, *Angew. Chem.-Int. Edit.*, 2007, **46**, 4464-4467.
80. B. A. Connolly, *Nucleic Acids Res.*, 1987, **15**, 3131-3139.
81. A. A. Mokhir, C. N. Tetzlaff, S. Herzberger, A. Mosbacher and C. Richert, *J. Comb. Chem.*, 2001, **3**, 374-386.
82. B. A. Connolly and P. Rider, *Nucleic Acids Res.*, 1985, **13**, 4485-4502.
83. J. L. Czlapinski and T. L. Sheppard, *J. Am. Chem. Soc.*, 2001, **123**, 8618-8619.
84. C. D. Claeboe, R. Gao and S. M. Hecht, *Nucleic Acids Res.*, 2003, **31**, 5685-5691.
85. J. G. Zendegui, K. M. Vasquez, J. H. Tinsley, D. J. Kessler and M. E. Hogan, *Nucleic Acids Res.*, 1992, **20**, 307-314.
86. G. R. Desiraju, *Nature*, 2001, **412**, 397-400.
87. S. Tyagi and F. R. Kramer, *Nat Biotech*, 1996, **14**, 303-308.
88. P. M. Holland, R. D. Abramson, R. Watson and D. H. Gelfand, *Proc. Natl. Acad. Sci. U. S. A.*, 1991, **88**, 7276-7280.
89. N. Thelwell, S. Millington, A. Solinas, J. Booth and T. Brown, *Nucleic Acids Res.*, 2000, **28**, 3752-3761.
90. D. J. French, C. L. Archard, T. Brown and D. G. McDowell, *Mol. Cell. Probes*, 2001, **15**, 363-374.
91. N. Moran, D. M. Bassani, J. P. Desvergne, S. Keiper, P. A. S. Lowden, J. S. Vyle and J. H. R. Tucker, *Chem. Commun.*, 2006, 5003-5005.
92. N. C. Seeman, *Journal of Theoretical Biology*, 1982, **99**, 237-247.
93. N. C. Seeman, *Angew. Chem., Int. Ed.*, 1998, **37**, 3220-3238.

94. N. C. Seeman, C. D. Mao and H. Yan, *Accounts of Chemical Research*, 2014, **47**, 1643-1644.
95. N. C. Seeman, *Annual Review of Biophysics and Biomolecular Structure*, 1998, **27**, 225-248.
96. E. Stulz, *Chemistry – A European Journal*, 2012, n/a-n/a.
97. N. R. Kallenbach, R. I. Ma and N. C. Seeman, *Nature*, 1983, **305**, 829-831.
98. J. H. Chen and N. C. Seeman, *Nature*, 1991, **350**, 631-633.
99. P. W. K. Rothemund, *Nature*, 2006, **440**, 297-302.
100. J. R. Burns, K. Gopfrich, J. W. Wood, V. V. Thacker, E. Stulz, U. F. Keyser and S. Howorka, *Angew. Chem.-Int. Edit.*, 2013, **52**, 12069-12072.
101. O. A. Vinogradova and D. V. Pyshnyi, *Russ. Chem. Rev.*, 2012, **81**, 130-157.
102. A. S. Walsh, H. F. Yin, C. M. Erben, M. J. A. Wood and A. J. Turberfield, *ACS Nano*, 2011, **5**, 5427-5432.
103. S. S. Simmel, P. C. Nickels and T. Liedl, *Accounts of Chemical Research*, 2014, **47**, 1691-1699.
104. S. M. Douglas, H. Dietz, T. Liedl, B. Hogberg, F. Graf and W. M. Shih, *Nature*, 2009, **459**, 414-418.
105. E. S. Andersen, M. Dong, M. M. Nielsen, K. Jahn, R. Subramani, W. Mamdouh, M. M. Golas, B. Sander, H. Stark, C. L. P. Oliveira, J. S. Pedersen, V. Birkedal, F. Besenbacher, K. V. Gothelf and J. Kjems, *Nature*, 2009, **459**, 73-U75.
106. D. H. Yoon, S. B. Lee, K. H. Yoo, J. Kim, J. K. Lim, N. Aratani, A. Tsuda, A. Osuka and D. Kim, *J. Am. Chem. Soc.*, 2003, **125**, 11062-11064.
107. A. Ambroise, R. W. Wagner, P. D. Rao, J. A. Riggs, P. Hascoat, J. R. Diers, J. Seth, R. K. Lammi, D. F. Bocian, D. Holten and J. S. Lindsey, *Chemistry of Materials*, 2001, **13**, 1023-1034.
108. S. Prathapan, T. E. Johnson and J. S. Lindsey, *J. Am. Chem. Soc.*, 1993, **115**, 7519-7520.
109. D. Furutsu, A. Satake and Y. Kobuke, *Inorg. Chem.*, 2005, **44**, 4460-4462.
110. M. K. Panda, K. Ladomenou and A. G. Coutsolelos, *Coord. Chem. Rev.*, 2012, **256**, 2601-2627.
111. V. L. Gunderson, A. L. Smeigh, C. H. Kim, D. T. Co and M. R. Wasielewski, *J. Am. Chem. Soc.*, 2012, **134**, 4363-4372.
112. M. Jurow, A. E. Schuckman, J. D. Batteas and C. M. Drain, *Coord. Chem. Rev.*, 2010, **254**, 2297-2310.
113. M. Endo, T. Shiroyama, M. Fujitsuka and T. Majima, *J. Org. Chem.*, 2005, **70**, 7468-7472.
114. I. Bouamaied, T. Nguyen, T. Ruhl and E. Stulz, *Org. Biomol. Chem.*, 2008, **6**, 3888-3891.
115. A. Brewer, G. Siligardi, C. Neylon and E. Stulz, *Org. Biomol. Chem.*, 2011, **9**, 777-782.
116. N. Zhang, X. Z. Chu, M. Fathalla and J. Jayawickramarajah, *Langmuir*, 2013, **29**, 10796-10806.
117. M. Vybornyi, A. L. Nussbaumer, S. M. Langenegger and R. Haner, *Bioconjugate Chem.*, 2014, **25**, 1785-1793.
118. W. B. Sherman and N. C. Seeman, *Nano Lett.*, 2004, **4**, 1203-1207.
119. J. S. Shin and N. A. Pierce, *J. Am. Chem. Soc.*, 2004, **126**, 10834-10835.
120. J. Bath, S. J. Green, K. E. Allen and A. J. Turberfield, *Small*, 2009, **5**, 1513-1516.

121. C. J. Murphy, M. R. Arkin, Y. Jenkins, N. D. Ghatlia, S. H. Bossmann, N. J. Turro and J. K. Barton, *Science*, 1993, **262**, 1025-1029.
122. N. B. Muren, E. D. Olmon and J. K. Barton, *Phys. Chem. Chem. Phys.*, 2012, **14**, 13754-13771.
123. C. H. Wohlgamuth, M. A. McWilliams and J. D. Slinker, *Anal. Chem.*, 2013, **85**, 8634-8640.
124. B. Giese, *Annu. Rev. Biochem.*, 2002, **71**, 51-70.
125. A. J. Storm, J. van Noort, S. de Vries and C. Dekker, *Appl. Phys. Lett.*, 2001, **79**, 3881-3883.
126. G. I. Livshits, A. Stern, D. Rotem, N. Borovok, G. Eidelshtein, A. Migliore, E. Penzo, S. J. Wind, R. Di Felice, S. S. Skourtis, J. C. Cuevas, L. Gurevich, A. B. Kotlyar and D. Porath, *Nat. Nanotechnol.*, 2014, **9**, 1040-1046.
127. A. Kuzyk, R. Schreiber, Z. Y. Fan, G. Pardatscher, E. M. Roller, A. Hogele, F. C. Simmel, A. O. Govorov and T. Liedl, *Nature*, 2012, **483**, 311-314.
128. P. K. Dutta, R. Varghese, J. Nangreave, S. Lin, H. Yan and Y. Liu, *J. Am. Chem. Soc.*, 2011, **133**, 11985-11993.
129. J. Hannant, J. H. Hedley, J. Pate, A. Walli, S. A. F. Al-Said, M. A. Galindo, B. A. Connolly, B. R. Horrocks, A. Houlton and A. R. Pike, *Chem. Commun.*, 2010, **46**, 5870-5872.
130. E. Braun, Y. Eichen, U. Sivan and G. Ben-Yoseph, *Nature*, 1998, **391**, 775-778.
131. Y. Eichen, E. Braun, U. Sivan and G. Ben-Yoseph, *Acta Polym.*, 1998, **49**, 663-670.
132. T. E. Ouldridge, *Mol. Phys.*, 2015, **113**, 1-15.
133. J. L. Fu, M. H. Liu, Y. Liu, N. W. Woodbury and H. Yan, *J. Am. Chem. Soc.*, 2012, **134**, 5516-5519.
134. J. L. Fu, Y. R. Yang, A. Johnson-Buck, M. H. Liu, Y. Liu, N. G. Walter, N. W. Woodbury and H. Yan, *Nat. Nanotechnol.*, 2014, **9**, 531-536.
135. C. M. Drain, *Proc. Natl. Acad. Sci. U. S. A.*, 2002, **99**, 5178-5182.
136. A. Stone and E. B. Fleischer, *J. Am. Chem. Soc.*, 1968, **90**, 2735-2748.
137. M. S. Choi, *Tetrahedron Lett.*, 2008, **49**, 7050-7053.
138. O. Ohno, Y. Kaizu and H. Kobayashi, *J. Chem. Phys.*, 1993, **99**, 4128-4139.
139. *http://www.atdbio.com/tools/oligo-calculator*, Accessed on 23.3.13.
140. I. Grabowska, D. G. Singleton, A. Stachyra, A. Gora-Sochacka, A. Sirko, W. Zagorski-Ostoja, H. Radecka, E. Stulz and J. Radecki, *Chem. Commun.*, 2014, **50**, 4196-4199.
141. G. Bratthauer, in *Immunocytochemical Methods and Protocols*, eds. C. Oliver and M. C. Jamur, Humana Press, Editon edn., 2010, vol. 588, pp. 257-270.
142. J. Olejnik, S. Sonar, E. Krzymanskaolejnik and K. J. Rothschild, *Proc. Natl. Acad. Sci. U. S. A.*, 1995, **92**, 7590-7594.
143. H. C. Kolb, M. G. Finn and K. B. Sharpless, *Angew. Chem.-Int. Edit.*, 2001, **40**, 2004-2021.
144. R. Huisgen, *Proceedings of the Chemical Society*, 1961, 357-396.
145. R. Huisgen, *Angewandte Chemie International Edition in English*, 1963, **2**, 565-598.
146. L. F. Tietze and G. Kettschau, *Stereoselective Heterocyclic Synthesis I*, 1997, **189**, 1-120.
147. H. Waldmann, *Synthesis*, 1994, 535-551.
148. H. C. Kolb and K. B. Sharpless, *Drug Discov. Today*, 2003, **8**, 1128-1137.
149. V. V. Rostovtsev, L. G. Green, V. V. Fokin and K. B. Sharpless, *Angew. Chem., Int. Ed.*, 2002, **41**, 2596-2599.

150. F. Himo, T. Lovell, R. Hilgraf, V. V. Rostovtsev, L. Noodleman, K. B. Sharpless and V. V. Fokin, *J. Am. Chem. Soc.*, 2005, **127**, 210-216.
151. M. G. Simmons, C. L. Merrill, L. J. Wilson, L. A. Bottomley and K. M. Kadish, *J. Chem. Soc.-Dalton Trans.*, 1980, 1827-1837.
152. T. R. Chan, R. Hilgraf, K. B. Sharpless and V. V. Fokin, *Org. Lett.*, 2004, **6**, 2853-2855.
153. C. J. Burrows and J. G. Muller, *Chem. Rev.*, 1998, **98**, 1109-1151.
154. V. Hong, S. I. Presolski, C. Ma and M. G. Finn, *Angew. Chem.-Int. Edit.*, 2009, **48**, 9879-9883.
155. V. Hong, N. F. Steinmetz, M. Manchester and M. G. Finn, *Bioconjugate Chem.*, 2010, **21**, 1912-1916.
156. M. P. Cervantes-Cervantes, J. V. Calderon-Salinas, A. Albores and J. L. Munoz-Sanchez, *Biol. Trace Elem. Res.*, 2005, **103**, 229-248.
157. J. C. Jewett and C. R. Bertozzi, *Chem. Soc. Rev.*, 2010, **39**, 1272-1279.
158. D. C. Kennedy, C. S. McKay, M. C. B. Legault, D. C. Danielson, J. A. Blake, A. F. Pegoraro, A. Stolow, Z. Mester and J. P. Pezacki, *J. Am. Chem. Soc.*, 2011, **133**, 17993-18001.
159. M. Dizdaroglu and P. Jaruga, *Free Radic. Res.*, 2012, **46**, 382-419.
160. J. Gierlich, G. A. Burley, P. M. E. Gramlich, D. M. Hammond and T. Carell, *Org. Lett.*, 2006, **8**, 3639-3642.
161. N. K. Devaraj, G. P. Miller, W. Ebina, B. Kakaradov, J. P. Collman, E. T. Kool and C. E. D. Chidsey, *J. Am. Chem. Soc.*, 2005, **127**, 8600-8601.
162. R. L. Weller and S. R. Rajski, *Org. Lett.*, 2005, **7**, 2141-2144.
163. K. Harju, M. Vahermo, I. Mutikainen and J. Yli-Kauhaluoma, *J. Comb. Chem.*, 2003, **5**, 826-833.
164. W. G. Lewis, L. G. Green, F. Grynszpan, Z. Radic, P. R. Carlier, P. Taylor, M. G. Finn and K. B. Sharpless, *Angew. Chem.-Int. Edit.*, 2002, **41**, 1053-1057.
165. Q. Wang, T. R. Chan, R. Hilgraf, V. V. Fokin, K. B. Sharpless and M. G. Finn, *J. Am. Chem. Soc.*, 2003, **125**, 3192-3193.
166. T. S. Seo, Z. M. Li, H. Ruparel and J. Y. Ju, *J. Org. Chem.*, 2003, **68**, 609-612.
167. A. H. El-Sagheer and T. Brown, *Chem. Soc. Rev.*, 2010, **39**, 1388-1405.
168. D. I. Rozkiewicz, J. Gierlich, G. A. Burley, K. Gutsmiedl, T. Carell, B. J. Ravoo and D. N. Reinhoudt, *ChemBioChem*, 2007, **8**, 1997-2002.
169. R. Kumar, A. El-Sagheer, J. Tumpane, P. Lincoln, L. M. Wilhelmsson and T. Brown, *J. Am. Chem. Soc.*, 2007, **129**, 6859-6864.
170. P. Kocalka, A. H. El-Sagheer and T. Brown, *ChemBioChem*, 2008, **9**, 1280-1285.
171. *http://www.baseclick.eu/products.php?IDCAT=16&IDSOTTOCAT=24*, Acessed on 13.3.15.
172. N. S. Hatzakis, H. Engelkamp, K. Velonia, J. Hofkens, P. C. M. Christianen, A. Svendsen, S. A. Patkar, J. Vind, J. C. Maan, A. E. Rowan and R. J. M. Nolte, *Chem. Commun.*, 2006, 2012-2014.
173. N. J. Agard, J. A. Prescher and C. R. Bertozzi, *J. Am. Chem. Soc.*, 2004, **126**, 15046-15047.
174. C. Bertozzi, *Abstr. Pap. Am. Chem. Soc.*, 2012, **244**.
175. C. G. Gordon, J. L. Mackey, J. C. Jewett, E. M. Sletten, K. N. Houk and C. R. Bertozzi, *J. Am. Chem. Soc.*, 2012, **134**, 9199-9208.
176. D. H. Ess, G. O. Jones and K. N. Houk, *Org. Lett.*, 2008, **10**, 1633-1636.
177. F. Schoenebeck, D. H. Ess, G. O. Jones and K. N. Houk, *J. Am. Chem. Soc.*, 2009, **131**, 8121-8133.
178. G. S. Hammond, *J. Am. Chem. Soc.*, 1955, **77**, 334-338.

179. J. C. Jewett, E. M. Sletten and C. R. Bertozzi, *J. Am. Chem. Soc.*, 2010, **132**, 3688-+.
180. N. J. Agard, J. M. Baskin, J. A. Prescher, A. Lo and C. R. Bertozzi, *ACS Chem. Biol.*, 2006, **1**, 644-648.
181. A. B. Neef and C. Schultz, *Angew. Chem.-Int. Edit.*, 2009, **48**, 1498-1500.
182. Y. K. Zou and J. Yin, *Bioorg. Med. Chem. Lett.*, 2008, **18**, 5664-5667.
183. M. Shelbourne, T. Brown and A. H. El-Sagheer, *Chem. Commun.*, 2012, **48**, 11184-11186.
184. G. H. Hur, J. L. Meier, J. Baskin, J. A. Codelli, C. R. Bertozzi, M. A. Marahiel and M. D. Burkart, *Chem. Biol.*, 2009, **16**, 372-381.
185. M. A. Nessen, G. Kramer, J. Back, J. M. Baskin, L. E. J. Smeenk, L. J. de Koning, J. H. van Maarseveen, L. de Jong, C. R. Bertozzi, H. Hiemstra and C. G. de Koster, *J. Proteome Res.*, 2009, **8**, 3702-3711.
186. *http://www.glenresearch.com/ProductFiles/10-1539.html*, Accessed on 12.3.15.
187. C. Stubinitzky, G. B. Cserep, E. Batzner, P. Kele and H. A. Wagenknecht, *Chem. Commun.*, 2014, **50**, 11218-11221.
188. J. M. Baskin, J. A. Prescher, S. T. Laughlin, N. J. Agard, P. V. Chang, I. A. Miller, A. Lo, J. A. Codelli and C. R. Bertozzi, *Proc. Natl. Acad. Sci. U. S. A.*, 2007, **104**, 16793-16797.
189. J. B. Ravnsbæk, M. F. Jacobsen, C. B. Rosen, N. V. Voigt and K. V. Gothelf, *Angew. Chem., Int. Ed.*, 2011, **50**, 10851-10854.
190. J. Jover, P. Spuhler, L. G. Zhao, C. McArdle and F. Maseras, *Catal. Sci. Technol.*, 2014, **4**, 4200-4209.
191. D. P. Arnold and G. A. Heath, *J. Am. Chem. Soc.*, 1993, **115**, 12197-12198.
192. V. S. Y. Lin, S. G. Dimagno and M. J. Therien, *Science*, 1994, **264**, 1105-1111.
193. C. Glaser, *Berichte der deutschen chemischen Gesellschaft*, 1869, **2**, 422-424.
194. C. Glaser, *Justus Liebigs Annalen der Chemie*, 1870, **154**, 137-171.
195. A. Hay, *The Journal of Organic Chemistry*, 1960, **25**, 1275-1276.
196. A. S. Hay, *The Journal of Organic Chemistry*, 1962, **27**, 3320-3321.
197. J. B. Armitage, E. R. H. Jones and M. C. Whiting, *Journal of the Chemical Society (Resumed)*, 1952, **0**, 2014-2018.
198. F. Sondheimer, Y. Amiel and R. Wolovsky, *J. Am. Chem. Soc.*, 1957, **79**, 4247-4248.
199. K. C. Nicolaou, R. E. Zipkin and N. A. Petasis, *J. Am. Chem. Soc.*, 1982, **104**, 5558-5560.
200. K. Balaraman and V. Kesavan, *Synthesis*, 2010, 3461-3466.
201. G. Sedghi, V. M. Garcia-Suarez, L. J. Esdaile, H. L. Anderson, C. J. Lambert, S. Martin, D. Bethell, S. J. Higgins, M. Elliott, N. Bennett, J. E. Macdonald and R. J. Nichols, *Nat. Nanotechnol.*, 2011, **6**, 517-523.
202. M. H. Vilhelmsen, J. Jensen, C. G. Tortzen and M. B. Nielsen, *Eur. J. Org. Chem.*, 2013, 701-711.
203. G. Eglinton and A. R. Galbraith, *Journal of the Chemical Society (Resumed)*, 1959, 889-896.
204. O. M. Behr, G. Eglinton, A. R. Galbraith and R. A. Raphael, *Journal of the Chemical Society (Resumed)*, 1960, 3614-3625.
205. D. P. Arnold, A. W. Johnson and M. Mahendran, *J. Chem. Soc.-Perkin Trans. 1*, 1978, 366-370.

206. H. L. Anderson and J. K. M. Sanders, *J. Chem. Soc.-Chem. Commun.*, 1989, 1714-1715.
207. D. P. Arnold and D. A. James, *J. Org. Chem.*, 1997, **62**, 3460-3469.
208. D. P. Arnold, G. A. Heath and D. A. James, *New J. Chem.*, 1998, **22**, 1377-1387.
209. J. D. Wilkinson, G. Wicks, A. Nowak-Krol, L. G. Lukasiewicz, C. J. Wilson, M. Drobizhev, A. Rebane, D. T. Gryko and H. L. Anderson, *J. Mater. Chem. C*, 2014, **2**, 6802-6809.
210. H. L. Anderson, S. J. Martin and D. D. C. Bradley, *Angew. Chem.-Int. Edit. Engl.*, 1994, **33**, 655-657.
211. S. G. DiMagno, V. S. Y. Lin and M. J. Therien, *The Journal of Organic Chemistry*, 1993, **58**, 5983-5993.
212. H. L. Anderson, *Inorg. Chem.*, 1994, **33**, 972-981.
213. E. V. Vinogradova, Y. Y. Enakieva, Y. G. Gorbunova and A. Y. Tsivadze, *Prot. Met. Phys. Chem. Surf.*, 2009, **45**, 529-534.
214. D. S. McClure, *The Journal of Chemical Physics*, 1949, **17**, 905-913.
215. M. N. Berberan Santos, *PhysChemComm*, 2000, **3**, 18-23.
216. M. Rae, F. Perez-Balderas, C. Baleizao, A. Fedorov, J. A. S. Cavaleiro, A. C. Tome and M. N. Berberan-Santos, *J. Phys. Chem. B*, 2006, **110**, 12809-12814.
217. A. Gonsalves, A. C. Serra, M. Pineiro, M. Laranjo, A. M. Abrantes, C. Goncalves, B. Oliveiros, A. B. Sarmento and M. Botelho, *Reporters, Markers, Dyes, Nanoparticles, and Molecular Probes for Biomedical Applications Iii*, 2011, **7910**.
218. P. M. E. Gramlich, S. Warncke, J. Gierlich and T. Carell, *Angew. Chem.-Int. Edit.*, 2008, **47**, 3442-3444.
219. G. W. Kabalka, M. Varma, R. S. Varma, P. C. Srivastava and F. F. Knapp, *J. Org. Chem.*, 1986, **51**, 2386-2388.
220. R. Ding, Y. He, X. Wang, J. L. Xu, Y. R. Chen, M. Feng and C. M. Qi, *Molecules*, 2011, **16**, 5665-5673.
221. G. C. Harrison and H. Diehl, *Org. Syn. Coll.*, 1955, **3**, 370.
222. R. S. Varma and K. P. Naicker, *Tetrahedron Lett.*, 1998, **39**, 2915-2918.
223. E. J. J. Grabowski and A. S. Thompson, Google Patents, Editon edn., 1995.
224. *http://www.glenresearch.com/ProductFiles/10-1935.html*, Accessed on 14.3.15.
225. C. Endisch, J. H. Fuhrhop, J. Buschmann, P. Luger and U. Siggel, *J. Am. Chem. Soc.*, 1996, **118**, 6671-6680.
226. L. Ruhlmann, A. Nakamura, J. G. Vos and J. H. Fuhrhop, *Inorg. Chem.*, 1998, **37**, 6052-6059.
227. W. Fudickar, J. Zimmermann, L. Ruhlmann, J. Schneider, B. Roder, U. Siggel and J. H. Fuhrhop, *J. Am. Chem. Soc.*, 1999, **121**, 9539-9545.
228. M. Regehly, T. Y. Wang, U. Siggel, J. H. Fuhrhop and B. Roeder, *J. Phys. Chem. B*, 2009, **113**, 2526-2534.
229. D. Chandler, *Nature*, 2005, **437**, 640-647.
230. C. A. Hunter and J. K. M. Sanders, *J. Am. Chem. Soc.*, 1990, **112**, 5525-5534.
231. N. Berova, L. Di Bari and G. Pescitelli, *Chem. Soc. Rev.*, 2007, **36**, 914-931.
232. G. Pescitelli, N. Sreerama, P. Salvadori, K. Nakanishi, N. Berova and R. W. Woody, *J. Am. Chem. Soc.*, 2008, **130**, 6170-6181.
233. *http://www.diamond.ac.uk/Science/Machine/Components.html*, Accessed on 24.3.15.

234. *http://commons.wikimedia.org/wiki/File:Circular.Polarization.Circularly.Polarized.Light_Circular.Polarizer_Creating.Left.Handed.Helix.View.svg*, Accessed on 1.3.15.
235. S. Georgakopoulou, R. van Grondelle and G. van der Zwan, *J. Phys. Chem. B*, 2006, **110**, 3344-3353.
236. S. Matile, N. Berova, K. Nakanishi, S. Novkova, I. Philipova and B. Blagoev, *J. Am. Chem. Soc.*, 1995, **117**, 7021-7022.
237. S. Matile, N. Berova, K. Nakanishi, J. Fleischhauer and R. W. Woody, *J. Am. Chem. Soc.*, 1996, **118**, 5198-5206.
238. M. Balaz, A. E. Holmes, M. Benedetti, P. C. Rodriguez, N. Berova, K. Nakanishi and G. Proni, *J. Am. Chem. Soc.*, 2005, **127**, 4172-4173.
239. M. Balaz, J. D. Steinkruger, G. A. Ellestad and N. Berova, *Org. Lett.*, 2005, **7**, 5613-5616.
240. A. Mammana, T. Asakawa, K. Bitsch-Jensen, A. Wolfe, S. Chaturantabut, Y. Otani, X. X. Li, Z. M. Li, K. Nakanishi, M. Balaz, G. A. Ellestad and N. Berova, *Bioorg. Med. Chem.*, 2008, **16**, 6544-6551.
241. J. K. Choi, A. Reed and M. Balaz, *Dalton Trans.*, 2014, **43**, 563-567.
242. A. D'Urso, M. E. Fragala and R. Purrello, *Chem. Commun.*, 2012, **48**, 8165-8176.
243. N. Berova, P. L. Polavarapu, Nakanishi.K and R. W. Woody, *Comprehensive Chiroptical Spectroscopy, Volume 2: Applications in Stereochemical Analysis of Synthetic Compounds, Natural Products, and Biomolecules*

2012.
244. A. S. Davydov, *Zhur. Eksptl. i Teoret. Fiz.*, 1948, **18**, 210-218.
245. M. J. Crossley, L. G. Mackay and A. C. Try, *J. Chem. Soc.-Chem. Commun.*, 1995, 1925-1927.
246. N. Harada, S. L. Chen and K. Nakanishi, *J. Am. Chem. Soc.*, 1975, **97**, 5345-5352.
247. M. P. Heyn, *J. Phys. Chem.*, 1975, **79**, 2424-2426.
248. *http://www.schrodinger.com/Maestro/*, Accessed on 10.12.13.
249. N. Harada and K. Nakanishi, *J. Am. Chem. Soc.*, 1969, **91**, 5896-5898.
250. N. Harada and Nakanish.K, *Accounts of Chemical Research*, 1972, **5**, 257-&.
251. S. Superchi, E. Giorgio and C. Rosini, *Chirality*, 2004, **16**, 422-451.
252. J. M. Bijvoet, A. F. Peerdeman and A. J. van Bommel, *Nature*, 1951, **168**, 271-272.
253. N. Harada, Y. Takuma and H. Uda, *J. Am. Chem. Soc.*, 1976, **98**, 5408-5409.
254. J. SantaLucia, *Proc. Natl. Acad. Sci. U. S. A.*, 1998, **95**, 1460-1465.
255. *http://www.entelechon.com/2008/08/dna-melting-temperature/*, Accessed 16.3.15.
256. M. Mandel and J. Marmur, in *Methods in Enzymology*, ed. K. M. Lawrence Grossman, Academic Press, Editon edn., 1968, vol. Volume 12, Part B, pp. 195-206.
257. R. B. Wallace, J. Shaffer, R. F. Murphy, J. Bonner, T. Hirose and K. Itakura, *Nucleic Acids Res.*, 1979, **6**, 3543-3557.
258. W. Rychlik, W. J. Spencer and R. E. Rhoads, *Nucleic Acids Res.*, 1990, **18**, 6409-6412.
259. *http://www.atdbio.com/content/53/DNA-duplex-stability*, Accessed on 16.3.15.

260. X. Jin, S. Yue, K. S. Wells and V. L. Singer, *Faseb J.*, 1994, **8**, A1266-A1266.
261. B. M. Znosko, T. W. Barnes, T. R. Krugh and D. H. Turner, *J. Am. Chem. Soc.*, 2003, **125**, 6090-6097.